Exhuming the core of collisional orogens,

the Tauern Window (Eastern-Alps)

A geochronological, modelling and structural study

Dissertation
von

Audrey Bertrand

Zur
Erlangung des Doktorgrades der Naturwissenschaften
im Fachbereich Geowissenschaften
an der
Freien Universität Berlin

……

Prof. Dr. Claudio L. Rosenberg (Erstgutachter)
UPMC – Paris VI Jussieu

Prof. Dr. Mark R. Handy (Zweitgutachter)
Freie Universität Berlin

Tag der Disputation: 06/12/2013

Erklärung

Hiermit erkläre ich, Audrey Bertrand, dass diese Arbeit ausschließlich auf Grundlage der angegebenen Hilfsmittel und Hilfen selbstständig von mir verfasst wurde. Diese Arbeit wurde nicht in einem früheren Promotionsverfahren eingereicht.

Berlin, den 11. Oktober 2013

Audrey Bertrand

Abstract

Exhumation of the Eastern Alps was largely localized within the Tauern Window, a thermal and structural dome located north of the Dolomite indenter and formed from the Oligocene to the Late Miocene times. The Tauern Window is composed by two main sub-domes that are dominated by upright folds. In particular, the western sub-dome is marked by upright folds, which reconstructed amplitudes attained more than 30 km. The western and eastern margins are delimited by the major Brenner and Katschberg normal fault systems, respectively. The presence of the upright folds in the internal parts of the Tauern Window and of the major normal faults at its borders suggest that both N-S shortening and E-W extension played an important role during the exhumation history of the Tauern Window.

This study attempts to assess the relative contribution of folding and erosion and of orogen-parallel extension during exhumation by a combined analysis of (1) the spatial and temporal evolution of late cooling of the Tauern Window, using apatite and zircon fission track ages; (2) the late, brittle deformation structures of the Tauern Window, providing new investigations of fault analyses and paleostress fields; and (3) the modelled, thermal evolution of a folded lithosphere based on 2D-thermal modelling, which predicts the surface distribution of fission track ages as a function of uplift rate and initial thermal state.

Cooling-age distribution based on previous and new apatite and zircon fission track ages indicate a heterogeneous cooling history along the Tauern Window. In general, ages of the western sub-dome are younger than ages in the eastern Tauern Window. Zircon fission track ages indicate that the eastern and western sub-dome were exhumed at similar rates between 22 and 12 Ma while apatite fission track ages indicate that after 12 Ma, the western sub-dome was exhumed at higher rates compared to the eastern sub-dome. Apatite and zircon fission track ages show elongate, concentric distribution following the map trace of the main axial planes of the folds, with younger ages in the core of the western sub-dome and more heterogeneous distributions in the eastern sub-dome. These distributions suggest that folding and erosion were responsible for the exhumation of the Tauern Window.

Brittle inversion and paleostress fields reveals a zoning within the Tauern Window with predominant strike-slip states of stress in the core of the investigated area, while the eastern and western margins of the dome are dominated by extensional regimes, with E-W to WNW-ESE extensional direction. Little evidence of compressive stress field has been highlighted, suggesting that brittle compressive structures that formed during folding have been eroded

since. During Late Miocene times, exhumation of the Tauern Window was mainly driven by E-W extension taking place along the Brenner and Katschberg normal fault systems and accommodated in the central part of the Tauern Window by major conjugate strike-slip faulting that was yielding N-S shortening.

Furthermore, results of 2D-thermal models that describe the thermal evolution of a crustal lithosphere undergoing folding and erosion indicate that a two-stage deformation history lead to a belle shape of low thermochronometer ages with younger ages where the maximum of exhumation exists. The first stage is marked by high uplift rates (2 $mm.yrs^{-1}$), lasting for ca. 10 Myrs, and bringing deep hot material to the surface, while the second event is marked by lower uplift rates (0,325 $mm.yrs^{-1}$), lasting from 20 Myrs, allowing the re-equilibration of the previous folded isotherms. This two-stage deformation history would explain both the fission track data results and the brittle deformations structures found in the Tauern Window.

Formation of upright folds and deformation of the isotherms occurred during the first stage of deformation, which is mainly driven by folding and erosion and substantial extension along the Brenner and Katschberg normal fault systems. Brittle N-S compressive structures that were associated to the folding event were eroded since. The second stage is mainly driven by orogen-parallel extension and strike-slip faulting. During this second stage, equilibration of the isotherms occurred providing the present-day cooling pattern observed in the Tauern Window. Brittle extensional and strike-slip fault measured in the field witness this second event and show that E-W to WNW-ESE extension mainly occurred along the Brenner and Katschberg normal fault systems while strike-slip faulting consistent with N-S shortening accommodated the deformation in the central Tauern Window.

Zusammenfassung

Die Exhumierung der Ostalpen, lokalisiert im Tauernfenster, erfolgte vom Oligozän bis zum späten Miozän. Das Tauernfenster ist ein thermischer und struktureller Dom, der nördlich des Dolomiten Indenters und südlich der Nördlichen Kalkalpen liegt. Ost-West gerichtete Extension ist entlang dem westlichen (Brenner Abschiebung) und östlichen Ende (Katschberg Abschiebung) des Fensters dokumentiert. Gleichzeitig zu der Ost-West Extension erfolgte eine Nord-Süd gerichtete Kompression, die sich durch einen intensiven Faltenbau im Inneren des Tauernfensters widerspiegelt. Im westlichen Bereich des Fensters erreichten die aufrechten Falten eine Amplitude von mehr als 20 km. Das gleichzeitige Vorkommen der Falten im inneren und der Abschiebungen entlang des äusseren Tauern Fenster suggeriert, dass die N-S gerichtete Verkürzunng und die E-W gerichtete Extension einen wesentlichen Beitrag zur Exhumierung des gesamten Fensters mit Beitragen hat.

Das Ziel dieser Dissertation ist den relativen Beitrag von Faltung, Erosion und der orogen-parallelen Extension mithilfe einer Kombination von Methoden zu bestimmen. Folgende methodische Ansätze wurden in dieser Arbeit verfolgt: (1) Die räumliche Anordnung und die zeitliche Entwicklung der Miozänen Abkühlung des Tauernfensters, basierend auf Apatit- und Zirkonspaltspuralter; (2) Die Analyse von späten spröden Strukturen im Tauernfensters mit Hilfe neuer tektonischer Analyseverfahren und Paläostress Inversion; (3) Durch numerischer Modellierung der 2D-thermischen Entwicklung der verfalteten Lithosphäre. Diese Modellierung prognostiziert die Verteilung der Spaltspurdaten an der Oberfläche mit Berücksichtigung von Hebungsrate und Initiale thermischen Bedingungen. Das Abkühlaltermuster, aufbauend auf bereits existierenden und eigenen Spaltspuraltern, enthüllt eine heterogene Abkühlungsgeschichte des Tauernfensters. Die Abkühlung des westlichen Tauernfensters ist überwiegend jünger und erfolgte bei größeren Hebungsraten als im östlichen Tauernfensters (Hochalm Dom). Zirkonspaltspuralter zeigen, dass zwischen 22 und 12 Myrs das westliche und östliche Tauernfester mit ähnlichen Hebungsraten exhumiert wurde. Apatitspaltspuralter zeigen, dass vor 12 Myrs das westliche Tauernfester mit höheren Hebungsraten exhumiert wurde. Die Abkühlaltermuster zeigen längliche, konzentrische Muster, parallel zur axialen Ebene der Tauern Dome, mit jüngeren Altersgruppen in den Kern der westlichen Tauernfenster und einer homogeneren Verteilung in den östlichen Tauernfester. Dieses Muster verursacht überwiegend durch Faltung und Erosion waren für Exhumierung des Tauernfensters verantwortlich.

Sprödstrukturenanalysen und Inversion von Paläostressdaten im Tauernfenster zeigen ein zoniertes Muster. Im Inneren des Fensters herrschen überwiegender seitverschiebende Strukturen vor, im Gegensatz zu den westlichen und östlichen Rand des Fensters, dort dominieren orogen-parallele extensionelle Strukturen. Die Tatsache dass kaum spröde kompressionelle Strukturen aufgenommen werden konnte, ist ein Hinweis für die Erosion der zuvor durch Faltung entstanden Strukturen. Die Miozäne Exhumierung im Tauernfenster wurde hauptsächlich durch den Ost-West gerichtete Extension entlang der Brenner- und Katschberg Abschiebung aufgenommen. Der zentrale Bereich des Fensters ist charakterisiert durch Blattverschiebungen, einhergehend mit dem Nord-Süd gerichtete Verkürzung.

Ergebnisse der 2D-thermischen Modellierung der krustalen Lithosphäre zeigen, dass eine zweiphasige Verformungsgeschichte mit einel glockenartigen Muster der Spaltspurabkühlalter erzeugt wird, wobei die jüngere Alter im Bereich der maximalen exhumiering zu finden sind. Die Erste Phase (10 Myrs) ist geprägt durch hohe Hebungsraten (2 $mm.yrs^{-1}$) das tiefes und heißes Gestein nahe an die Oberfläche exhumiert. Gefolgt von der Zweiten Phase mit geringeren Hebungsraten (0,325 $mm.yrs^{-1}$ während 20 Myrs). Aufgrund der geringeren Hebungsrate konnten sich die vorher verfalteten Isothermen äquilibrieren. Existierenden und neuen Spaltspuralten und Sprödstrukturen, deutet auf eine zweiphasige Miozäne Verformungsgeschichte im Tauernfenster hin, was im Einklang mit meiner Modellierung ist.

Die Bildung der vertikalen Falten und die Verformung der Isothermen erfolgte während der Ersten Phase, verursacht überwiegend durch Faltung und Erosion, sowie substantieller Extension am westlichen und östlichen Ende des Tauernfensters. Die zweite Phase, mit geringeren Hebungsraten, resultiert aus der orogen-parallelen Extension und den konjugierten Blattverschiebung. Während dieser Phase äquilibrierten die Isothermen und es wurde das heutige Muster der Spaltspurabkühlalter generiert. Gemessene extensionelle und blattverschiebende Sprödstrukturen sind Zeuge der Zweiten Exhumierungsphase und unterstreichen das orogen-parallele Extension hauptsächliche an den Rändern des Tauernfensters aufgenommen wurde. Nord-Süd-gerichtet Verkürzung, im zentralen Bereich des Fensters, wurde durch die konjugierten blattverschiebenden Strukturen aufgenommen.

Résumé

L’exhumation des Alpes de l’est a été en grande partie localisée depuis le début du Tertiaire au Miocène supérieur dans la fenêtre des Tauern, dôme thermique et structural situé au front nord de l'indenteur des Dolomites. L'extension E-W affectant la fenêtre des Tauern est bien documentée et est localisée le long des limites Ouest et Est du dôme, qui sont démarquées respectivement par le système de faille normale du Brenner et le système de faille normale du Katschberg. En même temps que l’extension E-W, des plis verticaux se forment et dominent la structure interne du dôme, en particulier dans sa partie occidentale, où les amplitudes de plis atteignent jusqu'à 30 km. La présence simultanée de grands plis dans la partie interne de la fenêtre des Tauern et de failles majeures le long des limites est et ouest suggère qu’une compression N-S et une extension E-W ont tous deux joué un rôle lors de l’exhumation Tertiaire de la fenêtre des Tauern.

La présente étude tente d'évaluer la contribution relative du plissement et de l’érosion et/ou de l'extension parallèle à l’orogène pendant l’exhumation de la fenêtre des Tauern par une analyse combinée de (1) l'évolution spatiale et temporelle du refroidissement de la fenêtre des Tauern à l’aide d’âges trace de fission sur apatite et zircon (2) l’étude de la déformation cassante a travers toute la fenêtre des Tauern ainsi que de leurs champs de paléocontraintes associés et (3) l'évolution thermique d'une lithosphère crustale plissée basée sur une modélisation thermique 2D permettant de décrire la distribution des âges traces de fission en surface en fonction des taux d’exhumation et de l'état thermique initial.

La distribution des âges de refroidissement basée sur des âges traces de fission sur apatite et zircon, issus de la littérature ainsi que sur des nouvelles données produite dans cette étude, indiquent une histoire de refroidissement non homogène sur l’ensemble de la fenêtre Tauern. Les âges trace de fission du dôme ouest sont généralement plus jeunes que dans la partie Est de la fenêtre des Tauern (Hochalm dome). Les âges traces de fission sur zircon indiquent que, entre 22 Ma et 12 Ma, dômes oriental et occidental ont été exhumés à des taux relativement similaires. Au contraire, les âges traces de fission sur apatite indiquent qu'après 12 Ma, l’exhumation du dôme ouest s’est faite à des taux plus élevés que celle du dôme est. Les âges apatite et zircon montrent distributions allongées et concentriaues parrallel à la trace du plan axial de la fenêtre des Tauern, avec des âges plus jeunes au cœur du dôme ouest et une répartition plus hétérogène dans le dôme est. Ces distributions suggèrent que plissement et érosion sont responsables sont les principaux acteurs de l'exhumation de la fenêtre de Tauern.

L'inversion des déformations cassantes et leurs champs de paléocontraintes associés montrent une zonation dans la fenêtre des Tauern avec une dominance de régimes décrochants au cœur de la zone d'étude, tandis que les marges orientales et occidentales du dôme sont dominées par des régimes extensifs avec une direction d'extension comprise entre E-W et WNW-ESE. Très peu de champ de contrainte en compression a été mis en évidence ce qui suggère que les déformations cassantes témoins la phase de plissement ont été érodées. Au cours du Miocène, l'exhumation de la fenêtre des Tauern a été principalement gouvernée par une extension E-W localisée le long des systèmes de failles normales du Katschberg et du Brenner et est accommodée, dans la partie centrale de la fenêtre des Tauern, par des systèmes décrochants compatibles avec un raccourcissement N-S.

Les résultats des modèles numériques 2-D decrivant l'évolution thermique d'une croûte litosphérique subissant une déformation par plissement, montrent qu'une déformation qui se fait en deux étapes conduit à la formation d'un profil thermique en forme de cloche avec les âges de refroidissement les plus jeunes au centre. La première phase est marquée par d'importants taux d'exhumation (ca. 2 $mm.yrs^{-1}$) qui font remonter de la matière chaude depuis la profondeur vers la surface tandis que la seconde phase de déformation est marqué par de faibles taux d'exhumation (0,325 $mm.yrs^{-1}$) permettant le rééquilibrage des isothermes déformés lors de la première phase de déformation. Une histoire d'exhumation en deux étapes pourrait expliquer à la fois la distribution des âges traces de fission et la distribution des déformations cassantes de la fenêtre des Tauern.

La formation de plis verticaux et la déformation des isothermes se sont produites lors de la première phase de déformation, phase principalement liée au plissement et à l'érosion. Durant cette phase une extension substantielle se produit le long des failles normales du Katschberg et du Brenner. La deuxième étape, marquée par des taux d'exhumation inférieurs, est principalement liée à une extension parallèle à l'orogène et des systèmes décrochants. Au cours de cette deuxième étape, le rééquilibrage des isothermes se fait et est ce réequilibrage est à l'origine de la distribution des âges de refroidissement actuelle observée actuellement dans la fenêtre des Tauern. Les systèmes décrochants et extensifs mesurés sur le terrain sont le témoin de cette deuxième phase de déformation et indiquent que l'extension E-W à WNW-ESE a eu lieu principalement le long des systèmes de failles normales du Katchberg et du Brenner et que les systèmes décrochants compatibles avec un raccourcissement N-S a accommodé la déformation dans la partie centrale de la fenêtre des Tauern.

Acknowledgment

Above all, I would like to thank my two supervisors, Claudio Rosenberg and Sebastian Garcia, from whom I have learned a lot and whose doors were always open for questions and discussions. I would especially like to thank Claudio for having spent so much time correcting my work as well as for his encouragements and his support.

I would like to thank Bernhard Fügenshuh and Hannah Pomella, who always so nicely welcomed me in Innsbruck, who introduced me to the fission track method and who explained me all the details of the method.

Many thanks to Frederic Gueydan for introducing me to the world of modeling and for providing models of the Tauern Window as well as for always kindly and promptly answering all the questions we had.

I am really grateful to Stefan Schmid, who kindly proposed me to correct my manuscript: thank you so much for the very interesting discussions concerning the Eastern Alps and the Tauern Window as well as for the comments and corrections of my manuscript.

Thanks a lot to Mark Handy, Andreas Scharf, Susanne Schneider and Silvia Favaro for the interesting and fruitful discussions we had concerning the Tauern Window, for the nice time that we spend on the field together.

I would like to thank Istvan Dunkl for always answering promptly and politely to my questions about fission track problems.

I wish to thank Cornelia Kitzig, Sandra Wollnik and Thomas Michalik, Anna Giribaldi, Martina Grundmann and Andrea Eberhöfer for their great professional help.

Many thanks to Andreas, Silvia, and Paula for the great time spent in the office. Special thanks to Andreas for the corrections of my poor german, as well as for always solving all the administrative issues for me.

Many grateful thanks to Bernhard, Hannah, Hugo, Michael, Martin and Neven for always so greatly welcoming me in the tectonic group of Innsbruck and for their helpful presence and support during difficult stage I had to pass through. Special thanks to Neven: for so much.

Thanks a lot to Paola, Franzi, Guillaume, Silvia, XioJuan, Andreas, Katy, Quentin and all the British Lions for the great time I spend during the three years in Berlin. Special thanks to Silvia, who was the best flatmate.

Thanks a lot to Hannah, Angelika and Anna, Cam and Nico, Gaby and Gelbi, Fred, Freddy and Patrick and finally to Elena, for providing me with a roof when I needed. Thanks for the nice time in all these flats.

Thanks to Antonio without whom I would have never became a structural geologist and whose advices had always been of great help.

Thanks to my parents and sisters for their support, their patience and for being there for me anytime I need.

Table of content

Chapter I. Introduction

I.1. Exhumation of metamorphic gneiss domes

Structural and metamorphic gneiss domes commonly form in the thickened crust of orogenic mountains belts. They are composed of a core of high-grade metamorphic or plutonic rocks, such as gneiss, granite or migmatite, overlain by upper crustal rocks of lower metamorphic grade, for example greenschist or gneiss (Eskola, 1949). The core has been differentially exhumed relatively to the surrounding host rocks (Whitney et al., 2004), the latter usually having been exhumed from shallower depths (Teyssier and Whitney, 2002). Gneiss domes are commonly elliptical in map view with their long axes parallel to the axial trend of the mountain chain. Large-scale folds often characterize the internal parts of the domes and their borders are marked by important shear-zones that accommodate the exhumation of the dome itself (Eskola, 1949).

The nature of the mechanisms that formed and exhumed the gneiss domes are still extensively debated (e.g., Coney, 1980; Burg et al., 1984; Mancktelow and Pavlis, 1994) because a given dome geometry may result from different mechanisms. Gneiss domes were originally assumed to result from two orogenic events (Eskola, 1949). A first stage was inferred to produce a granitic basement while a second event was thought to metamorphose and unroof this basement (Eskola, 1949). The modalities of the second event are strongly debated and several hypotheses have been proposed in the literature to describe the dynamic and kinematic development of gneiss domes (Figure I.1). At first, the origin of gneiss domes was attributed to diapirism driven by buoyancy forces with inversion of the rock densities due to melting of the granitic basement (Eskola, 1949) that allows metamorphic rocks to rise through denser host rocks (e.g. Eskola, 1949; Berner et al., 1972; Gilbert and Merle, 1987) (Figure I.1a). More recently it was suggested that gneiss domes owe their development to exhumation of mid-crustal rocks to shallower depth resulting from tectonic denudation localized along major low-dipping extensional detachments, which remove the overlying cover (e.g. Lister et al., 1984; Coney and Harms, 1984) (Figure I.1a) or from isostatic rebound caused by the extension along large-scale detachment (Axen et a., 1995) (Figure I.1c).

Alternatively, shortening resulting in duplex structures (Figure I.1d) (Brun, 1983) and/or folding (Figure I.1e), with fold axes perpendicular to the main compression direction, was also suggested to result in the formation of gneiss domes (e.g. Ramsay, 1967; Burg et al., 2004). It was also proposed that the mechanisms of extension and shortening described above acted simultaneously to form a gneiss dome (e.g. Selverstone, 1988). However, a single explanation for all regional examples does not exist so far and the relative importance of these processes for the formation of one and the same dome, and their spatial and temporal relationships are source of large debates (Burg et al., 2004; Lee et al., 2000).

Recently, gneiss domes related to extensional unroofing have been classified into two types (Jolivet et al., 2004): those that are elongate parallel to the extensional direction (“type a”) and those that are elongate perpendicular to the extensional direction (“type b”). The “type a” domes, which are the focus of this work, generally consist of upright folds with fold axes

parallel to the extensional direction and large-scale detachments that mark one or two sides of the dome.

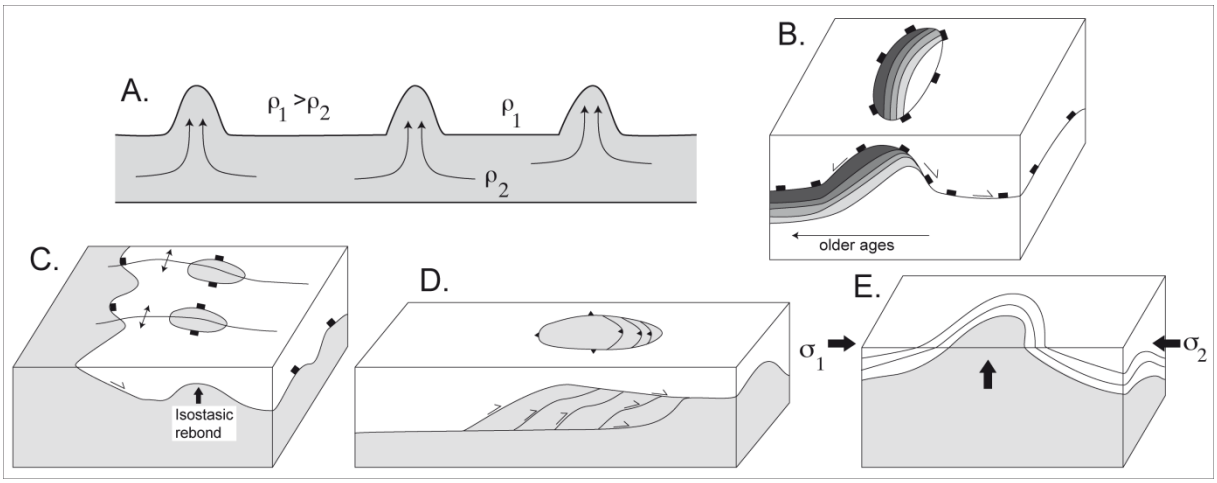

Figure I. 1. Exhumation mechanisms of gneiss domes. a. Diapirism due to buoyancy forces; b. Extension along major boundary normal faults; c. Extension-induced isostatic rebound ; d. thrust-duplex dome; e. Folding and erosion

An alpine example of these domes is the Lepontine dome (Central Alps), where low-angle detachment fault, exhumation of the Toce dome (the westernmost part of the Lepontine dome) and shortening perpendicular to the detachment occurred at the same time (Mancktelow, 1985; Merle et al., 1986; Steck and Hunziker, 1994). The dome is bordered along its western limit by the Simplon detachment, an extensional ductile shear zone of up to 2 km that was subsequently overprinted by brittle deformation (Mancktelow, 1985). The Lepontine dome is affected by upright to moderately inclined folds, which axes are parallel to the extension direction of the Simplon detachment and which are inferred to have formed simultaneously with extensional faulting (Mancktelow and Pavlis, 1994). The folds are transected by younger mylonitic foliations and low-angle detachment faults, which are themselves folded with similar fold axial planes. The interpolation of apatite and zircon fission track ages within the footwall of the fault indicates a younging of the ages toward the Simplon fault (Vernon, 2008; Campani, 2009; Rosenberg and Berger, 2009) and a clear jump across the Simplon fault. Older ages are consistently found in the hanging wall of the fault while younger ages are found in the footwall (Figure III.3 of Campani, 2009). The relationships between upright folds of the Lepontine dome and the Simplon mylonitic structures as well as the fission track data sets lead to the assumption that formation of the dome by folding occurred simultaneously with normal faulting along the Simplon fault (Mancktelow and Pavlis, 1994). The interplay between folding and faulting in the footwall reflects a component of shortening perpendicular to fold axial surfaces during extension parallel to fold axes (Mancktelow and Pavlis, 1994). The occurrence of both shortening and extension in such domes makes difficult to understand to which degree these mechanisms are responsible for the formation and exhumation of the dome.

To better understand the spatial and temporal relationships between folds and detachment faults in metamorphic core complexes, analogue models based on the natural case study of the Montagne Noire metamorphic core complex were recently performed (Malavieille, 2010). The Montagne Noire, the southernmost segment of the Massif Central, is a Variscan metamorphic core complex composed of a crystalline metamorphic core belonging to the lower plate and overlying metasediments of the upper plate (Ellenberger, 1967). The metamorphic core complex of the Montagne Noire is affected by large-scale, upright isoclinal folds (Ellenberger, 1967). Shortening and crustal thickening are responsible for the formation of the large upright antiformal structure of the axial zone while the following orogenic crustal tectonometamorphic extension developed along low-angle extensional and high-angle normal shear zones allowed for substantial differential uplift of the axial zone (Arthaud et al., 1966; Echtler and Malavieille, 1990). The late stages of crustal extension are marked by the formation of high-level, steeply dipping, brittle normal and strike-slip faults (Malavieille, 2010). Analogue models of the Montagne Noire indicate that the localisation of the deformation in the domain of underplating is the result of the combination between erosion, sedimentation and tectonics unroofing (Malavieielle, 2010). A duplex-type nappe stack described for the Montagne Noire is inferred to be the result of a first stage of rapid syn-convergence exhumation followed by a second stage of exhumation related to extension (Malavieille, 2010).

In some cases, the tectonic structures of the domes can be related to a specific formation mechanism. For instance, gneiss domes resulting from diapirism would be characterised by foliations dipping radially away from the core of the dome (Gapais et al., 1992). However, in many cases, the structures alone do not allow for an unequivocal interpretation of the formation and exhumation mechanisms, and additional sources of information are necessary to distinguish between the different mechanisms. Since the modalities of the exhumation of gneiss domes influence the evolution of the temperatures within the dome, the thermal history of a dome may help to identify a specific formation mechanism. Indeed, thermochronological data are appropriate tools to define the relative importance of folding and erosion during the exhumation of the rocks in metamorphic domes (Figure I.2).

For example, extensional domes delimited by large-scale detachment faults are expected to result in an asymmetric distribution of metamorphic isograds and cooling ages in map view, with isograds parallel to the detachment fault and cooling ages younging toward the fault (Figure I.2a; Wernicke, 1985; Foster et al., 2001; Yin, 2004; Burg et al., 2004). In contrast, in the case of upright fold-related domes, isograds are wrapped in such a way that the same temperature is found at shallower depth in the centre of the dome, resulting in a symmetrical and concentric distribution of cooling ages with younger ages centred in the middle of the dome (Figure I.2b; Burg et al., 2004). Two end-member cooling patterns are illustrated by two natural case studies (Figure I.3) that are the northern Idaho-Bitterroot metamorphic complex (Idaho, USA) (Figure I.3a and I.3b) and the Olympic Mountains dome (Washington, USA) (Figures I.3c, I.3d and I.3e) The northern Idaho-Bitterroot batholith is a

metamorphic core complex that consists of an extensional 500-1500 m thick, east-dipping shear zone that juxtaposes mid-crustal granitic and highly metamorphosed rocks of the Idaho-Biteroot batholith to shallower rocks of lower metamorphic grade of the hangingwall (Brandon et al., 1998; Figure I.3b).

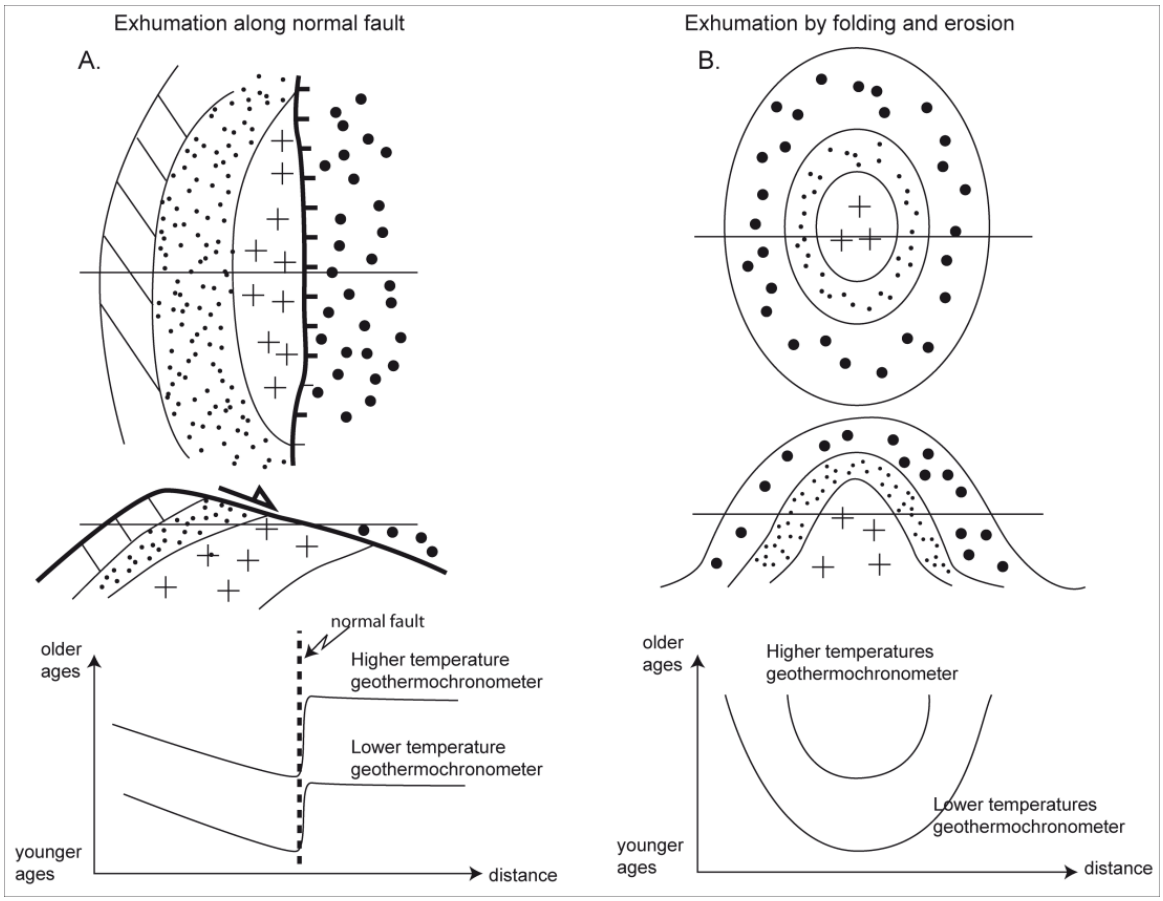

Figure I. 2. Map views, cross sections and age distributions expected in metamorphic core complexes in the case of A. Exhumation related to large-scale normal fault and B. Doming and exhumation controlled by folding and erosion

Apatite and zircon fission track ages and metamorphic grades decrease from the centre of the northern Idaho-Bitterroot metamorphic core complex toward the eastern, bordering detachment fault and isochrons are parallel to the fault trace (Figure I.3a) (Foster et al., 2001). The northern Idaho-Bitterroot batholith is thus described as a metamorphic core complex whereby high-grade metamorphic rocks have been exhumed by tectonic unroofing along the low-angle ductile to brittle detachment fault (Foster et al., 2001; Foster and John, 1999).

The Olympic Mountains expose a large dome consisting of an anticline plunging toward the East with highest topography found in the centre of the main fold (Figure I.3d). Cooling ages of the Olympic Mountains dome show a concentric pattern with youngest ages located in the areas of the highest topography (Brandon et al., 1998; Batt et al. 2001) (Figure I.3c to I.3e), which also corresponds to the core of the large anticline. The youngest ages correspond to rocks that are exhumed from the deepest levels and are located in the core of the antiform.

The cooling pattern of the Olympic Mountains dome is thus inferred to be linked to greater exhumation of the rocks in the core of the dome due to their faster exhumation rates (Brandon et al., 1998). Exhumation of the Olympic Mountains is thus inferred to have resulted from folding and erosion with fold axes perpendicular to the main compression direction (Brandon et al., 1998; Batt et al. 2001).

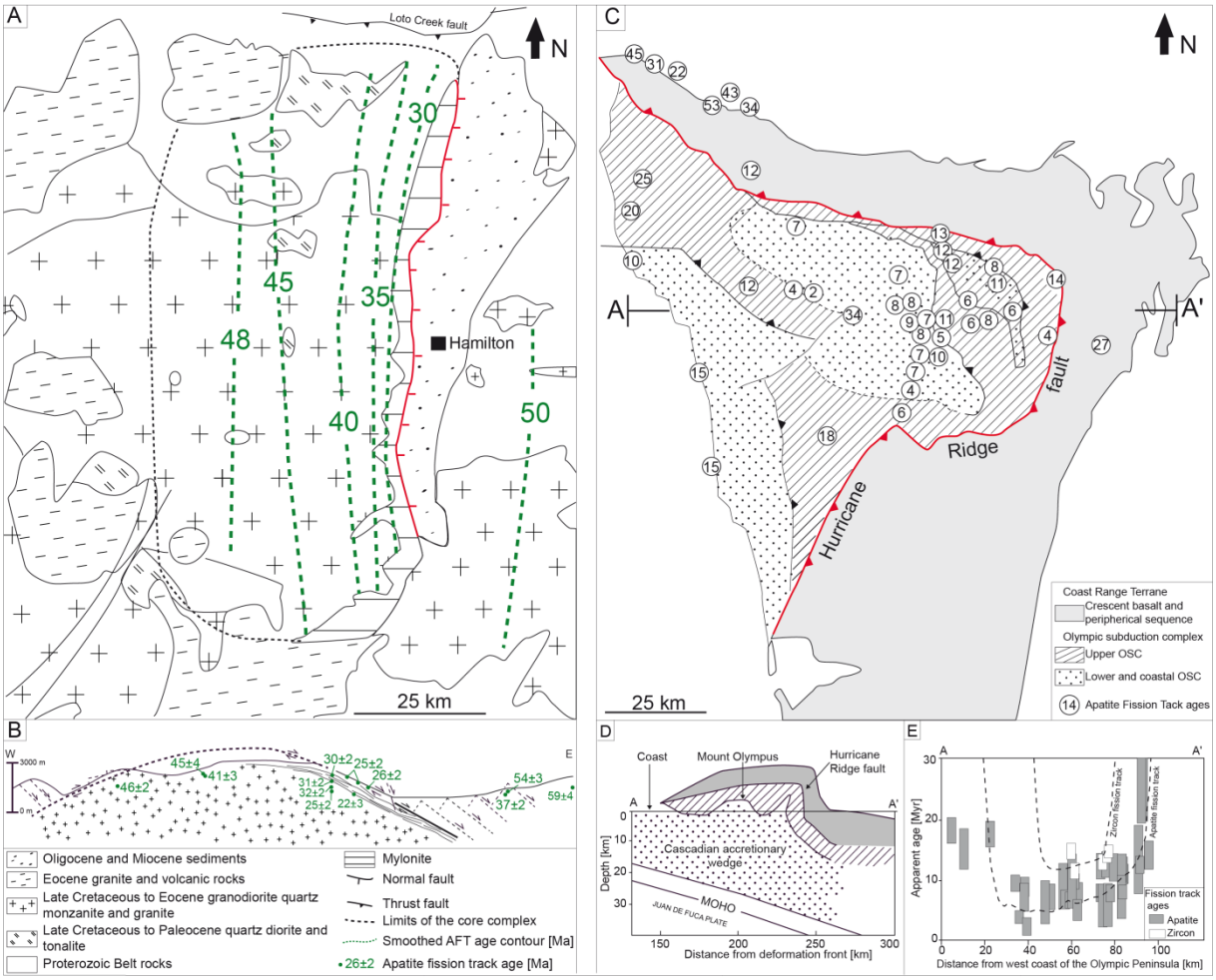

Figure I. 3. A. Apatite fission track ages of the Idaho-Bitterroot batholith (after Foster and Raza, 2002) B. Cross section of the Bitteroot fault system and apatite fission track ages (after Foster and Raza, 2002). C. Apatite fission track ages of the Olympic Mountains. D. Cross section of the Olympic Mountains and E. Apatite and zircon fission track ages along an W-E cross section through the Olympic Mountains (after Brandon et al., 1998).

The Tauern Window, in the core of the Eastern Alps is a metamorphic dome that localized the exhumation of the Eastern Alps during Tertiary times (Figure I.4) and that presents some tectonic structures similar to the one of the Olympic Mountains, i.e. antiformal folds) and some structures similar to the one of the Idaho-Bitterroot complex, i.e. bordering extensional shear zones (Figure I.5).

The prolonged, highly localised mode of exhumation (Figure I.4), in addition to the occurrence of large-scale upright folds and low-angle detachments (Figure I.5) makes the Tauern Window an ideal object for the investigation of exhumation mechanisms in a

metamorphic dome within a contemporaneously shortening orogen. Defining the relative contributions of folding and erosion and of extension and tectonic unroofing during Tertiary exhumation of the Tauern Window is a major target of the present work.

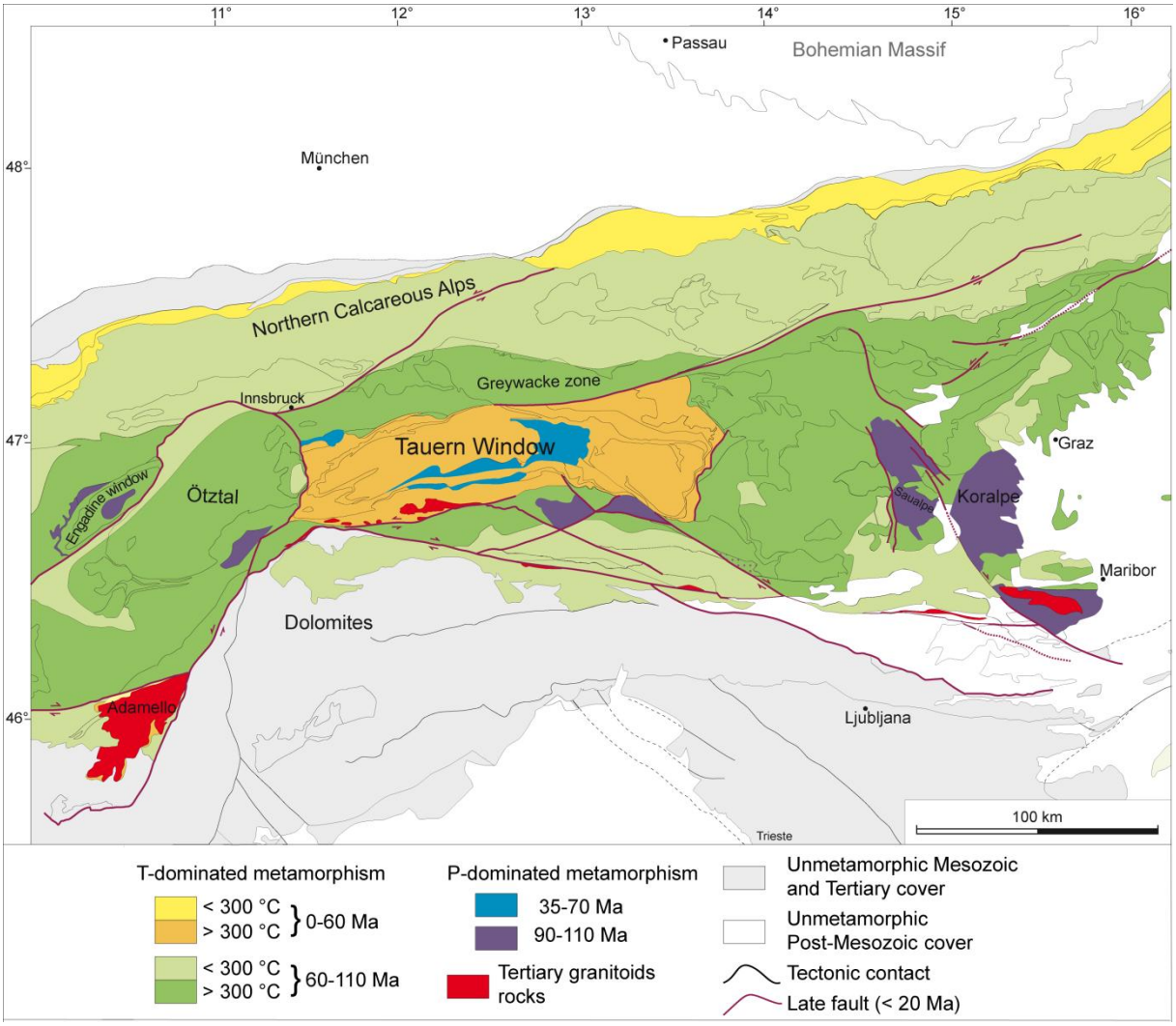

Figure I. 4. Age of T-dominated and P-dominated metamorphism in the Eastern Alps. Modified after Handy et al., 2010.

I.2. The Tauern Window in the Eastern Alps: Geological Setting

I.2.1. Overview of the Eastern Alps

The Eastern Alps are characterized by a stack of large-scale nappes (Termier, 1903) that are, from top to bottom, the Austroalpine, the Penninic and the Helvetic nappes (Figures I.5 and I.6). The tectonic units of the Eastern Alps are defined according to their paleogeographical origin, namely the Tethyan oceans and their adjacent paleo-continents. The Alpine Tethyan oceans comprised the Valais and Piemont-Liguria oceans whereas the Alpine Neo-Tethyan oceans (e.g. the Meliata and Vardar oceans) are largely restricted to the Western Carpathians and the Dinarides-Hellenides (Schmid et al., 2008; Handy et al., 2010).

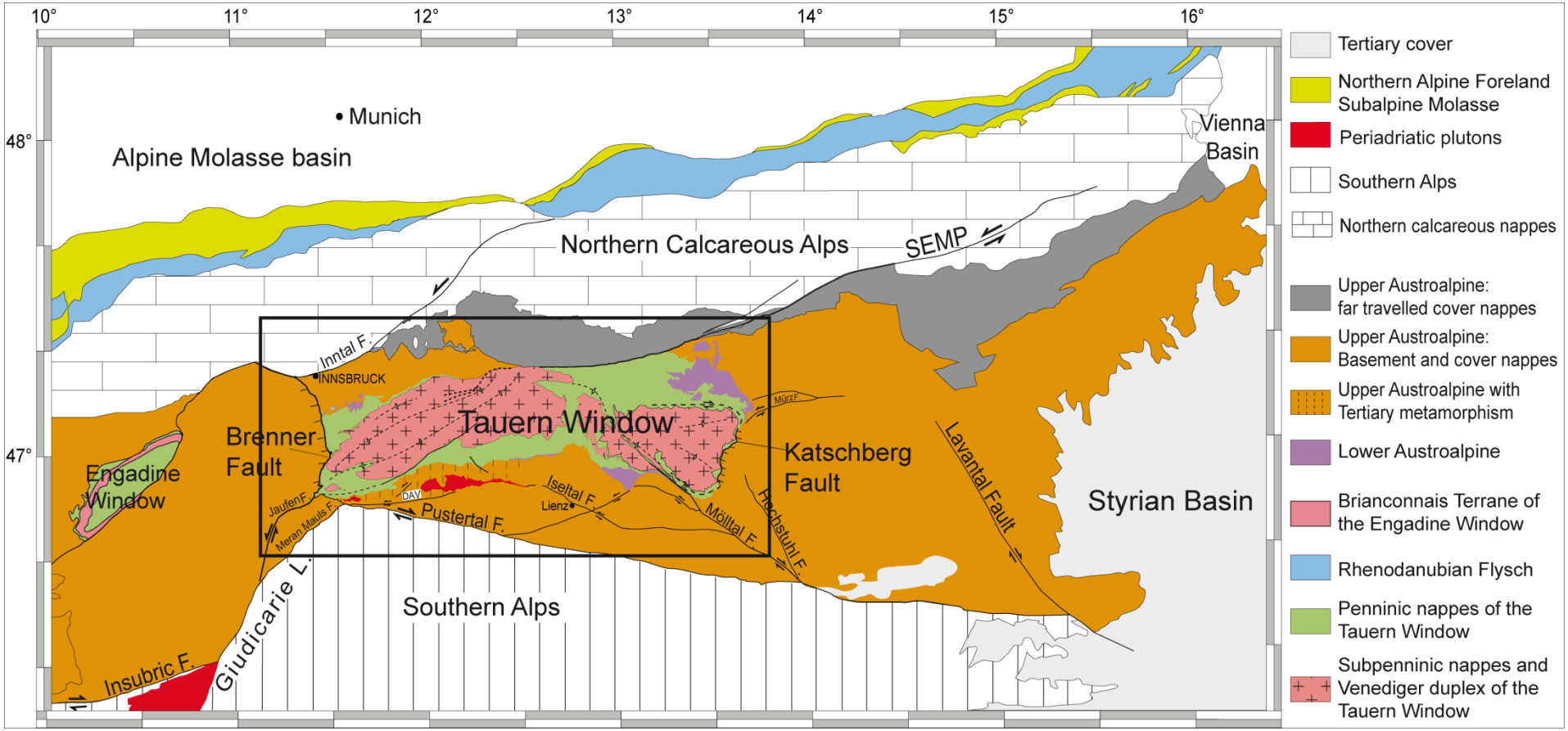

Figure I. 5. Simplified tectonic sketch map of the Eastern Alps with location of the study area (Based on the structural model of Italy map - 1.500000, Bigi et al., 1990 and on Schmid et al., 2013)

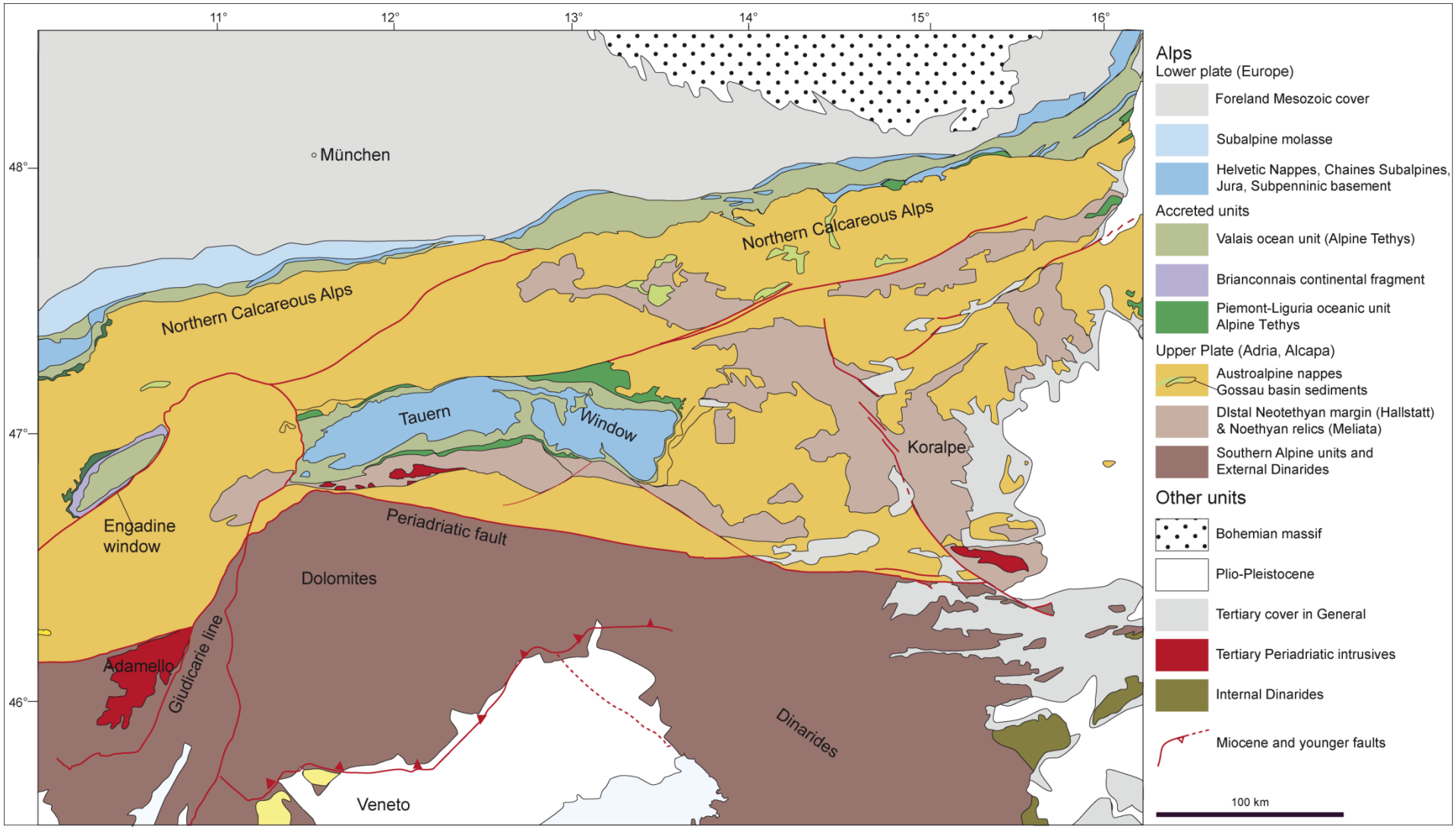

Figure I. 6. Tectonic provenance map of the Eastern Alps Modified after Handy et al., 2010).

Stacking and folding of the different units of the Eastern Alps resulted from two successive orogenies that occurred during Cretaceous and Tertiary times (Tollmann, 1963; Frisch, 1979, Frank, 1987; Behrmann, 1988; Dewey et al., 1989; Froitzheim et al., 1996). Cretaceous orogeny is characterized by the closure of Neotethys, nappe stacking within the Austroalpine nappes and accretion of parts of the Piemont-Liguria Ocean to the Austroalpine (Handy et al., 2010). Tertiary orogeny formed as a consequence of continent-continent collision (e.g., Dewey et al., 1973; Milnes, 1978) related to the closure of the two Alpine Tethyan oceans (Piemont-Liguria and Valais Oceans), which was completed by the Eocene times (Handy et al., 2010), resulting in the northward stacking and accretion of the Penninic basement and/or cover units (derived from the European distal margin, the Valais Ocean, the Briançonnais micro-continent and the Piemont-Liguria Ocean) beneath the Austroalpine (Figure I.7; Schmid et al., 1996, 2004). After Eocene collision, resulting from the collision between the Adriatic and European plates, shortening continued and led to post-nappe modifications in Oligocene to recent times, resulting in the present-day structural and topographic pattern of the Eastern Alps (Figure I.7; Schmid et al., 1996, 2004).

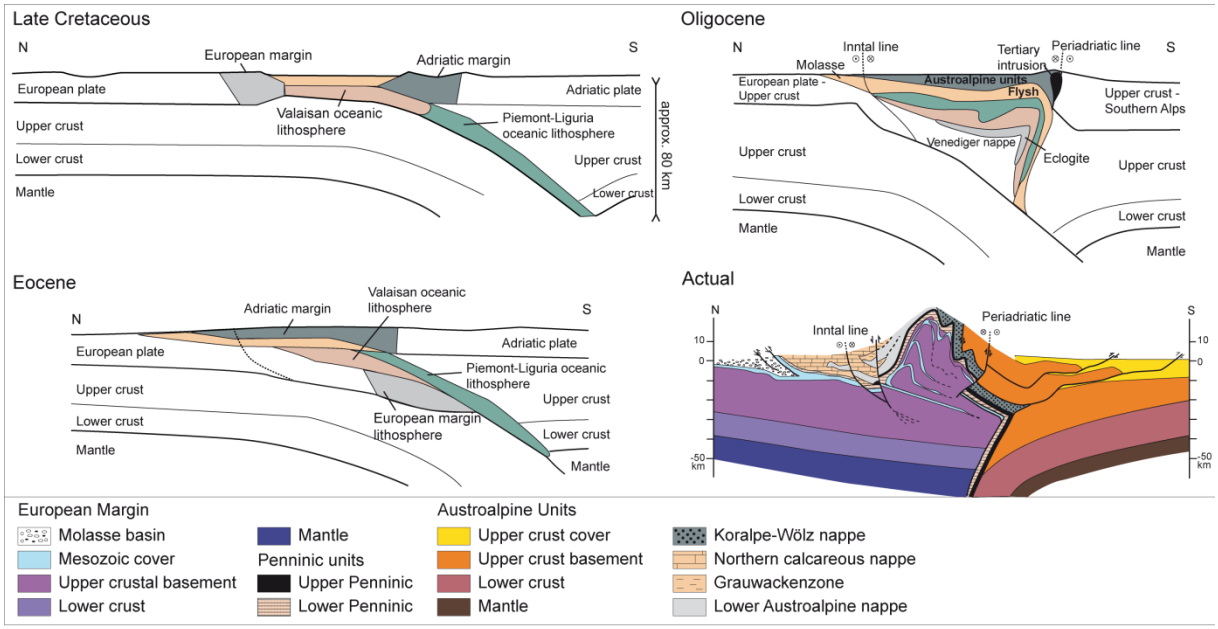

Figure I. 7. Paleogeographical evolution of the Eastern Alps (after Kurz et al. 2008; Handy et al., 2010) and present-day schematic cross-section through the Tauern Window along the Transalp transect (after Schmid et al., 2004)

The narrow Valais Ocean, i.e. the northern branch of the Alpine Tethys, was located south of the European margin and north of the Briançonnais micro-continent (Figure I.7; Schmid et al., 1996). The Valais Ocean opened in Early Cretaceous time (Frisch, 1979; Stampfli, 1993) and closed during the Middle to late Eocene (Schmid et al., 1996). The opening of the Valais Ocean resulted in the separation of the Briançonnais micro-continent from the European plate. The Piemont-Liguria Ocean, corresponding to the southern branch of the Alpine Tethys, was located between the Briançonnais ribbon and the Adriatic margin

(Schmid et al., 1996). It opened during Late Jurassic-Early Cretaceous time and closed, within the Alps, during Cretaceous-age Alpine orogeny (Handy et al., 2010).

The Austroalpine units, exposed over the major part of the Eastern Alps, consist of a crystalline basement and cover sequences derived from the distal Adriatic margin (Schmid et al., 1996). They were already exhumed in the Cretaceous and thrust over the Penninic units in Cenozoic times (Figure I.4) (Handy and Oberhänsli, 2004; Handy et al., 2010), and formed the upper Adria-derived plate during Tertiary collision and nappe stacking (Ratschbacher et al., 1989; Schmid et al., 1996; 2004).

I.2.2. The Tauern Window

Pattern and intensity of Late Miocene exhumation differ significantly along strike of the Alpine orogen. The area of enhanced exhumation characterised by Miocene fission track ages is much larger in the Central Alps than in the Eastern Alps (Bernet et al. 2001). This reflects a more localised mode of Miocene exhumation in the area of the Tauern Window, where the site of enhanced exhumation did not change from the Late Oligocene to the Late Miocene and occurred along an elongate, E-W striking zone, corresponding to the central axis of the Tauern Window (Figure I.4). It is characterised by two first order tectonic structures: (1) large-scale folds with axial plane sub-parallel to the axis of the east-alpine orogeny, which affect the entire nappe stack of Penninic and Austroalpine units (Figure I.8) (2) Two major normal fault systems, namely the Brenner and Katschberg fault systems that border the western and eastern limits of the study area, respectively (Figure I.8).

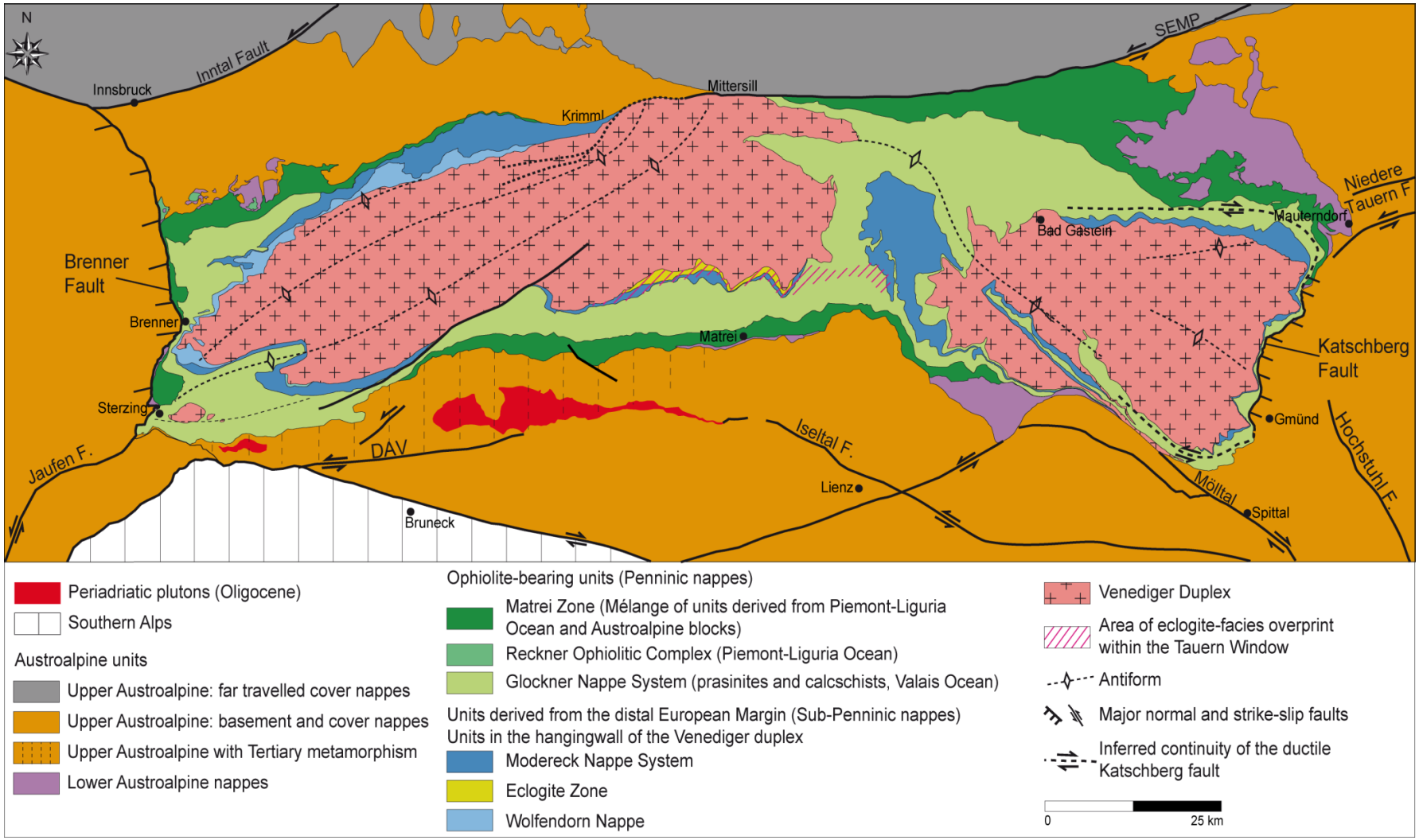

Figure I. 8. Simplified tectonic map of the Tauern Window (simplified after Schmid et al., 2013)

I.2.2.1. Tectonic setting

The Tauern Window is 170 km-long and 30 km-wide. It is located in front of the corner of the Dolomite Indenter (Figures I.5) and it represents the only area within the Eastern Alps, where the lower (European) plate of the Tertiary Alpine orogen is exposed (Figure I.6). The rest of the Eastern Alps is exclusively characterised by exposures of the Austroalpine units, which represent the upper plate during of the Tertiary Alpine orogeny, or exceptionally, within the Rechnitz Window, by the exposure of oceanic units of the Penninic realm.

The Tauern Window is composed of Sub-Penninic basement and cover units, overlain by Penninic units (Figures 8 and 9; Froitzheim et al., 1996; Schmid et al., 2013; Scharf et al., 2013). The Penninic nappes were derived from the Valais and Piemont-Liguria Oceans. The Subpenninic nappes were derived from the distal European margin (Milnes, 1974, Schmid et al. 2004) and consist of pre-Mesozoic basement and distal parts of the European upper crust (Figure I.9; Schmid et al., 2000). They include the Venediger duplex system composed of pre-Variscan and Variscan gneissic basement intruded by late to post-Variscan granitoids (Tollmann, 1975; Lammerer and Weger, 1998; Kurz et al., 1998; Schmid et al., 2013). In the southern central rim of the Tauern Window the Venediger duplex is overlain by the Eclogite zone (Figures I.8 and I.9), which is composed of Tertiary high-pressure metamorphic rocks (Zimmermann et al., 1994; Hoschek, 2001) that derived from the most distal European plate (Kurz and Neubauer, 1996; Lammerer, 1986, Kurz and Neubauer, 1996; Kurz et al., 1998; 2001). Rocks of the Modereck Nappe system consist of a series of Mesozoic metasediments and mafic rocks that underwent tertiary high-pressure metamorphism (Kurz and Neubauer, 1996).

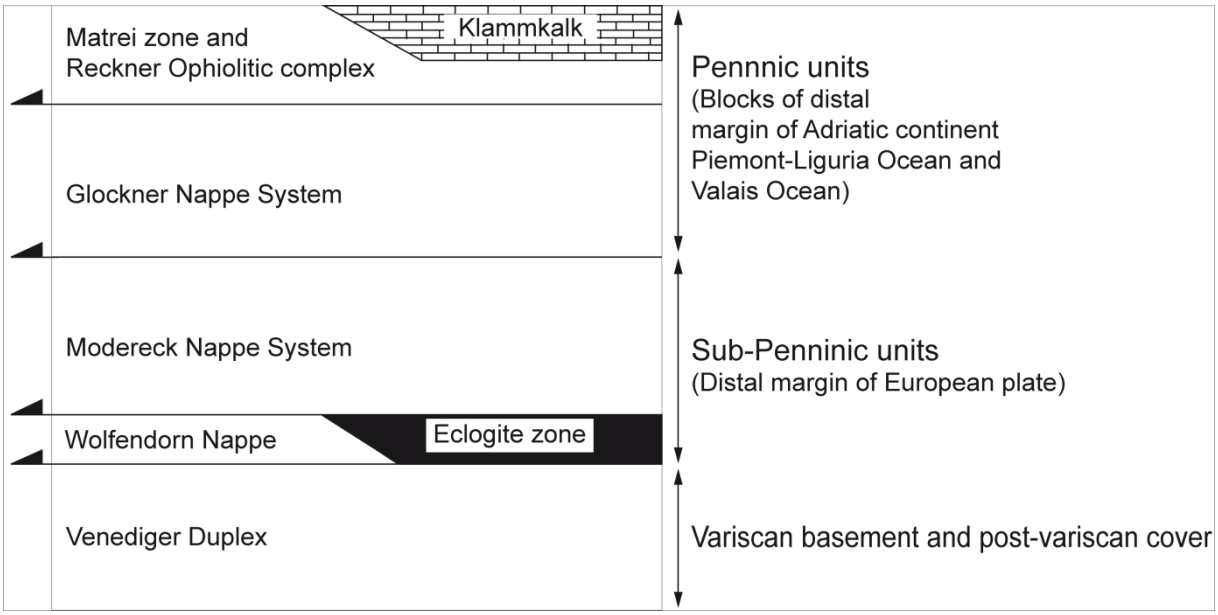

Figure I. 9. Stratigraphic column showing the nappe stack of the Tauern Window (Modified after Kurz et al., 2008)

The Glockner nappe system overrode the Modereck Nappe system (Figure I.9; Schmid et al., 2013). It is interpreted to either derive from one single Penninic Ocean (e.g. Kurz and Neubauer, 1996) or exclusively from the more northerly located Valais Ocean that opened later than the Piemont-Liguria Ocean (e.g. Schmid et al., 2004).

The topmost unit of the Tauern Window is the Matreier Zone (Figure I.9), characterised by a mélange of Mesozoic metamorphic flysch sediments and mafic rocks derived from the Piemont-Liguria Ocean and the immediately adjacent distal margin of the Adriatic continent (Schmid et al., 2004, 2013). The Middle Penninic nappes are commonly interpreted to derive from the Briançonnais micro-continent. However, no remnant of this continent is found east of the Engadine Window, whereas they are exposed over large parts of the Western and Central Alps (e.g. Froitzheim et al., 1996). As a consequence, within the Tauern Window, the Matreier Zone is in direct contact with the Glockner nappe (Figure I.8).

The different units of the Tauern Window are exposed in a series of domes formed by WSW-striking large-scale upright folds with a wavelength of up to 15 km (Figure 3 of Schmid et al., 2013) in the western part and by relatively more open upright folds striking ESE in the eastern part (see their axial traces indicated in Figure I.8). The margins of the structural Tauern Window are defined by the contact between the Austroalpine and the Penninic units (Selverstone, 1985). The Tauern Window is limited in the east and west by west-dipping and east-dipping N-S striking normal faults, termed the Brenner and the Katschberg Faults, respectively (Figure I.8).

The Brenner Fault is a low-angle, westward-dipping normal fault, whose formation and development is inferred to have played a major role during the exhumation of the Tauern Window. It is inferred to be the major structure accommodating orogen-parallel extension of the Eastern Alps (Behrmann, 1988; Selverstone 1988; Axen et al., 1995; Fügenschuh et al., 1997) but its importance, amount of offset and its southern continuation are a matter of debate.

Inferred horizontal offsets along the Brenner Normal Fault range from 5-20 km (Behrmann, 1988; Selverstone 1988; Rosenberg and Garcia, 2011; 2012) to up to 70 Km (Fügenschuh et al., 1997). According to the model of Axen et al. (1995), which states that the Brenner fault represents a rolling hinge system, the dip angle of the fault, i.e. the mean value between the dip of the foliation and the ramp dip, is estimated around 20 ° toward the West (Axen et al., 1995). Taking this dip angle, the formerly estimated displacement of ~10-20 km (Behrmann, 1988; Selverstone, 1988; Selverstone et al., 1995) along the Brenner fault would be under-estimated and the horizontal component of the Brenner fault is inferred by the authors to rather be in the order of 33-63 km (Axen et al., 1995).

Based on the vertical offset of a tectonic marker surface on both sides of the Brenner normal fault, namely the base of the Ötztal nappe in the hanging wall of the fault, and the base of the Patscherkofel unit in the footwall, Rosenberg and Garcia (2011) calculate an horizontal offset ranging from 2 to 14 km and propose that the major part of the exhumation of the western sub-dome of the Tauern Window was achieved by folding and erosion.

Using the difference in the temperature of metamorphism as offset markers between hangingwall and footwall, Fügenschuh et al. (1997) propose a horizontal displacement of 70 km. These 70 km of displacement are inferred to be the result of a two-stage deformation along the Brenner fault. A first stage involves ductile shearing that was contemporaneous with folding and erosion in the footwall while the second stage only involves a brittle extensional component. During the first stage the combined effects of faulting and folding would be the result of the contemporaneous activity of E-W extension and N-S Alpine convergence. The second brittle stage of the Brenner Fault activity would lead to a horizontal extensional displacement in the order of 4–5 km (Fügenschuh et al., 1997).

According to some authors, the Brenner fault is inferred to continue into the 500 m thick and 16 km long sinistral ductile shear zone of the Passeier-Jaufen Fault (Selverstone, 1988; Viola et al., 2001) with S-side up kinematics (Viola et al., 2001). Other authors proposed that the ductile component of the Brenner fault at least partly continues into the dextral strike-slip Pustertal Fault, a segment of the Periadriatic Line (Fügenschuh et al., 1997, 2012), whereas the brittle component would join the Jaufen Fault. The eastern border of the Tauern Window is defined by the low-angle (25-30°), SE-dipping Katschberg normal fault (Genser & Neubauer 1989) consisting of a 1 to 2 km thick mylonitic belt capped by a narrow cataclastic zone (Scharf et al., 2013). The northern continuation of the Katschberg fault consists of an E-W striking, dextral strike-slip fault (Scharf et al., 2013; Schmid et al., 2013) (Figure I.8). At its southern termination, the Katschberg fault transforms into a sub-vertical sinistral zone (Scharf, 2013; Schmid et al., 2013) (Figure I.8). The horizontal offset of the Katschberg has been estimated to at least 17.3 km (Genser and Neubauer, 1989) or to 26 km assuming an angle of 25-30° (Scharf et al., 2013).

To the north, the Tauern Window is partly limited by the E-W trending sinistral strike-slip SEMP fault (Salzach-Ennstal–Mariazell–Puchberg) (Decker and Peresson, 1996) (Figure I.8), whose lateral offset is estimated to up to 60-70 km (Linzer et al., 1997). The sinistral strike-slip movements along the SEMP are dated at ca 17 Ma based on deformed conglomerates of Carpathian ages (Steininger et al., 1989) that accommodated extension after the peak of metamorphism. These deformations are inferred to be related to the eastward extrusion of the Eastern Alps (Ratschbacher et al., 1991a and 1991b; Wang and Neubauer, 1998; Peresson and Decker, 1997; Scharf et al., 2013). At its western termination the SEMP bends into the interior of the Tauern Window, into the Ahorn shear zone (Rosenberg and Schneider, 2008) (Figure I.8), which marks the south-western limit of the Tauern Window.

The southern limit of the thermal dome is marked by the DAV fault (Defereggen-Antholz-Vals) (Figure I.8). The DAV was first defined on the base of cooling ages (Borsi et al., 1973) as a structure that delimits rocks that underwent Tertiary metamorphism from rocks that were already exhumed in Cretaceous times. The DAV was active during Oligo-Miocene times (Borsi et al., 1973) and, based on field observations of mylonitic zones and cataclasites along the fault, its sinistral lateral displacement is inferred to be in the order of 30 km (Kleinschrodt, 1987; Schulz 1989). Most of the displacement occurred during a brittle stage of

deformation as indicated by steeply dipping slickensides (Kleinschrodt, 1987; Schulz 1989). Further south, the Austro-alpine units are separated from the Southern Alps by the E-W striking dextral Pustertal fault (Figure I.8), which is part of the Periadriatic Fault System (Castellarin, 1992). The eastern part of the Periadriatic Fault System (Pustertal and Gailtal lines) is one of the largest tectonic structures of the Eastern Alps (700 km long) and based on K-Ar ages its activity ranges from 13 to 16 Ma (Zwingmann and Mancktelow, 2004).

I.2.2.2. Metamorphic conditions

Northward thrusting due to convergence between the Adriatic and European plates resulted in crustal thickening during the Cretaceous and Paleogene times (Dewey et al., 1973; Oxburgh and Turcotte, 1974; Behrmann, 1988). The high pressure rocks found in the Eclogite Zone indicate that crustal rocks were deeply buried before their exhumation (Selverstone, 1985; Behrmann, 1988) and metamorphic grade within the Tauern Window ranges from eclogitic, to greenschists facies conditions (Oberhänsli et al., 2004; Bousquet et al., 2008). In the following we describe the pressures and temperatures undergone by the rocks of the Tauern Window as well as the timing of the metamorphic peaks during Tertiary times (Figure I.10). The age determinations of the different metamorphic events were however performed on samples originating from different parts of the Window, whose cooling did not take place everywhere at the same time.

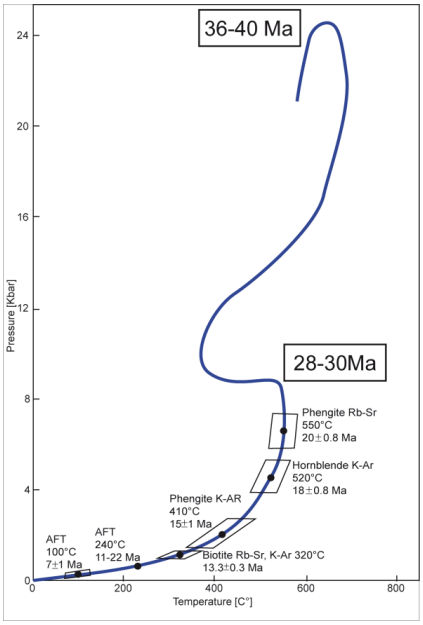

Figure I. 10. Pressure-temperature-time path of Penninic units of the Tauern window (modified after Kurz et al., 1998 and Von Blanckenburg et al., 1989).

The Penninic units of the Tauern Window experienced at least two tectono-metamorphic phases (Figure I.10) (Von Blanckenburg et al., 1989; Kurz et al., 1998). The first one, which only affected the Matreier zone and the overlying Austroalpine is of Cretaceous time and is linked to the initial stage of subduction of the Piemont-Liguria Ocean that followed the

closure of the Meliata Ocean (Schmid et al., 2004, 2013; Handy et al., 2010). The second one, of Tertiary age, led to the collision between Europe and Adria and registered low-grade metamorphism up to amphibolite facies grade. The temperature maximum during this second stage was attained around 30 Ma (Von Blanckenburg et al., 1989; Christensen et al., 1994; Inger and Cliff, 1994).

The Penninic units of the Tauern Window underwent amphibolite-facies metamorphism in the central part of the area and greenschist-facies metamorphism along its margins. The peak of high-pressure metamorphism (25 Kbar, 630 °C) (Hoschek, 2007; Glodny et al., 2008) is inferred to have occurred at around 38-40 Ma or earlier (Kurz et al., 2008; Raith et al., 1978) (Figure I.10). Based on a compilation of geochronological data sets, the peak of high-temperature metamorphism was most likely attained between 32-28 Ma in the highest structural levels (e.g., Selverstone et al., 1992, Reddy et al., 1993; Inger and Cliff, 1994; Glodny et al., 2005, 2008; Nagel et al., 2013) and 25-21.9 Ma in the deeper structural levels (Cliff et al., 1985; Von Blanckenburg, et al., 1989).

The rocks of the Modereck nappe system and of the Venediger duplex were buried to depths of 35-40 km, then heated to 550 °C ± 25 °C at P>10 Kbar (Axen et al., 1995; Zimmermann et al., 1994). The rocks of the Glockner nappe system were buried to lower depths when compared to the Modereck nappe system, since only parts of the Glockner nappe attained, at 32 ± 18 Ma, depths of 25 km yielding temperatures of 475 °C ± 25 °C and pressure of 5.5-7.5 Kbar (Selverstone et al., 1984; Selverstone, 1988; Cliff et al. 1985).

The peak of high-pressure metamorphism was followed by cooling and exhumation from Early Oligocene to Late Miocene time (e.g., Grundmann and Morteani, 1985; Von Blanckenburg et al., 1989).

After the thermal peak, in the western Tauern Window, rocks cooled below temperatures of 500-550 °C around 18-22 Ma and below 320 °C ± 25 °C around 18-13 Ma (Von Blanckenburg et al., 1989; Villa and Von Blanckenburg, 1992). Decompression from 7 to 2.5 Kbar occurred along an isothermal path and the rocks remained at temperatures of 350-400 °C until they reached 5 km depth (Selverstone, 1988). Both the Glockner and Modereck nappe systems cooled below 300 °C (based on biotite Rb/Sr and K/Ar) around 12-19 Ma within the western part of the Tauern Window (Franck et al., 1987; Selverstone, 1988). Based on apatite fission track ages, rocks of the Venediger duplex are assumed to have cooled below 110 °C between 4.6 and 14.4 Ma for the western sub-dome and 3.2 and 23.4 Ma for the eastern sub-dome (Grundmann and Morteani, 1985; Staufenberg, 1987; Fügenschuh et al., 1997; Most, 2003; Foeken et al., 2007; this study).

Biotite Rb/Sr and K/Ar ages range from 87 to 79 Ma (Miller et al., 1967; Satir, 1976; Franck et al., 1987) in the Austroalpine units of the hanging wall of the Brenner fault and from 19 to 12 Ma within the western part of the Tauern Window (Satir, 1976; Sassi et al., 1985). These data show that a major geochronological discontinuity separates the Austroalpine from the Penninic units across the western border of the window. The thermal metamorphic peak of the Austroalpine units of the hanging wall of the Brenner fault occurred

in Cretaceous times as cooling ages from Rb/Sr and K/Ar give 87 and 79 Ma (Miller et al., 1967; Thöni, 1981; Frank et al., 1987). The Austroalpine units cooled beneath 300°C before Tertiary times. This results in a marked contrast in the Tertiary metamorphic grade between Penninic units exposed within the Tauern Window and surrounding Austroalpine units. However, the Austroalpine units in the area located between the south-western part of the Tauern Window and the DAV fault also show Tertiary cooling ages (Borsi et al., 1973; 1978). Therefore the thermal Tauern Window also comprises this part of the Austroalpine units overprinted by Tertiary metamorphism.

I.2.2.3. Overview of previous studies and on-going controversies on the formation and exhumation mechanisms of the Tauern Window.

The location of the Tauern Window in front of the tip of the Adriatic indenter (Figure I.8) as well as the presence of large-scale upright folds and of major bordering normal faults lead to an ongoing debate concerning the relative contribution of folding and erosion and extension mechanisms to the exhumation of the Tauern Window during south-Alpine indentation (Figure I.11). Two coeval processes were suggested: folding associated with erosion of the hinge region of large-scale upright antiforms and extensional unroofing along the Brenner and Katschberg normal faults (Figure I.8). Exhumation models for the Tauern Window may be separated into two groups.

Since the relative contributions of the two faults to the exhumation of the Tauern Window are well debated, deformations along the Brenner and Katschberg normal faults are, in the following, described in detail. In the vicinity of the Brenner fault, mylonitic foliations are present in the Glockner and the Modereck nappe systems as well as in the upper part of the Venediger duplex (Axen et al., 1995). The mylonitic foliation is folded around WSW-plunging anticline and syncline folds. Stretching lineations giving an extension direction of N260 ° (Axen et al., 1995), kinematic indicators, and cooling ages show that structurally higher units moved WSW relative to structurally lower units during unroofing of Late Oligocene age (Selverstone, 1988; Axen et al., 1995). However, based on apatite and zircon fission track ages, unroofing along the Brenner normal fault is set to be of Miocene age (Fügenschuh et al., 1997). Within a few kilometres of the Brenner fault, the steep foliation on the fold limbs is overprinted by a gently west dipping mylonitic foliation that is folded with axial plane oriented WSW and bears top-to-the WSW shear sense (Axen et al., 1995). One group of interpretations suggests that the Tauern dome results primarily by folding and erosion with subordinate extension (Figure I.11a and I.11b; Laubscher, 1988; Lammerer, 1988; Behrman, 1988; Glodny et al., 2005; Rosenberg et al., 2004; 2007; Rosenberg and Garcia, 2011, 2012). Analogue models that test the impact of a NNE-ward movement of an indenter on the pattern of the deformations result in the formation of folds and faults with a geometry analogous to the presently observed large-scale tectonic structures of the Tauern Window (Figure I.11b; Rosenberg et al., 2004). For instance, upright WSW-ENE trending folds developed in the west and ESE-WNW trending ones in the east, in addition to E-W

extension in the area in front of the indenter tip that is the equivalent to the Brenner fault (Figure I.11b; Rosenberg et al., 2004).

Another group of investigations suggests that extension (Figure I.11c; Frisch et al., 1998; 2000) is the dominating process shaping and exhuming the Tauern Dome during Tertiary times and occurred in a regional N-S shortening setting (Figures I.11d, I.11e and I.11f; Axen et al., 1995; Neubauer et al., 1999; Fügenschuh, et al., 1997; Kuhlemann et al., 2001; Linzer et al., 2002; Genser and Neubauer, 1989; Wang and Neubauer, 1998). In these models, the exhumation of the Tauern Window is inferred to occur in a context of lateral extrusion resulting from the combination between extensional collapse of thickened crust and lateral escape of material towards the east during Early and Middle Miocene (Figure I.11d; Ratschbacher et al., 1991a and 1991b). The main driving forces inferred for these models would be a N-directed movement of the Adriatic indenter into an easterly unconfined orogen (Figure I.11d; Ratschbacher et al., 1991a and 1991b). In this context, extension of the upper crust would be accommodated, within the Tauern Window, by normal faulting along two major normal fault systems, i.e. the Brenner and the Katschberg faults. (Figures I.11c, I.11g and I.11h; e.g. Axen et al., 1995; Neubauer et al., 1999; Frisch et al., 1998; 2000; Kuhlemann et al., 2001; Linzer et al., 2002. Selverstone, 1988, Behrmann, 1988; Genser and Neubauer, 1989; Wang and Neubauer, 1998).

Based on apatite and zircon fission track data sets at the western limit of the Tauern Window, Fügenschuh, et al., 1997 propose a two-stage of deformation. In this model, it is proposed that the first stage includes both E-W extension along the Brenner fault and folding and erosion of the hanging wall of the fault, the later corresponding to the western sub-dome of the Tauern Window (Figure I.11e). The second stage involves a brittle purely extensional component along the Brenner fault whereby the Innsbrucker Quartzphyllite was transferred into the footwall of the Brenner normal fault (Figure I.11e; Fügenschuh, et al., 1997;).

Brittle-ductile structures showing west-dipping normal sense of shear are common features in the vicinity of the Brenner fault (Axen et al., 1995) and fluid inclusions indicate that they formed at depth of 12-23 km and at temperatures higher than 400 °C (Selverstone et al., 1995). West-down structures were formed at higher temperatures and depths than east-down structures, on which fluid inclusions give temperatures of only 250-400 °C and depths of 2-10 km (Selverstone et al., 1995). These datasets highlight a pressure span between the formation of the west-down structures and the formation of the east-down structures. Brittle structures (fractures, microfaults, veins, en-echelon fractures and kink bands) generally striking between N335 ° and N30 ° and dipping more than 50 ° toward the west (Axen et al., 1995) predominate and the east-down structures have mainly normal sense of shear, whereas west-down structures are equally normal or inverse structures (Axen et al., 1995). A model of rolling hinge is introduced by Axen et al. (1995) to explain the occurrence of the east-down and west-down structures (Figure I.11g). In a rolling hinge model, the movement along the normal fault would induce an isostatic answer of the upper crust, involving a rotation of the structures that is migrating towards the footwall as it is progressively unroofed (Figure I.11g;

Axen et al., 1995). The first normal fault, which is formed, is thus flattened and the formation of another steep normal fault occurred involving a higher amount of horizontal extension than along a normal fault without rolling hinges (Axen et al., 1995; Wawrzyniec et al., 2001).

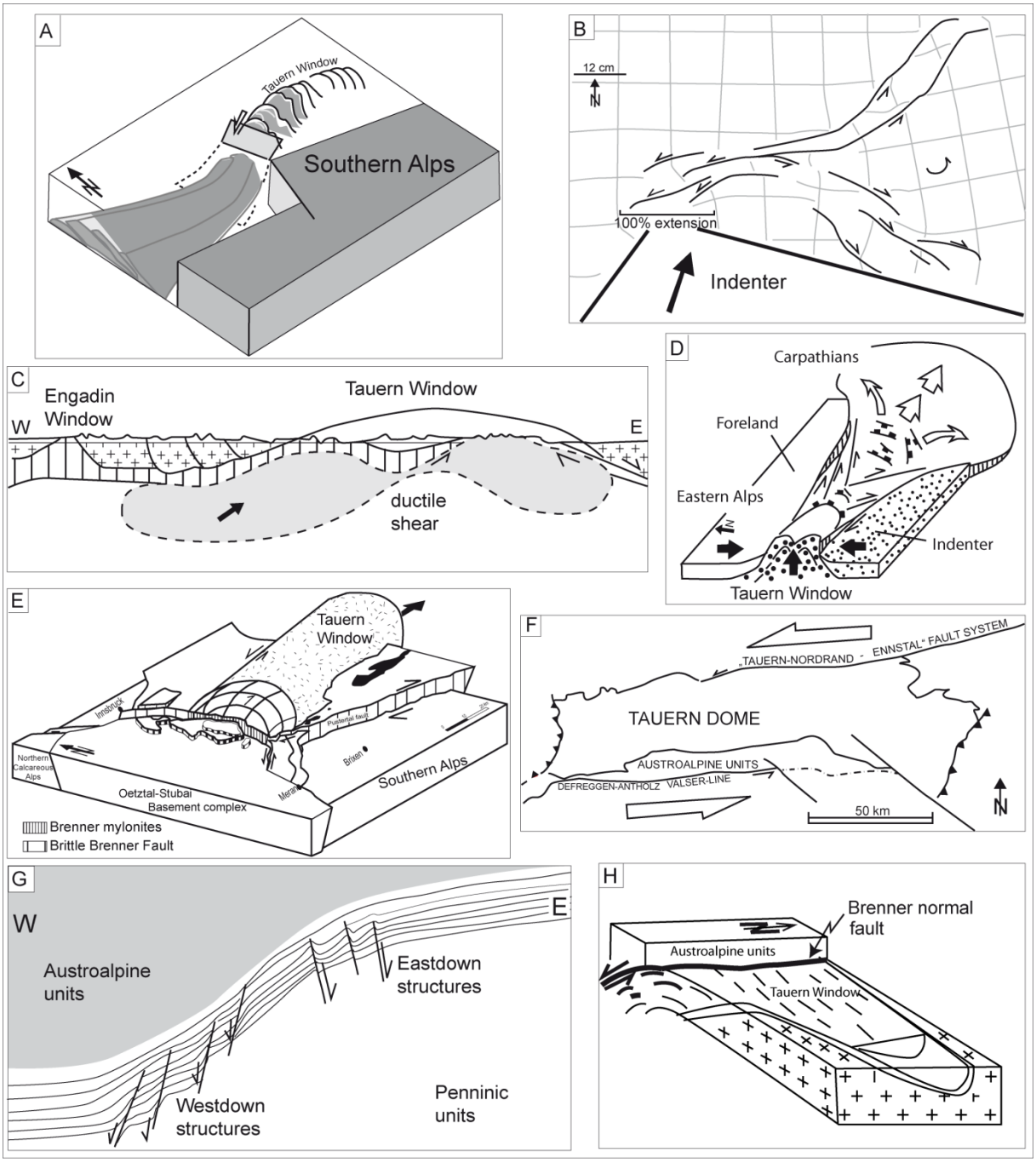

Figure I. 11. A. Differential shortening and exhumation due to shortening in front of the Dolomites indenter (Rosenberg and Garcia, 2011). B. Folding and erosion due to NNE-ward movement of the indenter (Rosenberg et al., 2004) C. Pure orogen-parallel extension (after Frisch et al., 2000) D. Large-scale lateral tectonic extrusion during alpine convergence (Ratschbacher et al., 1991) E. Extensional unroofing along the Brenner normal fault (Fügenschuh et al., 1997) F. Pull-apart comprised between sinistral faults parallel to the orogen (Genser and Neubauer, 1989) G. Rolling hinge model of the Brenner normal fault, (Axen et al. 1995) H. Isostatic uplift by E-W extension and tectonic denudation taking place along the Brenner normal fault system (Selverstone, 1988)

In general, if the footwall of an extensional fault is affected by folds with axial plane parallel to the extensional fault itself, the folds are assumed to result from isostatic uplift (Spencer, 1984) due to crustal thinning (Figure I.1h). In contrast, folds whose axial planes are perpendicular to the extensional fault, as observed in several core complexes (Mancktelow and Pavlis, 1994) are inferred to be related to shortening contemporaneous to extension.

In the Tauern Window, both types of folds are present. The first type would be linked to regional shortening with axial plane parallel to the extension direction (Figure I.11a; Rosenberg and Garcia, 2011, 2012) while a second type with axial plane perpendicular to the extension direction would result from isostatic rebound caused by the extension along large-scale detachment (Figure I.11h; Axen et a., 1995; Selverstone, 1988). Relationships between mylonitic foliation, folds and brittle structures along the Brenner fault thus indicate that E-W extension occurred simultaneously (Lammerer, 1988; Ratschbacher et al., 1991a, 1991b; Axen et al., 1995) with N-S shortening of the Tauern Window (Selverstone., 1988).

Alternative models propose that the exhumation of the Tauern Widow was driven by major extension along the Brenner and Katschberg normal faults accommodated by sinistral movements along the SEMP, north of the Tauern Window, and along the DAV, south of the area (Genser and Neubauer, 1989). The exhumation of the Tauern Window is thereby interpreted as a pull-apart, caused by ESE-WNW trending crustal stretching (Figure I.11f; Genser and Neubauer, 1989). In this model, space would be created between the SEMP and the DAV faults and uplift of the Penninic units would occur as an isostatic answer to the crustal thinning (Genser and Neubauer, 1989).

I.3. Goals of the study

The main goal of this study is to understand the mechanisms leading to a focused exhumation in the axial zone of the Eastern Alps, over a prolonged time interval, i.e. from the Late Oligocene to the present. We discuss the different processes of exhumation of the Tauern Window and their spatial and temporal relationships, focusing on the relative contribution of upright folding and erosion and E-W extension during the exhumation history of the Tauern Window. In order to do so, we assess the relationship between cooling pattern and cooling history of the Tauern dome and its major tectonic structures, as the large-scale upright folds and the two major detachment faults forming the eastern and western margins of the window (Figure I.8).

Many other eastern Alpine regions were probably affected by Late Miocene tectonic activity. However, excepted for rare and small areas where mid-Miocene sediments were deposited and deformed (e.g. Peresson and Decker, 1997) a distinction between Late Tertiary or Late Cretaceous to Early Tertiary tectonics is difficult outside of the Tauern Window, due to the overall late Cretaceous cooling of the Eastern Alps below the 300° C isotherm (Figure I.4; Handy and Oberhänsli, 2004). In the western Tauern Window, the age pattern indicated by apatite fission track shows an elongate structure, parallel to the major folds, with younger ages along the trace of the fold axial plane (Rosenberg and Berger, 2009). As stated in part

I.1, cooling age patterns can be related to two major process that are orogen parallel extension and shortening parallel to the Alpine convergence direction. Both mechanisms are assumed to be related to the northward movement of the Adriatic indenter (Wang and Neubauer, 1998). New apatite and zircon fission track ages are provided in this study in order, firstly to complete the existing data set, which do not cover the entire Tauern Window, especially for the zircon fission track dataset, secondly to constrain the cooling patterns provided by apatite and zircon fission track ages and thirdly to better define the spatial relationship between tectonic structures and cooling patterns. The fission track data are used to assess whether the "isochrones" mimic the contour lines of the major upright folds or of the major detachment. It is a major goal of this proposal to test the two possibilities.

The Tauern Window is the only area of the Eastern Alps exposing rocks, which cooled down below 300°C (Figure I.4; Handy and Oberhänsli, 2004) during Miocene times resulting from a late doming of a gently-dipping nappes stack (Schmid et al, 2013). Therefore, the Tauern Window is the only eastern Alpine area, in which the maximum age of Middle- to Late Miocene brittle structures can be, as first approximation, directly constrained by zircon fission track ages. The distribution of fault planes and their kinematic analysis was used to test whether the major fault patterns can be related to large-scale, distributed folding, or rather by localised large-scale detachment faulting. The description and kinematic interpretation of these brittle structures and their associated paleostress fields allow us to constrain the kinematics that affected the upper part of the crust during exhumation of the core of the Eastern Alps during the Mid- to Late Miocene.

The results of this combined thermo-chronological and structural study will allow us to, at least partly, bridge the gap between the well-known Early Miocene tectonics (Behrmann, 1988; Behrmann and Frisch, 1990; Selverstone, 1988; Neubauer et al., 1999; Ratschbacher et al., 1989; 1991a; 1991b; Linzer et al., 2002; Frisch et al., 1998; 2000; Peresson and Decker, 1997), and the present-day tectonic activity based on the interpretation of GPS and seismic data (Reinecker and Lehnhardt, 1999; Selverstone, 2005; D'Agostino et al., 2005; Reiter et al., 2005). This will show whether the long-term stress field in the axial zone of the Alpine orogen remained constant throughout the Miocene or whether significant changes took place.

In order to better interpret the age distribution of fission track thermochronometers in map view, the behaviour of isotherms during exhumation of rocks is assessed by folding a series of 2-D thermal models that mimics a large, upright antiform. In the models, the elements in the centre of the models are coming from deeper levels than the elements located at the borders of the models. The models illustrate the evolution of the temperature in a 50 km deep crustal section during the formation of the dome. The effects of uplift rates and of inherited temperature anomalies from the subduction event on the geothermal gradients and on the age distribution of fission tracks are investigated. The results of these 2D thermal models are then compared to the cooling pattern obtained from the apatite and zircon fission track datasets.

I.4. Methods

I.4.1 Apatite and zircon fission track dating

The low-temperature thermal history of the Tauern Window is determined using the apatite ($Ca_5(PO_4)_3(OH,Cl,F)$) and zircon ($ZrSiO_4$) fission track dating method. Fission tracks are radiation damage trails (Figure I.12) in uranium-bearing crystals produced by the spontaneous fission radioactive decay of the Uranium ^{238}U ($4.5x10^9$ half-life). The fission of ^{238}U expulses atoms at high velocity and high energy and creates a damage trail in the crystal.

The two particles produced by the fission of ^{238}U are expulsed in opposite directions leading to the creation, in the crystal lattice, of a straight track of approximately 10 to 20 µm length (Figure I.12) and 0,008 µm of diameter (Donelick et al., 1990; Paul and Fitzgerald, 1992; Dumitru, 2000). At high temperatures, modifications of the crystal lattice by diffusion mechanism may involve shortening and/or annealing of the fission track damages (Ravenhurst and Donelick, 1992), resulting in the decrease of the quantity of fission tracks in the crystal (Ravenhurst and Donelick, 1992).

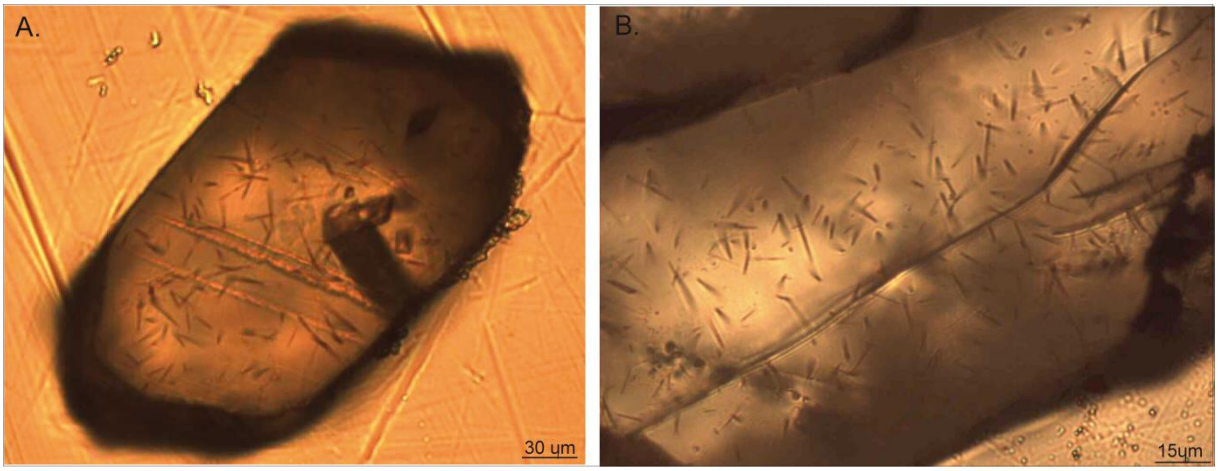

Figure I. 12. A- Polished and etched zircon crystal with fission track damage trails. B- Fission track damage trails in zircon crystal.

Fission tracks anneal completely at geological timescales at temperatures greater than the estimated "closure temperatures", which correspond to 110 ± 20 °C for apatite (Dodson, 1979; Naeser, 1981; Parrish, 1983; Green et al., 1989; Corrigan, 1991; Reiners and Brandon, 2006) and 240 ± 20 °C for zircon (Reiners and Brandon, 2006). When the temperature of the crystal falls below the closure temperature, damage fission tracks are preserved. The ratio and the length of fission tracks are thus proportional to the time spent by the crystal under the closure temperature. Longer time after the mineral cooled beneath its closure temperature, corresponds to higher density of tracks recorded in the crystal. Therefore, the density of fission tracks in a crystal gives, indirectly, the age, at which the rocks passed through their corresponding closure temperatures. As the density of fission tracks in the crystal is related to

the amount of uranium the crystal contains, knowledge of the uranium content is necessary in the determination of the cooling ages.

Fission track ages do not represent a specific closure temperature but rather a range of temperatures. Fission tracks can be shortened and partially erased (annealed) if the sample spent long time in the Partial annealing zone (PAZ) (Wagner, 1979), defined by a temperature range in which early formed tracks can (partially) anneal and the track lengths can be reduced. The temperatures of the zircon partial annealing zone (ZPAZ) range from 180 to 300°C (Hurford and Green 1983; Zaun and Wagner 1985) and the temperatures of apatite partial annealing zone (APAZ) range from 60 to120°C (Green et al. 1986; Gallagher et al. 1998).

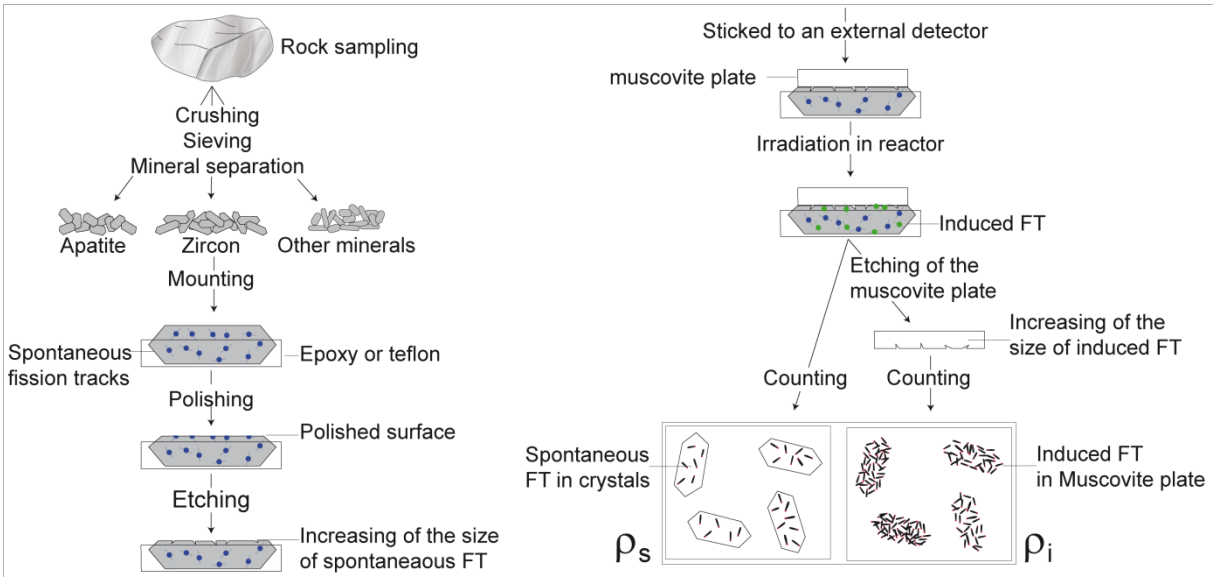

Figure I. 13. Successive steps of the preparation of apatite and zircon fission crystals for the external detector method of fission track analysis (modified after Naeser, 1979).

Great care is taken during sampling in order to collect rocks that were not affected by significant fluid circulations or alteration. The samples are crushed and sieved to separate the different grains sizes. A magnetic separator is used to separate the non-magnetic (including apatite and zircon) from the magnetic minerals (Figure I.13). In a third step, minerals are separated from lighter minerals using the heavy liquid Bromoform ($CHBr_3$; ρ= 2.9), as the density of the apatite and the zircon minerals are of 3.2 and 4.7, respectively. Apatite and zircon are finally split using Diiodomethane heavy liquid (I_2CH_4; ρ=3.3). The best quality crystals are finally chosen by handpicking under a binocular microscope. Crystals must present a section, which is large enough to count the maximum of fission tracks, and which contains enough fission tracks in order to get a reliable thermo-chronological result (Figure I.13). In order to obtain a clear polished internal surface of the minerals, the selected apatite and zircon crystals are mounted, in Epoxy resin and in Teflon® and then ground down using wet polished 1200 µm and 1000 µm grit carbide papers and then polished using a series of 9 µm, 6 µm and 3 µm diamond slurries on cloth (Figure I.13).

In order to increase the size of the tracks and to reveal horizontal confined tracks, apatite and zircon crystals are chemically etched, respectively, in chloridric acid (HNO_3) during 40 seconds at ambient temperature and in a NaOH-KOH eutectic melt for several hours at a temperature of 235 °C (Fleischer and Price, 1964a). To determine the parent uranium abundance, the samples are then sticked against an uranium-free mica plate and irradiated for several months in the FRM II research reactor (Garching, Germany) together with a standard and glass dosimeters. The glass dosimeters allow determining the neutron flux that is produced in the reactor. During irradiation of the samples, fission of ^{235}U produces induced fission that are revealed by etching the mica plate in 48% HF for 45 minutes at ambient temperature (Figure I.13).

The samples are finally dated using the external detector method with zeta calibration approach (Gleadow, 1981; Hurford and Green, 1983). In order to determine the Zeta factor, we use Durango apatites (31.4 ± 0.5 Ma) and Fish Canyon Tuff zircons (27.9 ± 0.5 Ma) (Hurford and Hammerschmidt, 1985; McDowell and Kreizer, 1977) as international age standards.

The amount of neutron flux in the reactor is calculated by counting the numbers of tracks present in the glass dosimeters and the newly formed induced tracks in the muscovite plates (Hurford, 1986). The induced fission tracks counted on the muscovite plates give the density of fission tracks produced by ^{235}U and thus the present-day ^{235}U content of the crystal. Since the abundance of ^{235}U is related to the ^{238}U concentration and the ratio $^{235}U/^{238}U$ in nature is known and fixed ($I = 7{,}26.10^{-3}$ yr^{-1}; Fleischer and Price, 1964b), the determination of the ^{235}U content directly provides the one of ^{238}U content. The dose ϕ (in neutron.cm²) necessary to produce a density ρ_i of induce fission tracks is given by the relation

$$\phi = \frac{\lambda_F . f . T}{\sigma . I}$$

Where λ_F is the spontaneous fission decay constant for ^{238}U (between $6.9.10^{-17}$ and $8.46.10^{-17}$ yr^{-1}; Fleischer and Price, 1964b; Wagner and Van den haute,1992), T is the age, σ is the cross-section for thermal neutron-induced fission of ^{235}U ($584.25.10^{-24}$ $cm^2.neutron^{-1}$; Fleischer and Price, 1964b) and f is a geometry factor of 2 for the external detector method (Gleadow and Lovering, 1977; Wagner and Van den Haute, 1992)

After irradiation of the crystals, the spontaneous (ρ_s) and induced (ρ_i) fission tracks densities in the sample and the mica plate, respectively, are measured per unit area. The ratio between the quantity of ^{238}U present in the crystal and the number of fission tracks allows for the calculation of the age of the crystal using the following equation:

$$\frac{\rho_s . \phi . \sigma . I}{\rho_i . \lambda_F . f} = \frac{e^{\lambda_D T} - 1}{\lambda_D}$$

The age can thus be calculated from the relation (Price and Walker, 1963; Naeser, 1967):

$$A = \frac{1}{\lambda_D} \ln\left(1 + \frac{\lambda_D . \rho_s . \phi . \sigma . I}{\rho_i . f . \lambda_F}\right)$$

Where λ_D is the total decay constant of ^{238}U ($1.5512.10^{-10}$ yr^{-1}; Hurford, 1990) For some samples it is not clear whether the single grain estimates are consistent with a common true age. In such a case, a chi-square test may help to define the homogeneity of the ages of the different crystals of a sample. The Chi-squared test (Galbraith, 1982) assess if the ratio between the density of spontaneous tracks in the crystal (ρ_S) and the density of induce tracks in the mica plate (ρ_i) is the same for each pair and if the data can be analysed by conventional Poissonian technique. If the sample passes the chi-squared test, thus the error can be estimated using the following Poissonian statistic technique:

$$\sigma(T) = T \sqrt{\frac{1}{N_s} + \frac{1}{N_i} + \frac{1}{N_d} + [\frac{\sigma(\xi)}{\xi}]^2}$$

Where N_s, N_i and N_d are the numbers of spontaneous, induced and dosimeter glass counted tracks, respectively and ζ is the personal mean zeta value. In that case, ages are considered as homogeneous, hence all the sampled grains had been reset before they started to register the presently measured ages and the mean value of the ages obtained from the different crystals gives the final cooling age of the sample. If the sample fails the chi-test, more careful attention has to be given to the sample in the calculation of the final age.

As soon as they are produced, the fission tracks tend to be healed (Donelick et al, 1990) depending, among others, on the chemical composition of the crystal and mostly on the ratio between chlorine and flurorine (Gleadow and Duddy, 1982; Green et al., 1985, 1986). The lengths of the intersection of the fission track with the c-axis etched and polished surface of the apatite crystal are characteristic for the different chemical composition of the apatite crystals and are thus measured in order to assess the mineral composition of each crystal. This value is named Dpar (for Diameter parallel to the c-axis of the crystal; Donelick, 1993). If Dpar is <1.75 µm, the apatite crystal is the common type apatite rich in fluorine whereas a crystal, whose Dpar is > 1.75 µm is richer in chlorite (Donelick et al., 2005). Fission tracks in chlorine-rich apatite are more resistant to annealing than in fluorine-rich apatite (Green et al. 1989, Crowley et al. 1991, Donelick et al., 1999). In Cl-apatite crystal, fission tracks are annealed at temperatures of ca. 120-130 °C (O'Sullivan and Parish, 1995) whereas in the F-rich apatites, fission tracks can be annealed at 95-110 °C (Green et al., 1986; Laslett et al., 1987).

I.4.2. Structural analysis of brittle deformation

In the field, minor brittle structures of faults planes, such as fault plane orientation and slickenside lineations, have been systematically measured throughout the Tauern Window. The latter are indicators of the sense of relative movement. The sense of shear is deduced from crystallisation behind steps, rough steps along the fault planes and Riedel fractures (Petit, 1987) (Figure I.14).

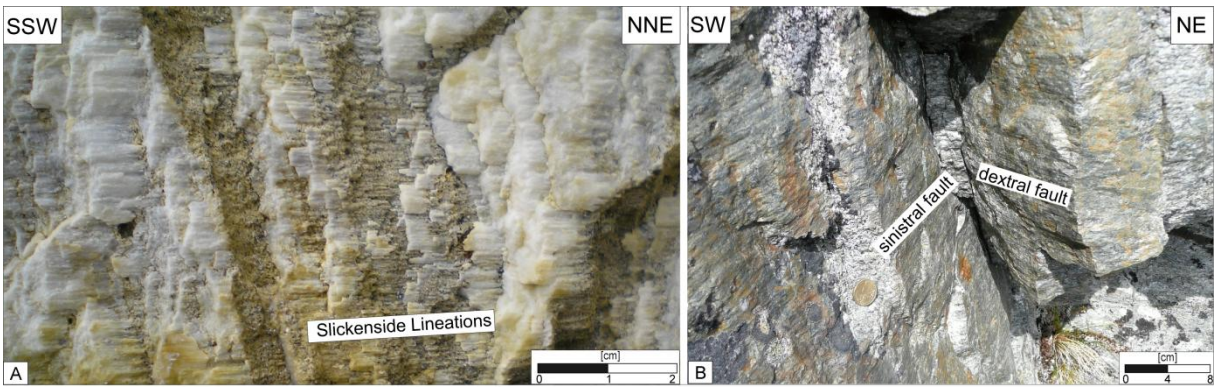

Figure I. 14. Typical brittle microstructures documenting brittle deformation in the Tauern Window. A- Calcite mineralised slickenside lineation indicating a sinistral sense of shear within schist of the Glockner nappe. B- Conjugate fault system.

We collected slickensides and striation lineations for analysis of paleostress fields formed during a succession of brittle deformation stages. Brittle data are then computed with the Tector 94 software produced and developed by J. Angelier (Angelier, 1989; 1990) in order to assess the associated paleo-stress fields. The analysis of the data is based on the direct inversion method (Carey and Brunier, 1974; Angelier, 1989; 1990) assuming that fault plane orientations may result from neo-formed fault planes or inherited faults, but each fault-slip direction corresponds to a particular stress tensor (Carey and Brunier, 1974; Angelier, 1989). The direct inversion method defines a stress tensor that best minimises the deviation between the theoretical shear stress for a given plane and slickenside, and the measured slickenside lineation. Calculations provide the orientations of the maximum (σ_1), intermediate (σ_2) and minimum (σ_3) principal stress axes based on the assumptions that (1) one of the principal stress axes is vertical (Anderson, 1942), (2) the rock volume is isotropic and homogeneous (Wallace, 1951) and (3) stress is homogeneous during the tectonic event (Angelier, 1989). The directions of compression and of extension are then deduced from σ_1 and σ_3, respectively, and paleostress regimes can be defined. If σ_1 is vertical, fault planes are inferred to have formed in an extensional context; if σ_3 is vertical, fault planes formed in a compressional context and if σ_2 is vertical fault planes formed in a transcurrent regime. The calculation also provides the Φ ratio ($\Phi = \frac{\sigma_2 - \sigma_3}{\sigma_1 - \sigma_3}$), with $0<\Phi<1$), which defines the relative magnitudes between the three principal stress axes.

We analysed the measured fault-orientation data using a classical routine in which the first processing involves the separation between strike-slip, normal and inverse faults, as they are mechanically incompatible in a single tensor of the same locality. If different types of faults (strike-slip, normal and inverse faults) were measured on the same outcrop, they were processed separately in order to obtain different stress tensors. Localities with complex deformation history can give rise to two or more paleostress tensors.

I.4.3. 2D-thermal modeling

Lithospheric-scale, 2D-thermal models were performed using the two-dimensional finite-element program SARP (Structural Analysis and Rock Physics, 2003), whose numerical code was produced and developed by F. Gueydan (Gueydan et al., 2004; Leroy et al., 2008). The models reproduce the thermal evolution of units that were exhumed by folding and erosion after subduction and nappe stacking. Selected locations within the finite-elements grid are tracked through this thermal structure so that the temperature can be recorded after each time-step. This procedure allows one to calculate the t-T history during exhumation.

The models are based on the time-dependent heat-transfer equation that requires the knowledge of conduction, advection and heat production. The thermal models require the definition of a geometrical cross section through the crust, a velocity field for the exhumation of the rocks, in addition to the boundary conditions. Thermal parameters (conductivity, specific heat, density, distribution and magnitude of radioactive heat generation) and initial temperature at each grid node are given.

A mesh composed of 440 elements and 1869 nodes provides the thermal evolution of a crustal section of 50 km length and 150 km depth (Figure I.15). The initial topography at the surface of the Earth is considered as planar and the surface temperatures are set to 0 °C. A velocity gradient field describes the movement of the rocks through the grid and the final deformation represented by a large-scale crustal fold composed of 4 nappes that have been stacked after subduction (Figure I.15).

In order to represent the shape of the western sub-dome of the Tauern Window, the deformation of the mesh is based on a half Gaussian equation as followed:

$$f(x) = \left(\frac{1}{\sigma\sqrt{2\pi}}\right) e^{\frac{-(x-\mu)^2}{2\sigma^2}}$$

where f(x) is the displacement, σ the width of the fold at half elevation and μ the width of the base of the fold.

The temperature is determined for each node of the mesh and the thermal evolution of the area is calculated based on the heat equation:

$$\frac{\varphi T(x,t)}{\varphi T} = D\Delta T(x,t) + \frac{P}{\rho c}$$

where Δ is the Laplace operator, D the coefficient of thermal diffusivity ($m^2.s^{-1}$); P the heat production ($W.m^{-3}$), ρ is the density of the material ($kg.m^{-3}$) and C the specific heat ($J.kg^{-1}\cdot K^{-1}$).

For the mathematical treatment, thermal diffusivity is considered as equal to 1. The initial conditions are fixed and considered as being equal to the temperatures that have been calculated by Carry et al. (2009) for subduction of a radiogenic crust.

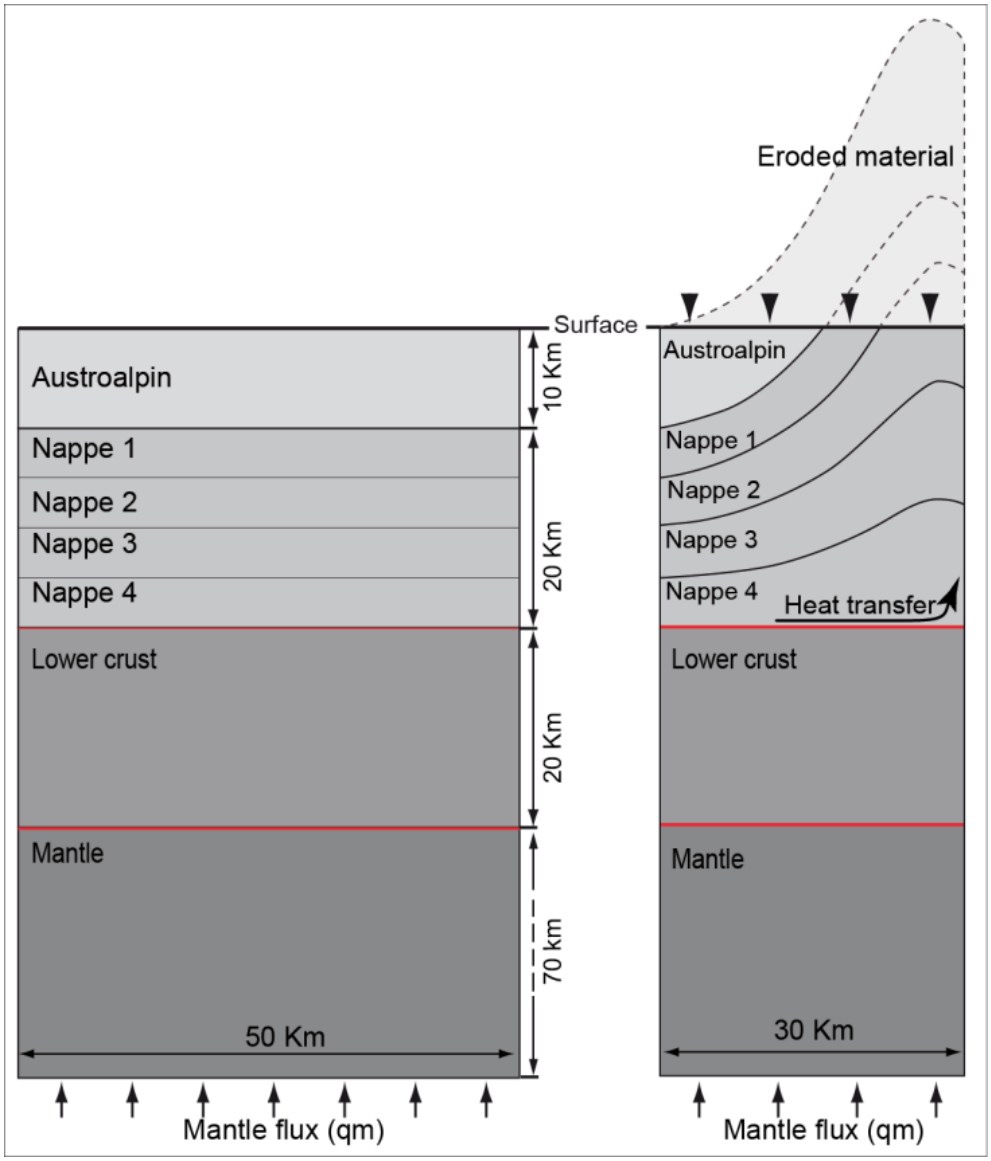

Figure I. 15. Model setup and boundary conditions. Transient heat conduction is solved in a layered segment with a top diffusive layer overlying the nappe pile.

The boundary conditions are as follow. Heat transfers are possible along the borders of the box and heat is produced from the bottom of the box. In order to represent erosion, the temperature is fixed to zero, when rocks pass a given elevation (arbitrarily fixed at 1000m).

Three different deformation histories are tested by changing the uplift rates of the rocks and the timing of deformation. Uplift rates and timing of the deformation are linked in a way

that final maximal exhumation has to be of 30 km in order to correspond to the maximal amount of exhumation that has been calculated for the Tauern Window by Schmid et al. (2004). Hence, higher uplift rates correspond to shorter bulk durations of deformation. The three models are thus as follow: Model 1 runs with uplift rates of 1.3 $mm.yr^{-1}$ during 20 Ma and then uplift rates of 0.325 $mm.yr^{-1}$ for the last 10 Ma; Model 2 runs with uplift rates of 2 $mm.yr^{-1}$ during 10 Ma and then of 0.5 $mm.yr^{-1}$ for the last 20 Ma whereas model 3 runs with constant uplift rates of 1 $mm.yr^{-1}$ during 30 Ma (Figure I. 16).

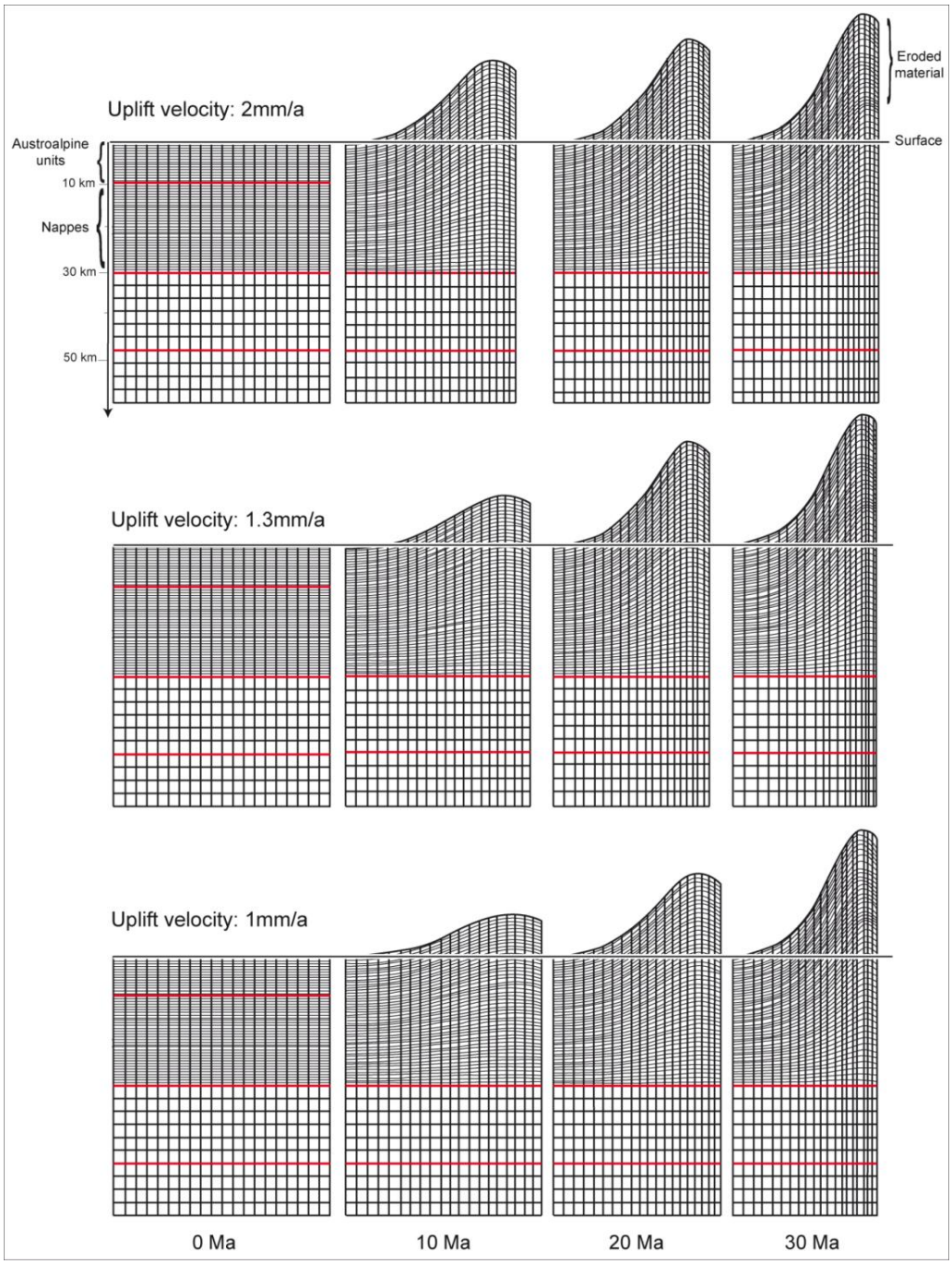

Figure I. 16. Deformation of the mesh for three models that underwent three different uplift rates with different timing of deformation.

Chapter II. Cooling history and late exhumation of the Tauern Window (Eastern Alps) inferred from apatite and zircon fission track thermochronology

Cooling history and late exhumation of the Tauern Window (Eastern Alps) inferred from Apatite and Zircon fission track thermochronology

Audrey Bertrand[1], Claudio Rosenberg[2] and Bernhard Fügenschuh[3]

1. Department of Tectonics and sedimentology, Freie Universität Berlin, Malteserstraße 74-100, 12449 Berlin, Germany
2. ISTEP, Université Paris 06-UPMC, 75252 Cedex 05 PARIS, France
3. Institute of Geology, University of Innsbruck, Innsbruck, Austria

Abstract

The relative contribution of two mechanisms for the exhumation of the Tauern Window, namely orogen-parallel extension and erosion triggered by folding is a matter of current debates. E-W extension is well documented at the western and eastern margins along the Brenner normal fault system of the Katschberg normal fault system, respectively. At the same time, upright folding dominates the internal structure of the dome, and in particular its western part, where reconstructed fold amplitudes, largely eroded during folding, attain more than 20 km. This study attempts to assess the relative importance of folding-induced erosion and orogen-parallel extension during exhumation by analysing the spatial and temporal evolution of cooling of the Tauern Window and its surrounding rocks. Age compilations based on previous and new apatite and zircon fission-track data show an elongate, concentric pattern following the map trace of the axial plane of the Tauern Dome, with younger ages in the core of the western sub-dome and a more homogeneous distribution in the eastern sub-dome. This pattern may suggest that folding and erosion were responsible for exhumation of the Tauern Window. E-W striking age profiles show that ages are younger in the western sub-dome than is the eastern sub-dome and that the youngest ages are located along the two bordering normal faults. This observation suggests that these structures were active until 3 Ma. Younger ages in the western sub-dome may suggest that exhumation of the eastern sub-dome terminated earlier than in the western subdome, hence that upright folding, associated with the Brenner normal fault lasted longer than folding associated with the Katschberg Fault. Alternatively, we propose that folding coupled with normal faulting was coeval throughout the Tauern Window, but the rates of shortening and exhumation were higher in the West. This rate increase, consistent with higher fold amplitudes and finite shortening, results in a shorter time interval between the transition of the partial annealing zone (PAZ) and the attainment of the surface, hence in younger fission track ages.

Because the age distributions show bell-shape along cross-sections perpendicular to the fold axial plane of the Tauern Window, we propose that folding and erosion were primarily responsible for exhuming the core of the Window. Younging of ages towards the normal faults only affects the immediate vicinity of those faults (5-10 km), suggesting that their activity did not significantly contribute to the exhumation of the Tauern Window on the large scale and that orogen-parallel extension played a subordinate role during unroofing.

II.1. Introduction

Structural and metamorphic gneiss domes, consisting of large-scale upright folds inside the dome and shear-zones along their boundaries are commonly observed in the cores of orogenic mountain belts (e.g. Eskola, 1949; Crittenden et al., 1980) and are inferred to have formed during or after the late stages of collision. Their formation was attributed to different mechanisms, such as diapirism (e.g. Eskola, 1949; Berner et al., 1972), tectonic denudation and erosion (e.g. Coney and Harms, 1984; Brun and Van Den Driessche, 1994) or folding and erosion (e.g. Ramsay, 1967; Burg et al., 2004).

Based on the relative orientation of fold axes and of extensional structures, two types of domes have been distinguished in the Aegean (Jolivet et al., 2004): type "a" domes, whose long axis is parallel to the direction of extension and perpendicular to shortening, and type "b" domes, whose long axis is perpendicular to extension (Jolivet et al., 2004). The majority of "a" domes shows that their axial planes are sub-parallel to the main extensional direction and perpendicular to the low-angle detachment faults bordering the dome (e.g. Yin, 1989). Natural examples of "a-type" domes are the Tertiary-age domes in the Alps (Lepontine and Tauern domes), the Naxos dome in the Cyclades (Greece) and the Montagne Noire in the Hercynian Massif (France). Some authors proposed that upright folds resulted from shortening perpendicular to the axial plane of the domes (e.g. Burg et al, 2004). On the other hand, extension along detachment faults bordering the domes may induce an isostatic-rebound of the crust triggering uplift and formation of domes (e.g. Coney, 1980; Crittenden et al., 1980). Whereas extension is unanimously recognised as the only cause of formation and exhumation of "b-type" domes, the role of shortening in the formation of "a-type" domes (e.g., Mancktelow and Pavlis, 1994) is more difficult to understand because they formed in different geodynamic settings. They are found within extensional domains, where the continental crust was severely thinned, as in the Aegean sea (Jolivet et al., 2004), but also within areas of constrictional deformation that did not undergo changes of crustal thickness as in the Devonian basins (western Norway; Osmundsen and Andersen, 2001) and within collisional settings with thickened crust, as in the Central and Eastern Alps.

The internal structure of the Tauern "a-type" dome, formed during Alpine N-S collisional shortening and orogen-parallel E-W extension is characterized by compressional structures, such as upright folds of large amplitude, and by extensional structures, such as the normal faults bordering the eastern and western margins of the dome. As a consequence, the mechanisms inferred to drive exhumation of the Tauern Window span between models suggesting that folding and erosion is the dominating process of exhumation (Cornelius, 1940; Laubscher, 1988; Lammerer, 1988; Glodny et al., 2008; Rosenberg et al., 2004; 2007; Rosenberg and Garcia, 2011, 2012) and models emphasising the role of orogen-parallel extension (Behrmann, 1988; Frisch et al., 1998; 2000; Selverstone, 1988; Kuhlemann et al., 2001; Linzer et al., 2002; Scharf et al., 2013). However, most authors agree that both processes are responsible for the exhumation of the Tauern Window (Selverstone, 1988;

Lammerer, 1988; Behrmann, 1988; Neubauer et al., 1999; Fügenschuh, et al., 1997, Kuhlemann et al., 2001; Linzer et al., 2002; Glodny et al., 2008; Rosenberg et al., 2004; 2007; Rosenberg and Garcia, 2011, 2012; Scharf et al., 2013; Schmid et al., 2013). Therefore, the present-day debate concerns the assessment of how much and when each of the two mechanisms contributed to the bulk exhumation of the Tauern Window.

The modalities of the exhumation of domes influence the evolution of the temperatures within the dome, (Chapter III, this study). Therefore thermochronological data are appropriate tools to test the relative importance of folding and erosion during the exhumation of the rocks of the study area.

In this paper, we investigate the distribution of cooling ages within the Tauern Window. Previous compilations (Luth and Willingshofer, 2008; Rosenberg and Berger, 2009) could not show a continuous picture of iso-age lines from the eastern to the western ends of the dome. We fill this gap by presenting new apatite and zircon fission-track ages, from different metamorphic units of the Tauern Window and surrounding areas, and integrate them into a compilation of previous ages from the literature.

The major aim of this paper is to assess whether the age distributions, the cooling rates and cooling history derived from thermochronological data can be related to the first-order structures observed in the Tauern dome, namely the large-scale upright folds and/or to the two major extensional detachment faults. This should help to assess the relative contribution of N-S shortening and E-W extension to the bulk exhumation of the Tauern Window.

II.2. Geological setting

The Tauern Window, located in Austria and northern Italy, is a 160 km-long and 30 km-wide dome, which strikes sub-parallel to the main axis of the Eastern Alpine orogen (Figure. II.1). The window exposes a nappe stack of European continental units and Alpine Tethyan oceanic units (Termier, 1903; Schmid et al., 2013) that are folded into an elongate dome shape (Figure. II.2).

The Tauern Window represents the only area of the Eastern Alps, where the European plate, i.e. the lower plate of the Tertiary alpine orogen, is exposed (Figure. II.1). The rest of the Eastern Alps is characterised by the exposure of the upper plate, corresponding to the Austroalpine units. European Units in the Tauern Window were exhumed through the brittle-ductile transition during Tertiary times, whereas most of the Austroalpine units had already cooled below 300°C in the Cretaceous (Figure. II.1; e.g. Oberhänsli et al., 2004; Handy et al., 2010). Therefore, Tertiary exhumation of the Eastern Alps was almost entirely localized within the Tauern Window.

The Austroalpine units in the area located between the south-western part of the Tauern Window and the DAV fault (Figure. II.1) are an exception, in that they also show Tertiary cooling ages (Figure. II.1; Borsi et al., 1973; 1978). Therefore, the latter units were included into the Tauern thermal dome (Frisch et al., 1998). This observation is consistent with the existing continuity of structures across the boundary between Austroalpine and Penninic

Units in the south-western Tauern Window (Nollau, 1969). Because this study deals with the cooling history of the Tauern Window based on thermochronological data, the term Tauern Window refers to the thermal dome in this work (Frisch et al., 2000).

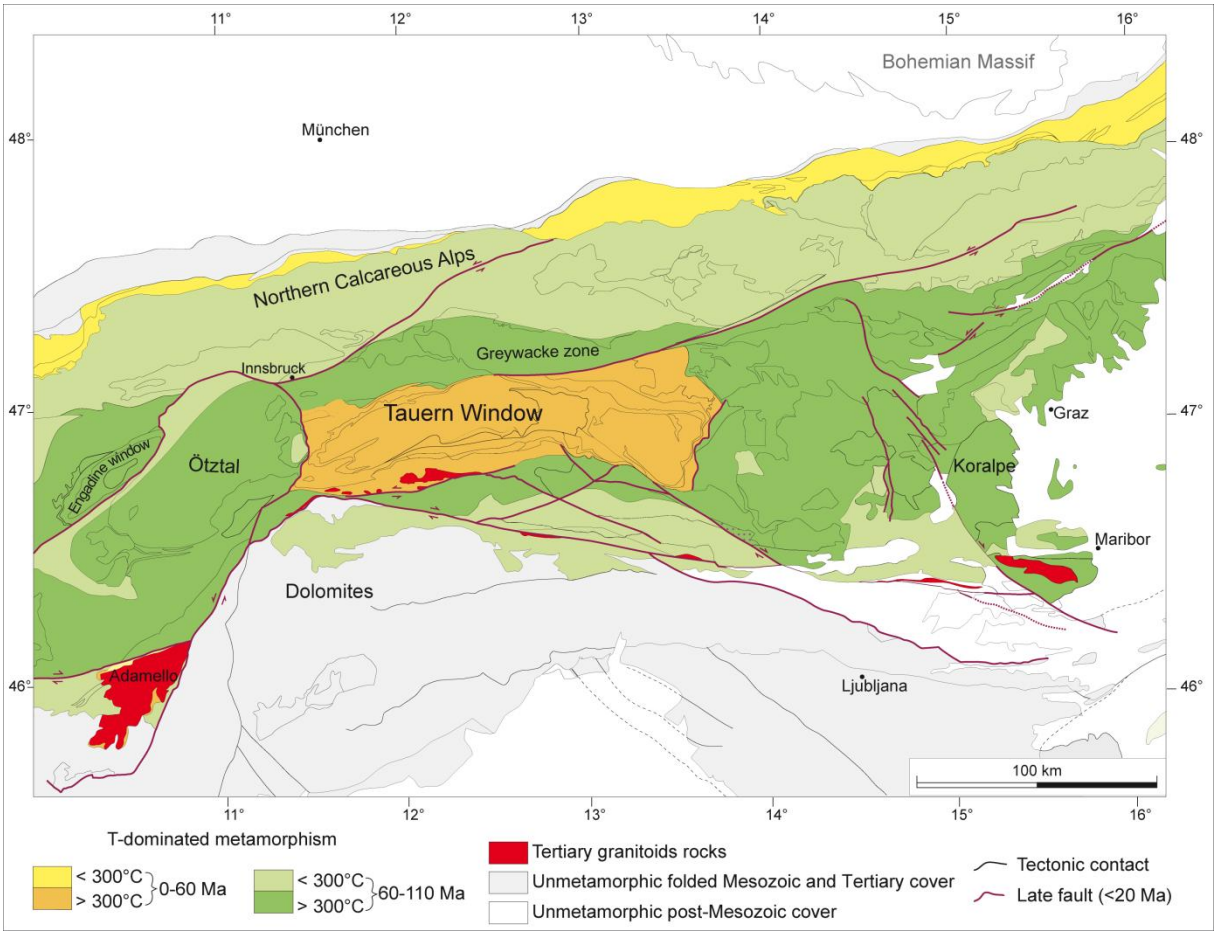

Figure II. 1. Age of temperature-dominated metamorphism in the Eastern Alps. Modified after Handy et al., 2010.

The internal structure of the Tauern Window is dominated by two elongate sub-domes, the western one, consisting of WSW-striking, tight upright folds of more than 20 km amplitude (Figure. II.2), and the eastern one consisting of ESE-striking folds of lower amplitude and larger wavelength (Schmid et al., 2013; Figure. II.2). Both the eastern and western margins of the window coincide with N-S striking normal faults, namely the west-dipping Brenner fault (Selverstone, 1988; Behrmann, 1988) in the west, and the east-dipping Katschberg fault in the east (Genser and Neubauer, 1989; Scharf et al., 2013) (Figure. II.2). These normal faults are suggested to be coeval with the upright folds of the sub-domes (Glodny et al., 2008; Rosenberg and Garcia, 2011; 2012; Scharf et al., 2013; Schmid et al., 2013). Large parts of the northern and southern margins of the Tauern Window are defined by strike-slip faults. In the north, the E-W striking, sinistral SEMP fault (Salzach-Ennstal–Mariazell–Puchberg) juxtaposes European continental and alpine Tethyan oceanic units to Austroalpine units (Figure. II.2). In the south, the sinistral transpressive DAV fault

(Kleinschrodt, 1987) marks the southern limit of Tertiary Alpine metamorphism (Figure. II.2; Hoinkes et al., 1999).

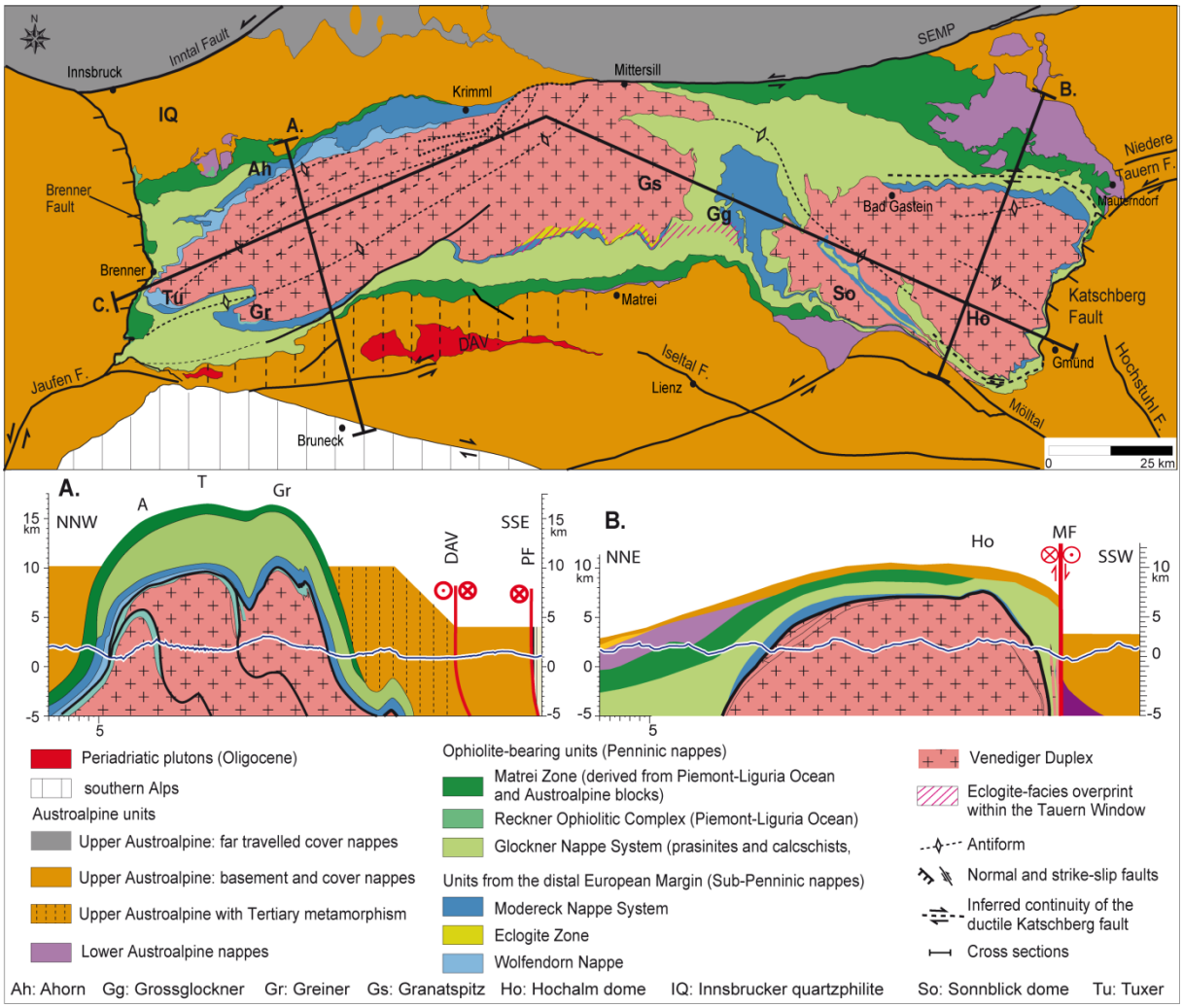

Figure II. 2. Simplified tectonic map of the Tauern Window and location of the cross sections through A. the western sub-dome and B. the eastern sub-dome (modified after Schmid et al., 2013); SEMP: Salzach-Ennstal–Mariazell–Puchberg; DAV: Defereggen-Antholz-Vals. Cross-section C is shown in Figure II.9a

The Tertiary metamorphic history of the Tauern Window started with subduction and was followed by a Barrow-type metamorphism (Bousquet et al., 2008), whose peak is inferred to have been attained between 31.5 Ma (Glodny et al., 2005) and 30-28 Ma (e.g. Inger and Cliff, 1994; Reddy et al., 1993; Selverstone et al., 1992; Christensen et al., 1994; Thöni 1999). Cooling and exhumation followed the peak of metamorphism from Early Oligocene to Late Miocene (e.g., Hoinkes et al., 1999; Handy and Oberhänsli, 2004). The metamorphic grade increases toward the centre of the two sub-domes (Hoernes and Friedrichsen, 1974; Luth and Willingshofer, 2008), as shown by the concentric, elongate pattern of the isograds in map view, both in the eastern and western sub-domes (Figure. II.3). The isograds are subparallel to the fold axial plane of the dome and symmetrically distributed about it (Figure. II.3), suggesting that they are either coeval with upright folding (D5 stage of Schmid et al.,

2013), which occurred during Miocene time and resulted in the present-day dome geometry of the Tauern Window (Schmid et al., 2013), or that they are older and were folded during upright folding. However, since they crosscut the nappe contacts, they post-date subduction and nappe-formation.

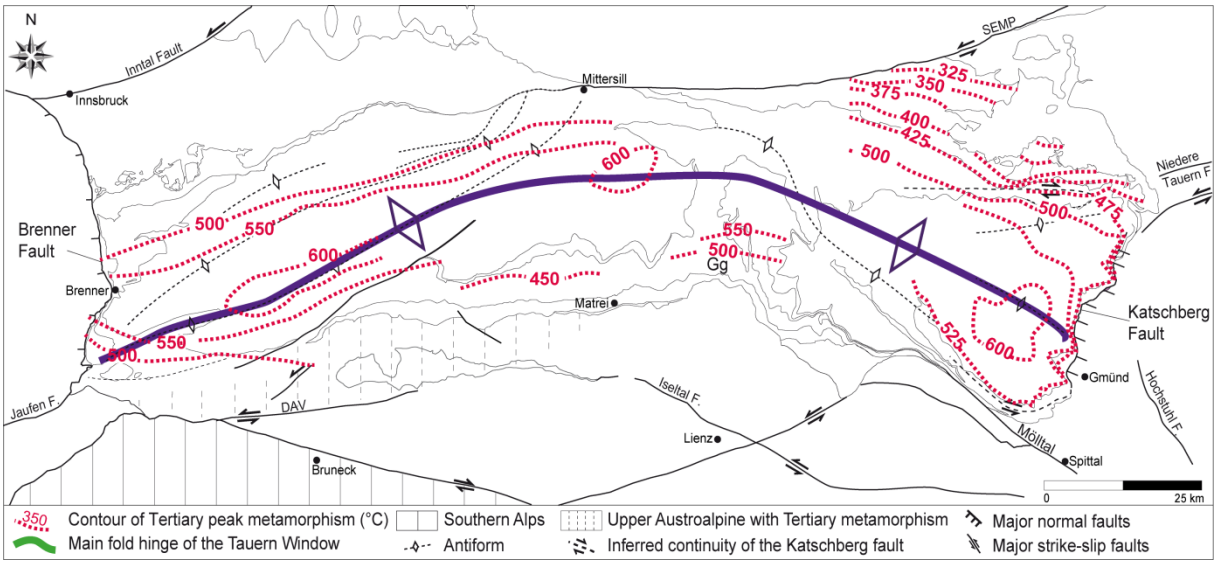

Figure II. 3. Simplified tectonic map of the Tauern Window showing isograds of tertiary metamorphism. Isograds in the central and western areas are based on oxygen thermometry on quartz-muscovite (modified after Hoernes and Friedrichsen, 1974); isograds in the Grossglockner (Gg) and eastern area are based on Raman microspectrometry of carbonaceous material (Scharf et al., 2013).

II.3. Method

II.3.1. Sampling and analytical procedures for fission track dating

91 samples from the basement and cover units of the Tauern Window and surrounding Austroalpine nappes were collected for apatite and zircon fission track dating. A total of 54 samples have been crushed in order to isolate apatite and zircon minerals. Only 22 apatites and 25 zircon samples could be dated (tables II.1 and II.2) because the remaining samples had an insufficient number of apatite and zircon grains of good quality and containing sufficient uranium for the dating process.

After crushing, sieving, and washing, apatite and zircon crystals were separated using a magnetic separator and heavy liquids, then handpicked and mounted in Epoxy and Teflon, respectively. To reveal the spontaneous tracks produced by the disintegration of the ^{238}U, apatites and zircons were etched, respectively in nitric acid (HNO3) and in a NaOH-KOH eutectic melt. The crystal were pressed against a muscovite plate and irradiated in the reactor of Garching (Germany) together with Durango apatite and Fish Canyon Tuff zircons standards (Hurford and Hammerschmidt, 1985; McDowell and Kreizer, 1977) and a glass dosimeter for several months.

The amount of uranium was calculated by counting the number of tracks present in the glass dosimeters. The muscovite plates were etched in fluoridric acid in order to reveal the

newly formed, induced fission tracks produced by the fission of ^{235}U. The samples were finally dated using the external detector method with zeta calibration approach (Gleadow, 1981; Hurford and Green, 1983) and the software Trackkey version 4.2.g written and developed by Istvan Dunkl (Dunkl, 2002).

Closure temperatures of apatite fission tracks were inferred to be 90 ± 30 °C (Green et al., 1989), 110 ± 10 °C (Wagner, 1968) or 105 ± 10 °C (Parrish, 1983). The closure temperature of zircon fission tracks is not well defined and several temperatures have been proposed: 175 ± 25 °C (Naeser, 1979), 260 ± 20 °C (Hurford, 1986), 240 ± 60 °C (Yamada et al., 1995), 260 ± 25 °C (Foster et al., 1996) and 280 ± 50 °C (Tagami and Shimada, 1996). The closure temperature depends, amongst others, on the cooling rates in a way that the slower the cooling rate, the lower is the closing temperature. Dodson (1979) and Reiners and Brandon (2006) calculated different closure temperatures according to different cooling rates. For apatite they obtained a closure temperature of 105 °C for a cooling rate of 30 °C.Myr^{-1}, 98 °C for a cooling rate of 10 °C.Myr^{-1}, and 92 °C for a cooling rate of 3 °C.Myr^{-1} (Dodson, 1979). Closure temperatures between 80 and 140 °C were determine for cooling rates varying between 0.1 and 100 °C.Myr^{-1} (Reiners and Brandon, 2006). For zircons, the closure temperatures are comprised between 190 and 260°C for cooling rates comprised, respectively, between 0.1 and 100 °C.Myr^{-1} (Reiners and Brandon, 2006). Taking the relationship between closure temperature and cooling rate proposed by Reiners and Brandon (2006) and assuming a cooling rate of around 25 to 50 °C.Myr^{-1} for the Tauern Window (Luth and Willingshofer, 2008), we assume closure temperatures of 110 ± 20 °C for the apatite and 240 ± 20°C for the zircon, respectively, for this study.

II.3.2. Extrapolation of compiled fission track ages

The modalities of the exhumation of gneiss domes influence the evolution of the temperatures within the dome. Therefore, the thermal characteristics of the domes can be related to a specific formation mechanism. For instance, domes delimited by large-scale extensional faults are expected to result in an asymmetric distribution of ages in map view, with ages younging toward the fault (Figure. II.4; Wernicke, 1985; Foster et al., 2001; Yin, 2004; Burg et al., 2004). In contrast, in the case of gneiss domes resulting from upright folding and erosion, isograds are wrapped in such a way that the same temperature is found at shallower depth in the centre of the dome, resulting in a symmetrical and concentric distribution of cooling ages with younger ages centred in the middle of the dome (Figure. II.4; Burg et al., 2004).

In order to discuss the cooling history of the Tauern Window, we compiled our new thermochronological data with those of the literature creating a database for zircon and apatite fission-track ages. These data cover the entire Tauern Window as well as the surrounding Austroalpine units. In order to facilitate reading and interpretation of the compiled data, we provide interpolated age maps using a natural-neighbour algorithm tool of ESRI-ArcMap10^{tm} GIS software.

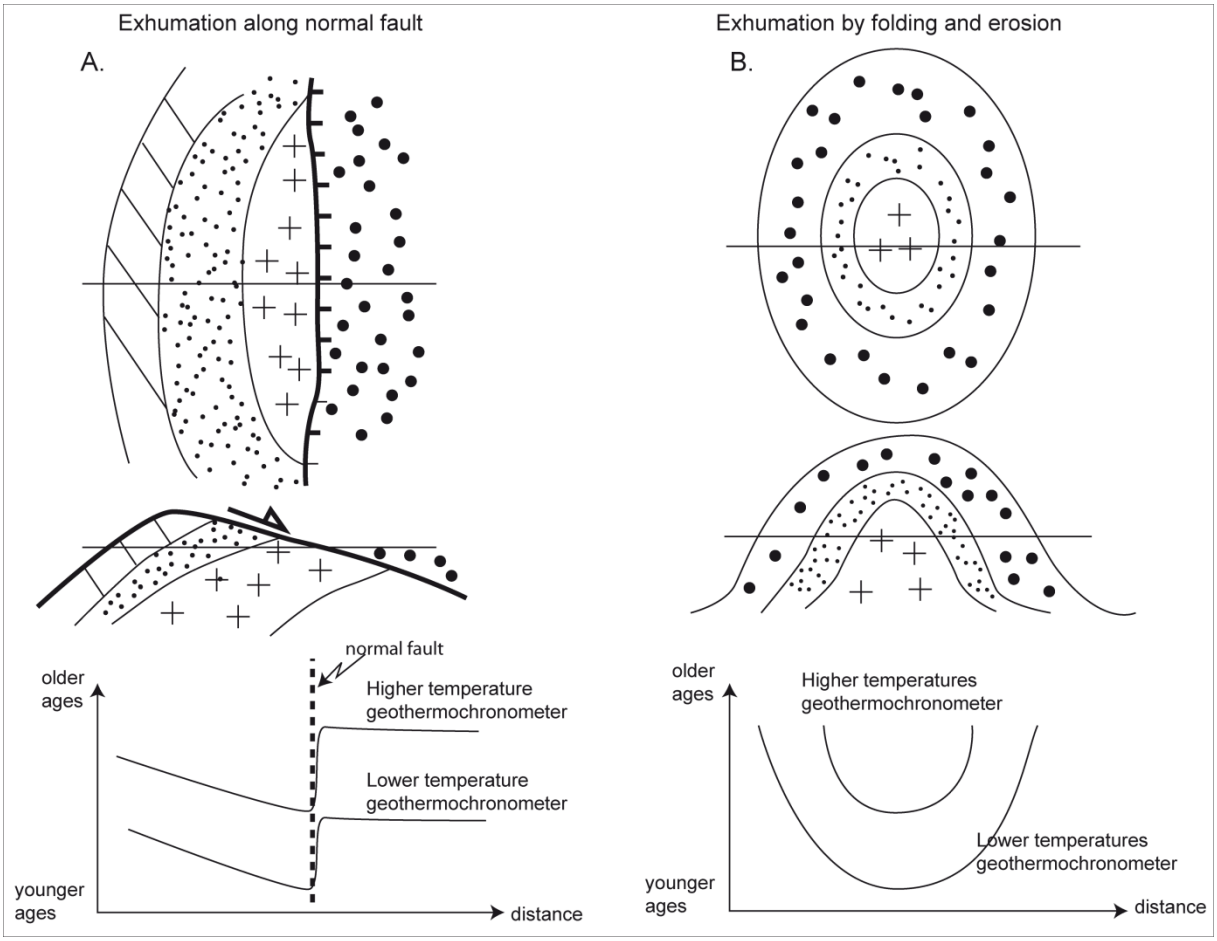

Figure II. 4. Map view cross section and expected age distribution of geothermochronometers data in the case of a. exhumation of a dome related to extensional denudation along a normal fault and b. Doming and exhumation controlled by folding and erosion.

II.4. Results

II.4.1. New zircon and apatite fission track ages

Numerous apatite ages from the Tauern Window exist in the literature (Luth and Willingshofer, 2008; Rosenberg and Berger, 2009 for review) and we attempted to complete the existing data with new measurements in areas that were poorly covered, such as the core of the western sub-dome and the eastern termination of the eastern sub-dome. Samples are mainly located in the central part of the western sub-dome and in the eastern part of the Tauern Window (Figure. II.5), where thermochronological data, particularly zircon fission-track ages, did not exist so far. Four samples are located in the westernmost part of the study area and four ages are provided for the surrounding Austroalpine units (Figure. II.5).

Sample	Longitude [DDEC]	Latitude [DDEC]	Elevation [m]	Location	Unit	Nbs of crystals	ρ_D [$10^5 cm^{-2}$]	ρ_S [$10^5 cm^{-2}$]	P_i [$10^5 cm^{-2}$]	χ (%)	Central age ± 1σ [Ma]
AB.08.04	11.5845	47.0389	1400	Valserbach	Zentralgneiss	13	0.50	2.57	9.09	0.0	13.8 ± 1.9
AB.08.11	12.2510	47.1003	2671	Schlieferturme	Zentralgneiss	17	0.50	2.45	6.30	95.98	18.2 ± 2.1
AB.08.14	12.2358	47.1102	2754	Schlieferspitz	Zentralgneiss	5	0.50	1.91	6.07	78.79	14.9 ± 2.0
AB.08.19	12.2683	47.0967	2730	WarnsdorferHutte	Zentralgneiss	16	0.49	3.29	9.91	0.0	15.3 ± 1.9
AB.08.25	12.3922	47.1198	2832	Neue Prager Hutte	Zentralgneiss	21	0.52	2.04	6.31	53,.56	15.7 ± 1.8
AB.08.31	12.3314	47.0852	2500	Dorfer Bach	Zentralgneiss	20	0.52	3.15	8.48	0.02	18.4 ± 2.2
AB.08.32	12.2484	47.0885	2547	Dorfer Bach	Zentralgneiss	19	0.41	2.84	6.38	32.95	17.4 ± 2.0
AB.08.47	11.7409	46.9406	2655	Pfeifholder Tal	Zentralgneiss	8	0.22	1.95	6.84	12.32	5.8 ± 0.8
AB.08.50	13.4043	46.8928	1939	Reinitzbach Tal	Zentralgneiss	6	0.24	5.93	11.55	4.04	11.8 ± 1.6
AB.08.58	13.5664	47.0800	1095	MuhrTal	Zentralgneiss	6	0.42	1.91	6.84	10.03	12.9 ± 1.8
AB.09.10	12.5315	47.1761	1473	FelberTauern Tal	Zentralgneiss	9	0.25	5.61	10.95	0.23	11.8 ± 1.4
AB.09.15	13.6807	47.1406	1196	Mautendorf	Austroalpine	2	0.41	2.49	7.48	58.47	12.5 ± 2.1
AB.09.16	13.1151	47.2177	906	Bad Hofgastein	Glockner nappe	2	0.42	2.64	5.87	2.68	18.0 ± 2.1
AB.09.18	13.4874	46.9681	1008	Malta Tal	Zentralgneiss	6	0.26	4.23	10.80	0.02	10.4 ± 2.1
AB.09.19	13.6162	46.9931	1196	Rennweg	Austroalpine	8	0.41	5.11	5.61	86.1	35.0 ± 4.2
AB.10.08	12.5050	47.1022	1523	Felbertauern Tal	Zentralgneiss	12	0.29	6.05	15.40	0.0	10.8 ± 1.4
AB.10.16	13.3513	47.1148	2405	Unterer Schwarzsee	Zentralgneiss	12	0.32	4.59	10,38	29.97	13.2 ± 1.5
AB.10.17	13.3441	47.1316	2030	Mururspung	Glockner nappe	16	0.33	3.96	10.04	0.08	11.9 ± 1.4
AB.10.18	13.3622	47.1975	2000	Rieding Tal	Austroalpine	16	0.34	0.69	1.19	0.29	19.2 ± 2.3
AB.10.25	11.4641	47.1294	1171	Matrei a. Brenner	Zentralgneiss	14	0.35	2.88	5.35	0.0	17.8 ± 2.2
AT.09.11	12.1361	47.0741	2645	Ahrn Tal	Zentralgneiss	9	0.37	2.87	6.59	1.08	15.1 ± 1.9
HT.09.01	12.3468	47.2176	1317	Habach Tal	Zentralgneiss	20	0.39	3.79	10.41	0.0	13.1 ± 1.6
PT.08.02B	11.7247	46.9647	2825	Pfunderer Tal	Zentralgneiss	2	0.40	4.01	13,68	53.54	10.7 ± 1.5
US.09.06	12.2933	47.1934	1375	Untersulzbach	Zentralgneiss	19	0.40	5.12	12.85	6.42	14.5 ± 1.7
WG.09.02	12.1214	47.1571	2429	Wildgerlos	Zentralgneiss	18	0.43	4.15	11.29	0.0	14.5 ± 1.7

Table II. 1.New zircon fission tracks ages - ρ_D: Track density of the dosimeter glass; ρ_s: Spontaneous track density ρ_i: Induced track density; χ: chi-square test. Zircon ages are calculated using a CN-1 dosimeter glass with a ζCN-1=189.0±11.1

Sample	Longitude [DDEC]	Latitude [DDEC]	Elevation [m]	Location	Unit	Nbs of Crystals	ρD [10^5cm^{-2}]	ρ_S [10^5cm^{-2}]	ρ_I [10^5cm^{-2}]	Dpar [µm]	χ (%)	Central age ±1σ [Ma]
AB.08.04	11.584514	47.038866	1400	Valserbach	Zentralgneiss	14	1.38	0.13	3.13	1.22	62.19	9.2 ± 1.5
AB.08.11	12.251013	47.100324	2671	Schlieferturme	Zentralgneiss	15	1.33	0.12	1.97	1.64	99.64	13.9 ± 2.4
AB.08.14	12.235809	47.110164	2754	Schlieferspitz	Zentralgneiss	8	0.99	0.12	1.53	1.72	92.91	13.0 ± 2.8
AB.08.19	12.268308	47.096653	2730	WarnsdorferHutte	Zentralgneiss	20	1.28	0.23	3.38	1.32	95.08	14.4 ± 1.7
AB.08.23	12.425885	47.158008	2294	Kratzenbergsee	Zentralgneiss	20	0.97	0.21	3.04	1.40	89.29	10.9 ± 1.3
AB.08.25	12.392237	47.119837	2832	Neue Prager Hutte	Zentralgneiss	7	0.95	0.11	1.67	-	98.2	11.0 ± 2,7
AB.08.26	12.624767	47.116438	2462	Weissee	Zentralgneiss	12	1.23	0.23	4.92	1.20	75.57	9.5 ± 1.4
AB.08.31	12.331387	47.085155	2500	Dorfer Bach	Zentralgneiss	21	1.37	0.11	1.91	1.47	99.98	13.3 ± 2.1
AB.08.32	12.248407	47.088509	2547	Dorfer Bach	Zentralgneiss	10	0.92	0.16	1.66	-	69.16	14.9 ± 2.7
AB.08.40	12.384651	46.942502	2618	Dorfer Bach	Zentralgneiss	20	0.91	0.20	2.22	1.33	99.94	13.3 ± 1.7
AB.09.15	13.680733	47.140600	1196	Mautendorf	Austroalpine	4	1.15	0.21	4.63	-	82.22	8.6 ± 2.3
AB.09.18	13.487412	46.968050	1008	Malta Tal	Zentralgneiss	20	0.29	0.14	2.17	1.39	94.45	3.0 ± 0.4
AB.09.22	13.289319	47.144935	1160	Grossarlbach Tal	Glockner Nappe	6	0.98	0.32	1.78	-	97.37	12.0 ± 2.8
AB.10.06	12.489841	47.233950	1014	Felbertauern Tal	Zentralgneiss	18	1.02	0.24	3.77	1.40	43.07	10.5 ± 1.3
AB.10.08	12.505044	47.102238	1523	Felbertauern Tal	Zentralgneiss	16	1.02	0.15	2.63	1.26	97.17	9.5 ± 1.4
AB.10.12	13.536402	46.861661	1440	Gmund	Austroalpine	20	1.03	0.34	4.49	1.27	80.45	12.9 ± 1.4
AB.10.14	13.346210	47.084398	1940	Malta Tal	Zentralgneiss	21	1.05	0.19	5.06	1.32	90.98	6.5 ± 0.8
AB.10.16	13.351317	47.114834	2405	Unterer Schwarzsee	Zentralgneiss	14	1.05	0.16	2.76	1.37	78.26	10.6 ± 1.4
AB.10.27	11.440938	46.797270	1557	Talver Tal	Austroalpine	14	1.07	0.17	1.73	1.72	99.13	17.2 ± 2.4
AT.09.11	12.136073	47.074116	2645	Ahrn Tal	Zentralgneiss	16	1.08	0.14	2.46	1.41	93.07	10.4 ± 1.4
GT.08.04	12.410298	47.083197	2783	Geschlossbach Tal	Zentralgneiss	20	1.09	0.17	3.12	1.37	83.86	9.8 ± 1.2
US.09.05	12.329273	47.153473	2174	Untersulzbach	Zentralgneiss	15	1.10	0.12	2.54	1.55	96.7	8.6 ± 1.3

Table II. 2. New apatite fission tracks ages; ρ_D: Track density of the dosimeter glass; ρ_s: Spontaneous track density ρ_i: Induced track density; χ: chi-square test. Dpar: length in µm of the intersection of the fission tracks with the c-axis surface of the apatite. Apatite ages are calculated using a CN-5 dosimeter glass with a ζ_{CN-5}=338.9±33.3

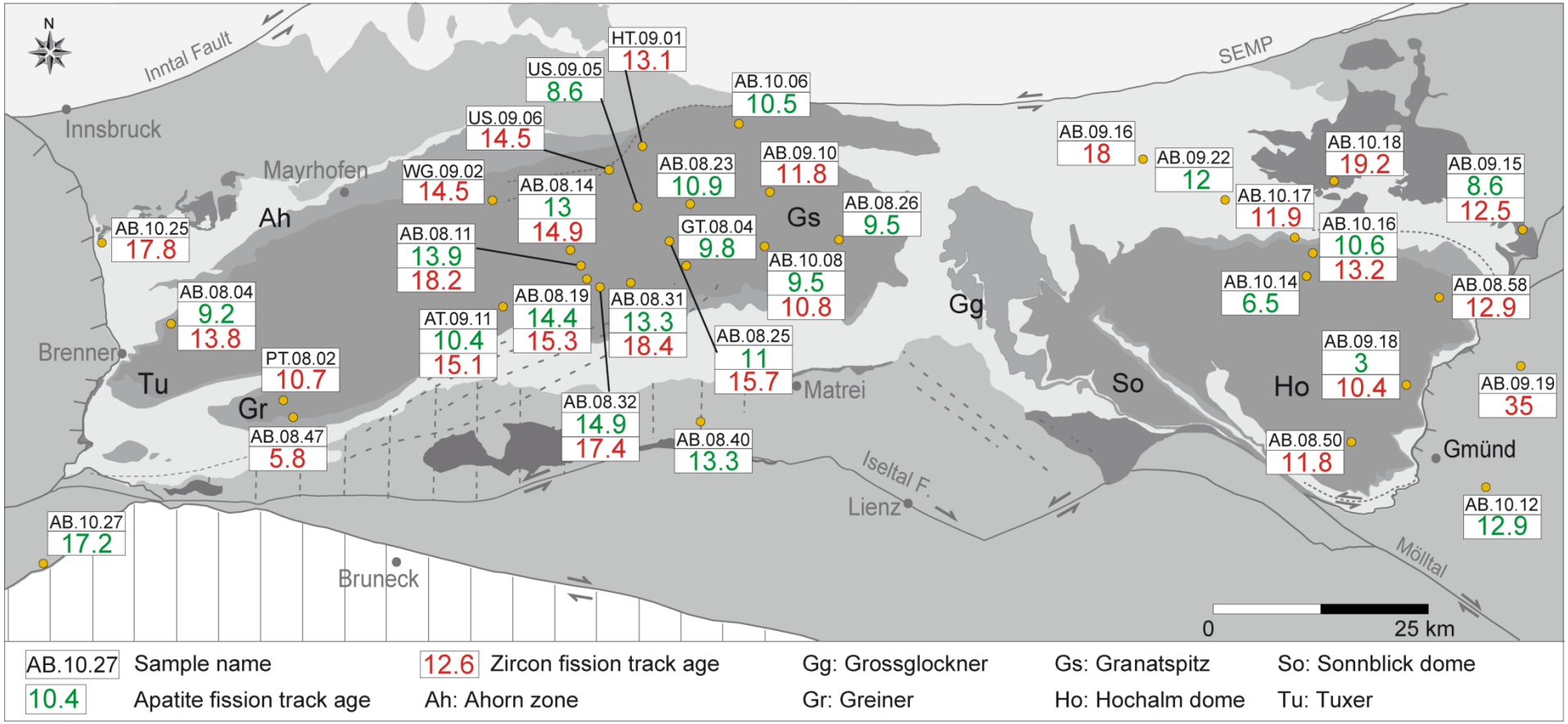

Figure II. 5. Structural sketch of the Tauern Window, with locations and ages of new apatite (red numbers) and zircon (blue numbers) fission track samples.

Zircon fission-track ages range between 5.8±0.8 Ma for a sample located in the south-western part of the Tauern Window (sample AB.08.47, Figure. II.5) and 35±4.2 Ma for an Austroalpine sample located in the hangingwall of the Katschberg fault (sample AB.09.19, Figure. II.5). Ages obtained for the western sub-dome vary between 13.1±1.6 Ma and 18.2±2.2 Ma, showing an age range similar but slightly younger than that of previous studies (11-22 Ma) that were focused on areas further west (Most, 2003). In the core of the Tauern Window, i.e. in the Granatspitz area (Figure. II.5), zircon fission-track ages vary between 10.8±1.4 Ma and 11.8±1.4 Ma. These ages are younger than those found in the eastern and western sub-domes (Figure. II.5). In the eastern sub-dome, zircon ages vary between 10.4±2.1 and 19.2±2.3 Ma (Figure. II.5). Within the Hochalm dome, fission-tracks yield ages that are distributed within a narrower time interval, namely between 10.4±2.1 and 13.2±1.5 Ma. These ages are significantly younger than those previously published for the same area (18-16 Ma; Dunkl et al., 2003; Figure. II.6).

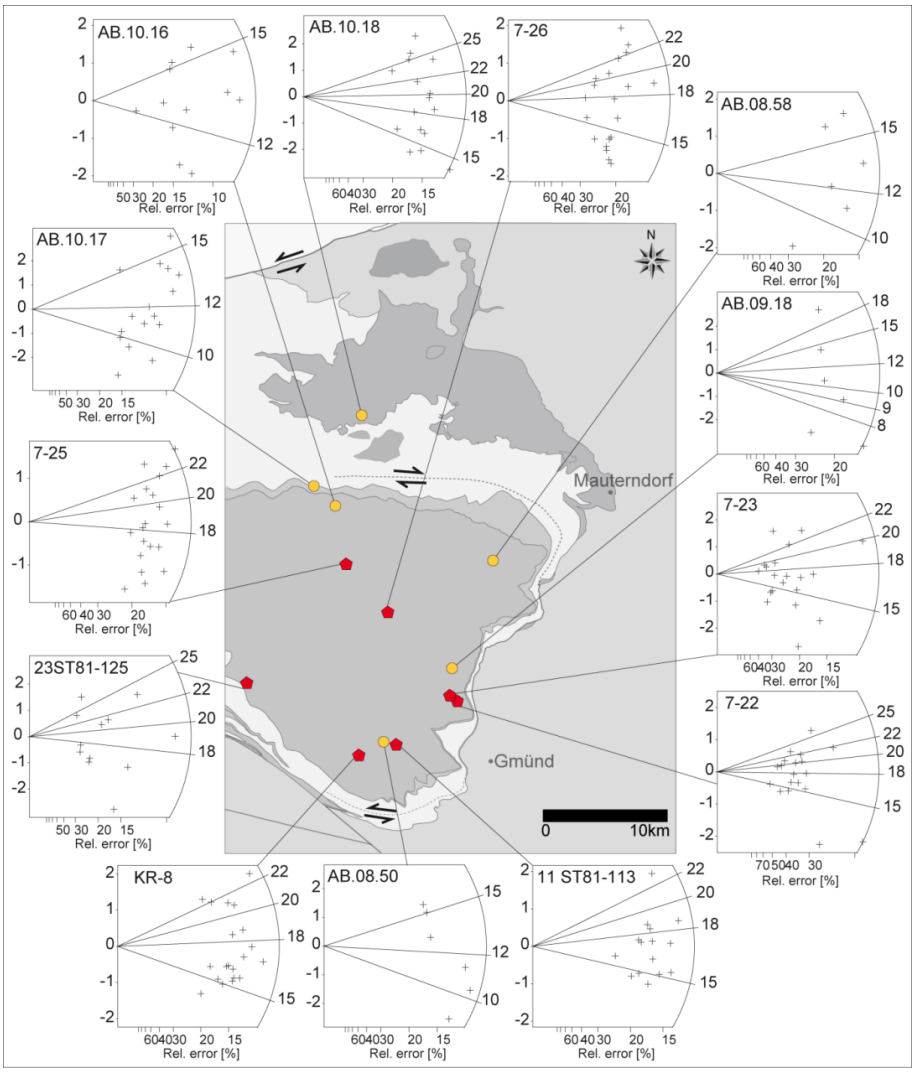

Figure II. 6. Radial plots showing the wide single grain range of zircon fission track ages of the Hochalm Dome. Data are from Dunkl et al., 2003 (red pentagons) and this study (yellow circles)

Even where samples were collected very close to those of Dunkl et al. (2003) (Figures. II.5 and II.6) an age difference of 5 Ma exists. This difference is not due to different elevations of the samples, nor to the vicinity to the Katschberg Fault, because no correlation between age and distance to this normal fault can be detected (Figure. II.6). However, the analysis of distribution of single-grain ages of the samples of the Hochalm dome shows that both sets of data (Dunkl et al., 2003, and this study) are characterised by a wide distribution of single-grain ages that overlap and range between 5.9 and 28.4 Ma in the case of this study and between 8.4 and 31 Ma in Dunkl et al. (2003). Therefore, the two data sets largely overlap, although the central ages of the different samples are different (Figure. II.6).

We consider a counting bias to be unlikely, especially in view of the consistent, broad range of single grain ages in both studies, that may result from slow cooling, implying a relatively long residence time within the PAZ (Wagner, 1979). Slow cooling is expected to result in a wide range of central fission-track ages (Yamada et al., 1995). The older ages, clustered around 25-28 Ma (Figure. II.6), may correspond to the time when the samples entered the PAZ while the younger ages, clustered around 5-8 Ma, may correspond to the time when the samples left the PAZ. Taken together we thus suggest that the rocks of the Hochalm dome cooled from 300 °C to 180 °C (Hurford and Green, 1983; Zaun and Wagner, 1985), between 25-28 and 5-8 Ma. The resulting cooling rates calculated for the Hochalm dome are around 5-7 °C/Myr^{-1}, thus rather low compared to other parts of the Tauern Window (Most, 2003; Foeken et al., 2007; Luth and Willingshofer, 2008).

Mean Dpar values of the tracks in apatites range from 1.2 to 1.72 µm indicating that there was no variation of composition between the different samples and that all of them are common, fluorine-rich apatites. Therefore, the closure temperature can be inferred to correspond to a closure temperature of 110±20 °C (Green et al., 1986). Apatite ages vary between 3±0.4 Ma in the footwall of the Katschberg normal fault, and 17.2±2.4 Ma in the Austroalpine units, along the Meran-Mauls fault (Figure. II.5). In the Granatspitz area, ages are slightly younger when compared to the western sub-dome (Figure. II.5). Taken together the data are consistent with ages previously obtained in neighbouring areas of the window and allow one to emphasise the along-strike continuity of iso-age lines (Luth and Willingshofer, 2008; Rosenberg and Berger, 2009).

One sample, located along the trace of the Katschberg normal fault, yields significantly younger apatite fission track age (3±0.4 Ma) than the rest of the samples. This may indicate that exhumation of the Tauern Window along the brittle part of this fault was still active during Pliocene times, or it may reflect a late thermal fluid event that affected the fault zone during its late stages of activity. Zircon fission-tracks of the same sample are not reset, hence the temperature of the fluids may have been comprised between ca. 110 °C and 240 °C, i.e. sufficiently high to reset apatite, but not zircon fission track ages

II.4.2. Iso-age maps

All available zircon and apatite fission-track ages from the Tauern Window and surrounding Austroalpine areas (Coyle, 1994; Dunkl et al., 2003; Foeken et al., 2007; Fügenschuh et al., 1997; Grundmann and Morteani, 1985; Most, 2003; Pomella, 2010; Staufenberg, 1987; Steenken et al., 2002; Viola et al., 2001, Wölfler et al., 2008 and Di Fiore, 2013) are compiled with the new data of this study (Figures. II.7a and II.8a) and interpolated in iso-age maps (Figures. II.7b and II.8b). As expected, zircon fission-track ages within the thermal dome of the Tauern Window, are younger than those outside the dome (Figure. II.7), excepted for the area bounded by the Jaufen and the Meran-Mauls faults, which displays zircon fission-track ages comprised between 14 and 19 Ma (Figure. II.7). Therefore, from a thermal point of view, this area, which is located directly in front of the Dolomites Indenter represents the south-western continuation of the Tauern Window.

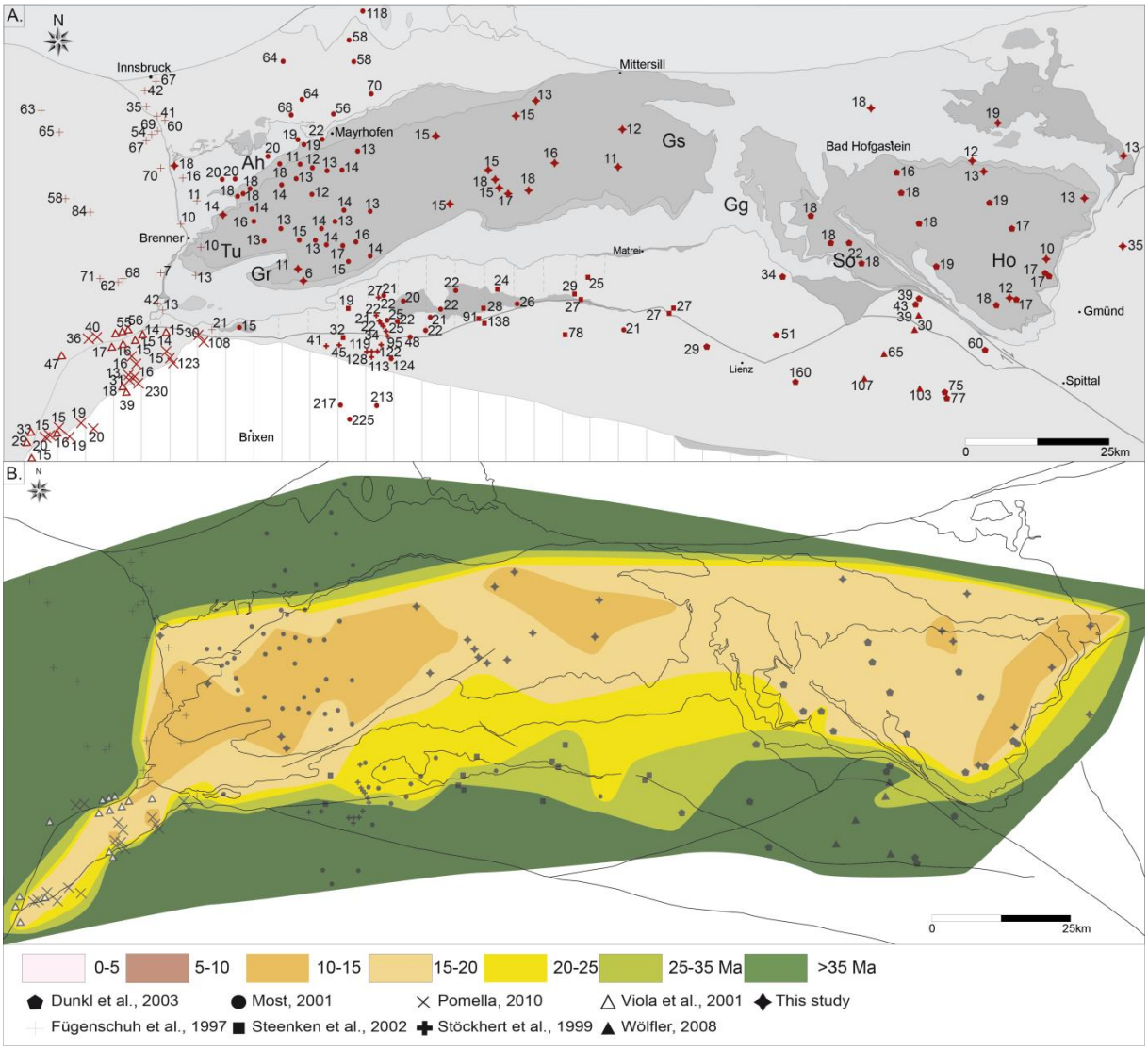

Figure II. 7. A. Distribution of compiled and new zircon fission track ages; B. Interpolation of zircon fission track ages using the natural neighbour tool provided by the computer program ArcGIS10®

Zircon fission-track ages in the western sub-dome become younger towards the core, however, the age pattern is asymmetric in that it shows a gradual age increase southward but an abrupt one northward, marked by a transition from ages younger than 20 Ma to ages older than 35 Ma within a few km distance (Figure. II.7). The long axis of the concentric and elongate contour, delimiting the youngest ages (Figure. II.7b) almost coincides with the hinge of the western sub-dome (Figure. II.2) and with the trace corresponding to the highest temperature isograds (Figure. II.3).

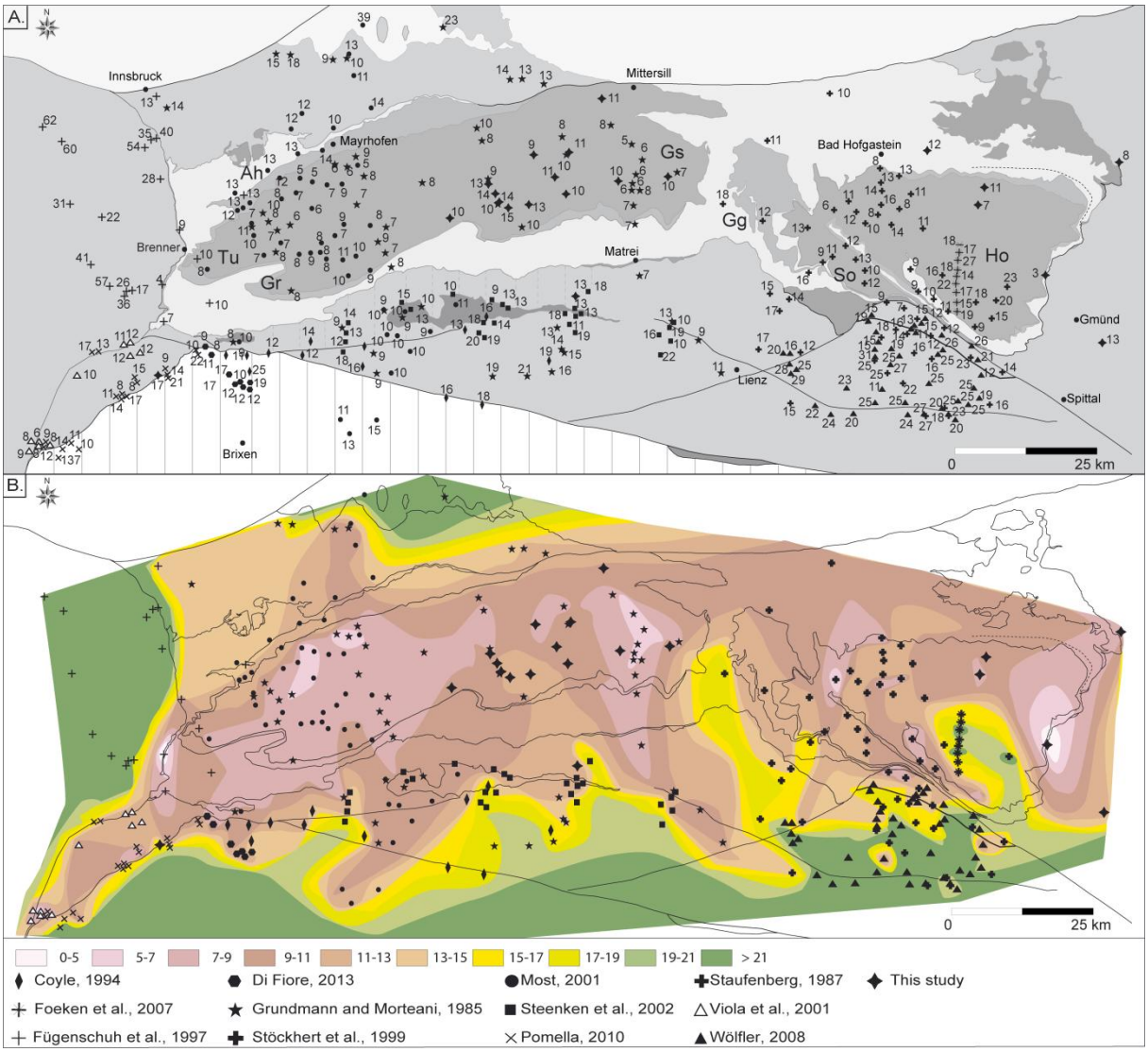

Figure II. 8. A. Distribution of compiled and new apatite fission track ages; B. Interpolation of apatite fission track data ages using the natural neighbour tool provided by the computer program ArcGIS10®.

Excepted for a young Austroalpine sample displaying a zircon fission-track age of 7.2±1.4 Ma (Fügenschuh et al., 1997) in the hanging wall of the Brenner fault (Figure. II.7) an important age gap coincides with the fault plane of the Brenner fault (Figure. II.7b), separating young Mioene ages in the footwall from older Cretaceous one in the hangingwall (Figure. II.7b). The same gap of ages is observed across the Jaufen fault (Figure. II.7b). In the

area located between the Jaufen and the Meran-Mauls faults, ages cluster between 12.9±1.3 Ma (Pomella, 2010) and 19.3±1 Ma (Viola et al., 2001), whereas north of the Jaufen fault they are older than 29±5.2 Ma (Viola et al., 2001). In the eastern sub-dome, the age distribution is very different and shows only small variations of ages over large part of the area (Figure. II.7b). Most of the eastern sub-dome cooled below 250 °C between 20 and 15 Ma and only along its margin, in the immediate footwall of the Katschberg normal fault the ages become younger (Figure. II.7b).

Apatite fission-track ages are systematically younger than zircon fission-track ages (Figures. II.7 and II.8). Within the western sub-dome of the Tauern Window, apatite fission-track ages display younger ages in the core of the sub-dome and older ages toward the north and the south (Most, 2003). As for the zircon ages, apatites from the Granatspitz area are younger than those from the rest of the Tauern Window (Figure. II.8).

Between the Jaufen and the Meran Maul faults, apatite ages, are similar to the ones of the western sub-dome of the Tauern Window as observed for the zircon ages. They cluster around 8.2±1.7 Ma and 17.2±2.4 Ma (Pomella, 2010; this study), but in contrast to zircon fission track ages no clear age jump is observed across the DAV fault. Apatite ages range between 9 and 15 Ma both in the Austroalpine units south of the DAV and in the basement of the Dolomites indenter (Figure. II.8), indicating that the DAV did not play an active role in the exhumation of the Austroalpine units during Late Miocene. Apatite ages also show a marked discontinuity across the Brenner fault, where ages pass from around 10 Ma in the footwall, to more than 28 Ma in the hangingwall (Figure. II.8). In contrast, no age jump is observed across the northern boundary of the Tauern Window (Figure. II.8).

II.4.3. Cross-sections

In order to highlight the relationship between the major tectonic structures and possible age discontinuities and trends, zircon and apatite fission track ages are plotted along an nearly E-W striking cross section striking parallel to the central axis of the entire Tauern Window (Figure. II.9a) and along NNW-SSE cross-section striking across the western sub-dome (Figure. II.9b). Due to the insufficient density of samples on the eastern sub-dome, especially for the zircon fission tracks, we do not show a section across the latter area. The first cross-section strikes parallel to the extension direction and to the main axial planes of the upright folds in the western and eastern sub-domes (Figure. II.9a). The second cross-section is perpendicular to the main axial plane of the upright fold (Figure. II.9b).

In the cross-sections, the distributions of zircon and apatite fission track ages follow similar trends (Figure. II.9). Age distributions along the E-W cross-section older zircon and apatite fission track ages in the eastern sub-dome and younger ages in the core of the Tauern Window, i.e. in the Granatspitz area (Figure. II.9a).

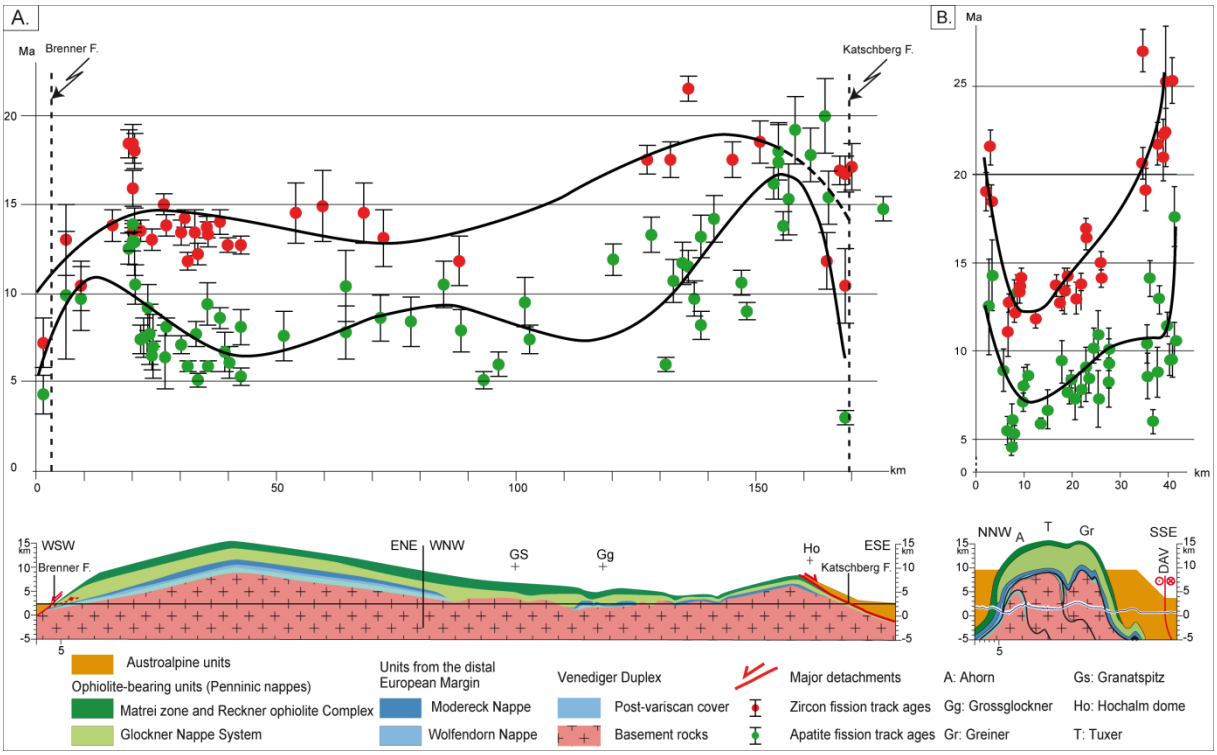

Figure II. 9. Zircon and apatite fission-track age distribution along a. a cross-section parallel to the main axial plane of the folds through the Tauern Window (See location of the cross section on Figure. II.2) and b. a N-S cross-section through the western sub-dome of the Tauern Window (See location of the cross section A in Figure. II.2. Ages were projected perpendicular to the cross-section from a distance of up to 5 km from each part of the cross-section trace. Cross section cross sections are based on Schmid et al., 2013).

A progressive younging from the central part of the window to its borders is not observed. In contrast a bell shape with older ages towards the margins is observed. However, ages are significantly younger in the areas immediately bordering the Brenner and the Katschberg extensional faults (Figure. II.9a). Along the NNW-SSE cross-section, the age versus distance diagrams display a bell shape for both the zircon and apatite fission track ages, with younger ages located in the hinge of the fold (Figure. II.9b), resembling that of (Figure. II.4b).

II.4.4. Exhumation and cooling rates

Based on paired samples providing both zircon and apatite fission-track ages, we determined cooling rates for 91 samples from the Tauern Window and surrounding areas (Figure. II.10), for the temperature interval comprised between the closure temperature of zircon and apatite fission tracks. In the eastern sub-dome only four samples were suitable for the analysis of both apatite and fission-track ages, hence a general pattern of exhumation rates in map view for this area cannot be assessed and we only show cooling rates of the western sub-dome and its surrounding Austroalpine units (Figure. II.10). For the units of the Tauern Window and the Austroalpine units, north of the DAV fault, cooling rates correspond to the Miocene and Pliocene times. In spite of local differences, all samples of the western Tauern

Window provide cooling rates higher than 20 °C.Ma^{-1} (Figure. II.10) and the cooling-rate ditribution is relatively symmetric about the ENE-striking trace of the Tauern Dome, but strongly dominated by two local maxima (Figure. II.10). One is centred in the middle part of the Brenner fault, close to the hinge of the Tauern dome (Figure. II.10), where tectonic omission across this normal fault is a maximum (Rosenberg and Garcia, 2012). The other maximum is located in the core of the Tauern Window, also along the hinge of the Tauern antiform (Figure. II.10). The maximum in the west could be attributed to the combine activity of the Brenner fault and an erosional component due to folding. The easternmost maximum is located in an area that is difficult to relate to any specific structure expected to cause enhanced exhumation. The NW-strike of contour lines in the easternmost part of the figure is an artefact due to the lack of data in this area.

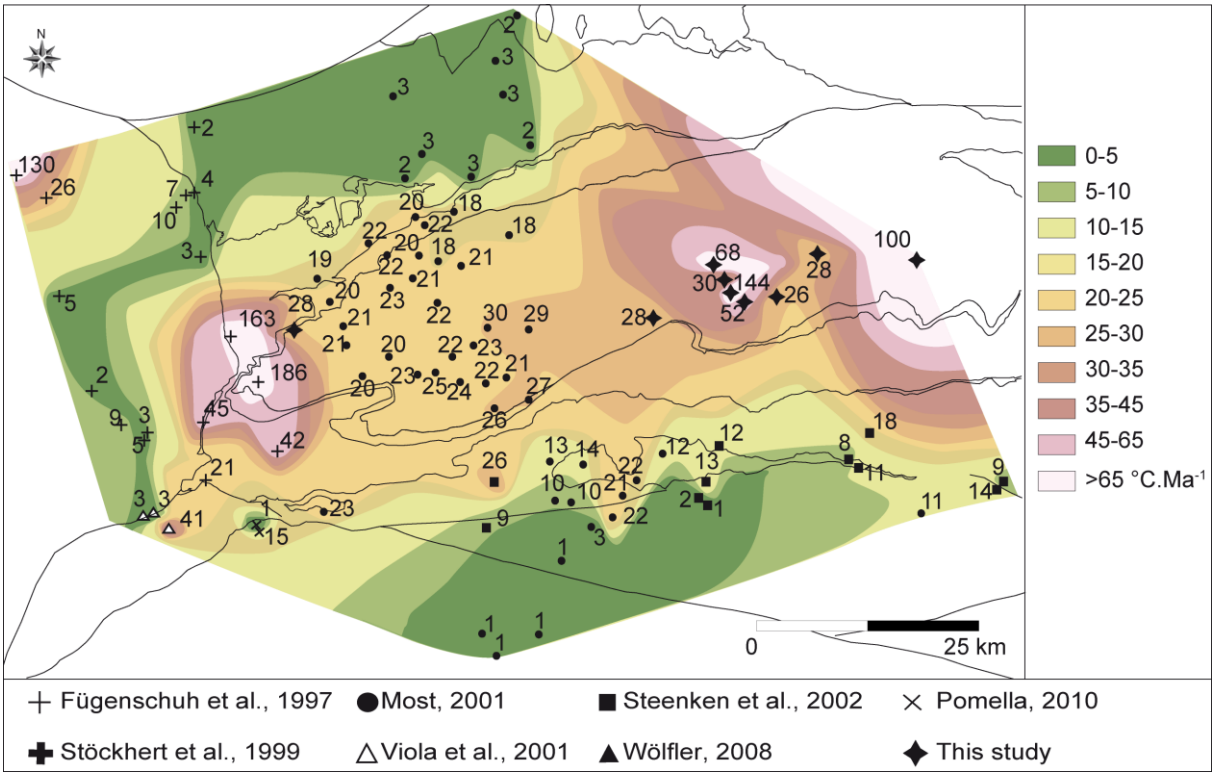

Figure II. 10. Cooling rates (in °C.Ma^{-1}) based on paired samples yielding both zircon and apatite fission track ages.

Exhumation rates could be deduced from cooling rates by assuming a given paleo-geothermal gradient. However, thermal models (chapter IV, this study) suggest that the geothermal gradient varied from one part of the Tauern Window to the other. For rocks that cooled at gradients higher than 10 °C.Ma^{-1} (ie. 0.3 mm.yr^{-1}) a linear regression of age/elevation relationships (Fitzgerald and Gleadow, 1988) can be used to determine exhumation rates if the correlation between fission-track ages and sample elevation is good enough, i.e. if the regression line passes through a maximum of data points (Gallagher et al., 1998). Age/elevation relationships provide reliable exhumation rates because they do not require any assumptions on the geothermal gradient nor on the closure temperatures (e.g.

Soom, 1990). Figure. II.11 shows the exhumation rates derived from age/elevation relationships for several areas where good linear correlations were found. Such relationships, calculated from apatite fission-track ages show that exhumation rates along the central axis of the Tauern Window were in the order of 0.5 to 1.0 mm.yr-1 (Figure. II.11; see also Grundmann and Morteani, 1985; Staufenberg, 1987; Most, 2003). Assuming that these rates were maintained until the present times, and considering that the temperature of the apatite PAZ, (60-120 °C; Gleadow and Duddy, 1982; Wagner and Van den Haute, 1992), corresponding to depths of 3 to 6 km (Braun et al., 2006), the time required to exhume the youngest samples (4-5 Ma; Figure. II.8a) from these depths to the present-day surface level closely coincides with their fission-track age. This suggests that their exhumation terminated in very recent time, and that the process may still be active at similar rates.

As noted previously (Most, 2003), the topographic wavelength of the valleys in the study area is probably insufficient to deflect the 110 °C isotherm corresponding to the closure temperature of the apatite fission-tracks. Therefore, the differences in zircon and apatite fission-track ages reflect different cooling histories due to local differences in the tectonic activity, hence in the timing, and/or amounts and rates of exhumation.

Exhumation rates in the Austroalpine units south of the Tauern Window are in the order of 0.1 to 0.2 $mm.yr^{-1}$ (Figure. II.11; Staufenberg, 1987; Steenken et al. 2002). During Miocene time the Austroalpine units south of the Tauern Window and North of the DAV were exhumed together with the units of the Tauern Window (Figures. II.7 and II.8) at similar rates than those in the southern part of the western sub-dome of the Tauern Window (Figure. II.11), suggesting that doming was not limited to the Tauern Window. This conclusion is consistent with the large-scale antiformal structure (Figure. II.2) that affects both the Tauern Window and its neighbouring Austroalpine units in the south.

Exhumation rates are rather homogeneous in the eastern sub-dome (Figure. II.11), whereas they vary in the western sub-dome, where rocks located along the central axis of the dome underwent higher exhumation rates compared to rocks along the northern and southern borders (Figure. II.11). This observation is consistent with the different geometries of the two sub-domes (Figure. II.2). The eastern one displays a plateau-type geometry (Figure. II.2) suggesting more homogeneously distributed uplift rates, whereas the western one (Figure. II.2) is characterized by higher amplitude and shorter wavelength, suggesting increasing uplift rates towards the hinge of the fold.

Mean exhumation rates derived from zircon age/elevation relationships are 0.24 $mm.yr^{-1}$ and 0.25 $mm.yr^{-1}$ (Figure. II.11) in the eastern and western sub-domes, respectively, suggesting that during Early Miocene times, the western and eastern sub-domes were exhumed at similar rates. Mean exhumation rates given by apatite ages are 0.16 $mm.yr^{-1}$ and 0.46 $mm.yr^{-1}$ in the eastern sub-dome and western sub-domes, respectively (Figure. II.11), indicating that later exhumation rates slowed down in the eastern sub-dome but increased in the western sub-dome. These data are an independent evidence for the existence of higher uplift rates in the western sub-dome.

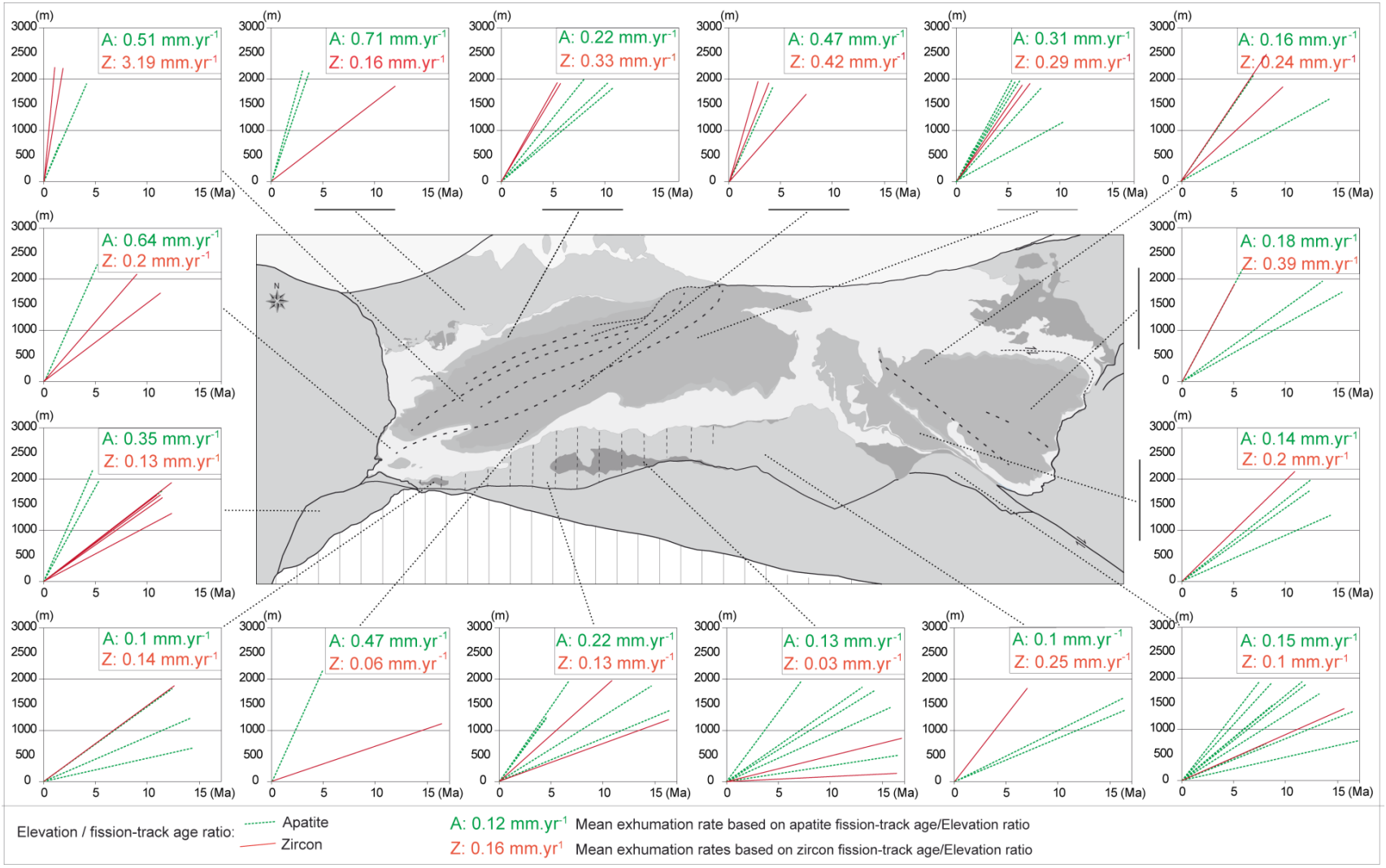

Figure II. 11. Exhumation rates (mm.yr^{-1}) determined from age/elevation relationships.

Excepted for one locality, in the hinge of the Tuxer antiform (Figure. II.11) exhumation rates are low, generally ≤ 0.5 mm/yr. If these rates are assumed to represent an average exhumation over the past 15 Ma, they can explain a maximum of 7.5 km of exhumation. In the western subdome, where ~20 km of exhumation may be inferred on the base of cross-sections (Figure. II.2), at least 40 Ma would be required in order to attain the present-day level of exposure. Such a time interval is by far longer than the one suggested in the literature on the base of different, independent, geological evidence (Schmid et al., 2013). As a consequence, exhumation rates in the time interval constrained by fission track ages of the Tauern Window must have been lower than in previous stages (Oligocene, Early Miocene) of the exhumation history.

II.5. Discussion

On the first order, the iso-age contours of zircon and apatite fission-tracks ages (Figures. II.7b and II.8b), show similar distributions: an elongate E-W trend, approximately following the outer shape of the Tauern Window that can be subdivided into three main domains, each of them characterized by a local minimum in the fission-track ages (hinge of the western sub-dome, Granatspitz area, and the easternmost part of the eastern sub-dome Figures. II.7b and II.8b).

The young ages found along the Brenner and the Katschberg faults (Figure. II.9a) suggest that these structures were still active during Pliocene times. However, especially in the case of the Katschberg Fault, the 3 Ma age is not associated to progressive younging of ages in the footwall when moving towards the fault plane. This age distribution suggests a late reactivation of the fault, rather than a significant exhumation event at 3 Ma. Progressive younging would be expected if extensional denudation associated to exhumation paths parallel to the normal fault plane (Figure. II.4) would have dominated unroofing of the Tauern Window. Natural examples of similar age patterns are described from metamorphic core complexes exhumed by extensional denudation (e.g., Foster and Raza, 2002). In contrast, what we observe is a rather flat age distribution (Figure. II.9a), which, on the scale of the entire dome, becomes older towards the extensional faults, and only decreases within the mylonitic belt of the latter faults (Figure. II.9a). This does point to the young activity of the faults.

In the western sub-dome, the orientation of the elongate and concentric iso-age contours (Figures. II.7b and II.8b) of zircon and apatite ages is sub-parallel to both the axial plane of the upright fold of the western sub-dome and the isograds of Barrowian metamorphism (Figure. II.3). The NNW-SSE cross-section (Figure. II.9b), shows that the youngest zircon and apatite fission-track ages are located in a broad zone corresponding to the core of the western sub-dome (Figure. II.9b), characterized by higher exhumation rates (Figure. II.11). This suggests that the cooling pattern of the western sub-dome, hence its cooling-age

distribution in map view, is primarily related to the formation of the upright fold (Figure. II.2), which forms the western Tauern dome. This fold also explains the elongate concentric pattern of the isograds, related to the Barrowian metamorphic event (Figure. II.3). Late deformation of the isograds by the upright folding event, or, contemporaneous upright folding and bending of the isotherms would result in such a pattern.

Because the Jaufen fault dips to the northwest with ca. 45°, the jump from Cretaceous ages Northwest of the Jaufen fault to Miocene ages southeast of the fault (Figure. II.7) was interpreted to reflect a normal sense of movement (Viola et al., 2001). Rocks southeast of the Jaufen fault have been sufficiently buried to erase older ages and have later been exhumed from a depth of around 10 km in the past 15 Ma (Viola et al., 2001). According to zircon and apatite fission track ages it is clear that the block southeast of the Jaufen fault was exhumed coevally with the Tauern Window, indicating that exhumation along the Jaufen and the Brenner faults occurred simultaneously, hence suggesting that the Jaufen fault may represent the termination of the Brenner fault as previously stated (Selverstone 1988).

The outward increase of fission-track ages within the western sub-dome (Figures. II. 7b, II.8b and II.9b) could result from higher exhumation rates within the central part of the sub-dome during amplification of folding. Rocks from the core of the antiform, stem from greater depth compared to the limbs, hence they were uplifted and exhumed at higher rates, and passed later through the PAZ. This explains their younger ages, as illustrated by 2D-thermal models of shortening accommodated by folding (Batt and Braun; 1997; chapter IV, this study), which predict that age of thermochronometers sampled at the eroded surface in a section parallel to convergence, form a bell shape in a distance-age diagram (Figure. II.4b; Batt and Braun, 1997; chapter IV, this study). The bell shapes of chronometers with highest closing temperature have higher amplitude and shorter wavelength with respect to the bell shapes of the lower-temperature chronometers (Batt and Braun, 1997; chapter IV, this study). These observations are in accordance to the distribution of zircon and apatite fission track ages across the western sub-dome of the Tauern Window (Figure. II.9b) indicating that the present-day cooling pattern of the western sub-dome is primarily related to the upright folding event.

The E-W age profile (Figure. II.9a) indicates a tendency for the eastern sub-dome to have cooled earlier than the western one (Figure. II.9a). Considering that cooling is the result of exhumation that brings the rocks to pass through the closure temperature, it was suggested that unroofing of the eastern sub-dome terminated earlier than unroofing of the western sub-dome (Dunkl et al., 2003; Luth and Willingshoffer, 2008; Scharf et al., 2013). These interpretations consider the age variations of thermochronometers at the surface as the expression of lateral temperature gradients. However, as shown by thermal models of folding designed to simulate the western sub-dome of the Tauern Window (chapter IV, this study), material points exhumed in the hinge of the antiform stem from deeper crustal levels

compared to the limbs, and hence they were uplifted at higher rates. Therefore, they passed later through PAZ of a given geochronometer. The same is true for material points located in the hinge of an antiform of high amplitude compared to those located in the hinge of a fold of low amplitude that underwent smaller amounts of shortening during the same time interval. The amplitude of the fold and the amount of shortening in the western sub-dome are higher than in the eastern sub-dome (Schmid et al., 2013; Figure. II.2). Therefore the younger ages of the western sub-dome may not result from an earlier exhumation of the eastern subd-dome (Luth and Willingshoffer, 2008; Scharf et al., 2013) but rather from faster exhumation of the western sub-dome during one and the same, coeval folding event, which affected both the western and eastern sub-domes. Our interpretation, which relies on lateral changes of uplift rates rather than on dramatic, horizontal temperature gradients, is consistent with lateral changes in the style of large-scale folding of the Tauern Window and with the results of thermal models (chapter IV, this study) showing that folding of the eastern Alpine crust does fold the isotherms, but never to such a degree, that it could explain lateral age differences observed in the Tauern Window. Significant gradients of uplift rates must be taken into account to explain such differences. Moreover, higher but coeval exhumation rates in the western sub-dome can easily be linked to larger scale tectonic processes of the Eastern Alps, such as the northward movement of the south-alpine Indenter, which is delimited by the straight, ESE-striking Periadriatic fault (Figure. II.1). An earlier interruption of shortening in the eastern Tauern Window, in order to explain older fission track ages is at odd with the continuous straight boundary of the Dolomite Indenter south of the Tauern Window. On the other hand, a westward increase of shortening, leading to a westward increase of uplift rates accommodating vertical thickening is documented by the following structures: (1) the amplitude of upright folds in the western subdome is higher by ca 10 km compared to the eastern sub-dome (Figure. II.2); (2) the width of the Austroalpine units south of the Tauern Window decreases progressively westward and this change of width is associated to tightening of upright folds in the Austroalpine, hence to an increase of shortening; (3) The Oligocene Periadriatic line was straight and E-W striking before being sinistrally offset by the Giudicarie fault, during Tertiary times, accommodating the northward movement of the southalpine Indenter (e.g., Laubscher 1971; Schmid et al. 1996; Schmid and Kissling 2000; Pomella, 2010). The change from its E-W strike to the present-day ESE-strike reflects a clockwise rotation of the Dolomites Indenter (Figure. II.12), leading to progressively larger northward displacement toward the indenter corner, hence progressively larger amounts of shortening westward in the area north of the indenter (Figure. II.12). Because the indenter moves as a coherent block, the larger northward displacement in the west occurs during the same time, but at higher rates than the smaller displacements in the east. This leads to progressively higher uplift rates in the western sub-dome of the Tauern window than in its eastern sub-dome.

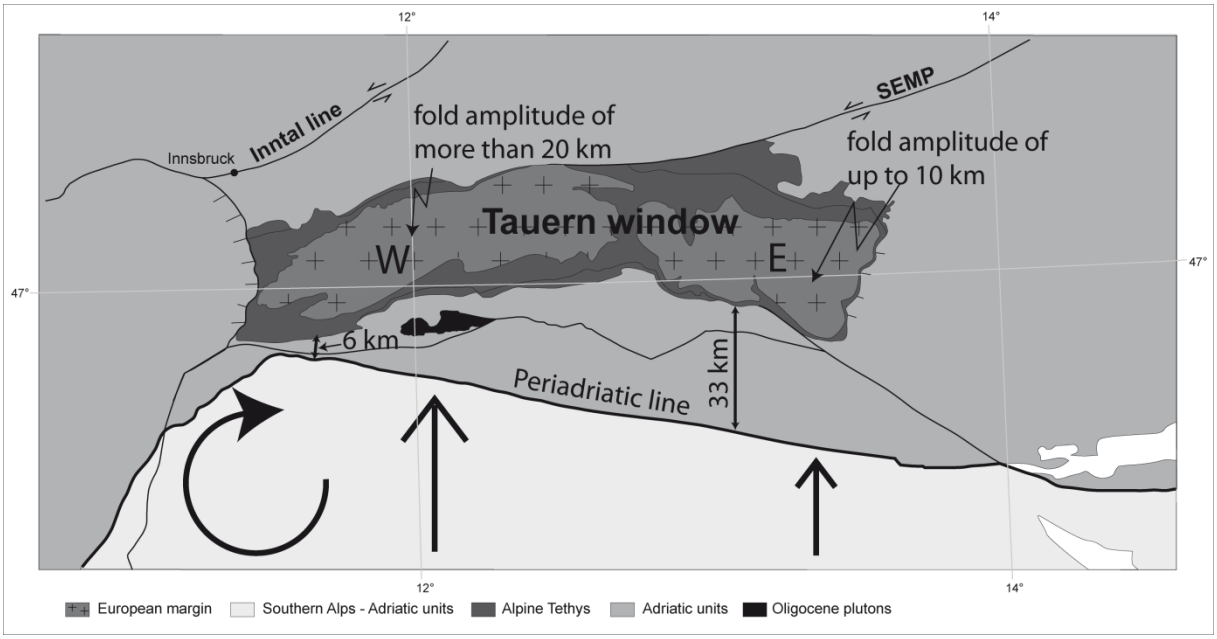

Figure II. 12. Simplified sketch map of the Eastern Alps illustrating a clockwise rotation of the Dolomites Indenter. Shortening is increasing westward; fold amplitude and uplift rates are higher in the western sub-dome of the Tauern window (W) that in its eastern sub-dome (E).

Conclusion

Compilations of previous and new zircon and apatite fission track ages provide a complete picture of the distribution of cooling ages over the Tauern Window and surrounding areas. In particular, the new zircon ages in the central Tauern Window allowed us to trace for the first time iso-age contour maps, linking the western and the eastern sub-domes.

The spatial coincidence between the antiformal structure and the bell shape of fission track ages on age/distance diagrams and the absence of large-scale younging from the sub-domes toward the major normal faults at the dome margins, suggest that upright folding and erosion were the major processes controlling exhumation of the Tauern dome, hence the cooling and the age distributions, at the time span given by zircon and apatite fission track ages, i.e during Miocene and Pliocene. However, on the smaller scale (10 km), abrupt younging of both zircon and apatite fission track ages occurs at the transition from the footwall to the mylonitic zones of the Katschberg and Brenner Normal Fault systems. This attests of a young and probably contemporaneous activity of the latter structures.

The previously described concentric iso-age pattern, elongated subparallel to the hinge of the western sub-dome for both zircon and apatite ages, corresponds to the expected age distributions resulting from antiformal folding. The older history of the Tauern Window, constrained by zircon fission-track ages, is marked by fast exhumation of the western sub-dome during early Miocene times with faster rates in the hinge of the upright antiform. At the same time, exhumation of the lower amplitude, flat-lying hinge area of the eastern dome occurred at lower rates. The younger history of exhumation, i.e. < 12 Ma, constrained by

apatite ages, indicates that a decrease of exhumation rates occurred in the eastern part of the Tauern Window while the western sub-dome was still being exhumed at high rates. The spatial, more homogeneous distribution of uplift rates in the eastern sub-dome compared to the increasing uplift rates towards the hinge of the western sub-dome is consistent with the plateau-type geometry of the former and the high-amplitude of the latter. The generally older ages and slower exhumation rates calculated for this sub-dome compared to the western one may be interpreted as the result of lower uplift rates during folding. Higher rates in the west may lead to younger cooling ages than in the east, even if folding terminated at the same time in both sub-domes. This interpretation is consistent with the idea of a single shortening and folding event in the Tauern Window, accommodating one and the same indentation process of the Dolomites indenter. As visible in map view, the relative displacement of the indenter probably increased westward causing higher amounts of shortening, higher exhumation rates, hence younger cooling ages. These relationships suggest a clockwise rotation of the Dolomite indenter and a control of upright folding on Miocene-Pliocene exhumation in the Tauern Window.

References

Batt, G. and Braun, J., 1997. On the thermomechanical evolution of compressional orogens. Geophys. J. Int., Vol. 128, p. 364-382.

Behrmann, J. H., 1988, Crustal-scale extension in a convergent orogen: The Sterzing-Steinach mylonite zone in the Eastern Alps. Geodynamica Acta, 2, 63-73.

Berner, H., Hamberg, H., and Stephansson, O., 1972. Diapirism in theory and experiment: tectonophysics, 15, 197-218.

Borsi, S., Del Moro, A., Sassi, F., 1973. Metamorphic evolution of the Austridic rocks to the south of the Tauern Window (Eastern Alps): radiometric and geopetrological data. - Mem. Soc. Geo. It., 12, 549-571.

Borsi, S., Del Moza, A., Sassi, F., Zanferrari, A. and Zirpoli, G. 1978. New geopetrologic and radiometeric data on the alpine history of the Austridic continental margin South of the Tauern window (Eastern Alps). Memorie dell'Istituto della Regia Universitá di Padova 32, 1–20.

Bousquet, R., Oberhänsli, R., Goffé, B., Wiederkehr, M., Koller, F., Schmid, S.M., Schuster, R., Engi, M., Berger, A. and Martinotti, G. 2008. Metamorphism of metasediments in the scale of an orogen: A key to the Tertiary geodynamic evolution of the Alps. In: Siegesmund, S. et al. (Eds.): Tectonic Aspects of the Alps-Dinarides- Carpathians system. Geological.

Braun, J., van der Beek, P., and Batt, G., 2006. Quantitative thermochronology. Cambridge University Press, pp. 258.

Brun, J.P., Van Den Driessche, J., 1994. Extensional gneiss domes and detachment fault-systems: structure and kinematics. Bulletin de la Société Géologique de France, 165, 519–530.

Burg, J.P., Klaus, B.J.P. and Podladchikov, Y.Y., 2004. Dome structures in collision orogens: Mechanical investigations of the gravity/compression interplay. In: Whitney, D.,

Teyssier, C., Siddoway, S. (eds.), Gneiss domes in orogeny: The Geological Society of America, Special Paper 380, 47-66.

Christensen, J. N., Selverstone, J., Rosenfeld, J. L. and DePaolo, D. J., 1994. Correlation by Rb- Sr geochronology of garnet growth histories from different structural levels within the Tauern Window, Eastern Alps. - Contrib. Mineral. Petrol., 118, 1-12.

Coney, P.J., 1980. Cordilleran metamorphic core complexes: An overview, in Crittenden, M.D, Coney, P.J., and Davis, G.H., eds., Cordilleran metamorphic core complexes : Boulder, Colorado, Geological Society of America Memoir 153, 7-34.

Coney, P.J. and Harms, T.A., 1984. Metamorphic core complexes: Cenozoic extensional relics of Mesozoic compression. Geology 12, 550-554.

Coyle, D.A, 1994. The application of apatite fission-track analysis to problem in tectonics. PhD thesis, La Trobe University, Bundoora, Victoria.

Cornelius, H.P., 1940. Zur Auffassung der Ostalpen im Sinne der Deckenlehre. Zeitsch. Deutsch. Geol. Ges., 92, 271-312.

Crittenden, M. D., Coney, P. J. and G. H. Davis (Eds.), 1980. Cordilleran Metamorphic Core Complexes, Geol. Soc. Am. Mem., 153, 490 pp.

Di Fiore, G., 2013. Evoluzione Morfotettonica delle aree alpine „Sempione“ e “Brennero“ attraverso studi termocronologici di bassa temperatura. Tesi di Dottorato, Università di Bologna, 2013.

Dunkl, I., 2002. TRAKKEY: a Windows program for calculating and graphical presentation of fission-track data. Comput. Geosci., 28, 3–12.

Dunkl, I., Frisch, W., and Grundmann, G., 2003. Zircon fission-track thermochronology of the south-eastern part of the TW and the adjacent Austroalpine margin, Eastern Alps. Eclogae geol. Helv., 96, 209-217.

Eskola, P.E., 1949. The problem of mantle gneiss domes: Geological Society of London, Quaterly Journal, 104, 253-283.

Fitzgerald, P.G and Gleadow, A.J.W, 1988. Fission-track geochronology, tectonics and structure of the transantartic Mountains – Nucl. Tracks 17, 351-357.

Foeken, J.P.T., Persano, C., Stuart, F. M. and ter Voorde, M. 2007. Role of topography in isotherm perturbation: Apatite (U-Th)/He and fission-track results from the Malta tunnel, Tauern Window, Austria. Tectonics, 26.

Foster, D. A., Schafer, C., Fanning, M.C., and Hyndmann D. W., 2001, Relationships between crustal partial melting, plutonism, orogeny, and exhumation: Idaho-Bitterroot batholith. Tectonophysics, 342, 313-350.

Foster, D. A. and Raza A., 2002. Low-temperature thermochronological record of exhumation of the Bitterroot metamorphic core complex, northern Cordilleran Orogen. Tectonophysics, 349, 23-36.

Frisch, W., Kuhlemann, A., Dunkl, I., and Brügel, A., 1998. Palinspastic reconstruction and topographic evolution of the Eastern Alps during late Tertiary tectonic extrusion. Tectonophysics, 297, 1-15.

Frisch, W., Dunkl, I., and Kuhlemann, J., 2000. Post-collisional orogen-parallel large-scale extension in the Eastern Alps. Tectonophysics, 327, 239-265.

Fügenschuh, B., Seward, D. and Mantckelow, N. S., 1997. Exhumation in a convergent orogen: the western Tauern Window. Terra Nova, 9, 213-217.

Gallagher, K., Brown, R. and Johnson, C., 1998. Fission-track analysis and its applications to geological problems. Annu. Rev. Earth Planet. Sci., 26, 519-572.

Genser, J. and Neubauer, F., 1989, Low angle normal faults at the eastern margin of the TW (Eastern Alps). Mitteilungen der Österreichische Geologische Gesellschaft, 81, 233-243.

Gleadow, A.J.W., 1981. Fission-track dating methods: what are the real alternatives? Nucl. Tracks, 5, 3-14.

Gleadow, A.J.W., and Duddy, I.R., 1982. A natural long-term annealing experiment for apatite. Nuclear Tracks Radiation Experiments, 5, 169-174.

Glodny, J., Ring, U., Kühn, A., Gleissner, P. and Franz, G., 2005. Crystallization and very rapid exhumation of the youngest Alpine eclogites (Tauern Window, Eastern Alps) from Rb/Sr mineral assemblage analysis, Contrib. Mineral. Petrol., 149, 699 – 712.

Glodny J., Ring, U. and Kühn A., 2008. Coeval high-pressure metamorphism, thrusting, strike-slip, and extensional shearing in the Tauern Window, Eastern Alps, Tectonics, 27, TC4004.

Green, P.F., Duddy, I.R., Gleadow, A.J.W., Tingate, P.R., Laslett, G.M., 1986. Thermal annealing of fission tracks in apatite. 1. A qualitative description. Chemical Geology (Isotope Geoscience Section), 59, pp. 237-253.

Green, P.F., Duddy, I.R., Laslett, G.M., Hegarty, A.J.W., Gleadow, A.J.W., and Lovering, J.F., 1989. Thermal annealing of fission-tracks in apatite. 4. Quantitative modeling techniques and extension to geological timescales. Chemical Geology (Isotope Geoscience Section), 79, 155-182.

Grundmann, G., and Morteani, G., 1985. The young uplift and thermal history of the central Eastern Alps (Austria/Italy), evidence from apatite fission-track ages. Jahrbuch der Geologischen Bundesanstalt, 128, 197-216.

Handy, M. and R. Oberhänsli, 2004. Age of the Metamorphic Structure of the Alps - Tectonic Interpretation and Outstanding Problems. In: Explanatory Notes to the Map: Metamorphic Structure of the Alps. edited by R. Oberhänsli. Mitteilungen der Österreichischen Mineralogischen Gesellschaft, 149, 97-121.

Handy, M.R., Schmid, S.M, Bousquet, R., Kissling, E. and Bernoulli, D., 2010. Reconciling plate-tectonic reconstructions of Alpine Tethys with the geological–geophysical record of spreading and subduction in the Alps. Earth-Science Reviews, vol. 102; issues 3-4, 121–158.

Hoernes, S. and Friedrichsen, H., 1974. Oxygen isotope studies of metamorphic rocks of the Western Hohe Tauern Area (Austria). SMPM 54, 769-788.

Hoinkes, G. Koller, F., Rantitsch, G., Dachs, E., Hock, V., Neubauer, F. and Schuster, R., 1999. Alpine metamorphism of the Eastern Alps. Schweizerische Mineralogische und petrographishe Mitteilungen 79, 155-181.

Hurford, A.J. and Green, P.F., 1983. The zeta age calibration of fission-track dating. Chem. Geol., 41, 285-317.

Inger, S. and Cliff, R.A., 1994. Timing of Metamorphism in the Tauern Window, Eastern Alps: Rb-Sr ages and fabric formation: J. met. Geol.12, 695-707.

Jolivet, L., Famin, V., Mehl, C., Parra, T., Avigad, D. and Aubourg, C., 2004. Progressive strain localisation, crustal-scale boudinage and extensional metamorphic domes in the Aegean Sea, American Geological Society, Special Paper 380: Gneiss Domes in Orogens, 185–210.

Kleinschrodt, R., 1987. Quarzkorngefügeanalyse im Altkristallin südlich des westlichen Tauernfensters (Südtirol/Italien). - Erlanger geol. Abh., 114, 1-82, Erlangen.

Kuhlemann, J., Frisch, W., Dunkl, I., Székely, B., 2001. Quantifying tectonic versus erosive denudation: The Miocene core complexes of the Alps.- Tectonophysics, 330, 1-23.

Lammerer, B., 1988. Thrust-regime and transpression regime tectonics in the Tauern Window (Eastern Alps), Geol. Rundsch., 77, 143-156.

Laubscher, H.P.V., 1971. Das Alpen-Dinariden-Problem und die Palinspastik der südlichen Tethys. International Journal of Earth Sciences, 40, 813-833

Laubscher, H.P., 1988. Material balance in Alpine orogeny. Geol. Soc. America, Bull., 100, 1313-1328.

Linzer, H.-G., Decker, K., Peresson, H., Dell'Mour, R., and Frisch, W., 2002. Balancing orogenic float of the Eastern Alps: Tectonophysics, 354, 211-237.

Luth, S.W., and Willingshofer, E. 2008. Mapping of the Post-Collisional Cooling History of the Eastern Alps. Swiss Journ. Geosci. 101, Sup1., 201-223.

Mancktelow, N. and Pavlis, T.L., 1994. Fold-fault relationships in low-angle detachment systems. Tectonics, 13, 668-685.

Most, P., 2003, Late Alpine cooling histories of tectonic blocks along the central part of the Transalp-Traverse (Inntal-Gadertal): constraints from geochronology. PhD Thesis.

Neubauer, F., Genser, J., Kurz, W. and Wang, X., 1999. Exhumation of the TW, Eastern Alps: Physics and chemistry of the Earth, ser. A, 24, 675-680.

Nollau, G., 1969. Kleintektonische Struktur en am Südrand des Tauernfensters und ihre Einbeziehung in großtektonische Konzepte. - Geol. Rundsch., 58. 755-788, Stuttgart 1969.

Oberhänsli, R. Bousquet, R., Engi, M., Goffé, B., Gosso, G., Handy, M.R., Höck, V., Koller, F., Lardeaux, J.-M., Polino, R., Rossi, Ph., Schuster, R., Schwartz, St., Spalla, 2004. Metamorphic structure of the Alps. Scale 1:1.000.000, Commission for the Geological Map of the World, Paris.

Osmundsen P.T. and Andersen, T.B., 2001. The middle Devonian basins of western Norway: sedimentary response to large-scale transtensional tectonics? Tectonophysics, 332, 51-68.

Parrish, R.R., 1983. Cenozoic thermal evolution and tectonics of the Coast Mountains of British Columbia, 1, Fission-track dating, apparent uplift rates, and patterns of uplift, Tectonics, 2, 601– 631.

Pomella, H., 2010. The Cenozoic evolution of the Giudicarie fault system (Eastern/Southern Alps, northern Italy) A geochronological, structural and paleomagnetic study. PhD thesis, Innsbruck, April 2010.

Ramsay, J.G., 1967. folding and fracturing of rocks : New York, McGrawHill, 568p.

Reddy, S.M., Cliff, R.A. and East, R., 1993. Thermal history of the Sonnblick Dome, South-East Tauern window, Austria: Implications for heterogeneous uplift within the Pennine basement. Geol. Rdsch. 82, 667-675.

Reiners, P.W., and Brandon, M. T., 2006. Using thermochronology to understand orogenic erosion. Annu. Rev. Earth. Planet. Sci. 34:419–66

Rosenberg, C.L., and Berger, A., 2009. On the causes and modes of lateral growth of the Alps. Tectonics 28, issue 6, TC6001.

Rosenberg, C.L., and Garcia, S., 2011. Estimating displacement along the Brenner fault and orogen parallel extension in the Eastern Alps. Int. J. Earth. Sci., 100, p.1129–1145.

Rosenberg, C.L., and Garcia, S., 2012. Reply to the comment of Fügenschuh et al. on the paper 'Estimating displacement along the Brenner Fault and orogen-parallel extension in

the Eastern Alps' by Rosenberg and Garcia, Int J Earth Sci (Geol Rundsch) 100:1129–1145. Int. J. Earth. Sci., 101, p.1457-1464.

Rosenberg, C. L., Brun, J.-P., and Gapais, D., 2004. An indentation model of the Eastern Alps and the origin of the Tauern Window. Geology, 32, 997-1000.

Rosenberg, C.L., Brun, J.P., Cagnard, F., and Gapais, D., 2007. Oblique indentation in the Eastern Alps: Insights from laboratory experiments. Tectonics, Vol. 26, TC2003.

Scharf, A., Handy, M.R., Favaro, S. ,Schmid, S. and Bertrand, A., 2013. Modes of orogen-parallel stretching and extensional exhumation in response to microplate indentation and roll-back subduction (Tauern Window, Eastern Alps). Int. J. Earth Sci. (Geol Rundsch.), 102, 1627-1654.

Schmid, S.M. and Kissling, E., 2000. The arc of the Western Alps in the light of geophysikal data on deep crustal structure. Tectonics, 19, 62-85.

Schmid S.M., Pfiffner O.A., Froitzheim N., Schönborn G. and Kissling E., 1996. Geophysical-geological transect and tectonic evolution of the Swiss-Italian Alps. Tectonics, 15, 1036-1064.

Schmid S. M., Scharf, A., Handy, M.R., Rosenberg, C.L, 2013. The Tauern Window (Eastern Alps. Austria): a new tectonic map, with cross-sections and a tectonometamorphic synthesis. Swiss J. Geosci., 106, 1-32.

Selverstone, J., 1988. Evidence for East-West crustal extension in the eastern Alps: implications for the unroofing history of the Tauern Window. Tectonics, 7, 87-105.

Selverstone, J., Franz, G., Thomas, S., Getty, S., 1992. Fluid variability in 2 GPa eclogites as an indicator of fluid behavior during subduction. Contributions to Mineralogy and Petrology 112, 341–357.

Soom, M. A., 1990. Abkühlungs- und Hebungsgeschichte der Externmassive und der penninischen Decken beidseits der Simplon-Rhone-Linie seit dem Oligozän: Spaltspurdatierungen an Apatit/Zirkon und K-Ar-Datierungen an Biotit/Muskowit (westliche Zentralalpen). PhD thesis, Universität Bern.

Staufenberg, H., 1987. Apatite fission-track evidence for postmetamorphic uplift and cooling history of the eastern Tauern Window and the surrounding Austroalpine (Central Eastern Alps, Austria). Jahrbuch der Geologischen Bundesanstalt, 130, 571-586.

Steenken, A., Siegesmund, S., Heinrichs, T., and Fügenschuh, B., 2002. Cooling and exhumation of the Rieserferner Pluton (Eastern Alps, Italy/Austria). International Journal of Earth Sciences, 91, 799–817.

Tagami, T., and Shimada, C., 1996. Natural long-term annealing of the zircon fission track system around a granitic pluton. J. Geophys. Res. 101, 8245-8255.

Termier, P. 1903. Les nappes des Alpes orientales et la synthèse des Alpes. Bull. Soc. Géol. France IVe Ser., vol. 3, 711-766.

Thöni, M., 1999. A review from geochronological data from the Eastern Alps, Schweizerische Mineralogische und petrographische Mitteilungen 79, 209-230.

Viola, G., Mancktelow, N. S. and Seward, D., 2001, Late Oligocene-Neogene evolution of Europe-Adria collision: New structural and geochronological evidence from the Giudicarie fault system (Italian Eastern Alps). Tectonics, 20, 999-1020.

Wagner GA. 1979. Correction and interpretation of fission-track ages In Lectures in Isotope Geology, ed. E Jaeger, JC Hunziker, 170 77. Berlin: Springer-Verlag.

Wagner, G. A., and Van den Haute, P., 1992. Fission-track dating: Dordrecht; Boston, Kluwer, 285 p.

Wagner, G.A., Coyle, D.A., Duyster, J., Henjes-Kunst, F., Peterek, A., Schröder, B., Stöckhert, B., Wemmer, K., Zulauf, G., Ahrendt, H., Bischoff, R., Hejl, E., Jacobs, J., Menzel, D., Nand Lal, P., Van den haute, P., Vercoutere, C., Welzel, B., 1997. Post-Variscan thermal and tectonic evolution of the KTB site and its surroundings. Journal of Geophysical Research 102, 18,221-232.

Wernicke, B., 1985. Uniform-sense normal simple shear of the continental lithosphere. Can. J. Earth Sci. 88, 108-125

Wölfler, A., Dekant, C., Danisìk, M., Kurz, W., Dunkl, I., Putis, M. and Frisch, W., 2008. Late stage differential exhumation of crustal blocks in the central Eastern Alps: evidence from fission-track and (U–Th)/He thermochronology. Terra Nova, 20, 378–384,

Yamada, R., Tagami, T. Nishimura, S. and Ito H., 1995. Annealing kinematics of fission-tracks in zircon: an experimental study. Chem. Geol. 122, 249-258.

Yin, A., 1989. Origin of regional, rooted low-angle normal faults: a mechanical model and its tectonic implications. Tectonics, 8, 469-482.

Yin, A, 2004. Gneiss domes and gneiss dome systems. In Whitney, D.L., Teyssier, C. and Siddoway, C.S., eds., Gneiss dome and orogeny : Boulder, Colorado. Geological Society of America Special Paper 380, p.1-14

Zaun P.E., and Wagner G.A., 1985. Fission-track stability in zircons under geological conditions. Nuclear Tracks, 10, 303–307.

Chapter III. Fault slip analysis and late exhumation of the Tauern Window

Fault slip analysis and late exhumation of the Penninic units of the Tauern Window, Eastern Alps

Audrey Bertrand[1], Claudio Rosenberg[2] and Sebastian Garcia[1]

1. Department of Tectonics and sedimentology, Freie Universität Berlin, Malteserstraße 74-100, 12449 Berlin, Germany
2. ISTEP, Université Paris 06-UPMC, 75252 Cedex 05 PARIS, France

Abstract

Exhumation of the Eastern Alps from the early Tertiary to the late Miocene was localized in the Tauern Window, a thermal and structural dome located in front of the Dolomite indenter. Based on new brittle structural investigations over the entire Tauern Window, stress inversions have been performed and indicate that a clear zoning of the paleostress field exists in the Tauern Window with a predominance of strike-slip state of stress in the core of the investigated area, while the eastern and western margins of the dome are dominated by extensional regimes. Few inverse fault structures have been highlighted. Since the internal structures of the Tauern Window are marked by large-scale folds with axis striking parallel to the main extension direction, we expected to measure large amount of compressive brittle structures associated to the formation of these folds. We propose at least two-stages of deformation to explain the paucity of inverse structures. During the first stage of exhumation of the Tauern Window, corresponding to the folding event, the brittle crust was probably dominated by N-S shortening and compression. The second stage of exhumation was marked by normal faulting at the margins of the dome and strike-slip faulting in the core of the study area. During the second stage, the brittle part of the crust that was previously affected by compressive structures belonging to the first stage was eroded leading to the lack of compressive structures that should be associated to the main folding event. At the same time, normal faulting associated to E-W direction of extension and taking place along the eastern and western borders of the Tauern Window was accommodated by strike-slip faulting located in the core of the Tauern Window, yielding E-W extension and N-S shortening.

III.1. Introduction

The Eastern Alps are characterized by a series of large-scale nappes (Helvetic, Austroalpine and Penninic nappes) (Termier, 1903; Dewey et al., 1989; Schmid et al., 2004) (Figure III.1), which started to be stacked during Cretaceous orogeny and were mainly exhumed during the Tertiary one. In contrast to the Western and Central Alps, this nappe stack was exhumed within a very confined area of the Eastern Alps, coinciding with the Tauern Window (Figure III.1b), where the upper and middle crust passed through the brittle-ductile transition in the Late Tertiary (Handy et al., 2010; Handy and Oberhänsli, 2004).

The Miocene to present tectonics of the Eastern Alps were marked by lateral extrusion, corresponding to the collapse of the chain and lateral escape of a crustal wedge comprised

between the Tertiary SEMP fault (Salzach-Ennstal–Mariazell–Puchberg) and the Periadriatic fault (Figure III.1) (e.g. Ratschbacher et al., 1991a; 1991b), thus explaining the present-day eastward decrease of topography in the Eastern Alps (Frisch et al., 1999).

Recent GPS measurements in the Eastern Alps (e.g. D'Agostino et al., 2005; Reiter et al., 2005; Caporali et al., 2013) and the records of seismic activity of the past century (Reiter et al., 2005) indicate that the Eastern Alps are still tectonically active (Reinecker and Lehnhardt, 1999; Reiter et al., 2005) and that eastward motion is still present East of the Tauern Window (Caporali et al., 2013). Areas of enhanced seismic activity seem to be bounded by fault systems that were already active in the Early Miocene, as for instance the Brenner fault (Reiter et al., 2005; Rosenberg and Garcia, 2011) (Figure III.1), and the SEMP fault (Reinecker and Lehnhardt, 1999) (Figure III.1). In contrast, the area characterized by the greatest exhumation in the Mid- to Late Miocene, i.e. the Tauern Window (Figure III.1), was hardly affected by seismic events in the past century (Reinecker and Lehnhardt, 1999). This might point to the termination of tectonic activity, or continuation of activity in a distributed, aseismic mode.

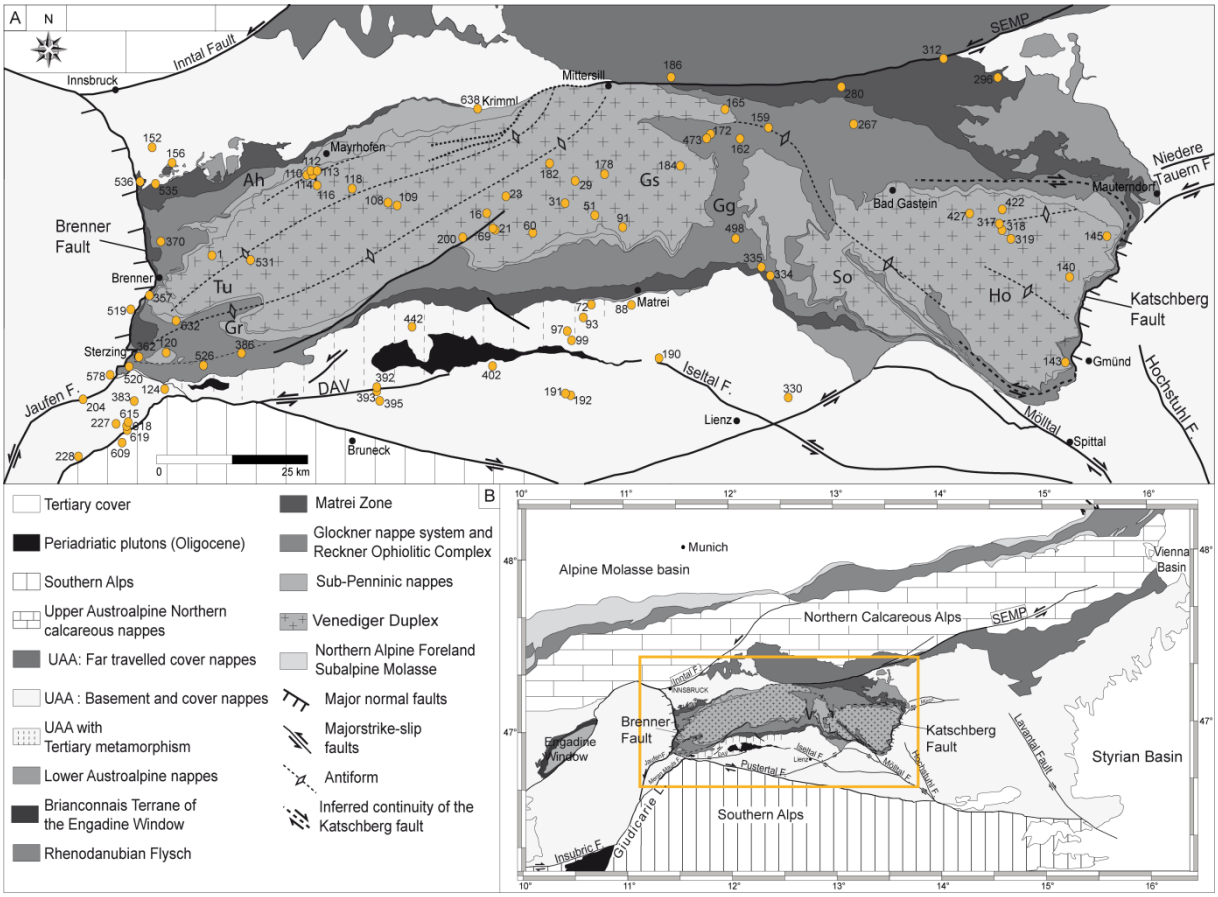

Figure III. 1. A. Simplified tectonic map of the Tauern Window. SEMP: Salzach-Ennstal–Mariazell–Puchberg Fault; DAV: Defereggen-Antholz-Vals Fault; Ah: Ahorn Kern; Tu: Tuxer Tal; Gg: Grossglockner; Gr: Greiner; Gs: Granatspitz; So: Sonnblick dome and Ho: Hochalm dome. Orange dots: location of outcrops with numbers referring to the tensors numbers in table 1) -Map modified after Schmid et al., 2013. B. Eastern Alps and location of the studied area (rectangle) -Map modified after Bigi et al., 1990

The seismic events and GPS data have not yet been related to specific, kinematically-constrained fault systems, known to have been active in the Late Miocene. Attempts to link the present-day seismicity and displacements inferred from GPS data to the well-investigated Early Miocene tectonics (Behrmann, 1988; Selverstone, 1988; Neubauer et al., 1999; Ratschbacher et al., 1989; 1991b; Peresson and Decker, 1997; Linzer et al., 2002) need to fill the information gap existing between the Miocene ductile structures of the Tauern Window and the present-day displacements. In order to do so, we investigate the orientation and sense of shear of brittle structures in the Tauern Window, which can be used to assess the strain and stress orientation during and after the Miocene orogenic history of the Eastern Alps. Miocene cooling of the Eastern Alps was mostly localized within the Tauern Window, whereas its surrounding areas cooled below 300°C during Cretaceous times (Oberhänsli et al., 2004). Zircon fission track ages date the cooling of rocks below 230 ± 20 °C (Hurford, 1986; Zaun and Wagner, 1985), a temperature that is below, but, within error, overlapping with the inferred brittle-ductile transition temperature, in quartz (Stipp et al., 2002). Therefore, in spite of several processes (e.g., fluid pressure, high strain rates) that may expand the brittle field to higher temperatures and as a first approximation, we consider that it is legitimate to interpret the brittle structures in the Tauern Window as contemporaneous as or younger than the zircon fission track ages of the rocks in which they are enclosed.

In the western sub-dome of the Tauern Window, zircon fission track ages vary from 17 ± 1 Ma along the northern and southern margins and are around 13 ± 1 Ma in the axial zone (Figure III.2). In the eastern part of the Tauern Window, zircon fission track ages cluster around 17 ± 1 Ma (Figure III.2), whereas along the Katschberg fault, zircon fission track ages are around 13 ± 1 Ma. Moreover, based on compilation of geochronological data sets of shear zones (Glodny et al., 2008), it has be shown that ductile deformation continued until 15 Ma, hence during the entire retrograde metamorphic history of the Tauern Window. These data thus put an upper limit on the age of the brittle deformation.

Therefore we infer that the brittle structures measured within the Tauern Window are all of Tertiary age, varying from the Late Miocene in the axial zone to the Early Miocene and Oligocene in the adjacent Austroalpine regions (Figure III.2). Since the rest of the Eastern Alpine rocks cooled below 300 °C in the Cretaceous (Oberhänsli et al., 2004), independent evidence is needed to distinguish brittle deformations belonging to the Cretaceous orogeny from those belonging to the Tertiary one.

Localization of deformation and exhumation mechanisms of the Tauern Window are the subject of an on-going debate centred on the relative importance of two distinct mechanisms: folding associated with erosion (Cornelius, 1940; Laubscher, 1988; Lammerer, 1988; Behrmann, 1988; Rosenberg et al., 2004; 2007; Rosenberg and Garcia, 2011; 2012) versus extensional unroofing located along the normal fault systems bordering the dome at its western and eastern margins (Ratschbacher et al., 1989; Axen et al., 1995; Neubauer et al., 1999; Fügenschuh, et al., 1997; 2012; Frisch et al., 1998; 2000; Kuhlemann et al., 2001; Linzer et al., 2002; Genser and Neubauer, 1989; Wang and Neubauer, 1998).

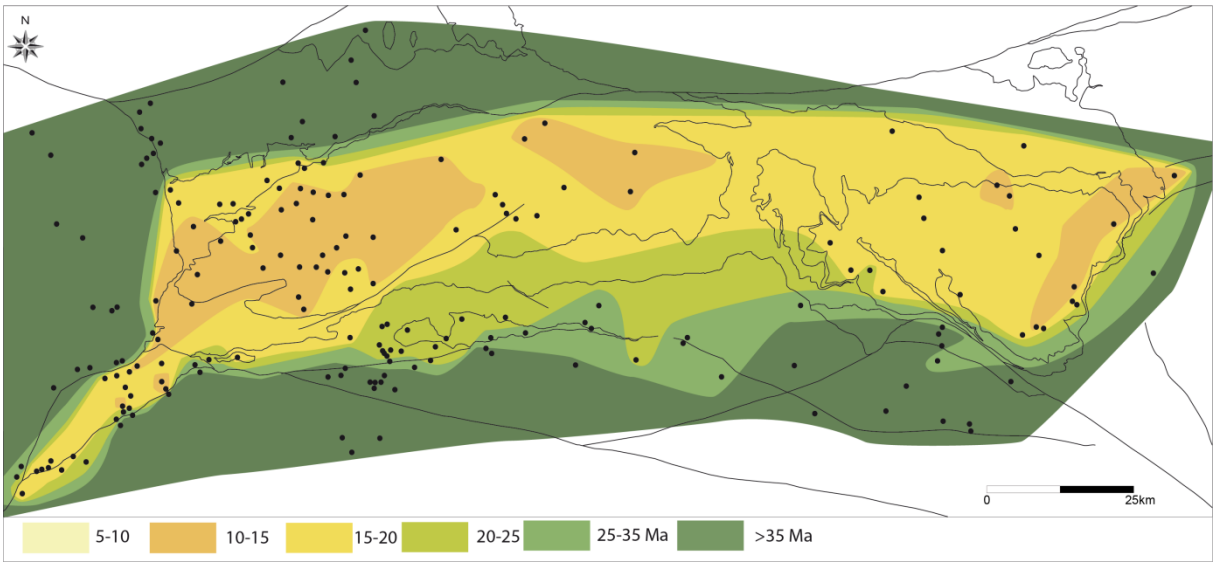

Figure III. 2. Map of zircon fission track ages within the Tauern Window and surrounding areas (See chapter II, this study). Ages are from Dunkl et al., 2003; Fügenschuh et al., 1997; Most, 2003; Pomella, 2010; Steenken et al., 2002; Stöckhert et al., 1999; Viola et al., 2001; Wölfler et al., 2008 and this study).

Previous works, emphasizing the role of extensional unroofing, are mainly focused on the western and eastern margins of the Tauern Window, where two N-S striking normal-fault systems, i.e. the Brenner and the Katschberg faults (Figure III.1a) are inferred to have largely, or even entirely exhumed the Penninic rocks of the Tauern Window (Axen et al., 1995; Neubauer et al., 1999; Fügenschuh, et al., 1997; Frisch et al., 1998; 2000; Kuhlemann et al., 2001; Linzer et al., 2002; Selverstone, 1988; Behrmann, 1988; Genser and Neubauer, 1989; Wang and Neubauer, 1998). Many authors suggest that E-W directed extension and exhumation of the metamorphic dome were coeval with indentation of the Adriatic plate during the Miocene. Based on analogue experiments, Ratschbacher et al. (1991a) propose a model in which the Early and middle Miocene tectonics of the Eastern Alps are controlled by lateral extrusion, which they define as the combination of extensional collapse of a thickened crust and lateral escape of materiel flowing toward the east. Orogen-parallel extension is inferred to be driven either only by the retreat of the plate boundary in the outer Carpathians (Royden, 1993) or by a combination of N-S compression driven by the Adriatic indenter (Ratschbacher et al., 1991a) and eastward retreat of the subducted slab below the Carpathians (Decker et al., 1993; Peresson and Decker, 1997).

The extensional displacements that occurred along the normal faults bordering the dome are often inferred to have been translated into strike-slip movements along E-W striking faults at the northern and southern borders of the area (Peresson and Decker, 1997; Frisch et al., 1999; Wang and Neubauer, 1998; Linzer et al., 2002; Scharf et al., 2013). For instance, the sinistral offset of 60-70 km that was estimated along the E-W trending SEMP fault (Linzer et al., 2002) (Figure III.1a) are inferred to be accommodated by an analogous extensional displacement along the Brenner fault (Linzer et al., 2002; Scharf et al., 2013).

Historically, exhumation of the Tauern Window was mainly discussed on the base of ductile structures (Selverstone, 1988; Behrmann, 1988; Genser and Neubauer, 1989) and of brittle structures that nucleated in a crustal segment that mainly behaved as a ductile medium (Axen et al., 1995; Selverstone et al., 1995). In contrast, only few studies investigate brittle deformations formed in the uppermost part of the crust within the Tauern Window (Kurz et al., 1993; Wang and Neubauer, 1998; Reiter et al., 2005; Decker and Reiter, 2006) and these studies are limited to small areas adjacent to the eastern and western margins of the dome.

A systematic investigation of brittle structures throughout the entire Tauern Window is the object of the present work. In addition to the kinematic analysis of brittle structures, we define the associated paleostress fields to determine the occurrence of extension and/or compression during the last stages of exhumation of the Tauern Window.

III.2. Tectonic overview on brittle deformation of the Tauern Window

Previous investigations on the brittle tectonics of the Tauern Window were mainly focused on the eastern and western margins, i.e. along the Katschberg (Genser and Neubauer, 1989; Kurz et al., 1993) and the Brenner Normal Fault systems (Axen et al., 1995; Wawrzyniec et al. 2001; Reiter et al., 2005; Decker and Reiter, 2006), where brittle structures mainly formed in response to extensional deformation. In the following we summarize these studies.

III.2.1. Western Tauern Window

The western border of the Tauern Window, marked by the Brenner normal fault, juxtaposes mid-crustal metamorphic Penninic rocks of the Tauern Window against upper crustal non-metamorphic Austroalpine units (Figure III.1). The Brenner fault is a low-angle, west-dipping normal fault, active since the Early Miocene (Selverstone, 1988; Fügenschuh et al., 1997). It is a N-S structure that can be followed from Sterzing to Innsbruck (Figure III.1) and is divided into a ductile part of the Brenner fault and brittle normal faulting. The ductile part of the Brenner fault is a low-angle (15° to 40°) WSW-dipping normal shear zone (Selverstone, 1988; Axen et al., 1995; Fügenschuh et al., 1997; Behrmann, 1988; Wawrzyniec et al., 2001) marked by a mylonitic zone of more than 200 m (Selverstone, 1988). The mylonitic zone is overprinted by a WSW-dipping normal brittle fault that is marked by several-meters thick cataclasite with a foliation dipping of 10 to 70° towards the SW (Selverstone, 1988). Mylonitic foliations and stretching lineations consistently dip toward the WSW (Axen et al., 1995; Selverstone, 1988).

Two main sets of ductile to brittle structures have been highlighted in the footwall of the Brenner normal fault. The first set consists of brittle and ductile sub-vertical fault planes showing west-dipping inverse and normal sense of shear. The second set is characterised by east-down, normal dip-slip brittle-ductile structures (Axen et al., 1995; Selverstone, 1995; Wawrzyniec et al., 1995). Fluid inclusions show that west-down structures formed at depth of

12-23 km and at temperatures higher than 400 °C (Selverstone et al., 1995), while fluid inclusions on east-down structures give lower temperatures of formation of 250-400 °C and shallower depths of 2-10 km (Selverstone et al., 1995). These datasets highlight the existence of a time span between the formation of the west-down and east-down structures, which is explained by a model of two rolling hinges (Axen et al., 1995). In this model, the footwall would first be affected by west-down structures, which form the lower hinge, and later by the east-down structures that form in the upper hinge. Axen et al. (1995) assume a low intensity of deformation in the upper hinge and a penetrative mylonitization in the lower hinge. Moreover, the steep late mylonitic foliation and younger mylonitic foliations of the Brenner fault are also deformed into WSW plunging anticlinal and synclinal folds (Axen et al., 1995). Such deformation at the vicinity of a detachment fault would result in the formation of fold sets with two main orientations; one is perpendicular to the detachment and the other one is parallel to it. The folds parallel to the fault are assumed to be due to buoyancy forces (Spencer, 1984) whereas the perpendicular folds are supposed to be related to perpendicular shortening, which is contemporaneous with and perpendicular to the extension direction (Mancktelow and Pavlis, 1994). Perpendicular and parallel folds are due to a migration of the rotation towards the footwall as it is progressively unroofed in response to buoyancy forces that accommodate the normal movement of the Brenner fault (Selverstone et al., 1995). In that case, subvertical simple shearing is assumed to accommodate the deformations of the footwall (Selverstone et al., 1995).

Rolling hinge models allow for higher amounts of horizontal extension in comparison with normal faults without a rolling hinge. Indeed, after the formation of a normal fault in the upper crust, the isostatic response to normal faulting induces a rotation of the structure, the fault is thus flattened and another steep normal fault can be formed (Axen et al., 1995). This model suggests that extension is entirely accommodated by normal faulting and that extension is the leading process during unroofing of the footwall of the Brenner fault (Axen et al., 1995; Wawrzyniec et al., 1995). By calculating the mean value between the dip of the foliation and the ramp dip, Axen et al. (1995) estimate that the dip angle of the rolling hinge of the Brenner fault is of 25°. The authors thus propose that the formerly estimated displacement of ~10-20 km (Behrmann, 1988; Selverstone, 1988; Selverstone et al., 1995) along the Brenner fault is under-estimated and they suggest a horizontal component of 33-63 km. However, the offset of the Brenner fault is still a matter of debate and the total displacement is assumed to be either around 10-20 km (Behrmann, 1988; Selverstone, 1988), 44 km (Fügenschuh et al., 2012), 70 km (Fügenschuh et al., 1997), or only of 2-14 km (Rosenberg and Garcia, 2011; 2012). The later assume that most of the vertical offset observed along the Brenner normal fault is due to folding and erosion of the footwall contemporaneous with the activity of the fault (Rosenberg and Garcia, 2012).

Based on GPS data and focal mechanisms of earthquakes, Reiter et al. (2005) postulated present-day NNW-directed shortening combined with E-W extension along the Brenner normal fault. The earthquake epicentres along the Brenner fault are scattered in an area, which

extends 15 km west of the Brenner fault and their depth increases toward the west (Reiter et al., 2005) suggesting that the Brenner fault is still active and that it is a moderately W-dipping active normal fault. The movement is slow (0.5 to 1 $mm.yr^{-1}$) (Reiter et al., 2005) and the geometry is similar to the Miocene one. Focal mechanisms indicate that E-W extension occurs along W to WSW dipping normal faults whereas N-S compression is taking place along E-W trending thrusts (Reiter et al., 2005).

III.2.2. Eastern Tauern Window

The eastern Tauern Window forms a dome composed by moderately E to SE-dipping units (Genser and Neubauer, 1989). The low-angle normal Katschberg fault system (Wang and Neubauer, 1998; Genser and Neubauer, 1989; Kurz et al., 1993; Scharf et al., 2013) marks the eastern limit of the Tauern Window, where the mid crustal Penninic rocks are juxtaposed to the upper crustal Austroalpine units (Figure III.1a). The horizontal stretch achieved by the Katschberg normal fault system is estimated between 17.3 km (Genser and Neubauer; 1989) and 23-29 km (Scharf et al., 2013). The Katschberg fault is a low-angle ductile fault marked by a mylonitic zone of several kilometres thickness (Scharf et al., 2013). Orientations of lineations and sense of shear criteria indicate ESE-directed downthrown of the upper plate across the fault zone (Genser and Neubauer, 1989; Scharf et al., 2013).

The north-western border of the eastern Tauern Window is marked by the E-W trending sinistral SEMP (Salzach-Enns-Mariazell-Puchberg) fault that juxtaposes Austroalpine units to Penninic units (Figure III.1a). The SEMP is steeply dipping toward the north (Wang and Neubauer, 1998) and its sinistral offset is estimated to 60-70 km (Linzer et al., 2002). West of Mittersil, its westward ductile continuation has been shown to terminate in a sequence of NE to ENE-trending sinistral, steeply dipping shear-zones, in the interior of the Tauern Window (Behrmann and Frisch, 1990; Rosenberg and Schneider, 2008) along which S-side-up movements accommodated the uplift of the Tauern dome (Rosenberg and Schneider, 2008).

The south-eastern border of the Tauern Dome is delimited by the dextral prolongation of the Katschberg fault system (Scharf et al., 2013) and by the brittle Mölltal fault. It is a NW-SE-trending subvertical dextral strike-slip fault that affects the Penninic units of the Sonnblick area as well as the Austroalpine units until the Periadriatic line (Figure III.1a). A dextral displacement of up to 30 Km (Kurz and Neubauer, 1996) is estimated along this structure.

D1	- NNW faults with ENE reverse slickenside lineations - NNE-trending dextral faults - Right-lateral en-echelon subvertical NE-trending extensional sulphid bearing quartz-veins	Compression 
D2	- NE-SW to E-W sinistral strike-slip faults along the SEMP fault - N-S dextral strike-slip faults along the Mölltal fault - NNE-SSW trending veins filled by muscovite, chlorite, quartz and sulphide-bearing minerals - Subvertical SE-NW trending strike-slip faults	Strike-slip 
D3	- Steeply-plunging NE-SW normal faults along the SEMP fault - NNE-SSW low-angle normal faults along the Mölltal fault	Extension 
D4	- E-W dextral shear striation and N-S sinistral shear striae	Compression 
D5	- Conjugate joints with vertical acute angle bisectors - Cataclasitics and fault gouges concentrated in the lower Austroalpine units - NNE-SSW normal faults	Extension 

Figure III. 3. The inferred brittle deformations phases of the eastern Tauern Window (Based on Genser and Neubauer, 1989; Wang and Neubauer, 1998; Kurz et al., 1993; Kurz and Neubauer, 1996)

Based on field measurements of brittle deformation along the SEMP, the Katschberg and Mölltal faults, five, kinematically distinct brittle stages of deformation were described (Figure III.3; Kurz et al., 1993; Wang and Neubauer, 1998; Genser and Neubauer, 1989).

At the north-western edge of the Mölltal fault and along the central part of the Katschberg fault, the oldest brittle deformations consist of subvertical NE-trending sulphide-bearing quartz veins organised in right-lateral, en-échelon structures and NNE-trending veins that have been filled by muscovite, chlorite, quartz and sulphide-bearing minerals (Kurz et al., 1993). These veins seem to occur within the same state of stress with ENE-trending slickensides indicating reverse sense of shear along the SEMP and dextral shearing along NNE-trending fault planes (Wang and Neubauer, 1998). The computation of these striae

indicates that the first brittle deformation event along the SEMP is a compressive one with NE-SW-trending subhorizontal σ_1 and subvertical σ_3. It is associated to a phase of compression oriented NE-SW (Wang and Neubauer, 1998) (Figure III.3). Crystallisation within the veins indicates that these brittle structures can have been formed within the ductile domain due to high fluid pressure (Kurz et al. 1993). Therefore these brittle deformations were assumed to have occurred simultaneously with brittle-ductile, low angle NNE-trending normal faulting that has been observed in the lower crustal level (Genser an Neubauer, 1989). The brittle veins and the brittle-ductile normal faults are inferred to be linked to the north-eastward movement of the South Alpine indenter (Wang and Neubauer, 1998; Kurz et al., 1993).

The second set of brittle deformation is characterised, along the SEMP, by gently west-plunging striae showing a sinistral sense of shear and minor N-S, subhorizontal striae showing a dextral sense of shear along the Mölltal fault (Wang and Neubauer, 1998). In this area, deformations are characterised by conjugate low-angle NNE-trending normal faults (Kurz et al., 1993) or by subvertical SE-NW trending fault surfaces associated with subhorizontal striae and Riedel fractures. Inversion of these brittle structures highlights in both cases a second deformation phase formed within a transcurrent paleostress field, compatible with a NNE-SSW subhorizontal σ_1 stress axis and a subhorizontal ESE-WNW σ_3 (Kurz et al., 1993; Wang and Neubauer, 1998). This stage of deformation is the main one along the SEMP (Wang and Neubauer, 1998) (Figure III.3).

The third set of brittle deformations along the SEMP displays subvertical striae indicating a normal sense of shear and an increase of the deformation towards the western part of the SEMP (Wang and Neubauer, 1998). Faults of the Mölltal area are filled with chlorite, calcite and quartz mineralization indicating that a high quantity of fluids was involved during this brittle deformation stage. This high hydrolytic pressure could have decreased the strength of the orogenic crust and lead to the formation of brittle structures within the ductile domain. A permutation from a strike-slip to an extensive regime may result from a permutation between σ_1 and σ_2 stress axes (Kurz et al., 1993). The third brittle phase may thus be an extensional to transcurrent one, resulting from a SE-NW subhorizontal σ_3 stress axis and a subvertical σ_1 (Kurz et al., 1993; Wang and Neubauer, 1998) (Figure III.3).

The fourth set of striae consists of E-W trending dextral faults and N-S trending sinistral ones measured along the SEMP fault system (Wang and Neubauer, 1998). Inversion of these striae results in a compressive paleostress field with subhorizontal NNW-SSE $\sigma 1$ orientation (Wang and Neubauer, 1998). This deformation stage has been proposed to be linked to the north-westward motion of the Adriatic indenter (Wang and Neubauer, 1998) (Figure III.3).

The last set of brittle deformations displays N-S trending, conjugate joints along the SEMP (Wang and Neubauer, 1998) as well as cataclasites and gouges associated to subvertical N-S trending joints and subvertical Riedel fractures along the Katschberg fault (Genser and Neubauer, 1989). The joints along the SEMP and the Katschberg faults are related to the latest stage of uplift, which is still active (Senftl and Exner, 1973; Reiter et al.,

2005). It indicates a mode III of fracturation associated to a paleostress field displaying vertical σ_1 and ESE-WNW subhorizontal σ_3 stress axes (Kurz et al., 1993; Wang and Neubauer, 1998) (Figure III.3).

III.3. Data acquisition and method of fault slip analysis

A total of 1740 brittle structures were measured over 172 localities (Figure III.1a) in the Tauern Window and additionally, in the Austroalpine units surrounding the Tauern Window. Most of the measured data are lineations and associated striated fault planes, but also veins, joints, Riedel planes. Particular attention was given to conjugate faults. Senses of shear along the investigated brittle structures are deduced from crystallisation behind steps, rough steps along the fault planes and Riedel fractures (Petit, 1987). The studied outcrops are heterogeneously distributed throughout the Tauern Window (Figure III.1a), reflecting the heterogeneous distribution of lithologies that do not always allow for the formation of striated fault planes, in particular within basement rocks.

The studied outcrops generally consisted of rocks that were first intensely deformed under ductile conditions during subduction and nappe stacking. Therefore, the brittle structures were superposed on anisotropic, more or less intensely banded and foliated rocks. In order to assess whether rock anisotropy possibly affected the orientation of fault surfaces, the main foliation and associated stretching lineations have also been measured. However, in most cases, fault planes in the studied area do not coincide with ductile foliation or schistosity planes. This lack of systematic relationship between the orientations of ductile and brittle planes of anisotropy is illustrated in figure III.4, where the orientations of fault planes and schistosity planes are plotted for one particular outcrop. This outcrop was chosen because it is characterised by a very intense foliation. Clearly, the fault planes are not parallel to the foliation planes; hence the latter do not control the nucleation and propagation of the deformation (Figure III.4).

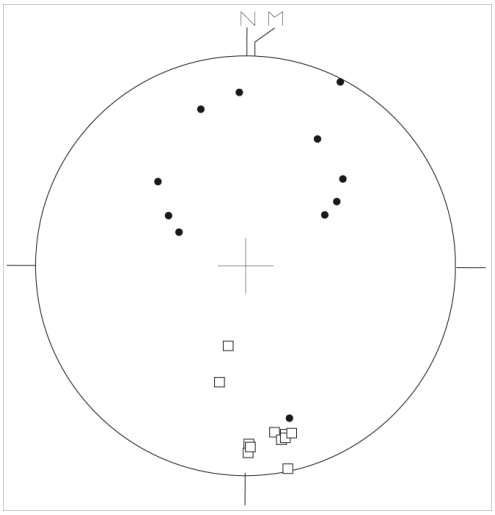

Figure III. 4. Poles of fault planes (dots) and schistosity planes (squares) measured at the outcrop 72 (see figure III.1a for its location).

Paleostress tensors associated to the measured faults are determined using the direct inversion method (Angelier, 1989, 1990), assuming that each slickenside lineation corresponds to a particular stress tensor (Carey and Brunier, 1974; Angelier, 1989). The fault plane orientations may result from neoformed fault planes or from inherited faults. The data sets are divided into groups formed during a given deformation stage and a stress tensor that best minimises the deviation between the expected and the measured slickenside lineation is defined. Calculations provide the orientations of the maximum, intermediate, and minimum principal stress axes, σ_1, σ_2, and σ_3, respectively, assuming that one of the principal stress axes is vertical (Anderson, 1942). We thus analyse the fault data using a classical routine in which the first processing is a separation between strike-slip, normal and inverse faults as they are mechanically incompatible in one and the same locality.

The calculation also gives the stress ratio $\Phi = \frac{\sigma_2 - \sigma_3}{\sigma_1 - \sigma_3}$ with $0<\Phi<1$), which defines the relative magnitudes between the three principal stress axes. Permutations of stress axes may occur during tectonic events. Indeed if Φ is equal 0 a permutation between σ_2 and σ_3 is possible whereas if Φ equals 1 a permutation between σ_2 and σ_1 may occur.

Some localities yield complex deformation patterns, with the necessity to consider several stress tensors in order to represent the complete stress field. The occurrence of different stress tensors is inferred to reflect different paleostrains that can be related to successive tectonic events. In this case, we systematically investigated the possible occurrence of structures pointing to a relative chronology, such as cross-cutting relationships between differently oriented striae, to establish a sequence of deformations. If this was not possible and if the quality of the tensor (in terms of the Andersonian criteria) could be improved by rotating a set of faults, we assumed that a tectonic event following the formation of the measured fault was responsible for tilting of the fault planes.

III.4. Results: paleostress patterns

Ninety-eight stress tensors (Table III.1) distributed over eighty-one localities (Figure III.1a) have been obtained out of the 1740 measured slickenslide lineations by the direct inversion method (Angelier, 1989). The tensors have been separated into three main groups according to the orientation of the three principal stress axes, σ_1, σ_2 and σ_3. Some outcrops (for instance site Nr. 172, Table III.1), highlight a complex deformation that does not allow one to determine a single stress tensor. In such sites, mechanical incompatibilities between the different collected data suggest a polyphase deformation that leads to the calculation of several stress states for one and the same site. Out of the 98 tensors, 60% indicate a transcurrent regime, 33% an extensional regime and only 7% a compressive one (Table III.1).

Site	Unit	Nb of fault slip data	Axis σ_1 trend / plunge	Axis σ_2 trend / plunge	Axis σ_3 trend / plunge	Φ	ANG	RUP
1	Venediger Nappe	6	116 / 69	355 / 11	262 / 17	0.8	11	7
16	Venediger Nappe	4	351 / 15	085 / 14	216 / 69	0.2	11	30
21	Venediger Nappe	13	012 / 15	243 / 68	107 / 16	0.6	9	25
21	Venediger Nappe	12	130 / 07	025 / 65	222 / 24	0.1	10	26
23	Venediger Nappe	14	325 / 03	056 / 27	229 / 62	0.3	11	37
23	Venediger Nappe	10	172 / 19	009 / 71	264 / 05	0.3	3	13
23	Venediger Nappe	4	256 / 07	151 / 65	349 / 24	0. 3	3	13
29	Venediger Nappe	6	017 / 10	230 / 78	108 / 06	0.3	10	27
29	Venediger Nappe	5	106 / 15	241 / 69	012 / 14	0.5	7	27
31	Venediger Nappe	4	346 / 21	173 / 69	077 / 02	0.4	14	33
51	Venediger Nappe	5	108 / 70	016 / 01	286 / 20	0.7	14	36
60	Venediger Nappe	7	147 / 02	246 / 79	056 / 11	0.4	10	26
60	Venediger Nappe	5	023 / 05	182 / 84	293 / 02	0.2	6	26
69	Venediger Nappe	7	207 / 01	117 / 26	299 / 64	0.1	8	31
69	Venediger Nappe	6	341 / 03	227 / 83	071 / 06	0.8	9	25
72	Upper Austroalpine	8	004 / 17	192 / 73	095 / 02	0.2	9	28
88	Upper Austroalpine	7	042 / 18	140 / 23	278 / 60	0.2	9	27
91	Venediger Nappe	4	146 / 87	318 / 03	048 / 00	0.9	8	22
93	Upper Austroalpine	9	156 / 01	050 / 87	246 / 03	0.2	7	29
97	Upper Austroalpine	8	164 / 20	338 / 70	073 / 02	0.7	7	23
99	Upper Austroalpine	13	137 / 05	293 / 85	047 / 02	0.4	9	26
99	Upper Austroalpine	6	315 / 77	155 / 12	064 / 04	0.9	12	29
99	Upper Austroalpine	5	110 / 08	223 / 70	017 / 18	0.4	7	28
108	Venediger Nappe	11	178 / 09	076 / 53	274 / 35	0.5	7	22
109	Venediger Nappe	7	111 / 03	231 / 84	021 / 05	0.4	12	34
110	Venediger Nappe	6	112 / 04	275 / 85	022 / 01	0.3	10	29
112	Venediger Nappe	26	130 / 68	395 / 21	027 / 05	0.1	11	29
112	Venediger Nappe	17	105 / 67	311 / 21	217 / 09	0.5	7	30
113	Venediger Nappe	7	020 / 07	140 / 76	289 / 12	0.4	7	26
114	Venediger Nappe	11	164 / 01	072 / 77	254 / 13	0.6	14	30
116	Venediger Nappe	13	205 / 14	338 / 71	111 / 14	0.2	10	25
118	Venediger Nappe	4	306 / 08	057 / 67	213 / 21	0.3	5	19
120	Rote Wand Modereck	6	163 / 16	343 / 75	253 / 00	0.5	5	22
124	Upper Austroalpine	4	245 / 00	154 / 81	335 / 09	0.1	9	21
143	Venediger Nappe	4	273 / 68	050 / 17	145 / 14	0.4	7	24
145	Venediger Nappe	13	228 / 66	029 / 22	122 / 07	0.3	7	23
152	Upper Austroalpine	4	228 / 65	351 / 15	087 / 21	0.7	2	22
156	Upper Austroalpine	6	226 / 67	011 / 19	105 / 12	0.8	3	16
159	Rote Wand Modereck	5	176 / 08	067 / 67	270 / 21	0.6	6	18
162	Glockner Nappe	4	267 / 10	023 / 68	173 / 20	0.6	7	29
165	Venediger Nappe	19	195 / 18	005 / 72	104 / 03	0.7	7	16
165	Venediger Nappe	9	072 / 09	324 / 63	167 / 25	0.6	9	28
172	Glockner Nappe	15	233 / 06	002 / 81	142 / 07	0.3	11	28
172	Glockner Nappe	8	192 / 06	323 / 81	102 / 07	0.4	4	11
172	Glockner Nappe	5	258 /74	105 / 15	013 / 07	0.4	4	11
178	Venediger Nappe	5	330 / 08	091 / 74	238 / 13	0.5	11	31
182	Venediger Nappe	4	019 / 09	197 / 81	289 / 00	0.4	5	26
184	Venediger Nappe	24	005 / 02	266 / 76	095 / 15	1	10	27
184	Venediger Nappe	9	034 / 01	124 / 15	302 / 75	0.1	11	35

186	Upper Austroalpine	24	234 / 70	063 / 20	332 / 03	0.5	7	21
190	Upper Austroalpine	4	013 / 17	175 / 72	281 / 05	0.5	8	28
191	Upper Austroalpine	4	327 / 10	078 / 63	232 / 25	1	9	22
192	Upper Austroalpine	4	159 / 63	014 / 23	278 / 14	0	10	27
200	Venediger Nappe	5	207 / 01	116 / 71	297 / 19	0	9	27
204	Upper Austroalpine	5	111 / 77	224 / 05	315 / 12	0.6	6	22
227	Upper Austroalpine	17	099 / 37	275 / 53	008 / 02	0.5	8	21
228	Upper Austroalpine	8	155 / 62	356 / 26	262 / 09	0.2	12	32
267	Rote Wand Modereck	15	178 / 66	033 / 20	298 / 13	0.4	8	25
280	Glockner Nappe	6	062 / 30	269 / 60	331 / 01	0.5	6	26
296	Glockner Nappe	5	250 / 70	154 / 02	063 / 10	0.4	5	31
312	Upper Austroalpine	14	250 / 71	033 / 15	126 / 11	0.5	9	31
312	Upper Austroalpine	4	045 / 02	135 / 23	311 / 67	0.8	11	28
317	Venediger Nappe	4	086 / 61	267 / 29	177 / 00	0.1	4	24
318	Venediger Nappe	8	189 / 02	070 / 65	283 / 21	0.8	5	25
319	Venediger Nappe	4	145 / 68	026 / 11	293 / 19	0.5	4	32
330	Upper Austroalpine	4	130 / 15	333 / 74	222 / 06	0.7	7	42
334	Glockner Nappe	25	029 / 04	287 / 70	121 / 20	0.4	9	31
335	Glockner Nappe	12	094 / 74	187 / 01	277 / 16	0.6	6	22
357	Rote Wand Modereck	12	129 / 75	017 / 06	286 / 14	0.9	8	24
362	Glockner Nappe	5	141 / 70	033 / 06	301 / 19	0.5	8	29
370	Glockner Nappe	7	017 / 05	263 / 80	108 / 10	0.8	4	21
383	Upper Austroalpine	5	285 / 81	072 / 07	162 / 05	0.5	7	21
386	Glockner Nappe	9	339 / 34	161 / 56	069 / 01	0.8	4	23
392	Upper Austroalpine	4	214 / 67	025 / 02	116 / 03	0.6	6	29
393	Upper Austroalpine	5	195 / 07	320 / 78	104 / 10	0.4	4	33
395	Upper Austroalpine	7	189 / 31	013 / 59	280 / 02	0.5	3	21
395	Upper Austroalpine	5	250 / 73	008 / 08	101 / 15	0.5	4	19
402	Upper Austroalpine	12	192 / 16	064 / 65	288 / 19	0.3	7	25
422	Venediger Nappe	19	170 / 64	011 / 24	277 / 08	0.2	9	25
427	Venediger Nappe	8	029 / 67	215 / 23	124 / 02	0.3	5	23
442	Upper Austroalpine	5	115 / 07	022 / 19	225 / 70	0.3	6	23
473	Glockner Nappe	13	196 / 03	011 / 87	106 / 00	0.4	8	25
498	Glockner Nappe	11	018 / 88	205 / 02	115 / 00	0.4	9	31
519	Glockner Nappe	7	194 / 65	317 / 14	052 / 20	0.2	12	35
520	Glockner Nappe	5	162 / 11	042 / 70	256 / 17	0.4	4	18
526	Glockner Nappe	12	171 / 27	345 / 63	080 / 03	0.5	5	13
531	Venediger Nappe	10	175 / 22	349 / 68	084 / 02	0.5	9	20
535	Glockner Nappe	4	082 / 73	192 / 06	283 / 16	0.5	9	24
536	Upper Austroalpine	7	360 / 85	195 / 05	105 / 01	0.5	5	18
578	Upper Austroalpine	11	186 / 11	032 / 78	277 / 05	0.8	10	27
578	Upper Austroalpine	5	192 / 75	059 / 13	326 / 12	0.8	11	33
609	Southern Alps	15	290 / 03	190 / 74	021 / 15	0.5	9	28
609	Southern Alps	7	154 / 07	285 / 79	063 / 08	0.9	12	27
615	Upper Austroalpine	8	109 / 04	201 / 30	012 / 60	0.9	8	25
618	Upper Austroalpine	5	301 / 12	185 / 64	036 / 23	0.8	7	33
619	Upper Austroalpine	4	321 / 74	167 / 14	075 / 07	0.2	10	22
632	Glockner Nappe	6	165 / 14	343 / 76	075 / 01	0.5	9	24
638	Upper Austroalpine	5	170 / 10	076 / 22	284 / 65	0.5	2	11

Table III. 1. Results of stress tensors obtained from inversion of striated faults. The Φ ratio represents the relative ratio between the principal stress axes; Φ = (σ2-σ3) / (σ1-σ3). RUP: misfit estimation ranging from 0 and 100% (good estimations are between 0 and 50%). ANG: average angle between the computed shear stress and the slip vector. See figure III.2a for location of the outcrops.

In order to visualise the orientation of the principal stress axes for the extensional and transcurrent tensors, the orientation of the principal stress axis σ_3 is plotted in rose diagrams (Figure III.5a and III.5b). For the compressive states of stress, the orientation of the principal stress axis σ_1 is plotted (Figure III.5c).

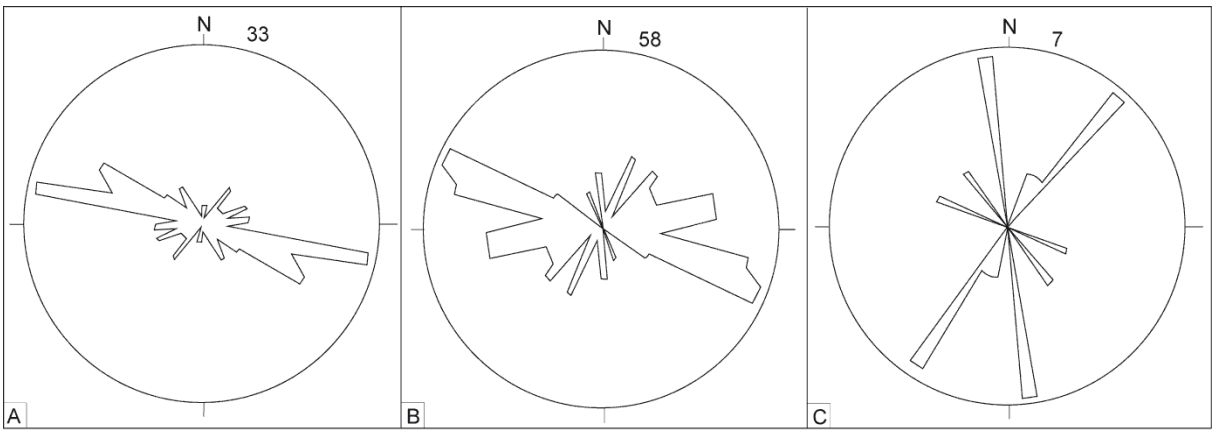

Figure III. 5. A. Orientation of σ_3 principal stress axes for the extensional regimes. B. Orientation of σ_3 principal stress axes for the transcurrent regimes. C. Orientation of σ_1 principal stress axes for the compressive regimes. In each rose diagram, the data have been separated by cluster of 10°; Numbers represent the numbers of tensors included in each rose diagrams.

Tensors belonging to extensional regimes (Figure III.5a) shows one main direction of extension comprised between N 100° and N 132°, with a maximum oriented between N100° and N 105°. Extensional regimes display a second, minor peak (Figure III.5a) that may be attributed to noise and which ranges between NNW and ENE. The rose diagram of the transcurrent regimes highlights three groups having different directions of σ_3 (Figure III.5b). In the first group, σ_3 is oriented between N 100° and N 115° with a maximum orientation between N 100° and N 105°, in the second group between N 70° and N75° and in the third group between N 20° and N 40°. Only few tensors corresponding to a compressive regime have been found, and they represent the last group with NNW to NE orientation of σ_1.

In the following, we discuss the spatial distribution of the 6 different groups of tensors. In order to simplify this description, we distinguish different areas in the Tauern Window and surrounding Austroalpine units. Firstly, we define a large area along the western border of the Tauern Window comprising the Brenner normal fault and approximately 5 km to both sides of this fault (Figure III.1a). The south-western part of the Tauern Window corresponds to the corridor of Austroalpine units located between the Jaufen and the Meran-Maul faults (Figure III.1a) and the southwestern tip of the Tauern Window. The part of the Tauern Window laterally delimited by the towns of Mayrhofen and Mittersill as well as the Austroalpine units that are located between the southern limit of the Tauern Window and the DAV fault (Figure III.1a) corresponds to the western part of the Tauern Window. The area named the core of the Tauern Window represents the central part of the dome, around the Granatsptiz area (Figure III.1a). The Sonnblick and Hochalm domes compose the eastern part of the Tauern Window.

Finally, the area along the Katschberg fault comprises the Katschberg fault including an approximately 5 km wide area on both sides of the fault defines the Katschberg fault area (Figure III.1a).

III.4.1. Transcurrent regimes

Tensors displaing a transcurrent regime are the most common ones within the Tauern Window and represent 60 % of the entire data set. The tensors of the transcurrent regimes can be separated into three different groups according to the three predominant orientations of their σ_3 principal stress axes (Figure III.5b). They are presented in the Figures III.6, III.7 and III.8.

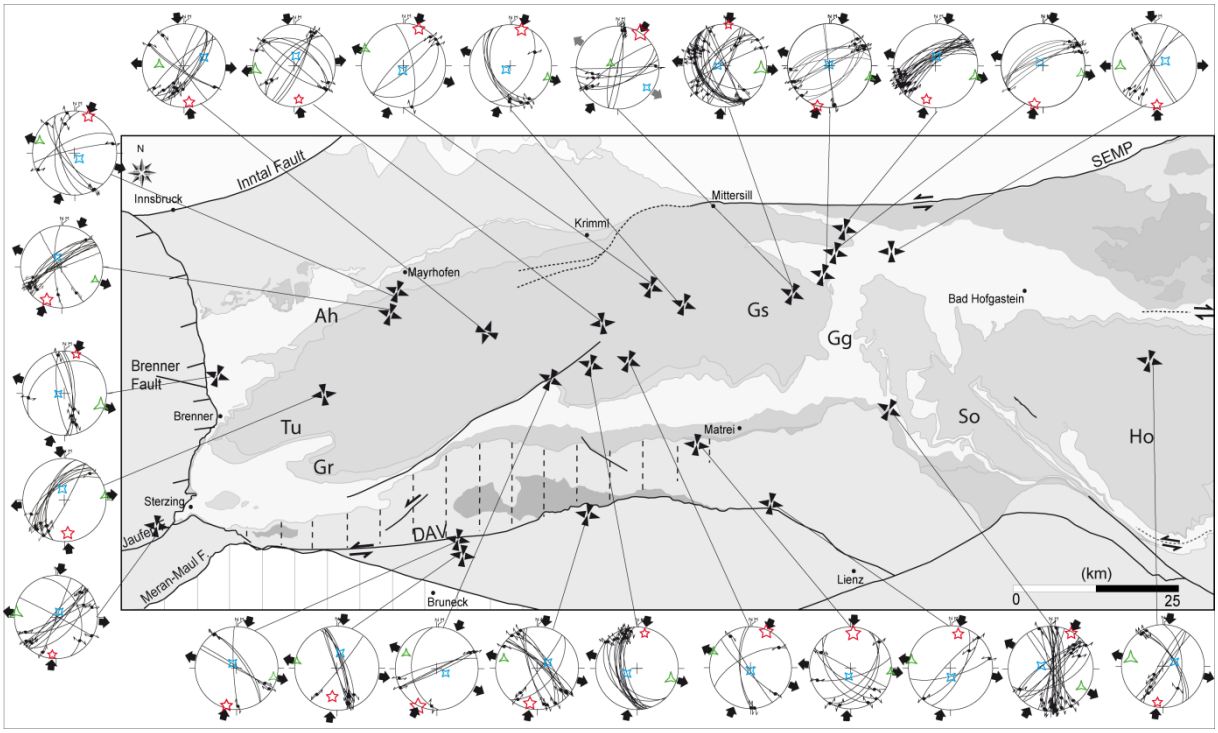

Figure III. 6. Transcurrent stress tensors with E-W to ESE -WNW trend of σ_3 (Group 1). Fault planes are represented as thin lines, slickenside-lineations as dots with arrows and extension or compression direction as large-black arrows. Single centrifugal arrows are normal faults, single centripetal arrows are inverse faults and double-left or –right arrows are sinistral or dextral strike-slip faults, respectively. The three-, four- and five-branched stars represent maximum (σ_1), intermediate (σ_2) and minimal (σ_3) stresses axes, respectively. N: geographic north; M: magnetic north. Ah: Ahorn Kern; Tu: Tuxer Tal; Gg: Grossglockner; Gr: Greiner; Gs: Granatspitz; So: Sonnblick dome and Ho: Hochalm dome

The overwhelming majority of these transcurrent tensors is located within the core and south-western parts of the Tauern Window (Figures III.6, III.7 and III.8). Outside of the Tauern Window, transcurrent paleostress regimes are found between the south-western border of the Tauern Window and the DAV fault as well as along the Meran-Mauls fault (Figures III.6, III.7 and III.8). In the eastern Tauern Window there is only one locality indicating a strike-slip tensor (Figure III.6).

43% of the transcurrent stress tensors display an EW to ESE-WNW oriented subhorizontal σ_3 (group 1, Figure III.6). These are mostly located within the previously defined central part of the Tauern Window as well as in the Austroalpine units south of the Tauern Window (Figure III.6). Only a few of them are located along the eastern and south-eastern borders of the Tauern Window (Figure III.6).

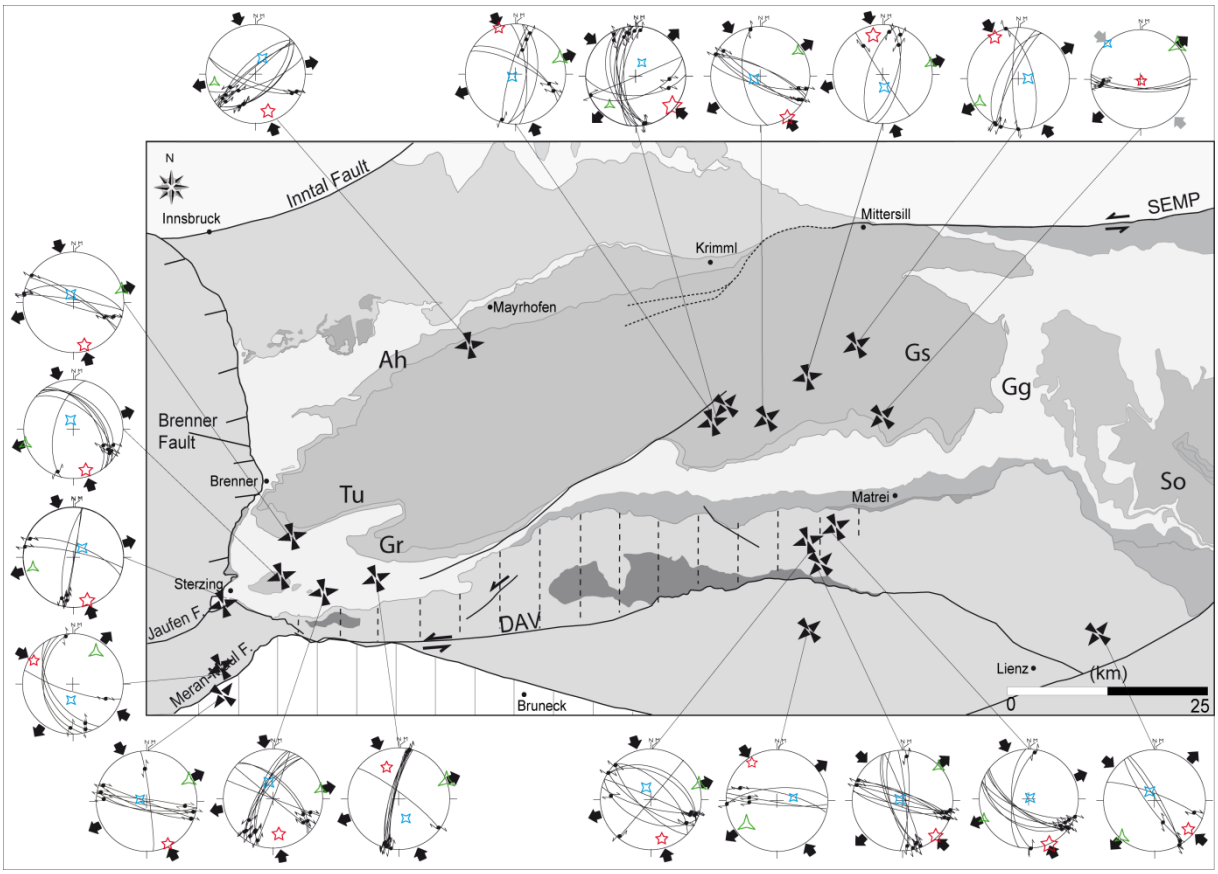

Figure III. 7. Transcurrent regimes with an ENE-WSW to NE-SW trend of σ_3 (Group 2). See figure III.6 for a detailed legend.

The 19 transcurrent tensors with SW-NE to SSW-NNE direction of σ_3 (group 2, Figure III.7) represent 32% of the transcurrent regimes. They are located within the south-western part of the Tauern Window and along the Meran-Mauls fault (Figure III.7) as well as in the central part of the Tauern Window. As the Φ ratio of the tensor 91 is equal to 0.9 (Table III.1), a stress permutation between σ_1 and σ_2 can be invoked and this extensive tensor can be considered as a strike-slip one. As the orientation of σ_3 and as the latter two tensors are located in the same area than the tensors of the group 2 (Figure III.7), the tensor 91 is included in the group 2 (Figure III.7).

Strike-slip regimes with σ_3 trending N-S are found over 13 localities (group 3, Figure III.8) corresponding to 24% of the studied outcrops. These outcrops are located mostly in the central part of the Tauern Window and in the Austroalpine units bordering the western tip of the Adriatic indenter.

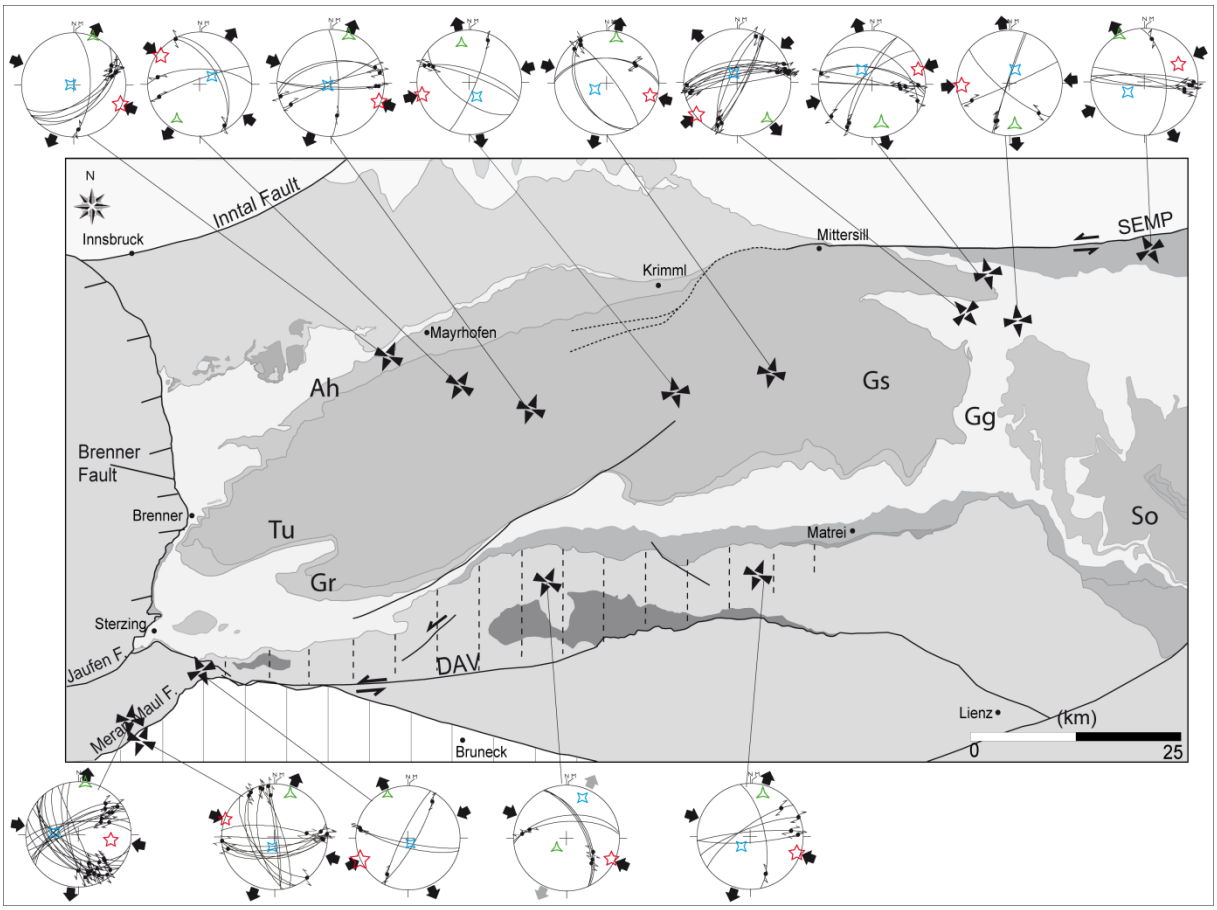

Figure III. 8. Transcurrent regimes with a NNW-SSE to NNE-SSW trend of σ_3 (Group 3). See figure III.6 for a detailed legend.

III.4.2. Extensional regimes

Based on the rose diagrams (Figure III.5a), we separated extensional tensors into two groups (group 4 and 5) according to the orientation of their minimal stress axis, σ_3. They are represented in Figures III.9 and III.10.

82% of the extensive tensors display σ_3 oriented ESE-WNW to SE-NW (group 4, Figure III.9). These tensors, which represent the largest group amongst the 6 groups of tensors, are mostly located in the vicinity of the Brenner normal fault and within the eastern part of the Tauern Window. Only a few of them have been found in the central part of the studied area (Figure III.9). This ESE-WNW to SE-NW direction of σ_3 is sub-parallel to the maximum of σ_3 deduced for the largest group of the transcurrent tensors (Group 1, Figure III.6).

A smaller number of the extensional tensors (18%) show a direction of σ_3 varying between NNW-SSE to NNE-SSW (group 5, Figure III.10). Out of these 6 tensors, 4 of them are along the northern border of the Tauern Window.

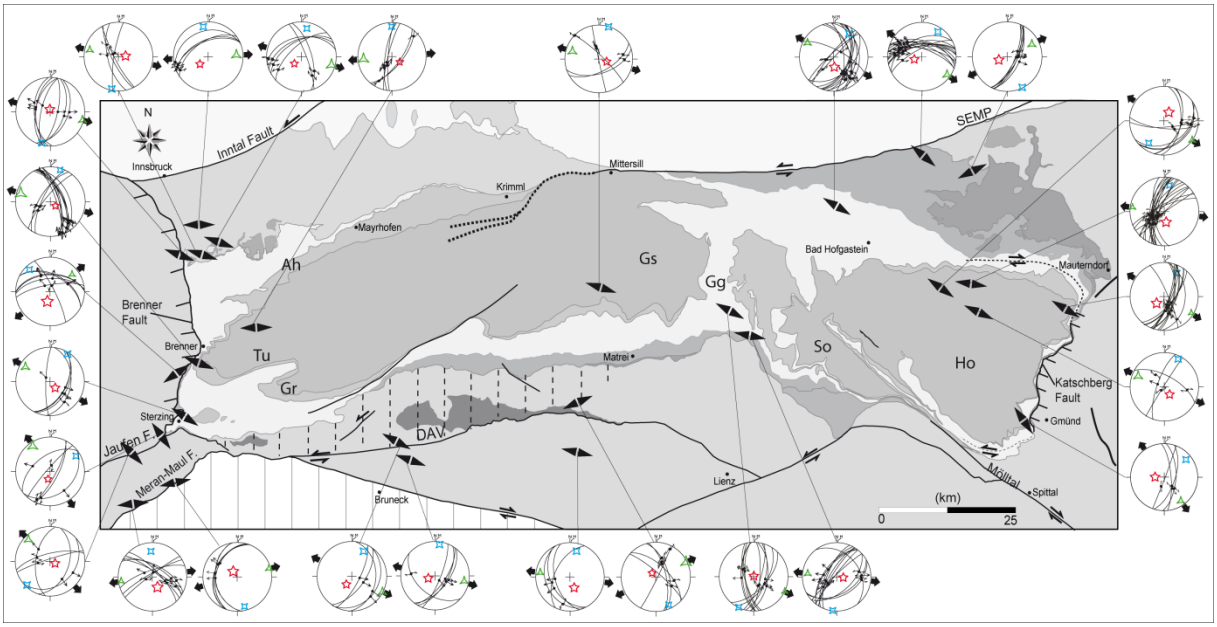

Figure III. 9. Extensional regimes with an ESE-WNW to SE-NW trend of σ_3 (Group 4). See figure III.6 for a detailed legend.

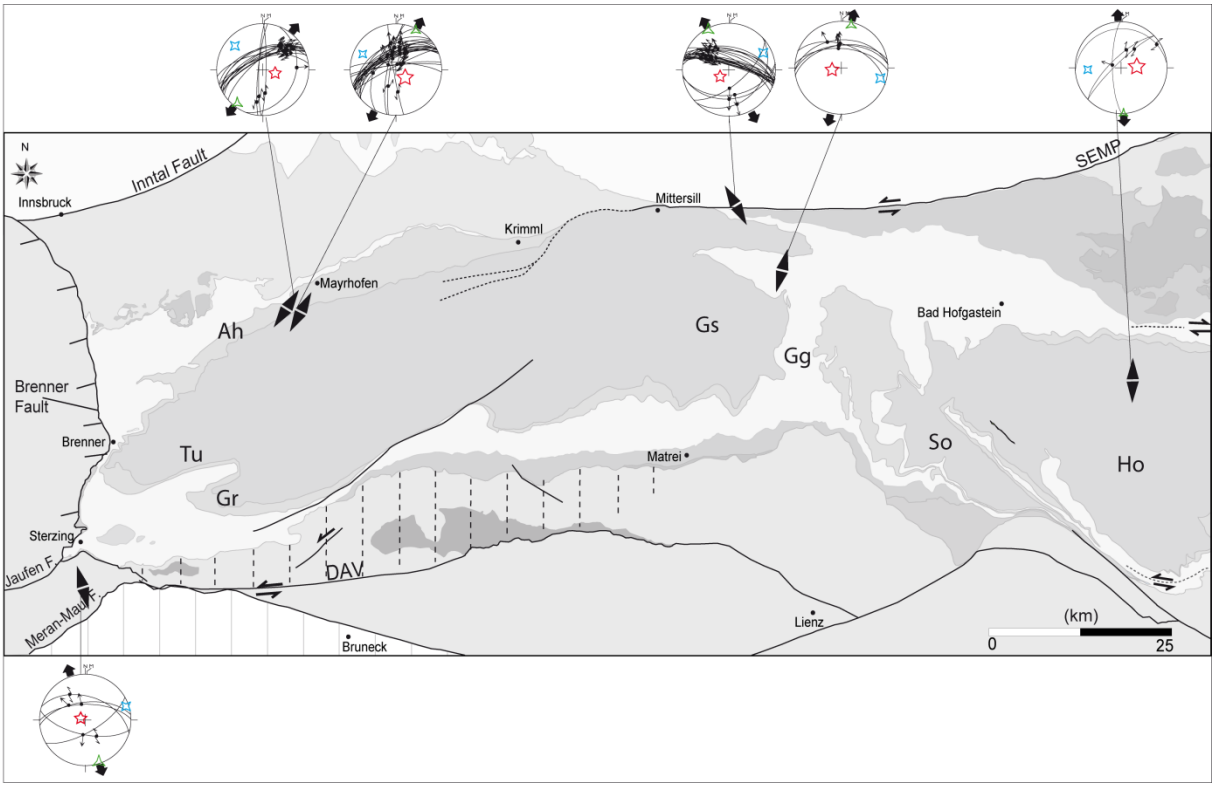

Figure III. 10. Extensional regimes with a NNW-SSE to NNE-SSW trend of σ_3 (Group 5). See figure III.6 for a detailed legend.

III.4.3. Compressive regimes

Very few tensors display a compressive state of stress, (7% of the total data set) (Table III.1; Figure III.11). These tensors are mostly located in the central part of the studied area,

where σ_1 is always oriented NNW-SSE to NNE-SSW (group 6, Figure III.11). One tensor is located along the SEMP fault and it shows a direction of σ_1 oriented NE-SW. This orientation is compatible with a sinistral movement along the SEMP fault. The last compressive state of stress has been determined along the Meran-Mauls fault and the direction of σ_1 is ESE-WNW (Figure III.11).

No compressive tensors were found in the western and eastern parts of the Tauern Window (Figure III.11).

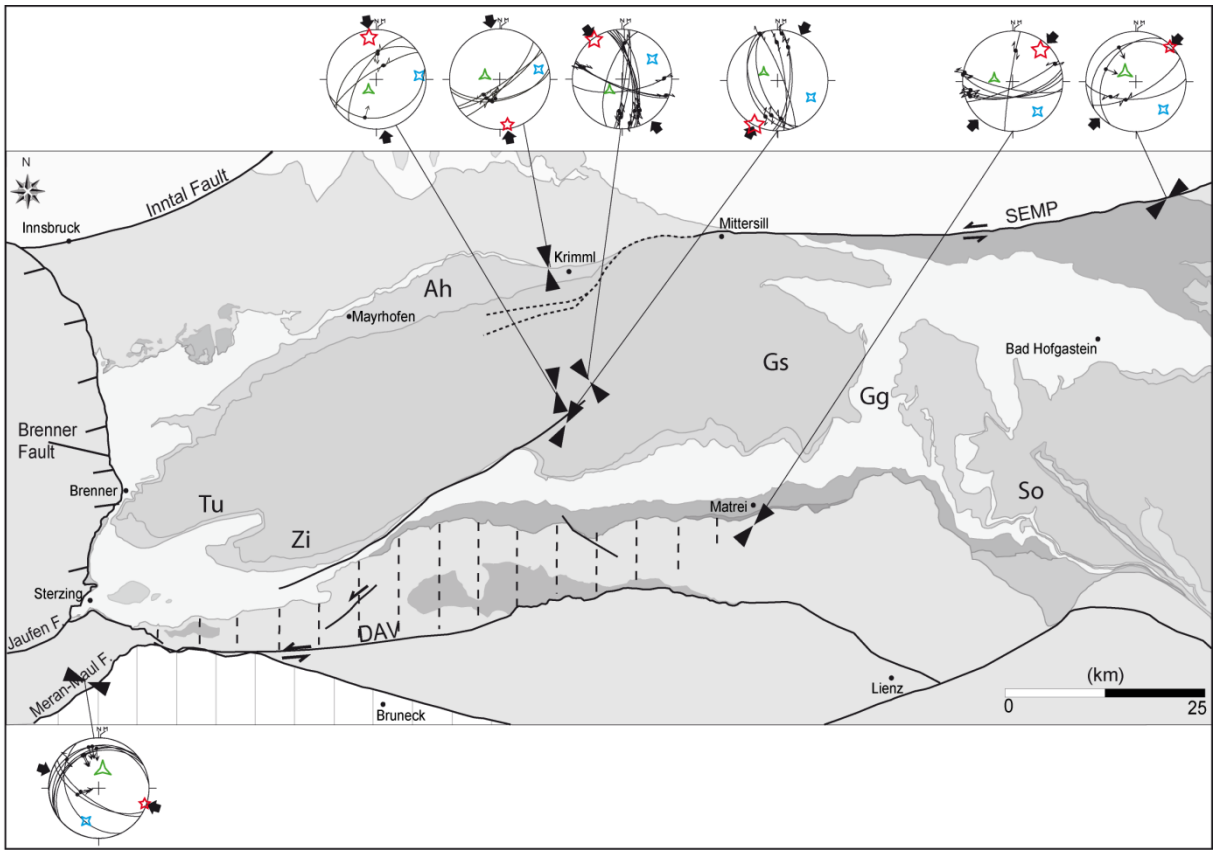

Figure III. 11. Stress tensors indicating compressive regimes in the central part of the Tauern Window (Group 6). See figure III.6 for a detailed legend.

III.5. Discussion

Brittle deformations within the Tauern Window are dominantly related to strike-slip faulting in the central part of the studied area and to extensional regimes at the western and eastern margins of the dome (Figures III.6, III.7 and III.9), where a SE-NW to ESE-WNW-oriented σ_3 direction dominates. These regimes represent 72% of the obtained tensors. Due to the lack of overprinting relationships in the investigated outcrops, it was not possible to determine any temporal sequence between different sets of striae, hence between the different types of tensors of each studied outcrop. Nevertheless, based on the different orientations of the inferred stress axe, we assume that several deformation phases may have affected the

investigated area. Different states of stress can be coeval in an area as large as the Tauern Window, representing local answers to a larger scale regional state of stress (Angelier, 1984).

In the rose diagram of figure III.5.b, the two peaks corresponding to the orientation of σ_3 in the strike-slip regime are close to each other (ENE-WSW) and (ESE-WNW), but clearly distinct. In order to test whether these orientations belong to regionally distinct areas, we plotted them separately in figures III.6 and III.7. Because there is no systematic, regional separation of these orientations, and no systematic overprinting relationships, we consider them to belong to one and the same stress field, with σ_3 statistically oriented E-W.

The orientation of σ_3 shows a third peak (Figure III.5.b), but of subordinate importance, compared to the previous ones. It is oriented N to NNE (Figure III.5.b) and its distribution in map view (Figure III.8), if anything can be concluded based on the small amount of data, appears to be weakly associated to the central axis of the window.

The orientation of σ_3 calculated from the extensional states of stress shows a single peak oriented WNW (Figure III.5a). However, other orientations, although poorly represented do exist, and their orientation is between NNW and NNE (Figure III.5a). As for the transcurrent tensors, we plotted these orientations separately in map view (Figures III.9 and III.10) to assess whether they occur in a specific area. In spite of the small number of data we note that they are spread throughout the dome, but mainly in the vicinity of the central axis.

Based on these considerations, and on the orientation of the σ_3 axis we can arrange the above tensors into 3 groups: the pure N-S compressive paleostress regime (Figure III.11), both the strike-slip and the extensional regimes with E-W orientation of σ_3 (Figures III.6 and III.7 and III.9) and both strike-slip and extensional tensors with σ_3 oriented N-S (Figures III.8 and III.10). In principle, the 6 groups described in Figures III.6 to III.11 could be interpreted as 6 separate tectonic events, but for the following reasons we prefer to group them as above: 1) we observed no overprinting relationships on the outcrop scale; 2) a regional stress field is expected to be partitioned into coeval but separate local strains and stress fields, especially in front of an indenter corner; 3) the main direction of extension given by the extensional tensors at the western margin of the Tauern Window is coherent with the azimuth of extension of 260°N that has been estimated in the Brenner area based on stretching lineations in mylonitic foliation and ductile to brittle-ductile shears bands (Axen et al., 1995). The orientations of stretching lineations and σ_3, and of the maximum shortening direction and σ_1 being similar for the overwhelming majority of the measured structures (the ones represented by the peaks of Figure III.5), we suggest a kinematic continuity between ductile and brittle structures.

In summary, most of the data point to E-W oriented σ_3, but two additional, small groups of tensors indicate either subvertical or N-S oriented σ_3. As shown in Figure III.5 the number of tensors in these groups is so limited, that they may be considered as “noise”, hence it is questionable whether they should be interpreted as representing distinct tectonic events. Keeping this in mind, we can speculate about the tectonic events responsible for such stress fields. The compressive structures that generally indicate a NNW-SSE to NNE-SSW direction

of σ_1 are compatible with two main regional tectonic events that affected the Tauern Window. The first one is the nappe stacking stage (Schmid et al., 2013). The second one is the formation of the Tauern dome by refolding of the nappe stack in Early Miocene times (Schmid et al., 2013). Given the Miocene age of the zircon fission tracks (Figure III.2), the oldest possible ages for the brittle compressive structures within the Tauern dome are Miocene, hence post-subduction stage. Therefore, the compressive structures must have formed during or after upright folding.

The tensors showing N-S oriented σ_3, show a weak spatial affinity to the central axis of the Tauern Window. Such orogen-perpendicular extension direction recalls that observed in the core of the western Alps (Sue et al, 2007) and of the Central Alps (Allanic, 2013). Orogenic collapse was invoked to explain these structures (Sue et al, 2007) but significantly more data would be needed for analogue statements on the Tauern Window.

Since the iso-age contours of zircon and apatite fission track ages (Figure III.2) follow the trend of the main axial planes of the major folds in the western part of the Tauern Window (Figure III.1), one could expect that the cooling pattern, hence exhumation of the western dome of the Tauern Window, resulted from folding and erosion. As a consequence, a large number of tensors indicating N-S compression would be expected in this area. However, only few structures indicating compressive states of stress have been found (Table III.1, Figure III.11). Several interpretations that we discuss below may explain this contradiction:

1. The brittle crust of the Tauern Window was affected by a transtensive regime throughout its exhumation history. This model largely explains the type and distribution of brittle structures, but not the age pattern shown by low-temperature geochronometers.

2. A two-phase evolution in which dominant compression is followed by dominant extension. Compressive structures associated to the first stage are probably largely eroded and the upper crust is mostly overprinted by the younger extensional/strike-slip faults. The fact that the low-temperature age pattern follows the upright folds rather than the normal faults, suggests however that exhumation associated to the second, extensional phase was not sufficient to reset apatite ages, except for the areas located along the faults themselves. As a consequence a maximum exhumation of 7-8 km may have occurred in this phase.

3. Vertical partitioning between shortening at lower crustal levels and extension in the upper crust has often been invoked (e.g., Platt, 1986), based on critical wedge models. These models may explain the overprinting of ductile compressional folds by extensional brittle structures, when the latter are exhumed in the upper part of the crust. However, the iso-age pattern of apatite fission tracks, which reflects cooling in the upper crust, does show a close relationship to the upright folds, suggesting that the upper crust was not affected by dominant extension for a time lapse that was sufficiently long to modify the cooling, hence the iso-age pattern of the Tauern Window. Therefore, such a one-stage exhumation model must always be dominated by compression in order to be consistent with our thermo-chronological data in the Tauern Window. This would be in conflict with the analysis of brittle deformation showing a clear domination of extensional/strike-slip faults.

4. Physical analogue models of doming (Withjack and Shiner, 1982) were invoked to explain the presence of extensional structures in the Tauern Window that was inferred to form under compressive conditions (Laubscher, 1990). Models result in an elliptical dome displaying N-S compression in the northern and southern boundary, transtension at the western boundary and in the core of the dome, extension at the eastern boundary, and strike-slip faulting in the central part of the dome. These extensional structures at the western and eastern boundaries are associated to the Brenner and to the Pannonian basin, respectively. The compressive structures could be associated to the TNBF (Lammerer et al., 2008) in the north and the limit of the indenter in the south while strike-slip fault could be associated to the SEMP and the DAV fault. However, the occurrence of extensional structures in the central part of the analogue model cannot be linked to any structures in the Tauern Window and these extensional structures can only be explain by the fact that in the analogues models uplift of the rock is due to inflation from below (Withjack and Shiner, 1982). In addition, the orientation of the strike-slip fault in the models display an angle that is not coherent with the orientation of the SEMP and the DAV strike-slip faults and no N-S shortening can be yield by such orientation of strike-slip displayed by the models. Moreover, as stated before in point 3., a one-stage model of exhumation cannot explained both the lack of compression and the iso-age pattern of the apatite and fission track data-sets.

In summary, model 2 is more appropriate to explain both the brittle deformation and the thermo-chronological data. The late character of the extensional phase is consistent with the young ages along the extensional faults bordering the dome. This does not preclude their longer and older activity.

We suggested that the paucity of compressive structures compared to the extensional and transcurrent ones may indicate that erosion removed most of the upper crustal levels that were affected by brittle deformation during the first phases of deformation and exhumation of the Tauern Dome. Provided that this explanation is correct, the compressive brittle structures would be older than the extensive and transcurrent ones. We thus assume that after N-S shortening during the folding event, compression became of subordinate importance in the Late Miocene. This implies that combined extensional displacements and strike-slip faulting accommodated the late stages of exhumation in the brittle field, with substantial N-S shortening accommodated along strike-slip faults. The occurrence of N-S compression and shortening during the first event due not preclude a coeval occurrence of E-W extension that would take place along the Katschberg and the Brenner normal faults.

In contrast to Wang and Neubauer (1998), who proposed five stages of brittle deformation, we only described two-stages (Figure III.12). Our systematic investigation of brittle structures, even in the eastern Tauern Window, did not reveal any complex, overprinting relationships, leading to numerous phases of deformation. Based on our own observations, a simpler and more realistic history consisting of only two, brittle deformation events, is more likely.

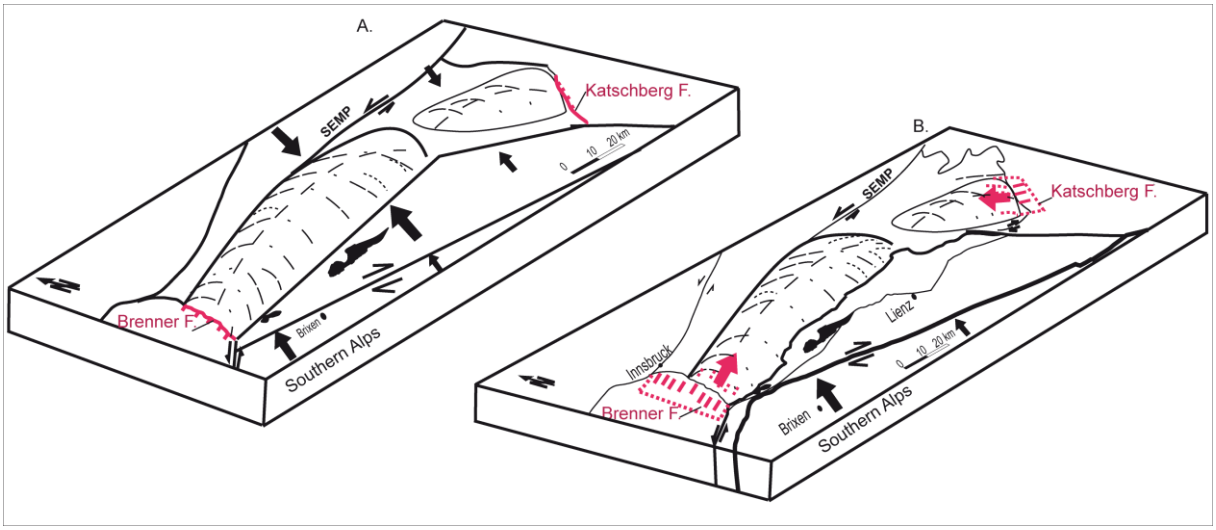

Figure III. 12. Tectonic evolution of the Tauern Window. A. first stage majoritarily driven by shortening and N-S compression with higher amount of shortening in front of the tip of the indenter; formation of the western and eastern sub-domes of the Tauern Window. B. second stage dominated by E-W extension and strike-slip faulting

The location of the Tauern Window in front of the tip of the Adriatic indenter invokes a possible link of extensional and strike-slip faulting with the NS to NNE motion of the Adriatic indenter. It is compatible with the results of the analogue models of Ratschbacher et al. (1991) and Rosenberg et al. (2004) showing that in a context of lateral extrusion for the Eastern Alps, the Tauern Window can still undergo compression due to its position at the tip of the indenter. We thus propose that the motion of the Adriatic indenter was initially accommodated by a pure NNW-SSE compression and later by normal faulting combined with strike-slip faulting, both yielding a ENE-WSW to SE-NW direction of extension and strike-slip yielding a global N-S shortening.

Conclusion

A large number of brittle structures has been collected throughout the Tauern Window and surrounding areas, and inversion of these data results in six different paleostress fields that provide a two-stage brittle deformation history of the Tauern Dome. In contrast to our first expectation that were based on the iso-age pattern of fission track data, really few inverse fault structures have been highlighted and the Tauern Window is mainly affected by strike-slip faulting passing into extensional regimes at the eastern and at the western margins of the Window. Our results suggest that the brittle crust of the Tauern Window was mostly affected by a strike-slip state of stress, which graded into extension at the eastern and western margins of the dome. We propose that the few inverse structures could be the remains of a N-S shortening event related to the folding event (Schmid et al., 2013) and to the formation of the large-scale folds of the Tauern Window. The majority of the upper brittle crust affected by brittle compressive structure has been eroded since and only few remnants of the event still exist. We thus propose that the transcurrent and extensional regimes postdate the reverse one.

Distribution of paleostresses within the Tauern Window indicates a transition from extension to strike-slip, when passing from the eastern and western boundaries towards the internal part of the Window suggesting that E-W extension affecting the Eastern Alps during late Miocene time (or even later) was accommodated, within the Tauern Window, by E-W extension along the Katschberg and Brenner normal faults and by strike-slip faulting in the core of the Tauern Window. We finally propose that a first stage of exhumation of the Tauern Window, during which large-scale folds were formed, was dominated by N-S shortening and compression while significant amounts of extension occurred at the margins of the Tauern Window during a second stage of deformation.

References

Allanic, C., 2013. Kinematics, Age and Dynamic of the brittle deformation within the Lepontine Dome (Central Alps), PhD, Orléans, 272p.

Anderson, E.M., 1942. The Dynamics of faulting (2nd edn). Olivier & Boyd, Edinburgh.

Angelier, J., 1984. Tectonic analysis of fault slip data sets. Journal of Geophysical Research, 89, 5835-5848.

Angelier, J, 1989. From orientation to magnitudes in paleostress determinations using fault slip data. Journal of Structural Geology, 11, 37-50.

Angelier, J., 1990. Inversion of field data in fault tectonics to obtain the regional stress – III. A new rapid direct inversion method by analytical means. Geophysical Journal International, 103, 363-376.

Axen, G. J., Bartley, J.M., and Selverstone, J., 1995. Structural expression of a rolling hinge in the footwall of the Brenner Line normal fault, Eastern Alps. Tectonics, 14, 1380-1392.

Behrmann, J. H., 1988, Crustal-scale extension in a convergent orogen: The Sterzing-Steinach mylonite zone in the Eastern Alps. Geodynamica Acta, 2, 63-73.

Behrman, J.H., and Frisch, W., 1990. Sinistral ductile shearing associated with metamorphic decompression in the Tauern Window, Eastern Alps: Jahrbuch der Geologischen Bundesansalt, 133, 135-146.

Bigi, G., Castellarin, A., Coli M., Dalpiaz, G.V. and Vai, G.B., 1990. Structural model of Italy sheet 1 & 2, 1:500000. Consiglio Naz. Ricerche, Progetto Finalizzato Geodinamica, Selca Firenze.

Caporali, A., Neubauer, F., Ostini, L., Stangl, G. and Zuliani, D., 2013. Modeling surface GPS velocities in the southern and Eastern Alps by finite dislocations at crustal depths. Tectonophysics, 590, 136-150.

Carey, E. and Brunier, B., 1974. Analyse théorique et numérique d'un modèle mécanique élémentaire appliquée à l'étude d'une population de failles. C.r. Acad. Sci., Paris D179, 891-894.

Cornelius, H.P., 1940. Zur Auffassung der Ostalpen im Sinne der Deckenlehre. Zeitsch. Deutsch. Geol. Ges., 92, 271-312.

D'Agostino, N., D. Cheloni, S. Mantenuto, G. Selvaggi, A. Michelini, and D. Zuliani, 2005. Strain accumulation in the southern Alps (NE Italy) and deformation at the north-eastern boundary of Adria observed by GPS measurements. Geophysical Research Letters, 32, L19306.

Decker, K., and Reiter, F., 2006. Depth-extrapolated models of fracture orientation and fracture density for the Brenner Base Tunnel. In: *Pangeo Austria 2006*, Tessadri-Wackerle, E. (ed.), 44-45, Innsbruck University Press.

Decker, K., Meschede M. and Ring, U., 1993. Fault slip analysis along the northern margin of the Eastern Alps (Molasse, Helvetic nappes, North and South Penninic flysch, and the Northern Calcareous Alps). Tectonophysics, 223, 291-312.

Dewey, J.F., Helman, M. L., Knott, S.D., Turco, E., and Hutton, D.H.W., 1989. Kinematics of the western Mediterranean, in *Alpine tectonics*, M.P. Coward, D. Dietrich and R.G. Park. (eds.). Geol. Soc. Spec.. Publ., London, 45, 265-283.

Dunkl, I., Frisch, W., and Grundmann, G., 2003. Zircon fission track thermochronology of the south-eastern part of the TW and the adjacent Austroalpine margin, Eastern Alps. Eclogae geol. Helv., 96, 209-217.

Frisch, W., Dunkl, I., and Kuhlemann, J., 2000. Post-collisional orogen-parallel large-scale extension in the Eastern Alps. Tectonophysics, 327, 239-265.

Frisch, W., Kuhlemann, A., Dunkl, I., and Brügel, A., 1998. Palinspastic reconstruction and topographic evolution of the Eastern Alps during late Tertiary tectonic extrusion. Tectonophysics, 297, 1-15.

Frisch, W., Szekely, B., Kuhlemann, A., and Dunkl, I., 1999. Geomorphological evolution of the Eastern Alps in response to Miocene tectonics. Zeitschrift für Geomorphologie N.F., 44, 103-138.

Fügenschuh B, Mantckelow N.S, Schmid S.M., 2012. Comment on ‘‘Estimating displacement along the Brenner Fault and orogenparallel extension in the Eastern Alps’’ by Rosenberg and Garcia. Int J Earth Sci (Geol Rundsch) (2011). Int. J. Earth. Sci., 101, 1451–1455

Fügenschuh, B., Seward, D. and Mantckelow, N. S., 1997. Exhumation in a convergent orogen: the western TW. Terra Nova, 9, 213-217.

Genser, J. and Neubauer, F., 1989. Low angle normal faults at the eastern margin of the TW (Eastern Alps). Mitteilungen der Österreichische Geologische Gesellschaft, 81, 233-243.

Glodny J., Ring, U. and Kühn A., 2008. Coeval high-pressure metamorphism, thrusting, strike-slip, and extensional shearing in the Tauern Window, Eastern Alps, Tectonics, 27, TC4004.

Handy, M. and Oberhänsli, R., 2004. Age of the Metamorphic Structure of the Alps - Tectonic Interpretation and Outstanding Problems. In: *Explanatory Notes to the Map: Metamorphic Structure of the Alps*. Oberhänsli., R. (eds). Mitteilungen der Österreichischen Mineralogischen Gesellschaft, 149, 97-121.

Handy, M.R., Schmid, S.M, Bousquet, R., Kissling, E. and Bernoulli, D., 2010. Reconciling plate-tectonic reconstructions of Alpine Tethys with the geological–geophysical record of spreading and subduction in the Alps. Earth-Science Reviews, vol. 102; issues 3-4, 121–158.

Hurford, A.J., 1986. Cooling and uplift patterns in the Lepontine Alps, South Central Switzerland and an age of vertical movement on the Insubric fault line: Contributions to Mineralogy and Petrology, 92, 413-427.

Kuhlemann, J., Frisch, W., Dunkl, I., Székely, B., 2001. Quantifying tectonic versus erosive denudation: The Miocene core complexes of the Alps.- Tectonophysics, 330, 1-23.

Kurz, W. and Neubauer, F, 1996. Deformation partitioning during updoming of the Sonnblick area in the TW (Eastern Alps, Austria). Journal of Structural Geology, 18, 11, pp. 1327-1343.

Kurz, W., Neubauer, F., Genser, J., and Horner, H., 1993. Sequence of Tertiary Brittle Deformations in the Eastern TW (Eastern Alps). Mitt. Österr. Geol. Ges., 86, 153-164.

Lammerer, B., 1988. Thrust-regime and transpressionregime tectonics in the Tauern Window (Eastern Alps), Geol. Rundsch., 77, 143-156.

Lammerer, B. Gebrande, H., Lüschen, E. and Vesela, P., 2008. A crustal-scale cross-section through the Tauern Window (Eastern Alps) from geophysical and geological data. In: *Tectonic Aspects of the Alpsine-Carpathian-Dinaride System*, edited by Siegesmund, S., Fügenschuh, B. and Froitzheim, N., Geol. Soc. Spec. Publ., 219-229.

Laubscher, H.P., 1988. Material balance in Alpine orogeny. Geol. Soc. America, Bull., 100, 1313-1328.

Laubscher, H.P., 1990. The problem of the Moho in the Alps. Tectonophysics 182, 9-20.

Linzer, H.-G., Decker, K., Peresson, H., Dell'Mour, R., and Frisch, W., 2002. Balancing orogenic float of the Eastern Alps: Tectonophysics, 354, 211-237.

Mancktelow, N. and Pavlis, T.L., 1994. Fold-fault relationships in low-angle detachment systems. Tectonics, 13, 668-685.

Most, P., 2003. Late Alpine cooling histories of tectonic blocks along the central part of the Transalp-Traverse (Inntal-Gadertal): constraints from geochronology. PhD Thesis, University of Tübingen, pp. 97.

Neubauer, F., Genser, J., Kurz, W. and Wang, X., 1999. Exhumation of the TW, Eastern Alps: Physics and chemistry of the Earth, ser. A, v.24, p.675-680.

Oberhänsli, R. Bousquet, R., Engi, M., Goffé, B., Gosso, G., Handy, M.R., Höck, V., Koller, F., Lardeaux, J.-M., Polino, R., Rossi, Ph., Schuster, R., Schwartz, St., Spalla, 2004. Metamorphic structure of the Alps. Scale 1:1.000.000, Commission for the Geological Map of the World, Paris.

Peresson, H., and Decker, K., 1997. Far-field effects of late Miocene subduction in the Eastern Carpathians: E-W compression and inversion of structures in the Alpine-Carpathian-Pannonian region. Tectonics, 16, 38-56.

Petit, J.P., 1987. Criteria for the sense of movement on fault surfaces in brittle rocks. Journal of structural Geology, vol. 9, No. 5/6, pp. 597-608.

Platt, J.P., 1986. Dynamics of orogenic wedges and the uplift of high pressure metamorphic rocks. Geological Society of American Bulletin, 97, 1037-1053.

Pomella, H., 2010. The Cenozoic evolution of the Giudicarie fault system (Eastern/Southern Alps, northern Italy) A geochronological, structural and paleomagnetic study. PhD thesis, Innsbruck, April 2010

Ratschbacher, L., Frisch, W., Neubauer, F., Schmid, S. M., and Neugebauer, J., 1989. Extension in compressional orogenic belts: The Eastern Alps. Geology, 17, 404-407.

Ratschbacher, L., Merle, O., Davy, P., and Cobbold, P., 1991a. Lateral extrusion in the Eastern Alps, Part. 1: Boundary conditions and experiments scaled for gravity. Tectonics, 10, 245-256.

Ratschbacher, L., Frisch, W., and Linzer, H.-G., 1991b. Lateral extrusion in the Eastern Alps: Part II. Structural analysis. Tectonics, 10, 257-271.

Reinecker, J. and A.W. Lehnhardt, 1999. Present-day stress field and deformation in eastern Austria, Int J Earth Sciences, 88, 532–550.

Reiter, F., Lenhardt, W.A., and Brandner, R., 2005. Indications for activity of the Brenner Normal Fault zone (Tyrol, Austria) from seismological and GPS data. Austrian journal of Earth Sciences, 97, 16-23.

Rosenberg, C.L., and Garcia, S., 2011. Estimating displacement along the Brenner fault and orogen parallel extension in the Eastern Alps.

Rosenberg, C.L., and Garcia, S., 2012. Reply to the comment of Fügenschuh et al. on the paper 'Estimating displacement along the Brenner Fault and orogen-parallel extension in the Eastern Alps' by Rosenberg and Garcia, Int J Earth Sci (Geol Rundsch) (2011) 100:1129–1145. Int J Earth Sci (Geol Rundsch) (2012) 101:1457–1464.

Rosenberg, C.L., and Schneider, S. 2008. The western termination of the SEMP fault (Eastern Alps) and its bearing on the exhumation of the Tauern Window. In: Siegesmund, S., Fügenschuh, B., Froitzheim, N. (eds) Tectonic aspects of the alpine-dinaride-carpathian system. Geol. Soc. Lond 298: 197-218.

Rosenberg, C. L., Brun, J.-P., and Gapais, D., 2004. An indentation model of the Eastern Alps and the origin of the Tauern Window. Geology, 32, 997-1000.

Rosenberg, C. L., Brun, J.-P., Cagnard, F., and Gapais, D., 2007 Oblique indentation in the Eastern Alps: Insights from laboratory experiments. Tectonics, 26.

Royden, L.H., 1993. Evolution of retreating subduction boundaries formed during continental collision. Tectonophysics, v.12, p.629-638.

Scharf, A., Handy, M.R., Favaro, S., Schmid, S. M. and Bertrand, A., 2013. Modes of orogen-parallel stretching and extensional exhumation in response to microplate indentation and roll-back subduction (Tauern Window, Eastern Alps) Int J Earth Sci (Geol Rundsch), 102, 1627-1654.

Schmid, S.M., Fügenschuh, B., Kissling, E. and Schuster, R., 2004. Tectonic map and overall architecture of the Alpine orogen. Eclogae Geol. Helv., 97, 93-117.

Schmid S. M., Scharf, A., Handy, M.R., Rosenberg, C.L, 2013. The Tauern Window (Eastern Alps. Austria): a new tectonic map, with cross-sections and a tectonometamorphic synthesis. Swiss J. Geosci., 106, 1-32.

Selverstone, J., 1988. Evidence for East-West crustal extension in the Eastern Alps: implications for the unroofing history of the TW. Tectonics, 7, 87-105.

Selverstone, J., Axen, G., and Bartley, J., 1995. Fluid inclusion constraints on the kinematics of footwall uplift beneath the Brenner Line normal fault, Eastern Alps. Tectonics 14, 264-278.

Senftl, E. and Exner, C., 1973. Rezente Hebung der Hohen Tauern und geologische Interpretation. Verhandlungen der Geologischen Bundesansalt, 1973, 209-234.

Spencer, J.E., 1984. The role of tectonic denudation in the wrapping and uplift of low-angle normal faults. Geology, 12, 95-98

Steenken, A., Siegesmund, S., Heinrichs, T., and Fügenschuh, B., 2002. Cooling and exhumation of the Rieserferner Pluton (Eastern Alps, Italy/Austria). Int. J. of Earth Sci., 91, 799–817.

Stipp, M., Stünitz, H., Heilbronner, R., Schmid S.M., 2002. The eastern Tonale fault zone: a "natural laboratory" for crystal plastic deformation of quartz over a temperature range from 250 to 700 °C. Journal of Structural Geology, 24, 1861-1884.

Stöckhert, B., Brix, M.R., Kleinschrodt, R., Hurford, A.J., and Wirth, R., 1999. Thermochronometry and the microstructures of quartz - A comparison with experimental flow laws and predictions on the temperature of the brittle-plastic transition. Journal of Structural Geology, 21, 351–369.

Sue, C., Delacou, B., Champagnac, J-D., Allanic, C., Tricart, P. and Burkhard, M., 2007. Extensional neotectonics around the bend of the Western / Central Alps: an overview. Int. J. of Earth Sci., 96, 1101-1129.

Termier, P. 1903. Les nappes des Alpes orientales et la synthèse des Alpes. Bull. Soc. Géol. France Série 4., vol. 3, 711-766.

Viola, G., Mancktelow, N. S. and Seward, D., 2001. Late Oligocene-Neogene evolution of Europe-Adria collision: New structural and geochronological evidence from the Giudicarie fault system (Italian Eastern Alps). Tectonics, 20, 999-1020.

Wang, X., and Neubauer, F., 1998. Orogen-parallel strike-slip faults bordering metamorphic core complexes: the Salzach-Enns fault zone in the Eastern Alps. Journal of Structural Geology, 20, 799-818.

Wawrzyniec, T.F., Selverstone, J., and Axen, G.J., 2001. Styles of footwall uplift along the Simplon and Brenner normal fault systems, central and Eastern Alps. Tectonics, 20, 748-770.

Withjack, M.O. and Sheiner, C., 1982. Fault Patterns Associated with Domes – An Experimental and Analytical Study. The American Association of Petroleum Geologists Bulletin, 66, 302-316.

Wölfler, A., Dekant, C., Danisìk, M., Kurz, W., Dunkl, I., Putis, M. and Frisch, W., 2008. Late stage differential exhumation of crustal blocks in the central Eastern Alps: evidence from fission track and (U–Th)/He thermochronology. Terra Nova, 20, 378–384,

Zaun P.E., and Wagner G.A., 1985. Fission track stability in zircons under geological conditions. Nuclear Tracks, 10, 303–307.

Chapter IV. 2D-thermal modelling of a structural and thermal dome based on a natural example, the Tauern Window (Eastern Alps)

2D-thermal modelling of a structural and thermal dome based on a natural example, the Tauern Window (Eastern Alps)

Audrey Bertrand[1], Frédéric Gueydan[2] and Claudio Rosenberg[3]

1. Department of Tectonics and sedimentology, Freie Universität Berlin, Malteserstraße 74-100, 12449 Berlin, Germany
2. Laboratoire Géosciences Montpellier, Université Montpellier II, CNRS, France, Montpellier, France
3. ISTEP, Université Paris 06-UPMC, 75252 Cedex 05 PARIS, France

Abstract

Interpretations of low-temperatures thermochronologic data sets to assess cooling histories of gneiss domes are generally based on the assumption that deformation of the isotherms is directly related to the amount of uplift of the rocks during deformation. These models are thus valid only if the uplift velocities of the rocks are important enough to render insignificant the effect of re-equilibration of the isotherms. We provide a series of two-dimensional thermal models of a lithosphere that undergoes folding and we compare them to a natural case study (the Tauern Window). Models show that Models show that High uplift rates induce a deformation of the isotherms due to convective heat transfer, while thermal equilibration of the system occurs when the uplift rates decrease. The thermal re-equilibration significantly counterbalances folding of the isotherms and isograds. Comparison of the results to the ages obtained within the Tauern Window, indicate that the Tauern Window an age distribution most similar to that age distribution of models that result from a two-stage uplift event. The first stage is marked by high uplift rates that bring deep, hot material to the surface. The isotherms and isograds are thus folded due to convection resulting from the advection of hot deep material. A second stage is marked by uplift rates that are too low to counterbalance equilibration of the isotherms. This sequence of two-stages with different uplift rates provides a cooling pattern that is most similar to the one observed in the Tauern Window.

IV.1. Introduction

Structural and metamorphic gneiss domes, composed by cores of high-grade metamorphic or plutonic rocks overlain by upper crustal rocks of lower metamorphic grade, commonly form in the core of orogenic mountain belts (Eskola, 1949; Whitney et al., 2004). They are exhumed from deeper crustal levels relatively to their surrounding host rocks (Teyssier and Whitney, 2002) and are usually elliptical in map view with their long axes parallel to the axial trend of the mountain chain. Gneiss domes are mostly characterized by large-scale folds inside the dome and major detachment faults along their borders (Eskola, 1949). The relative contributions of orogen-parallel extension (e.g. Coney, 1980; Crittenden, 1980; Frisch et al., 2000) and folding and erosion (e.g. Ramsay, 1967; Rosenberg and Garcia; 2011; 2012) for the exhumation and cooling history of gneiss domes is still debated.

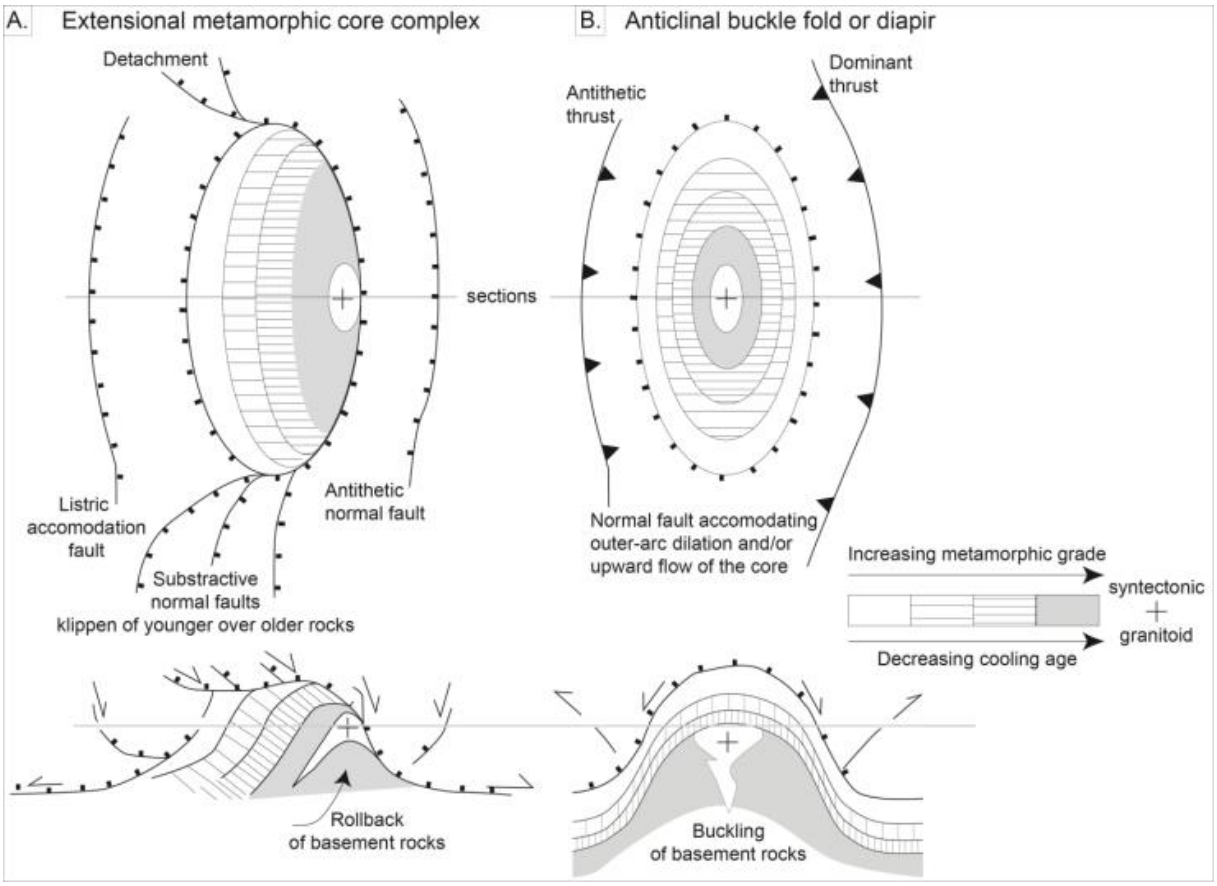

Figure IV. 1. Distribution of metamorphic facies in map view and cross sections in the case of A. extensional metamorphic core complex and A. folding and buckling of diapiric dome (after figure 1 of Burg et al., 2004)

Thermal histories of rocks provide important constraints on geological models and particularly in orogenic belts that are characterised by rapid uplift and denudation (Batt and Brandon, 2002). Thermochronological ages of exposed rocks of metamorphic domes are directly related to the cooling and exhumation history underwent by the dome (Batt and Brandon, 2002; Hurley et al., 1962), hence cooling patterns may be diagnostic for the formation mechanisms of a dome (Burg et al., 2004) (Figure IV.1). For example, extensional unroofing along large-scale detachments is expected to result in a linear pattern of isochrones, striking parallel to the extensional fault plane and younging toward its surface (Foster et al., 2001; Burg et al., 2004) (Figure IV.1a). On the contrary, domes resulting from upright folds are characterised by concentric isograds and isochrones, symmetrically distributed about the axial plane, with younger ages centred in the middle of the dome (Burg et al., 2004) (Figure IV.1b).

Two natural examples of metamorphic and structural domes formed during collision of the Central and Eastern Alps are given by the Lepontine and the Tauern dome, respectively. The westernmost part of the Lepontine dome (Swiss/Italian Alps), named the Toce dome, (Mancktelow, 1985; Merle et al., 1986; Steck and Hunziker, 1994) and the westernmost part of the Tauern Window (Austrian/Italian Alps) are sub-domes presenting some structural and

thermal similarities. Both sub-domes are approximately parallel to the axial trend of the Alpine Chain, both delimited by a large-scale W-dipping detachment fault, known as the Simplon fault for the Lepontine dome and the Brenner fault for the Tauern Window. Based on apatite and zircon fission track ages, two major cooling trends can be recognised for the Toce and western Tauern sub-domes. Both show at first order, concentric patterns with younger ages in the core of the domes and, at second order, cooling ages younging toward the major detachment faults (Vernon, 2008; Campani, 2009; Luth and Willingshoffer, 2008; Chapter II, this study). Overprinting relationships between upright folds of the Lepontine dome and the Simplon mylonitic structures lead to the assumption that orogen-perpendicular folding occurred simultaneously with orogen-parallel extension accommodated by the Simplon normal fault (Mancktelow and Pavlis, 1994). The extension-parallel folds of the Toce dome are thus interpreted as being the result of horizontal contraction perpendicular to the stretching direction in a transpressional continental collision-extrusion (Mancktelow, 1992; Mancktelow and Pavlis, 1994; Wawrzyniec et al., 2001). Similarly, orogen-perpendicular shortening within the Tauern Window is inferred to be coeval with orogen-parallel extension along the Brenner normal fault, but the relative roles played by extension along the Brenner fault and folding in its footwall for the bulk exhumation of the Tauern Window is still debated (Fügenschuh et al., 2012; Rosenberg and Garcia, 2011; 2012).

Models proposing that exhumation of gneiss domes is mainly related to folding assume a direct relationship between uplift of the rocks and deformation of the isotherms resulting from the fact that exhumation of hot, deep material induces advective heat transport during exhumation (Mancktelow and Grasemann, 1997). In that case, deformation of the isograds is directly related to the amount of uplift of the rocks during the deformation stage. These models do not take into account that re-equilibration of the isotherms may occurs and counterbalance the bending of the isotherms (Sleep, 1979). It has been proposed that significant bending of the isotherm can only occur if the uplift velocities of the rocks are fast enough to render insignificant the effect of re-equilibration of the isotherms (Sleep, 1979).

In this study, we model the two-dimensional thermal evolution of a dome during its uplift and exhumation using boundary conditions derived from the regional geologic setting of the Tauern Window, in order to investigate 1- the influence of thermal inheritance from subduction and nappe stacking on the thermal structure during collision; 2- the deformation of the isotherms during shortening, as a function of shortening rates; 3- the influence of uplift velocities and amount of deformation on cooling ages and cooling patterns and 4. Whether fission track age differences in the Tauern window result from the re-equilibration of isotherms following the folding event or from differential exhumation during folding. By comparing the models provided of this study to apatite and zircon fission track data ages provided for the Tauern Window (Chapter II, this study), we discuss the tectonic significance of age patterns derived from thermochronological data in the Tauern Window.

IV.2. Two-dimension thermal modelling

IV.2.1. Geometrical, thermal and rheological input parameters

A lithospheric-scale 2D-thermal evolution of a 50 km-wide lithospheric segment is provided using the finite element method and the SARPP (Structural Analysis and Rock Physics, 2003) numerical code (Gueydan et al., 2004; Leroy et al., 2008; Carry et al., 2009). This model reproduces the evolution of temperatures through time of continental lithospheric rocks undergoing exhumation by folding and erosion. In the following, we focus on the exhumation history of the retrograde PT path of a pile of stacked nappes, which initial thermal state derives from the inferred thermal history of subduction of the Tauern Window.

In order to compare the models to the natural example of the western Tauern Window, the input parameters of the thermal models are the ones that can mimic the best the geometrical, physical properties of the Tauern Window. These are described below.

The southward subduction of the European plate has been active since the Cretaceous (Handy et al., 2010), resulting in the accretion of different paleogeographic domains to the southern margin of the European plate beneath the Austroalpine units (Figure IV.2). The Tauern Window is a gneiss dome exposing the lower plate of the Alpine orogen in the form of the folded nappe stack of the European basement, the Valais Ocean and the Piemont-Liguria Ocean. This dome is surrounded by the upper plate of the Tertiary Alpine orogen, corresponding to the Austroalpine Units (Figure IV.2).

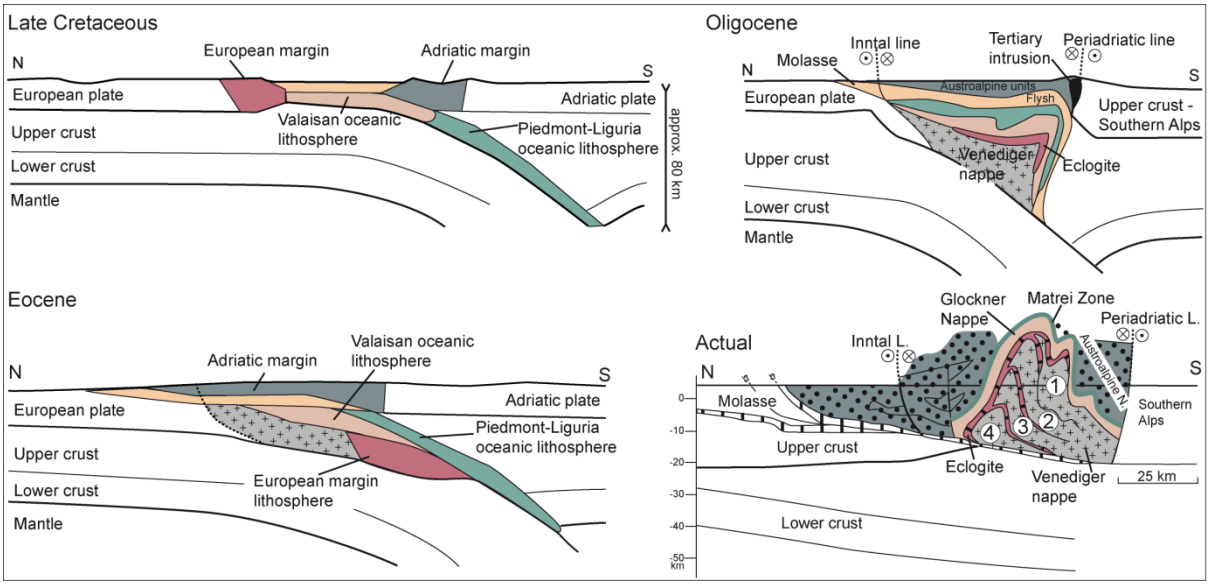

Figure IV. 2. Plate tectonic evolution of the Eastern Alps (after Kurz et al., 2008) and schematic cross-section of the western sub-dome of the Tauern Window and (after Schmid et al. 2004 and Laubscher; 2010). Numbers refer to the successive imbricate nappes that have been stacked as a duplex.

Based on a series of cross-sections of the Tauern Window (Schmid et al., 2004) the number and the thickness of the nappes of the alpine stack can be calculated. The western sub-dome of the Tauern Window consists of a stack of four nappes of basement metamorphic

rocks derived from the European plate (Venediger duplex) (Schmid et al., 2013) and cover metasediments with minor basement units deriving from the Valais ocean (Glockner nappe) and the Piemont-Liguria Ocean (Matrei zone) (Schmid et al., 2013). Each nappe is approximately 5 km thick (Schmid et al., 2004) and the nappe pile lies below the Austroalpine units, whose thickness is estimated to ~ 10 km (Figure IV.2). At present, the western sub-dome of the Tauern Window displays an asymmetric half-dome shape with steep northern limb and more gently dipping southern limb (Schmid et al., 2004; Schmid et al., 2013) (Figure IV.2).

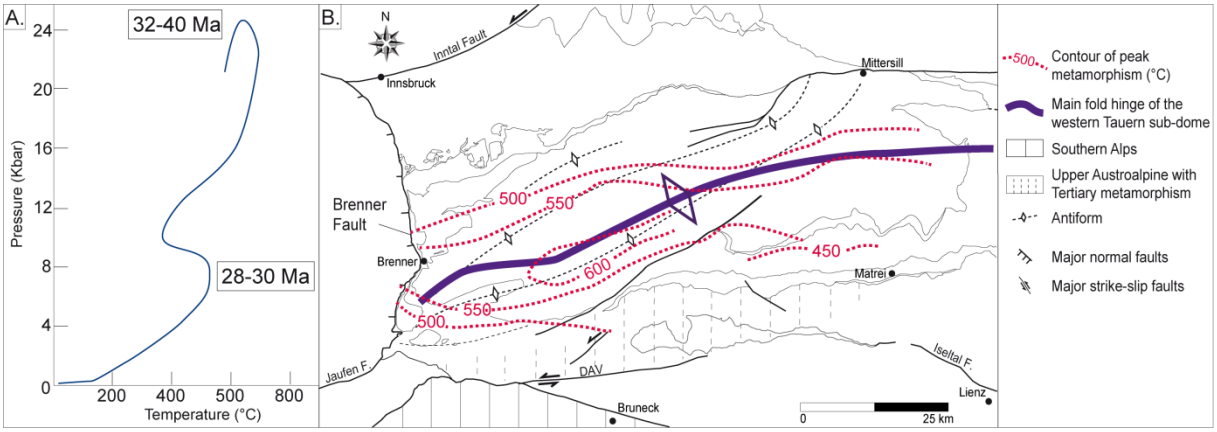

Figure IV. 3. A. PTt path of the Penninic units of the Tauern Window (after Kurz et al., 1998). B. Isograds of Tertiary metamorphism in western sub-dome of the Tauern Window - based on oxygen thermometry on quartz-muscovite (Hoernes and Friedrichsen, 1974)-

Thermal history of the Penninic rocks of the Tauern Window is complex and derives from two successive orogenies that occurred during Cretaceous and Tertiary times (e.g. Dewey et al., 1989; Froitzheim et al., 1996) (Figure IV.3a). Nappe stacking occurred at ca. 35-40 Ma (Schmid et al., 2004) during the subduction of the Penninic units, which were metamorphosed into eclogitic facies (Höck, 1980; Holland and Ray, 1985; Selverstone, 1988) (Figure IV.3a). High pressure metamorphism is inferred to have attained 600° C and 20-23 kbar (e.g. Zimmermann et al., 1994; Kurz et al., 2008). The age of high pressure metamorphism (Figure IV.3a) is controversially debated, due to different results from several geochronological methods. Zimmermann et al. (1994) suggest that high-pressure metamorphism was older than 36 Ma, because phengites of the Eclogite zone, yielding Ar/Ar ages between 36 and 32 Ma, are inferred to be cooling ages, hence following the high-pressure event. In contrast, Rb/Sr isochrones on several mineral phases of the eclogite (Glodny et al., 2005) and Lu-Hf garnet ages (Nagel et al., 2013) both yielding ages of ca. 32 Ma, are inferred to date the high-pressure event.

High-temperature Barrovian metamorphism is characterised by a concentric, elongate pattern symmetrically distributed around the axial trace of the Tauern antiform (Hoernes and Friedrichsen, 1974; Oberhänsli et al., 2004) (Figure IV.3b). High-temperature metamorphism attained a maximum of more than 600 °C (Hoernes and Friedrichsen, 1974) around 30-28 Ma (Schmid et al., 204; 2013) (Figure IV.3a). Therefore, a time span of only 2 to 8 Ma separates

the high-pressure from the high-temperature metamorphic events. Given the short time span between these two events that correspond to subduction and collision, the thermal structure of the subducted nappes may have influenced the thermal structure of the crust during collision and high-temperature metamorphism.

The entire nappe stack is folded during the Miocene but the maximum exhumation occurred in the core of the western sub-dome, where it is manifested by an eroded upright antiform of approximately 30 km wavelength and 30 km amplitude (Schmid et al., 2004; 2013). In order to investigate this structure, shortening of the model is entirely accommodated by uplift within an antiformal structure (Figures IV.4 and IV.5).

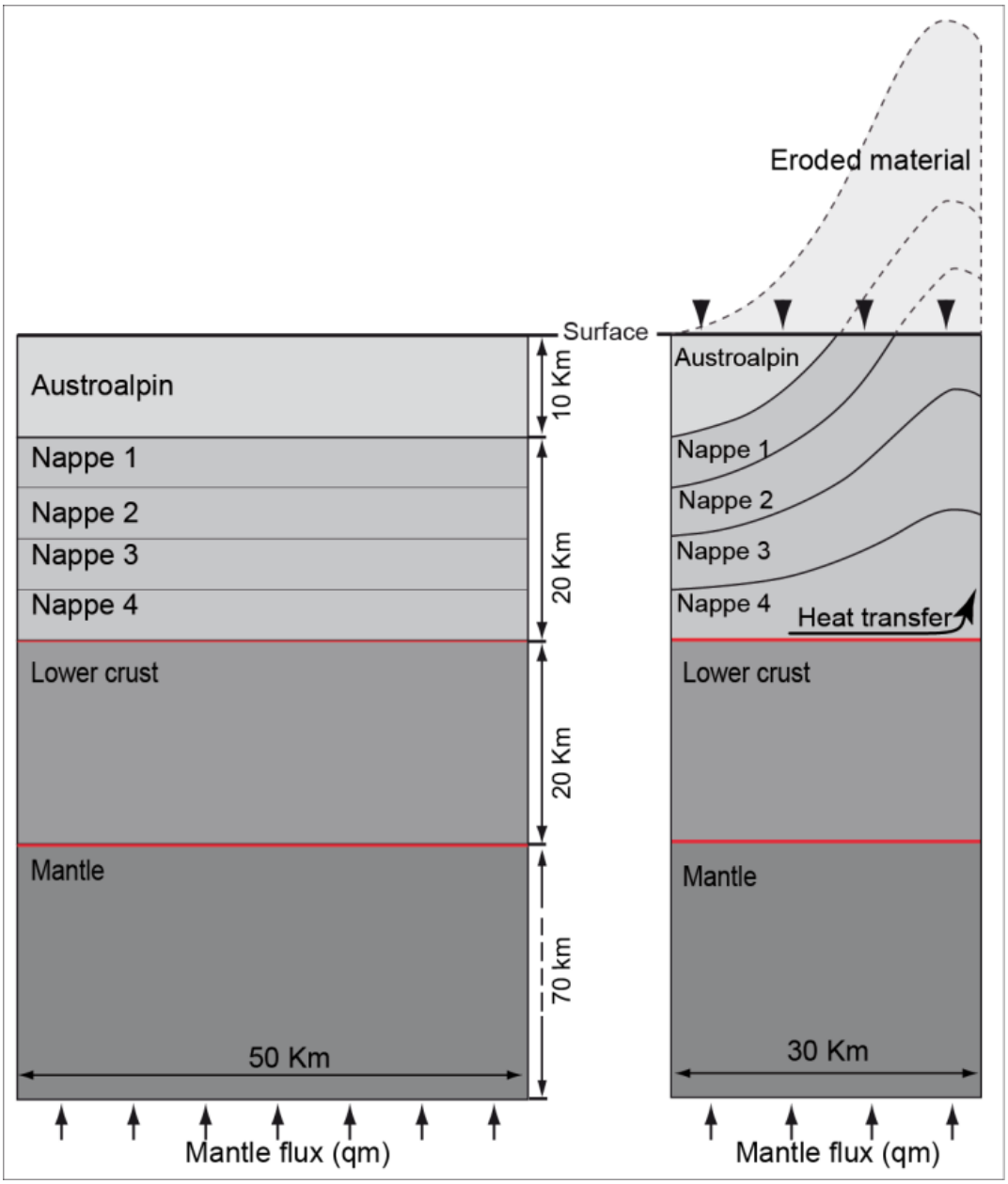

Figure IV. 4. Model setup and boundary conditions. Transient heat conduction is solved in a layered segment with a top diffusive layer overlying the nappe pile.

Exhumation rates are inferred to be between 3.2 and 0.1 mm (Fügenschuh et al., 1997; Chapter II, this study), for the period between 20 Ma and the present. The time span comprised between the ages of zircon and apatite fission tracks, i.e. between 14 Ma and 5 Ma in the latter study, is characterised by exhumation rates of 0.1 mm.yr^{-1}.

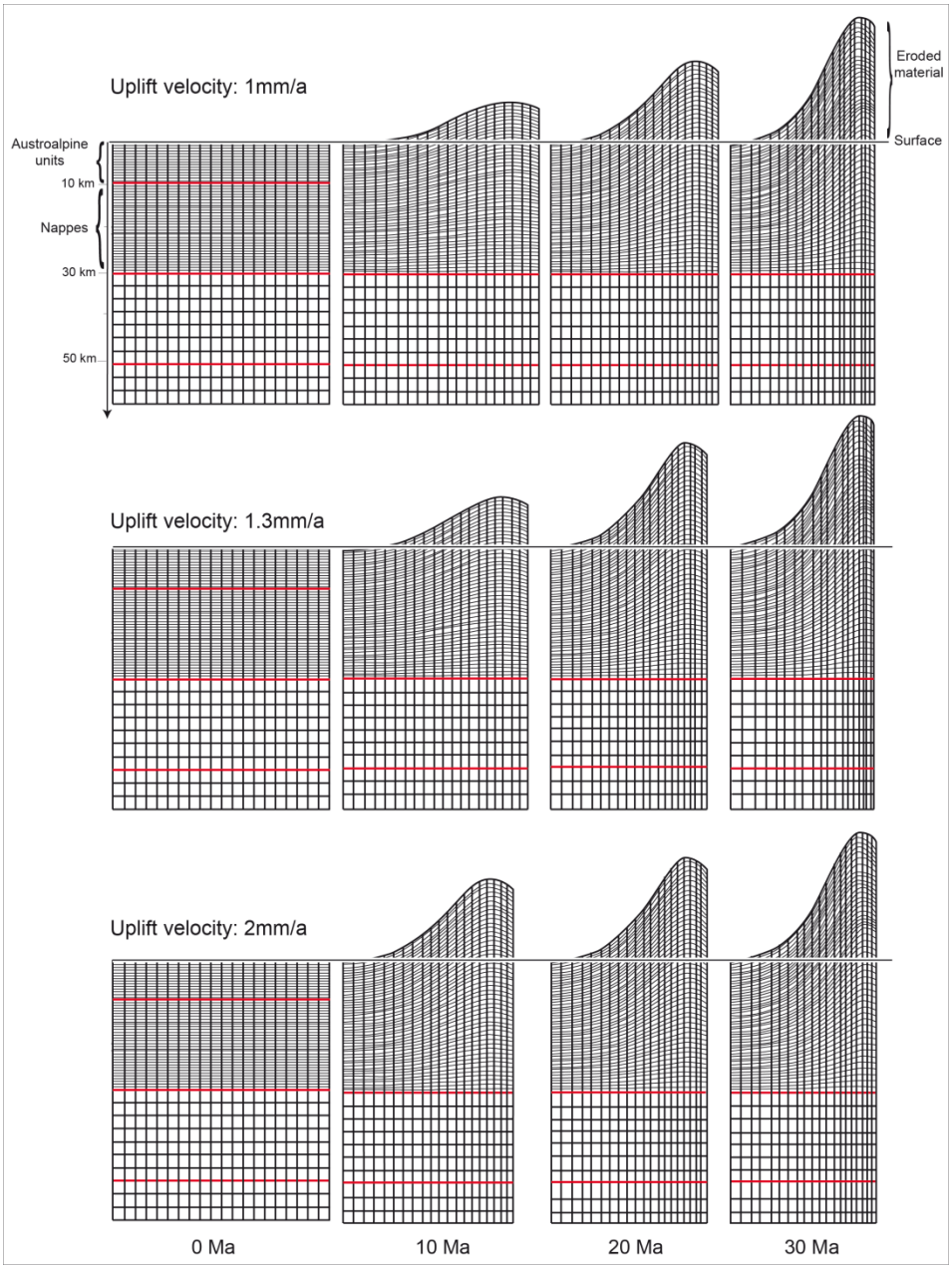

Figure IV. 5. Deformation of the mesh for three models that underwent three different uplift rates with different timing of deformation.

The Moho under the Tauern Window strikes parallel to the long axis of the orogen and is located at a depth of 40 to 50 km (Müller et al., 2001; Giese et al., 1982; Ebbing et al., 2001). Since the Austroalpine units did not undergo subduction during the Tertiary, we attribute them physical characteristics of a non-radiogenic crust. The resulting mesh represents a 50 km

wide and 150 km depth area divided into 4 main domains corresponding to the mantle, the radiogenic lower crust, the radiogenic nappes and the non-radiogenic Austroalpine units (Figure IV.4). The models are represented by a mesh composed of 440 elements and 1869 nodes that mimic the shape of the Tauern Window (Figure IV.5).

IV.2.2 Model equations and boundary conditions

We aim at modelling the two-dimensional thermal evolution of the Tauern Window, with a particular focus on the role of the initial, subduction-related temperature distribution. The novelty of these models is to account for the initial, unsteady thermal conditions during the following deformation.

IV.2.2.1 Heat equation

The thermal evolution of the area is calculated based on the heat equation:

$$\frac{\varphi T(x,t)}{\varphi t} = D\Delta T(x,t) + \frac{P}{\rho c}$$

where Δ is the Laplace operator, D the coefficient of thermal diffusivity ($m^2.s^{-1}$); P the heat production ($W.m^{-3}$), ρ is the density of the material ($kg.m^{-3}$) and C the specific heat ($J.kg^{-1}\cdot K^{-1}$). For the mathematical treatment, thermal diffusivity is considered as equal to 1.

IV.2.2.2 Kinematics of folding: grid deformation/advection and erosion

We use the following physical laws to simplify the studied natural system in such a way that it can be easily described numerically. The imposed kinematic pattern results in a highly asymmetric type of folding, where one side terminate against an area that was affected by the nearly highest uplift rates. This asymmetry in the rates of uplift is manifest in the asymmetry of the fold that is cut just behind its hinge region, forming a half-dome (Figure IV.2). This half-dome shape is represented by a half Gaussian equation:

$$f(x) = \left(\frac{1}{\sigma\sqrt{2\pi}}\right) e^{\frac{-(x-\mu)^2}{2\sigma^2}}$$

where f(x) is the displacement, σ the width of the fold at half elevation and μ the width of the base of the fold.

Erosional laws are not integrated in these experiments, but we simulated the effect of erosion on the thermal state of the model, by setting an arbitrarily fixed elevation of 1000 m at which the surface temperature, Ts, is equal to zero. Hence, when rocks pass the 1000 m elevation they cool down to 0 °C; a constant mantle heat flux, qm of 30 $m.W.m^{-2}$ is applied at the bottom of the box in order to represent a continuous income of accreted material and to maintain the base of the orogen at a fixed temperature. Heat transfers are possible along the

borders of the box and advection is modelled by applying a change in the temperature after deformation of the mesh. Thermal exchanges occur across the surface, with the fixed surface temperature equal to zero. Input parameters of the models are summarized in the table IV.1.

Symbol	Parameters	Value
r	Radiogenic heat production	$2{,}4.10^{-6}$ $W.m^{-3}$
k_c	Diffusion coefficient in the crust	2.1 $W.m^{-1}.K^{-1}$
k_m	Diffusion coefficient in the mantle	3.0 $W.m^{-1}.K^{1}$
q_m	Basal heat flux	30 $mW.m^{-2}$
p_c	Density of the crust	2700 $kg.m^{-3}$
p_m	Density of the Mantle	3300 $kg.m^{-3}$
T_s	Surface temperature	0 °C
T_b	Base temperature	1200 °C
alpha	Thermal diffusivity	1.10^{-6} $m^{-2}.s^{-1}$
C	Specific heat capacity	1100 $J.kg.^{-1}.K^{-1}$
G	Geothermal gradient	15 $°C.km^{-1}$

Table IV. 1. Models parameters used for the 2D thermal models

	Uplift Velocity of 1 $mm.yr^{-1}$ during 30Ma	**Uplift Velocity of 1.3 $mm.yr^{-1}$ during 20Myrs and of 0.325 $mm.yr^{-1}$ during 10 Myrs**	**Uplift Velocity of 2 $mm.yr^{-1}$ during 10Myrs and of 0.5 $mm.yr^{-1}$ during 20 Myrs**
Initial thermal state 1 steady geothermal gradient	Model 1 (Figure 9a)	Model 2 (Figure 9b)	Model 3 (Figure 9c)
Initial thermal state 2 geotherm disturbed by 4 nappes that underwent low temperatures during subduction	Model 4 (Figure 10a)	Model 5 (Figure 10b)	Model 6 (Figure 10c)
Initial thermal state 3 geotherm disturbed by 4 nappes that underwent high temperatures during subduction	Model 7 (Figure 11a)	Model 8 (Figure 11b)	Model 9 (Figure 11c)

Table IV. 2. The different models based on different uplift rates and initial thermal states.

In order to investigate the effect of different uplift rates and different initial thermal states on the cooling of the upper crust, we varied these two parameters in the models and kept the total amount of shortening and the time of bulk shortening constant. All models have been shortened by 30 km in a time interval of 30 Myrs. Therefore, models with higher uplift rates imply higher shortening rates and require shorter time intervals to achieve the imposed, total amount of shortening. We thus conceived the latter models as sequences of two uplift phases taking place at different uplift rates. If the uplift rate was increased with respect to the standard uplift of 1 $mm.yr^{-1}$, uplift of the model was completed by an uplift phase at a rate

lower than 1 mm.yr^{-1}. Hence the models with uplift rate of 1,3 mm.yr^{-1} are followed by a phase of uplift at 0,5 mm.yr^{-1}, and those starting at 2 mm.yr^{-1} are followed by a phase of uplift at 0,324 mm.yr^{-1} (Figure IV.5; Table IV.2). These two-phase models that we provide with the purpose of maintaining constant finite shortening and time in all experiments, may be of particular interest for the Tauern Window, where such two-phase cooling histories have been inferred on the base on thermochrononological data (Fügenschuh et al., 1997).

IV.2.2.3 Initial temperature distribution

Different initial thermal states are modelled in order to test the influence of the temperatures inherited from a subduction event (Figures IV.6).

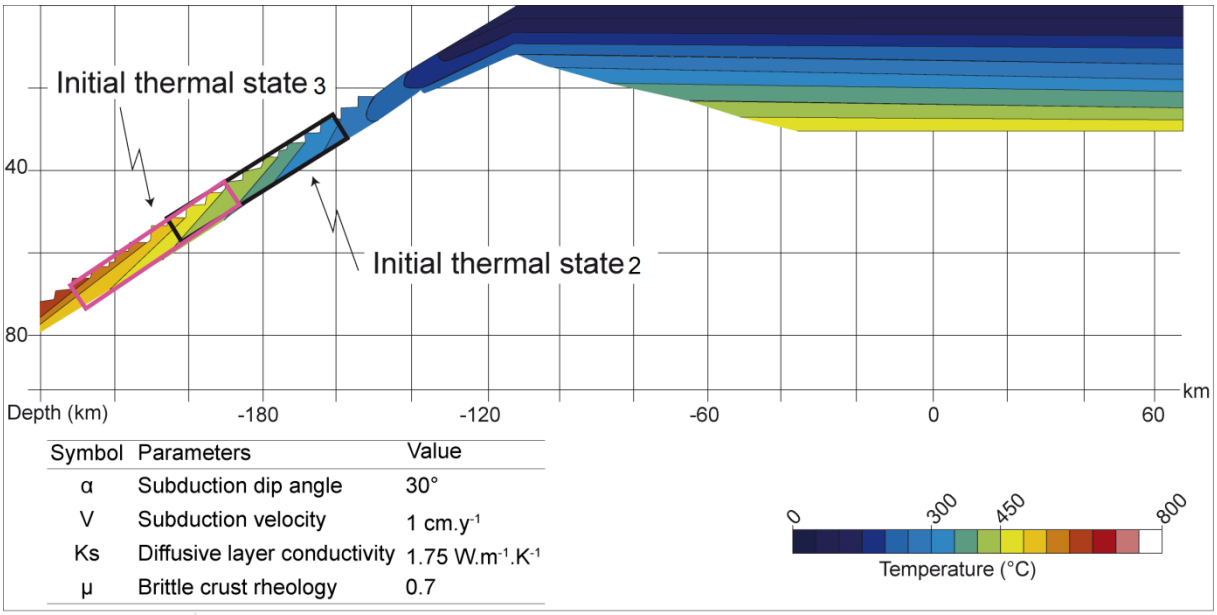

Figure IV. 6. Temperature profile of a subducted crust after 9 Ma. Subduction dip angle of 30° and velocity of 1 cm.yr-1 (after Carry et al., 2009)

Assuming a reasonable geothermal gradient of 15 °C.km^{-1} within subduction zones, the initial thermal state 1 (Figure IV.7a) is a reference system with steady geothermal gradient of 15 °C.km^{-1}. The two other models are systems with 4 nappes that are stacked below Austroalpine units (Figures IV.7b and IV7.c).

The initial thermal state 2 represents the thermal state of a crust affected by stacking of 4 nappes that underwent a lower-temperature subduction (≤ 600 °C) history (Figure IV.7b). Initial thermal state 2 (LT - Figure IV.7b) yields temperatures that correspond to a subducted passive margin that reached 30 to 60 km, 9 Ma after subduction has begun as it has been modelled by previous studies (Carry et al., 2009) (Figure IV.6). Therefore, the initial thermal state of the models incorporates a thermal gradient increasing laterally from ca. 300 °C to ca. 600 °C (Figure IV.7b). Temperatures of Initial thermal state 3 are those of a subducted passive margin crust reaching 50 to 70 km depth, 9 Ma after subduction has begun as it has been modelled by previous studies (Carry et al., 2009) (Figure IV.6). Therefore, the initial

thermal state of these models incorporates a thermal gradient increasing laterally from ca. 400 °C to ca. 700 °C (HT - Figure IV.7c) in order to account for the southward increase of temperature during the subduction phase (Figure IV.6).

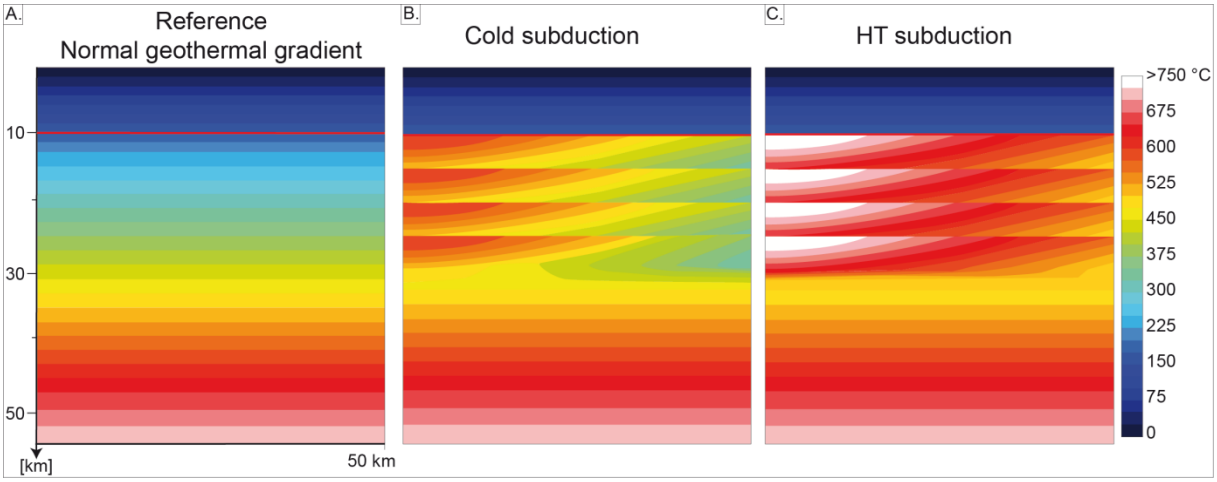

Figure IV. 7. The three different initial thermal states corresponding to A. initial thermal state 1 (SS): lithosphere with steady geothermal gradient; B. initial thermal gradient 2 (LT): lithosphere with a geothermal gradient disturbed by 4 nappes that were initially affected by temperatures up to 600 °C during subduction, and C. initial thermal gradient 3 (HT): lithosphere with a geothermal gradient disturbed by 4 nappes that were initially affected by temperatures up to 700 °C during subduction.

The initial thermal state 3 (Figure IV.7c) represents the thermal state of a crust affected by stacking of 4 nappes that underwent high-temperature subduction (≤ 700 °C). Both models introduce a high-temperature anomaly in the otherwise horizontally stratified thermal state of the steady-state model 1.

Initial thermal states 2 and 3 (Figures IV.7b and IV.7c) show a complex thermal stratiphications within the nappe stack, due to the repetition of one and the same vertical temperature profile within each nappe and to the horizontal temperature gradient inherited from the subduction event. Such a temperature distribution implies that the left side of the nappes was subducted to lower depths as shown in figure IV.6, and that their superposition occurred instantaneously with respect to the temperature equilibration within each nappe.

In the following we will term these models steady state (SS – Figure IV.7a), low temperature subduction (LT - Figure IV.7b), and high temperature subduction (HT – Figure IV.7c).

We are aware of the fact that the first initial thermal state (SS - Figure IV.7a) is unrealistic to model the thermal conditions of the Tauern Window but it provides an end-member system that allows for a good comprehension of the influence of initial thermal conditions on the following evolution of the system.

IV.3. Results

The results of the models consist of a series of crustal sections showing the evolution of the temperature distribution through time, hence the geometry of isotherms as a function of

time and uplift rates. For each initial thermal state (Figure IV.7), we model three different folding histories by applying different uplift rates and durations of shortening. In order to compare the results of different models and to compare models with the natural case study of the Tauern Window, uplift rates and bulk duration of shortening are linked in a way that final maximal exhumation always results in 30 km as inferred for the Tauern Window (Schmid et al., 2004; 2013) (Figure IV.5). Therefore, higher experimental uplift rates were coupled with shorter durations of deformation. In summary, the three models performed are as follows: Models 1, 4 and 7 run with constant uplift rates of 1 mm.yr^{-1} during 30 Myrs. Models 2, 5 and 8 run with uplift rates of 2 mm.yr^{-1} during 10 Ma and then of 0.5 mm.yr^{-1} for the last 20 Myrs, whereas models 3, 6 and 9 runs with uplift rates of 1.3 mm.yr^{-1} during 20 Myrs and uplift rates of 0.325 mm.yr^{-1} during the last 10 Myrs (Table IV.2).

IV.3.1 Thermal re-equilibration of initial high temperature stacked nappes without shortening

We aim to study the time required to "passively" re-equilibrate an initial temperature distribution reflecting a perturbation due to hot stacked nappes that underwent subduction. In other words, we investigate the time needed to re-equilibrate isotherm perturbations in the absence of deformation. Figure IV.8 illustrates a standard experiment performed with a thermal perturbation after subduction to a depth of 40 to 60 km and incorporation into a crust reaching 50 km thickness as a consequence of nappe stacking, without subsequent shortening.

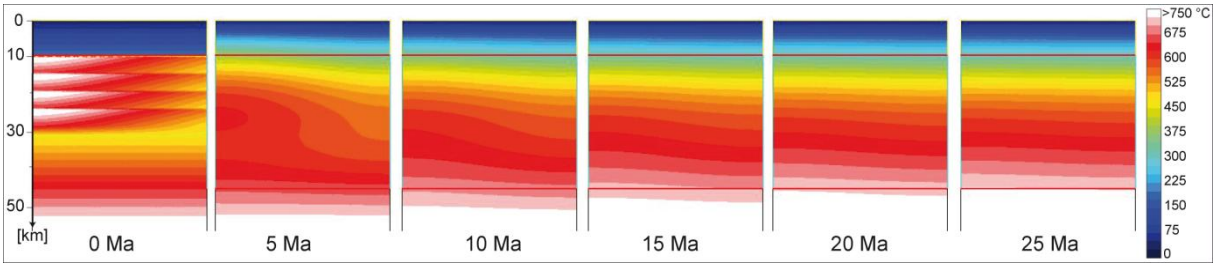

Figure IV. 8. Evolution of the temperature after subduction and stacking of high temperature nappes

The initial thermal state is disturbed by the stacking of 4 nappes that bring high temperatures of up to 700 °C in contact with overlying and underlying lower temperatures. Because the model was run without applying any deformation, the evolution of the temperature distribution in time was only driven by heat conduction. After 5 Myrs the individual thermal anomalies of each nappe cannot be recognized anymore, and a single high-temperature anomaly forms in the area that reached the highest temperature during subduction (Figure IV.8). This anomaly progressively disappears with time being only visible in the lower crust after 15 Myrs. The cooling effect of the surface that is set at 0 °C, resulting in a much more rapid re-equilibration of the isotherms in the upper crust compared to the lower crust, where the anomaly becomes smaller but still persists until the end of the experiment (Figure IV.8). After 25 Ma, the geothermal gradient is still significantly increased in the 10 first kilometres of the upper crust compared to the steady state initial conditions of figure

IV.7a, with a geothermal gradient of 15 °C.km^{-1} (Figure IV.7a). Between 10 and 50 km depth, the geothermal gradient is slightly higher than the one of the initial steady state initial conditions (Figure IV.8).

IV.3.2 Initial thermal steady-state and folding/erosion

The thermal evolution of a lithosphere with an initially undisturbed thermal stratification changes if the model is shortened and these changes depend on the imposed uplift rates (Figure IV.9).

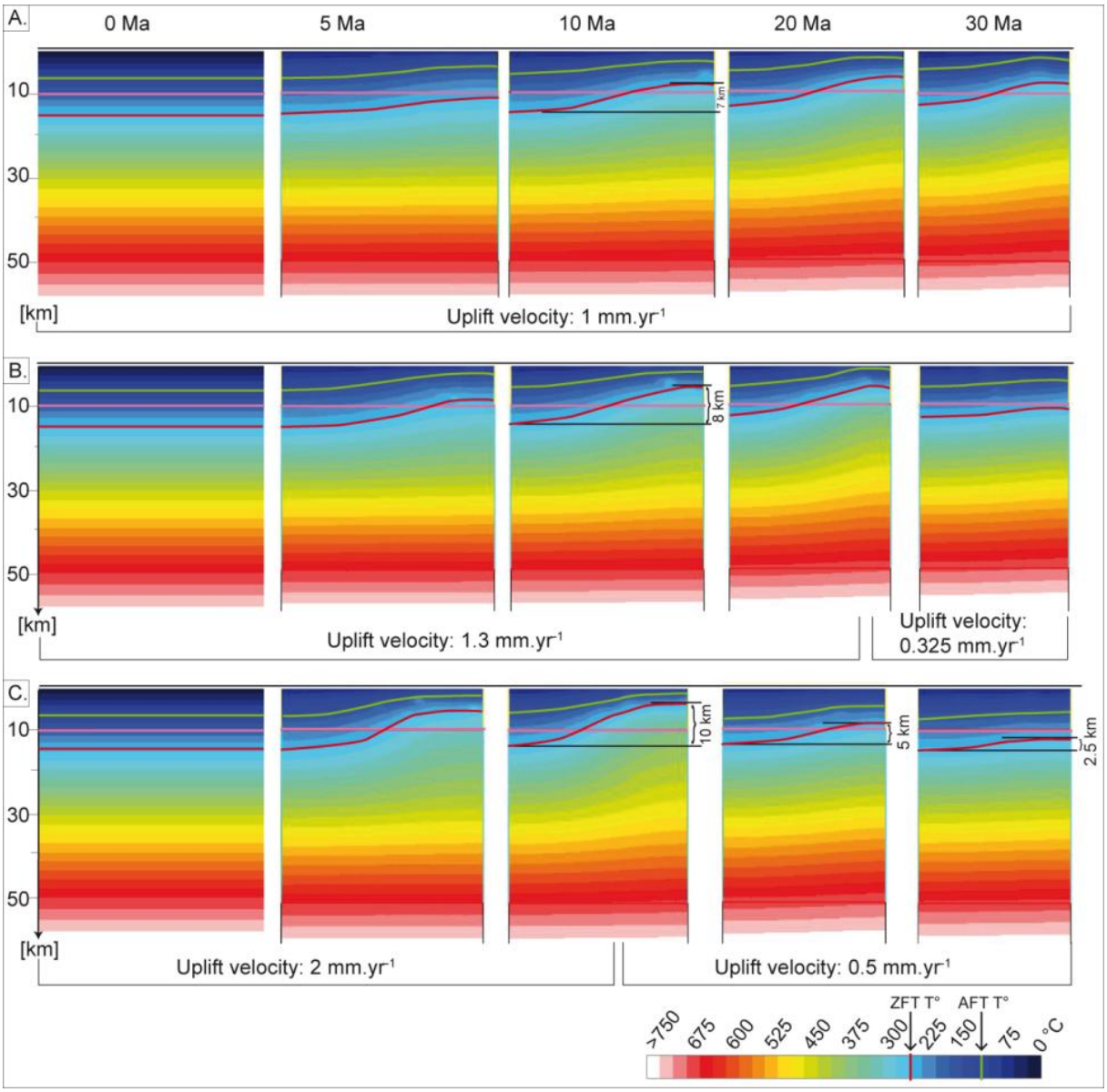

Figure IV. 9. Folding and erosion of a lithosphere with an initial thermal steady-state for three models with different uplift rates. A. Model 1: constant uplift rates of 1 mm.yr^{-1} during 30 Myrs; Model 2: uplift rates of 2 mm.yr^{-1} during 10 Ma and of 0.5 mm.yr^{-1} for the last 20 Myrs; C. Model 3: uplift rates of 1.3 mm.yr^{-1} during 20 Myrs and of 0.325 mm.yr^{-1} for the last 10 Myrs. Temperatures at the surface are set to 0 °C. Green and red lines represent the isotherms corresponding to the apatite and zircon fission track closure temperatures, respectively. Pink line marks the 10 km depth.

Constant uplift rate of 1 mm.yr^{-1} involves a constant deformation of the isotherms during 30 Myrs (Figure IV.9a). At 10 Myrs, a referenced line defined by material point that were lying on an horizontal surface before shortening is folded with an amplitude of 10 km while the isotherms are folded into an antiform, whose amplitude attains 7 km (Figure IV.9a).

If the uplift rate is increased to1.3 mm.yr^{-1}, bending of the isotherms is more intense than for uplift rates of 1 mm.yr^{-1}. Folded isotherms attain amplitudes of 8 km after 10 Myrs, while the amplitude of a folded material line attains 16 km (Figure IV.9b). If the uplift rate is reduced to 0.325 mm.yr^{-1} in the final stages of the experiment, thernal re-equilibration reduces the amplitude of the folded isotherms to less than 1 km (Figure IV.9b).

Fast uplift rates of 2 mm.yr^{-1} rapidly induce higher bending of the isotherms (Figure IV.9c). After 10 Myrs, material lines shortened into an antiform of 20 km amplitude and the isotherm into one of 10 km amplitude (Figure IV.9c). When the uplift rate is reduced from 2 mm.yr^{-1} to 0.5 mm.yr^{-1}, re-equilibration of the isotherms reduces the amplitude of their flexure to about 2.5 km after 10 Myrs (Figure IV.9c).

IV.3.3 Initial low-temperature stacked nappes and folding/erosion

Models with initial thermal anomaly resulting from the stacking of nappes that underwent low temperature subduction (Initial steady state 2; Figure II.7b) display higher geothermal gradients than models with initial steady state temperature distribution (Figure IV.9). The boundary conditions along the surface cause a larger perturbation of the geothermal gradient in the lower part of the model, i.e. below 15 km, compared to the upper part of the model. The geothermal gradient is higher and the temperature increases considerably with depth in comparison with models with initial steady thermal state (Figures IV.9 and IV.10).

The disturbance of the isotherms is amplified when applying a deformation to the models. Constant uplift rate of 1 mm.yr^{-1} involves an important increase of temperatures with depth associated with a high geothermal gradient in the right part of the model (Figure IV.10). Models with uplift rates of 2 mm.yr^{-1} during the first 10 Ma, followed by lower uplift rates of 0.5 mm.yr^{-1} show large disturbance of the isotherms during the 10 first Myrs and a slight re-equilibration of the isotherms during the following phase of slower uplift, although the geothermal gradient still remains important (Figure IV.10).

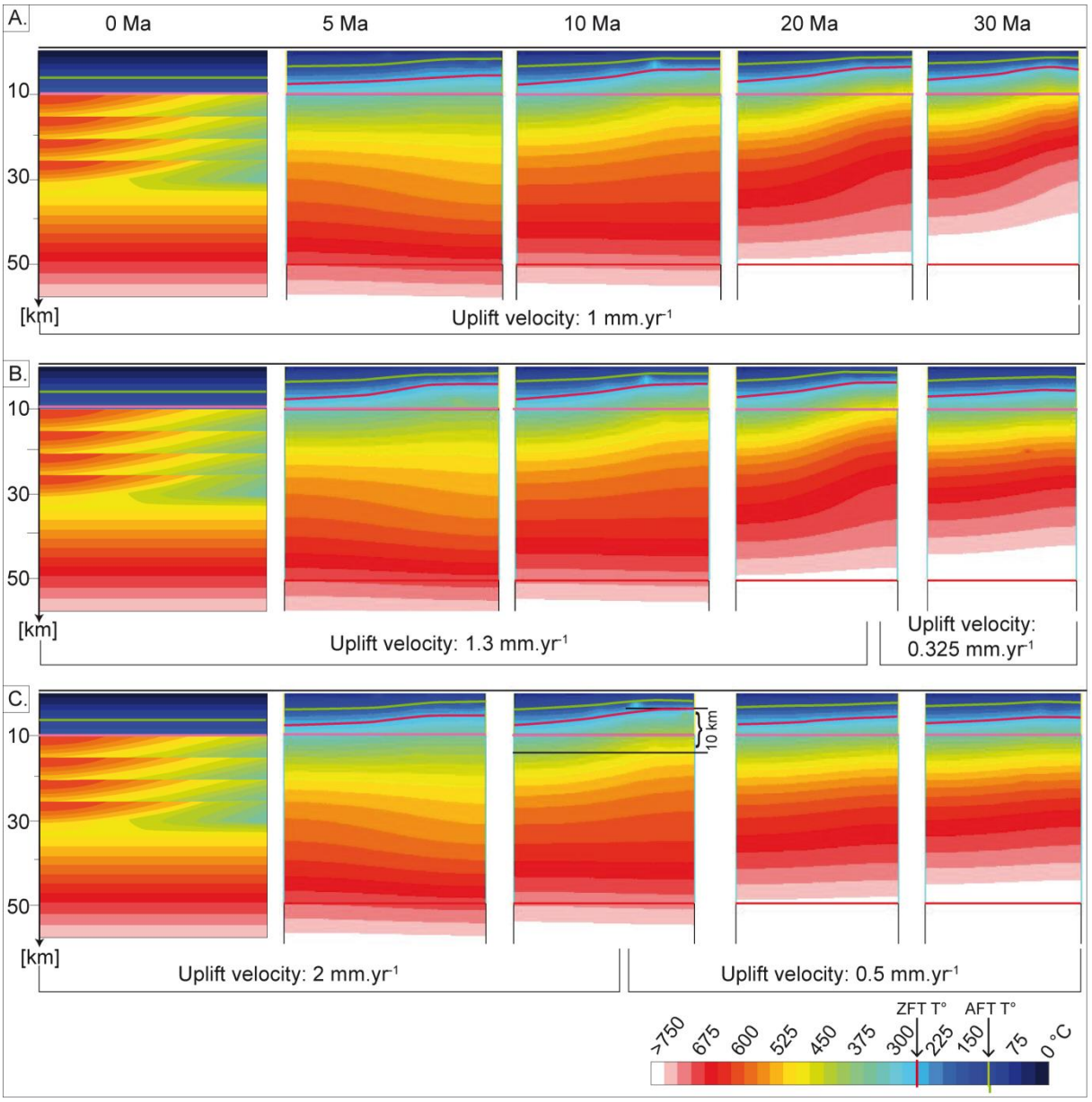

Figure IV. 10. Folding and erosion of a lithosphere with an initial thermal steady-state consisting of nappes that were initially affected by temperatures up to 600 °C during subduction. A. Model 4: constant uplift rates of 1 mm.yr^{-1} during 30 Myrs; B. Model 5: uplift rates of 2 mm.yr^{-1} during 10 Ma and of 0.5 mm.yr^{-1} for the last 20 Myrs; C. Model 6: uplift rates of 1.3 mm.yr^{-1} during 20 Myrs and of 0.325 mm.yr^{-1} for the last 10 Myrs.. See legend in figure IV.9.

IV.3.4 Lithosphere with initial hot stacked nappes and folding/erosion

Models including an initial thermal anomaly, which results from the stacking of hot nappes (Figure IV.11) display a geothermal gradient twice as high as the models consisting of an initial thermal steady state (Figure IV.9) with a difference of temperature of ca 200 °C (Figure IV.9 and IV.11). For an initially undisturbed thermal state, an asymmetry is only visible in the upper part of the crust and the lateral difference in the temperatures is of c.a. 100 °C (Figure IV.9) while for an initially disturbed thermal state the asymmetry is more important in the lower part of the model (Figure IV.10 and IV.11). The asymmetry due to the

initial thermal anomaly is still visible after 30 Ma and it is more important for models with lower uplift rates (1 mm.yr^{-1}) than for the models with uplift rates of 2 mm.yr^{-1} (Figures IV.10 and IV.11).

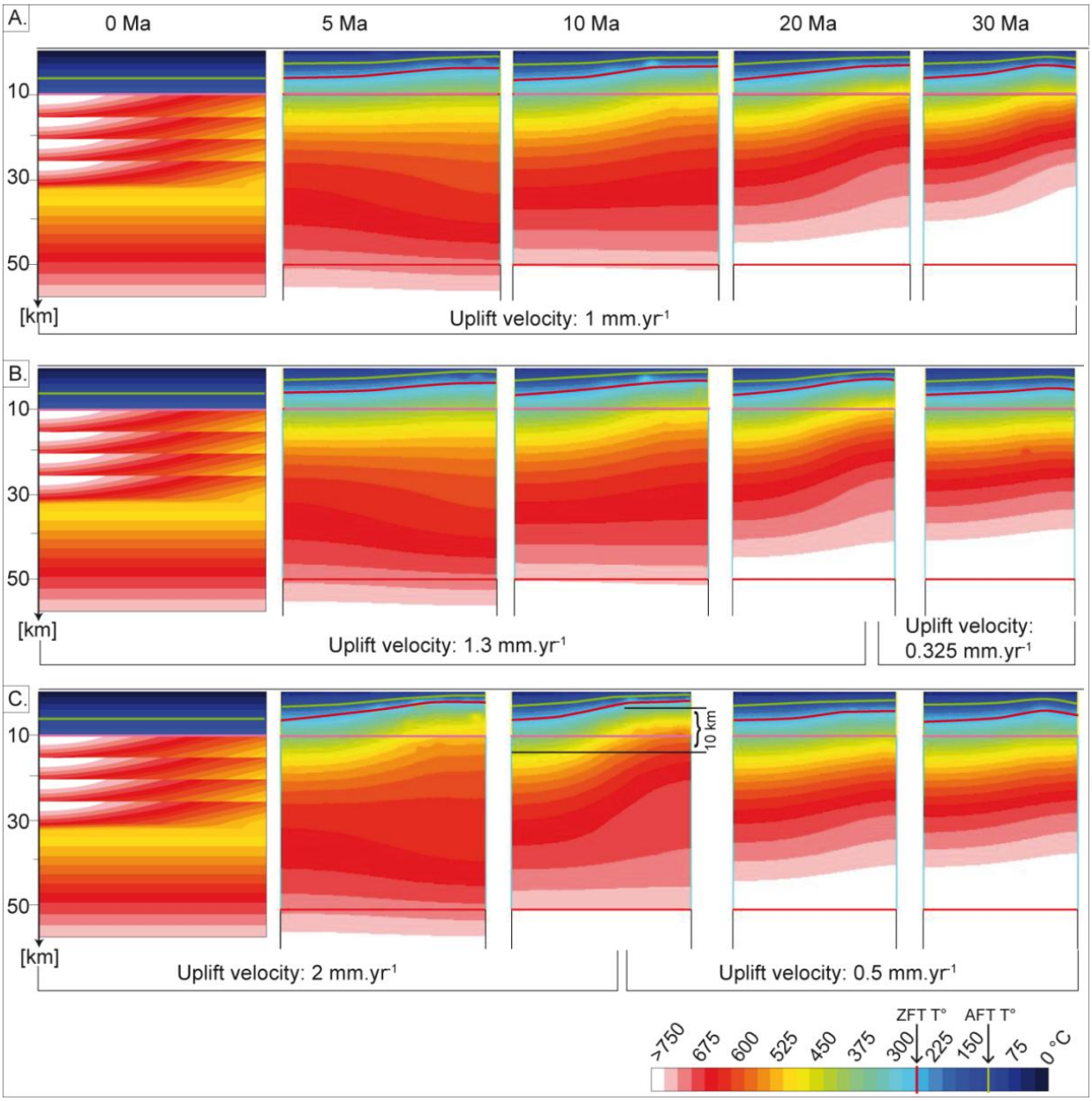

Figure IV. 11. Thermal evolution of a lithosphere including nappes that were initially affected by temperatures up to 700 °C during subduction. 3 different uplift rates are shown. A. Model 7: constant uplift rates of 1 mm.yr^{-1} during 30 Myrs; Model 8: uplift rates of 2 mm.yr^{-1} during 10 Ma and of 0.5 mm.yr^{-1} for the last 20 Myrs; C. Model 9: uplift rates of 1.3 mm.yr^{-1} during 20 Myrs and of 0.325 mm.yr^{-1} for the last 10 Myrs. See legend in figure IV.9.

IV.3.5 Predicted thermal history

A major result of the models is the conversion of the PT paths of material points into thermo-chronological ages. The models track the transition time of material points through the

isotherms of 110 ° and 240 °C, corresponding to the inferred closing temperatures of fission tracks in apatite (Dodson, 1979; Naeser, 1981; Parrish, 1983; Corrigan, 1991; Reiners and Brandon, 2006) and zircon (Reiners and Brandon, 2006), respectively. The results illustrate the exhumation path through the last ca. 16 km of the crust, assuming an average geothermal gradient of 15 °C.Km^{-1}. Models with different initial thermal conditions and uplift rates result in different thermo-chronologic ages of the material points that attained the surface in the final stage of the models (Figures IV.9, IV.10 and IV.11). The results of the nine different models in terms of low-temperature ages are presented in Figures IV.12 in a series of ages vs. distance diagrams, where the horizontal distance corresponds to the one of the model box at its initial stage. The ages refer to material points at the surface of the model and correspond to the time-span spent between the transition of the isotherm corresponding to the closing temperature of fission tracks and the end of the 30 Myrs modelled time.

All cross-sections performed along the surface of the mesh at the end of the models show bell-shaped curves with younger ages in the central part (Figure IV.12). As expected apatite ages are always younger than the zircon and the initial thermal state and the uplift velocities cause different age patterns, as shown by the variations along columns and rows of figure IV.12, respectively.

A general trend can be recognised as followed: Models with low uplift rates during longer time (Models 3, 6 and 9; Figure IV.12) result in older apatite and zircon fission track ages, and initially colder thermal states result in older apatite and zircon fission track ages (Models 1, 2 and 3; Figure IV.12). In contrast, the difference in time lag between apatite and zircon fission track ages does not follow a trend. While the offset between apatite and zircon ages is of 6 Ma for the steady state geothermal gradient, it is of 5 to 9 Ma for the LT subduction and of 3 Ma for the HT subduction (Figure IV.12).

Similarly, no correlation occurs between uplift rates and the time lag between apatite and zircon fission track ages. Therefore, the initial thermal states as well as the uplift velocities do influence apatite and zircon fission track ages and the two isotherms, corresponding to the closure temperature of apatite and zircon fission track systems, react differently to changes in the latter parameters.

Model 3 (steady state and uplift rates of 2mm.yr^{-1}) (Figure IV. 12) does not provide any zircon fission track ages due to its cold initial thermal state. The points that are at the surface after 30 Myrs were already above the “closure temperature” at time zero of the model. Under natural conditions, these points would give ages that are older than 30 Ma, but our model does not allow for the calculation of ages older than 30 Myrs, i.e. older than the bulk modelled time interval.

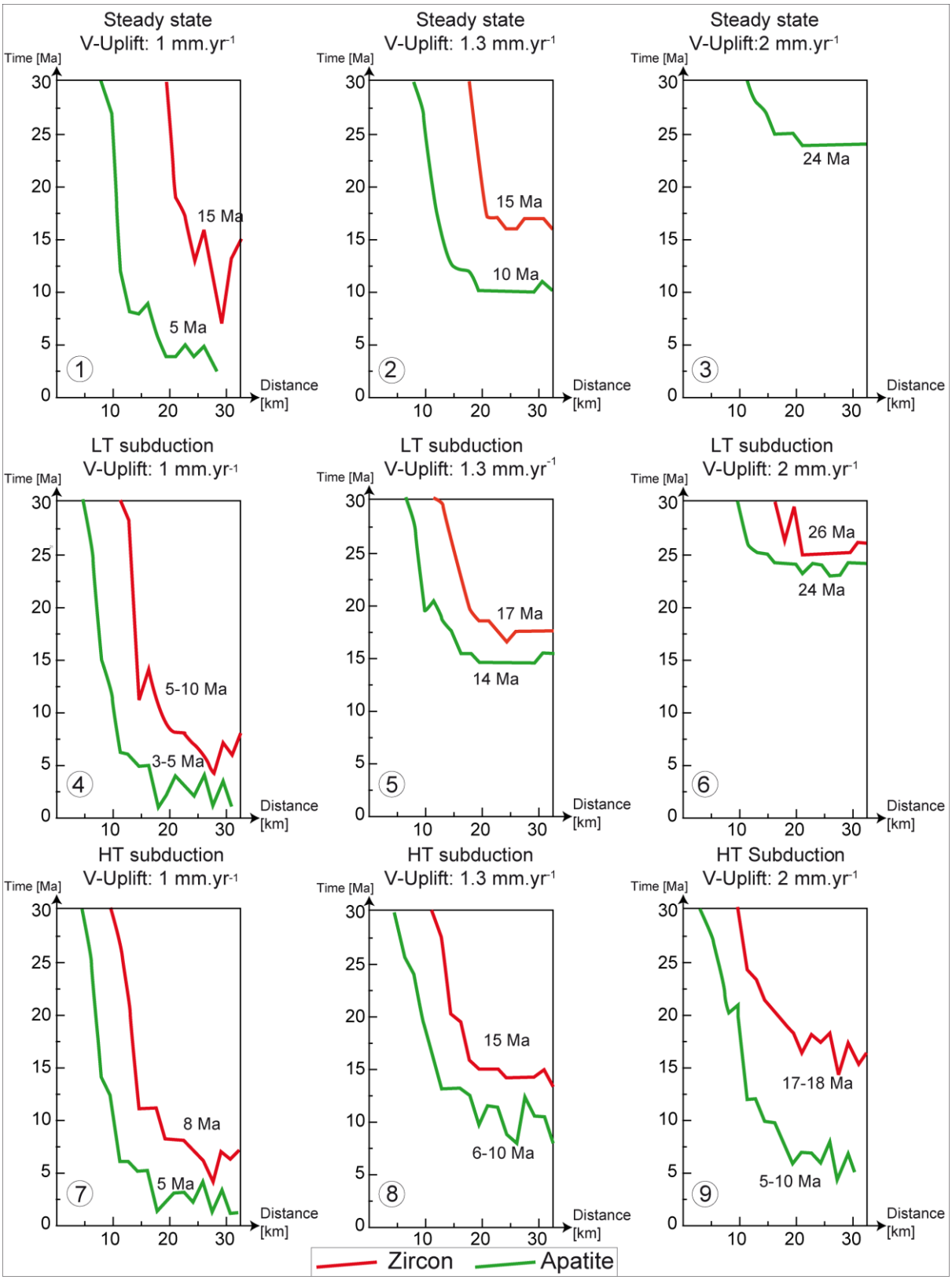

Figure IV. 12. Apatite and zircon fission track age profiles along the surface at the end of the experimental runs.

In the following we discuss in detail the relative contribution of the initial thermal state and the uplift velocities on the resulting apatite and zircon fission track ages before comparing modelled ages to the apatite and zircon fission track data in the Tauern Window.

IV.4. Discussion

IV.4.1 Effect of the initial thermal state

The initial thermal states are disturbed until the end of the runs, hence affecting the absolute ages and age distributions (Figure IV.12). The younger ages predicted by the HT experiments (models 7, 8 and 9 Figure IV.12) in comparison with the models of LT subduction (graphs 4, 5, 6 Figure IV.12) and steady-state geothermal gradient (graphs 1, 2, 3 Figure IV.12) are due to the hot anomaly imposed to the initial thermal state, which causes higher temperatures at shallower depths even in the final stages of the experiments. Therefore, for a given uplift rate, material points of the HT models passed through their "closure temperature" later than for a colder initial thermal state.

For a constant uplift rate of 1 $mm.yr^{-1}$, initial thermal anomalies generated by the stacking of low temperature nappes (≤ 600 °C; Figures IV.7b and IV.10) seems to be rapidly annealed (after 5 Ma) by re-equilibration of the isotherms. However, comparison of the latter experiments (Figure IV.10) with others performed at the same uplift rates (1 $mm.yr^{-1}$) but with higher temperature anomalies (stacking of hot nappes at T ≤ 700 °C; Figure IV.11) shows that the geothermal gradient, even where the model is not significantly shortened, remains higher in the hot nappes model. This effect shifts the level of the partial annealing zone of the entire crust closer to the surface, even where shortening is modest (left side of the model). As a consequence, the wavelength of the area with reset ages, i.e. of the area showing fission track ages in the models, correlates with the initial temperature of the models. Initially higher temperature anomalies (LT subduction and HT subduction; Figures IV.7b and IV.7c) always increase the initial geothermal gradient, widening the area affected by exhumation of material points that passed across their PAZ, i.e. widening the area comprised within the half-bell shaped curves of the distance vs. age diagrams (Figure IV. 12), for any given uplift rate. This effect is due to the lateral diffusion of heat from the initial site of the temperature anomaly to the area located in the hinge of the antiform (Figures IV.10 and IV. 11). In other words, whereas the steady state model creates a bend of the isotherms that is only dependent on the area of uplift, the other models widen this bend by thermal diffusion, hence widening the associated age distributions.

The models with initial thermal state disturbed by hot nappes (Figures IV. 10 and IV.11) do not reach a steady thermal state at the end of the runs. The hot isotherms are still bended after 30 Myrs on the contrary to the isotherms of the models with initial steady thermal state (Figure IV.9) that are subhorizontal after 30 Myrs. The low temperature isotherms of the models LT and HT subduction tend to be horizontal after 30 Myrs (Figures IV. 10 and IV.11). This means that hot initial temperatures induce a slower re-equilibration of the high

temperatures isotherms than of the low temperature isotherms after decreasing of the uplift rates compared to colder initial thermal states. As a consequence, the resulting apatite and zircon ages are expected to be older if the initial temperatures are colder.

IV.4.2 Effect of uplift rates

Slower uplift rates result in younger apatite and zircon fission track ages (Figure IV.12). Assuming horizontal isotherms before the initiation of uplift, the time span required for a material point to cover the distance between the level of its "closure temperature" and its exposure at the surface of the model is shorter for higher uplift rates (Figures IV.12). Such a process should generally go together with younger thermochronological ages, but this is not the case in the present experiment (Figure IV.12) because higher uplift rates are always followed by very slow ones, in order to maintain constant bulk shortening and constant bulk duration in all experiments (Figure IV.5). As a consequence, fast uplift rates rapidly expose material points at the surface of the model in the first stages of the experiment (Figure IV.5), while a second stage with lower uplift rates "freezes" olds ages at the surface. Young ages cannot form because the remaining uplift rate is too low to bring material points from their level of closing temperature to the surface.

This discussion does not take into account folding of the isotherms that may occur during shortening of the mesh. Such a folding shifts the partial annealing zone of a given thermochronometer to higher crustal levels, reducing the distance between closing temperature and surface exposure. Therefore, higher uplift rates increase the ages of cooling on the one hand, but partly reduce them in the core of antiforms by deflecting the isotherms, hence shortening the distance between the level of the partial annealing zone and the surface. In such cases, a complex interplay exists between the perturbation of the isotherm due to material advection and the increase of uplift rate.

Results of the models based on three different uplift rates starting with the same initial steady thermal state (Figures IV.9) allow one to quantify the ratio between uplift rates and re-equilibration of the isotherms during deformation of the mesh. Since the initial thermal conditions are the ones of an equilibrated geothermal gradient, the thermal evolution in these three experiments is not affected by any inherited thermal anomaly, but entirely driven by heat advection during folding. The first and second models (Figures IV.9b and 9c) show that uplift of 0.325 $mm.yr^{-1}$ and 0.5 $mm.yr^{-1}$ are not sufficient to counterbalance the re-equilibration of the isotherm. Upward advection of material points is not fast enough to allow for the upward flow of heat. Thus, a partial equilibration occurs and the thermal state of the system tends to go back to a state of thermal equilibrium (Figures IV.9b and 9c). In contrast uplift rates higher than 1 $mm.yr^{-1}$ induce folding of the isotherms. Exhumations rates of 2 $mm.yr^{-1}$ (Figure IV. 9c) are fast enough to counterbalance the re-equilibration of the isotherms and to bend them. Nevertheless, the amplitude of the fold created by differential exhumation of material points is by far larger than that of the upward bent isotherms. In the first model (Figure IV.9a), after 10 Ma of shortening and uplift, the amplitude of the folded mesh is twice

as much as the amplitude of the folded isotherms. Deformation must occur with sufficient velocities that thermal equilibrium of the system cannot be obtained. We thus propose that the resulting thermochronological ages of modelled surface points after shortening of the mesh are mostly related to the differential exhumation path followed by the material points and in a second order from deformation of the isotherms. Higher uplift rates induce higher amplitude of folding of the isotherms, increasing the geothermal gradient in the hinge of the antiform. However, this effect is counterbalanced by thermal re-equilibration following the high uplift rate experiments, re-increasing the distance between the isotherms, hence the age difference between apatite and zircon fission track ages.

In other words, increasing uplift rates strongly enhances the amplitude of bending of the isotherms (Figures IV.9c). However, the reduction of such amplitude is fast (less than 5 Ma) if the uplift rate is reduced to values ≤ 0.5 mm.yr^{-1} (Figures IV.9c). The range of uplift rates comprised between 1 mm.yr^{-1} and 0.5 mm.yr^{-1} seems to represent a threshold between rates that cause very significant bending of the isotherms and rates that barely affect the geometry of the isotherms.

IV.4.3 End-members models for the interpretation of fission track ages and implications for the thermal evolution and exhumation of the Tauern Window

Apatite and zircon fission track ages of the western sub-dome of the Tauern Window indicate a concentric iso-age pattern with ages younging toward the core (Figure IV.13) and with the long axis of this structure oriented parallel to the axial plane of the main fold of the dome. A similar structure has been observed within other domes characterised by large-scale antiforms (e.g. Olympic Mountains, Batt et al., 2001).

The close spatial relationship between iso-age pattern and folded structures in these areas suggests a correlation between folding and cooling pattern. However, the precise temporal relationship between these two processes is not easy to assess, as shown by the results of our numerical models. We discuss below why younger ages may be found in the core of these antiformal structures, describing two end-member processes that relate the thermochronological ages at the surface with uplift of the rocks, bending of the isotherms, and re-equilibration of the isotherms (Figure IV. 14).

Previous interpretations of apatite and zircon fission track ages of the Tauern Window tacitly assume that isotherms and isograds were folded during exhumation of the Tauern Window because of heat convection provided by upward advection of hot deep material during folding (Luth and Willingshofer, 2008). As a consequence, these authors point to horizontal thermal gradients of approximately 300°C during their Miocene reconstruction of the area, implying a very significant folding of the isotherms. As in our models, Sleep (1979) shows that thermal equilibration may counterbalance folding of the isotherms if the upward movement of the rocks is not sufficiently rapid. Therefore, interpretations of apatite and zircon fission track ages from mountain chains, which assume that the isotherms are folded

due to heat advection, are valid only if the uplift velocities are sufficient to prevent equilibration of the isotherms.

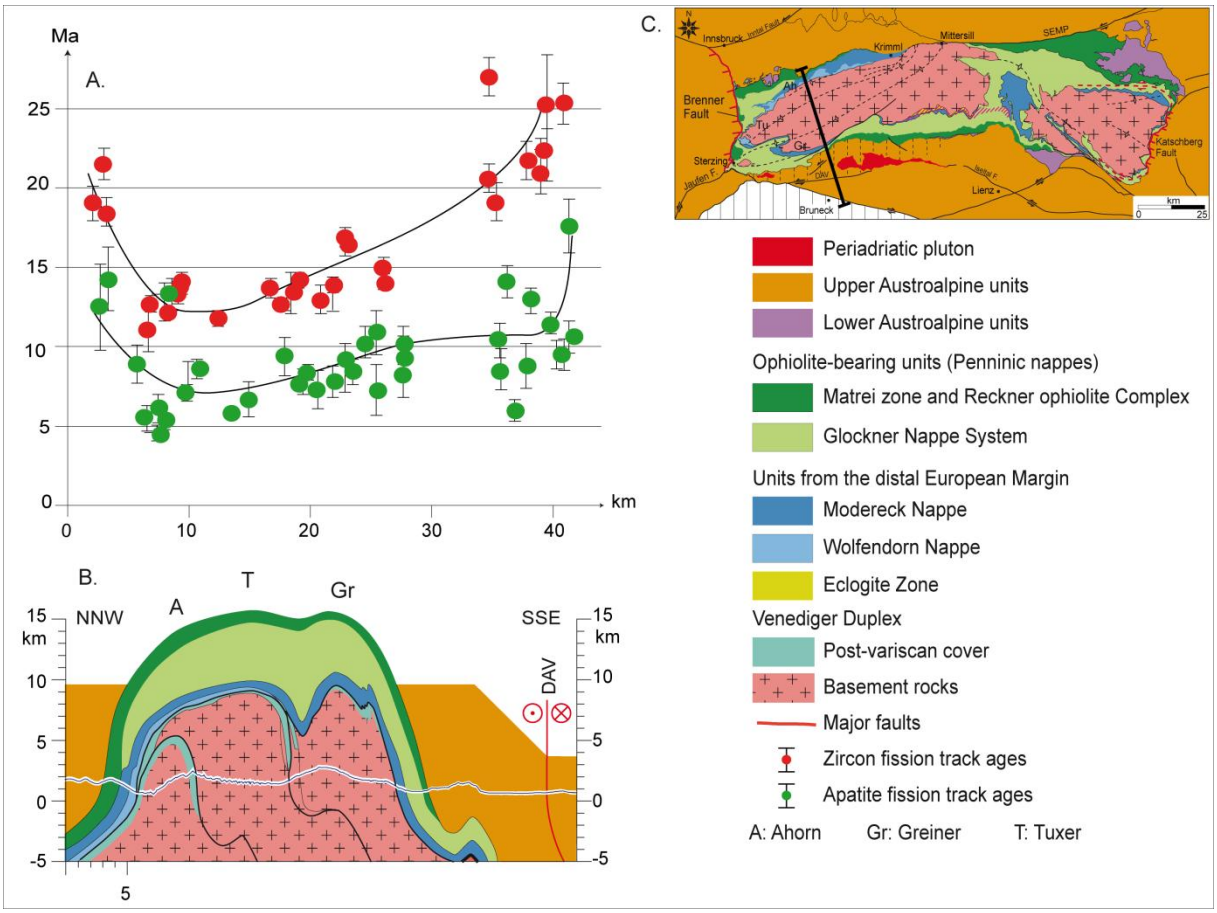

Figure IV. 13. A. Apatite (green) and zircon (red) fission track ages versus distance along a cross-section that strikes perpendicular to the fold axe; (Grundmann and Morteani, 1985 and Chapter II, this study . B. NNW-SSE profil throught the western sub-dome of the Tauern Window based on Schmid et al., 2013. C. Simplified geological map of the Tauern Window with location of the cross-section (based on Scharf et al., 2013).

Sleep (1979) proposes that the high temperatures in the warmest parts of the system may be maintained after cessation of folding if thermal equilibration does not occur. As a consequence, temperatures could increase in the cooler parts of the system even after cessation of the deformation, implying that the peak of metamorphism in the lower temperature regions may postdate the folding (Sleep, 1979). However, the models presented in this work show that equilibration of disturbed isotherms occurs within a time span of maximum 5 Myrs after cessation of deformation (Figure IV.8). Although a variation of 100° C in the initial thermal state affects the geothermal gradients of the models until the end of the experiments, the anomaly itself, which causes a lateral bending of the isotherms, is eliminated within a time span of approximately 5 Ma, inhibiting lateral heat diffusion that would heat the limb regions of the antiform (Figure IV.8). Under these conditions, and, in contrast to Sleep (1979), the peak of thermal metamorphism cannot be attained after cessation of the

deformation. The difference between the results of Sleep (1979) and our results is due to differences in the boundary conditions. The models of Sleep (1979) are based on the natural case study of Acadian folding (U.S.A), where exhumation rates are considerably higher (30 to 45 mm.yr^{-1}) and the bulk duration of deformation is shorter (0.16 and 0.59 Myrs). In contrast, our models are inspired from thermochronological data in the Tauern Window that display much lower uplift rates of maximum 2 mm.yr^{-1} (Grundmann and Morteani, 1985; Fügenshuh et al. 1997; Chapter II, this study), inducing smaller lateral thermal gradient preventing post-tectonic heating of the cooler parts. The maximum temperatures in the core of the fold and thermal gradient between the core and the rims of the folds are thus much higher in the models of Sleep (1979) compared to our models.

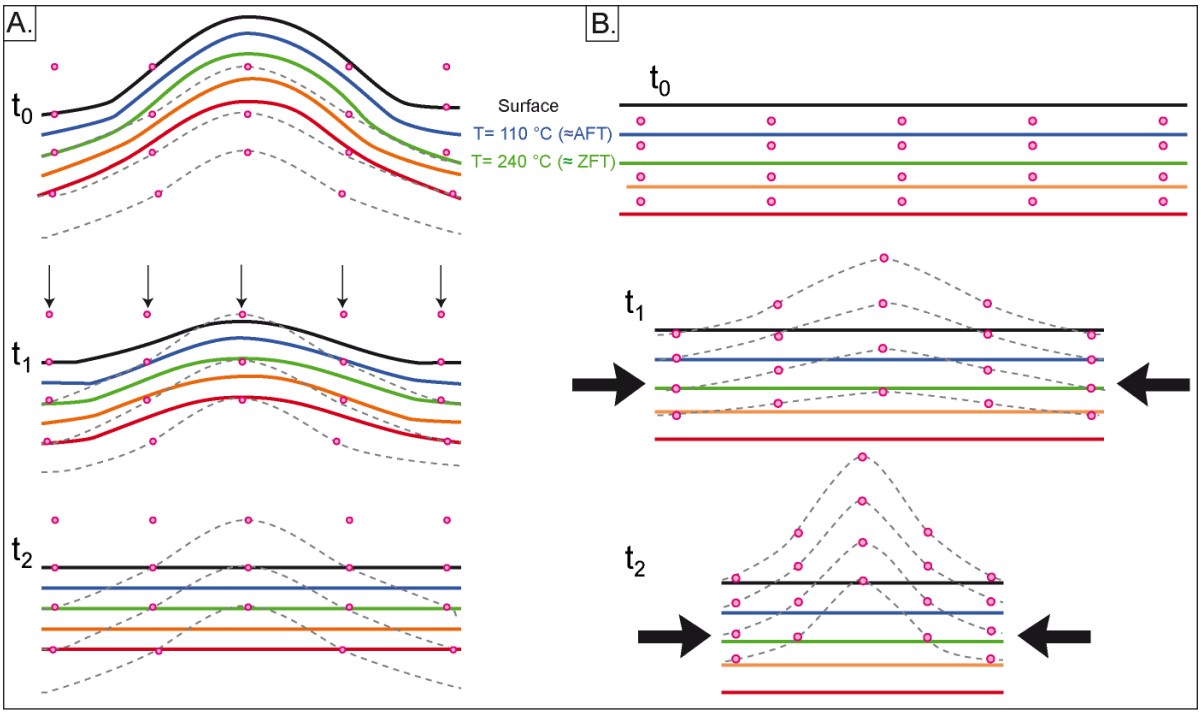

Figure IV. 14. End-member conceptual models showing A. deformation of the isotherms during formation of the dome followed by thermal re-equilibration, and B. Differential uplift increasing in the core of the dome without bending of the isotherms. Pink dots represent material points. Coloured lines represent the isotherms.

In the absence of lateral heat diffusion, thermochronological ages of a folded region may result either from re-equilibration of the isotherms after folding (Figure IV.14a), hence from downward displacement of the isotherms through a nearly stationary rock unit, or from exhumation, hence the transition of a rock through a nearly stationary partial annealing zone (Figure IV.14b) due to vertical displacement towards the surface.

The first model (Figure IV.14a) assumes that uplift rates during folding were sufficiently high to inhibit re-equilibration of the isotherms. Hence, advection driven by upward movement of deep, hot material results in folded isotherms (Figure IV. 14a). For the sake of clarity, we show that the isotherms are folded with the same amplitude of the folded material lines, a situation that could only exist for instantaneous folding. After crustal folding and

upward bending of the isotherms, progressive cooling displaces the isotherms downward through the previously folded crust (Figure IV. 14a). As shown in figure IV.14a, a given isotherm descending to its horizontal equilibrium position, reaches the material points of a horizontal plane first along the limbs border and later within the core of the antiform. In other words, the time needed to cool the central part of the dome is longer than the one needed to cool its limbs. Resulting ages thus provide a pattern similar to the one of the Tauern Window (Figure IV.13) and of our models (Figure IV.12), i.e. younger ages in the hinge of the fold and older ones in the limbs.

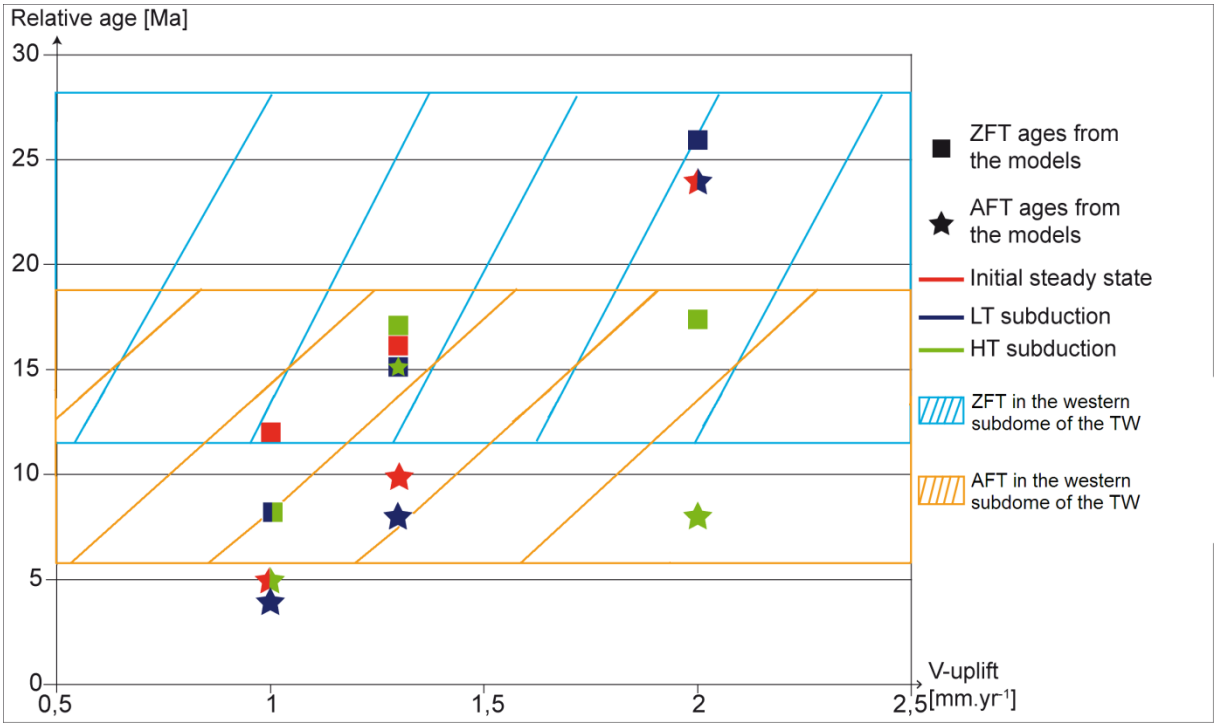

Figure IV. 15. Apatite and zircon fission tracks calculated for a point located in the central part of the surface after running the models.

The second end-member model proposes that uplift of the rocks is too slow to counterbalance, the re-equilibration of the isotherms. For the sake of clarity we sketch three stages of a folding event in which the isotherms are not folded at all (Figure IV.14b). In this case, the ages of surface samples date their upward movement through a given fixed isotherm, during folding and erosion of the crust. Since uplift rates are higher in the hinge of the fold compared to the limbs, the time span between the transition of the isotherm corresponding to the closure temperature and the attainment of the surface is longer in the limbs than in the centre (Figure IV.14b). As a consequence, this model results in the same cooling pattern than the previously one, i.e. younging of ages towards the centre of the fold. However, the significance of the ages is very different. In the first case they date post-tectonic folding; in the second case they date syn-tectonic folding.

Both models are expected to result in similar cooling-age patterns, in the sense that younger ages form in the core of the folded area. Therefore, it is difficult to decipher which

model is more appropriate to describe the thermal evolution of the crust during exhumation of the Tauern Window. A comparison of the central ages obtained from the different models and the mean apatite and zircon fission track ages of the Tauern Window (Figure IV.15) may help to discriminate between the two models.

Along the cross-section parallel to the maximum shortening direction and in the western sub-dome of the Tauern Window and adjacent Austroalpine units, apatite display ages comprise between 14 Ma and 18 Ma and zircon fission track ages are comprised between 11 Ma and 29 Ma (Figure IV.13).

Taking in account the initial thermal state, which mimics best the present-day age distribution of the Tauern Window, only the model with uplift rates of 2 $mm.yr^{-1}$ and a HT subduction history provides ages corresponding to the apatite and zircon fission track ages of the Tauern Window (Figures IV.11c and IV.15). Models with uplift rates of 1 $mm.yr^{-1}$ yield ages that are too young in comparison with the natural data sets, whereas models with uplift rates of 1.3 $mm.yr^{-1}$ provide apatite ages that are too old. We previously showed that, after 10 Myrs, for exhumation rates of 2 $mm.yr^{-1}$ the amount of maximal uplift of the rock is twice higher than the maximal deformation of the isotherms (Figure IV.11c) indicating that folding and equilibration of the isotherms occur simultaneously.

The spatial variations of thermochronological ages in the Tauern Window was interpreted in terms of lateral temperature gradients, in excess of 40° $C.km^{-1}$ (Luth and Willingshofer, 2008) during the Miocene, hence severe folding of the isotherms over short wavelengths. Such horizontal temperature gradients are otherwise only known from contact aureoles around magmatic bodies. This interpretation tacitly assumes that uplift velocities (exhumation rates) were the same for all samples after they passed the partial annealing zone. If this is the case, where the same age is obtained in different areas for different thermochronological systems, the closure temperatures of the latter can be used to track horizontal temperature differences at one and the same time (Luth and Willingshofer, 2008). However, if uplift rates between the PAZ and the surface are not constant throughout the study area, the latter interpretation of thermochronological ages is not applicable. In the hinge of an antiform, ages may be younger due to higher uplift rates, because these samples passed later through the PAZ.

The model results may be compared to the thermochronological ages from the Tauern Window (Figures IV.12, IV.13 and IV.15). The models show that the ages of the hinge region, which always form an irregular plateau in the age vs. distance plots (Figure IV.12) vary strongly as a function of uplift rates and of the initial thermal conditions of the models. The youngest ages may vary between 2 Ma and 24 Ma for the apatite and 5 and 15 Ma for the zircon (Figure IV.12), although the folding process lasts for 30 Ma in all models. If the results of the model can be used to interpret the apatite and zircon fission track ages of the Tauern Window it may be concluded that the ages of the hinge area do not date the initiation nor the termination of folding, whereas the oldest ages on the limbs of the antiform, which do not vary from one experiment to the other, do date the initiation of folding. Under natural

conditions, the limbs of the antiform are characterised by the transition from reset ages within the fold to older ages outside of the fold, not existing in the models. In this natural case study, zircon FT ages between 25 and 30 Ma (Figure IV.13), would date the beginning of folding, inferring that it is significantly older compared to recent interpretations (Scharf et al., 2013).

It is important to state here, that this interpretation, suggesting initiation of folding between 25 and 30 Ma, does not result from the boundary conditions of the models, which impose 30 Ma of folding. It is the general geometry of the age vs. distance curves, not its absolute age values, that allows us to draw this conclusion, by comparing them to the age-distance curves of the Tauern Window (Figure IV.13). We emphasize, that all models including a phase of slower uplift in their final stages, yield fission track ages that are more than 10 Ma younger than the termination of folding. We thus propose that cooling patterns of the Tauern window, derived from apatite and zircon fission track ages (Luth and Willingshofer, 2008; Chapter II, this study) result from a two-stage deformation event. During the first stage of the deformation, Penninic units of the Tauern Window are exhumed with uplift rates that are high enough to fold the isotherms. At the surface and along a cross section perpendicular to the fold axis, rocks coming from higher depth and yielding younger ages are found in the core of the fold. After this event uplift rates slow down and equilibration of the isotherms occurred with cooling of the hinge area preceding the cooling in the limbs, inducing younger ages in the core of the fold.

Conclusion

In order to have a quantitative base to interpret the thermochronological data of the Eastern Alps, we explored a set of different boundary conditions that may have affected the Tauern Window and its surrounding areas during Tertiary times. We tested the effect of different initial temperature distribution and uplift rates on the cooling history and age distribution of a lithosphere undergoing folding and erosion.

All experiments reproduce the first order age distribution observed in the Tauern Window, i.e. the (half-) bell shape of the ages plotted against distance. However, they show that the precise relationship between fission track ages, and the age of folding as well as the relationship between area of the fold and area of reset ages is strongly dependent on the thermal and tectonic history of the folded area.

The thermal inheritance of the subducted crust has a dramatic effect on the age distribution of apatite and zircon fission track age distribution, provided a fast uplift rate (2 $mm.yr^{-1}$). If this is the case, cooling ages are significantly younger for a crust that was affected by HT subduction. If uplift rates are slower the thermal structure inherited from the subduction stage does not strongly affect later low-temperature geochronometers as shown by all models run at 1.3 and 1 $mm.yr^{-1}$ and different initial thermal states.

Within each model, irrespective of the chosen boundary conditions, the amplitude of the folded isotherms increases downward in the crust. As a consequence, the lateral age difference between limbs and hinge of the antiform is higher for thermochronometers with

higher closing temperature. These features are also observed in the age distribution across the Tauern Window and even more clearly if higher-temperature thermo-chronometers are considered, as Rb/Sr and K/Ar on biotite (Luth and Willingshofer, 2008).

Equilibration of deformed isotherms starts immediately after the cessation of the deformation. Therefore, in contrast to the statement of Sleep (1979), the peak of thermal metamorphism is contemporaneous to the deformation phase, if the uplift rates correspond to those of our experiments, which are consistent with independent geological data of the Tauern Window. We have shown that a competition occurs between equilibration of the isotherms and deformation of the system. By comparing the models with the natural study case of the Tauern Window, we conclude that the apatite and zircon fission track ages are primarily resulting from the initial thermal state and differential uplift rates between the core and the rims of the dome. Initial thermal state results from hot subducted and stacked nappes that vertically disturb the geothermal gradient over the system with higher geothermal gradient in the 30 shallower kilometres of the upper crust and lower geothermal gradient in the lower part of the crust. Differential uplift rates bring to the surface hot material originating from higher depth in the core of the area. Then uplift rates slow down and equilibration of the isotherms occurred. Hotter material of the core of the fold thus cooled later than rocks located at the rims, inducing younger ages in the core of the fold.

The absolute ages of the modelled geochronometers in the core of the antiform are strongly dependent on the initial thermal state of the model and on its uplift rates; hence they cannot be used to date the initiation nor the termination of the folding process. The more reliable way of dating the initiation of folding is given by the ages of the thermochronometers in the most external part of the limb of the antiform, where both thermochronometers yield the same age. These ages are analogous to the oldest reset ages under the natural conditions of the Tauern Window, where they vary between 20 and 25Ma.

References

Batt, G. E., Brandon, M. T., Farley, K. A. and Roden-Tice, M., 2001. Tectonic synthesis of the Olympic Mountains segment of the Cascadia wedge, using two-dimensional thermal and kinematic modeling of thermochronological ages, J. Geophys. Res., 106, 26,731–26,746.

Batt, G., and Brandon M.T, 2002. Lateral thinking: 2D interpretation of thermochronology in convergent orogenic settings, Tectonophysics, 349, 185 –201.

Burg, J.P., Klaus, B.J.P. and Podladchikov, Y.Y., 2004. Dome structures in collision orogens: Mechanical investigations of the gravity/compression interplay. In: *Gneiss domes in orogeny*. Whitney, D., Teyssier, C., Siddoway, S. (eds.), The Geological Society of America, Special Paper 380, 47-66.

Campani, M., 2009. Temporal and spatial evolution of a syn-orogenic extensional system: the Simplon Fault Zone (Central Alps). PhD thesis, ETH Zurich.

Carry, N., Gueydan, F., Brun, J.P. and Marquer, D., 2009. Mechanical decoupling of high-pressure crustal units during continental subduction. Earth and planetary Sciences Letters, 278, 13-25.

Coney, P.J., 1980. Cordilleran metamorphic core complexes: An overview, In: *Cordilleran Metamorphic Core Complexes*, Crittenden, M. D., Coney, P. J. and Davis, G. H. (Eds.), 1980. Geol. Soc. Am. Mem., 153, 7-34.

Corrigan JD, 1991. Inversion of apatite fission track data for thermal history information. J Geophys Res 96: 10347-10360.

Crittenden, M. D., 1980. Metamorphic core complexes of the North American Cordillera: Summary. In: *Cordilleran Metamorphic Core Complexes*, Crittenden, M. D., Coney, P. J. and Davis, G. H. (Eds.), 1980. Geol. Soc. Am. Mem., 153, 485-590.

Dewey, J.F., Helman, M. L., Knott, S.D., Turco, E., and Hutton, D.H.W., 1989. Kinematics of the western Mediterranean, in *Alpine tectonics*, M.P. Coward, D. Dietrich and R.G. Park. (eds.). Geol. Soc. Spec.. Publ., London, 45, 265-283.

Dodson, M.H., 1979. Theory of cooling ages. In: *Isotope Geology* Jäger, E. and Hunziker, J.C (Eds), Lectures in Isotope Geology. Springer-Verlag, Berlin (1979), 194–202.

Ebbing, J., Braitenberg, C. and Goetze, H.J., 2001. Forward and inverse modelling of gravity revealing insight into crustal structures of the Eastern Alps. Tectonophysics 337/3-4, 191–208.

Eskola, P.E., 1949. The problem of mantle gneiss domes. Geological Society of London, Quaterly Journal, 104, 253-283.

Foster, D. A., Schafer, C., Fanning, M.C., and Hyndmann D. W., 2001. Relationships between crustal partial melting, plutonism, orogeny, and exhumation: Idaho-Bitterroot batholith. Tectonophysics, 342, 313-350.

Frisch, W., Dunkl, I., and Kuhlemann, J., 2000. Post-collisional orogen-parallel large-scale extension in the Eastern Alps. Tectonophysics, 327, 239-265.

Froitzheim, N., Schmid, S.M., Frey, M., 1996. Mesozoic paleogeography and the timing of eclogite facies metamorphism in the Alps: a working hypothesis. Eclogae Geologicae Helvetiae, 89, 81–110.

Fügenschuh, B., Seward, D. and Mantckelow, N. S., 1997. Exhumation in a convergent orogen: the western TW. Terra Nova, 9, 213-217.

Giese, P., Reutter, K.-J., Jacobshagen, V., Nicolich, R., 1982. Explosion seismic crustal studies in the Alpine Mediterranean region and their implications for tectonic processes. In: *Alpine-Mediterranean Geodynamics*. Berckhemer, H., Hsü, K.J. (Eds.), Geodynamics Series, 7. American Geophysical Union, pp. 39–73.

Glodny J., Ring, U. Kühn, Gleissner, P. and Franz, G., 2005. Crystallization and very rapid exhumation of the youngest Alpine eclogites (Tauern Window, Eastern Alps) from Rb/Sr mineral assemblage analysis, Contrib. Mineral. Petrol. 149, 699-712.

Grundmann, G., and Morteani, G., 1985. The young uplift and thermal history of the central Eastern Alps (Austria/Italy), evidence from apatite fission track ages. Jahrbuch der Geologischen Bundesanstalt, 128, 197-216.

Gueydan, F., Leroy, Y.M. and Jolivet, L., 2004. Mechanics of low-angle extensional shearzones at the brittle–ductile transition. J. Geophys. Res. 109, B12407.

Handy, M.R., Schmid, S.M, Bousquet, R., Kissling, E. and Bernoulli, D., 2010. Reconciling plate-tectonic reconstructions of Alpine Tethys with the geological–geophysical record of spreading and subduction in the Alps. Earth-Science Reviews, vol. 102; issues 3-4, 121–158.

Höck, V., 1980. Distribution of minerals of the Alpine metamorphism on the Penninic Tauern Window, Austria, Mitt. Österr. Geol. Ges., 71/72, 119-127.

Hoernes, S. and Friedrichsen, H., 1974. Oxygen isotope studies of metamorphic rocks of the Western Hohe Tauern Area (Austria). SMPM 54, 769-788.

Holland, T.J.B and Ray, N.J., 1985. Glaucophane and pyroxene breakdown reactions in the Pennine units of the Eastern Alps. J. metamorph. Geol., 3, 417-438.

Hurley, P.M., Hughes, H., Pinson Jr., W.H. and Fairbairn, H.W. 1962. Radiogenic argon and strontium diffusion parameters in biotite at low temperatures obtained from Alpine Fault uplift in New Zealand. Geochimica et Cosmochimica Acta 26, 67– 80.

Kurz, W., Neubauer, F., Genser, J. and Dachs, E., 1998. Alpine geodynamic evolution of passive and active continenetal margin sequences in the Tauern window. (Eastern Alps, Austria, Italy), Rev. Geol. Rundschau, 87, 225-242.

Kurz, W., Handler, R. and Bertoldi., C., 2008. Tracing the exhumation oft he eclogite zone (Tauern Window, Eastern Alps) by 40Ar/39Ar dating of the white mica in eclogites. Swiss journal of Geosciences 101, 1, 191-206.

Laubscher, H.P., 2010. Jura, Alps and the boundary of the Adria subplate. Tectonophysics, v. 483, pp.223-239.

Leroy, M., Gueydan, F. and Dauteuil, O., 2008. Uplift and strength evolution of passive margins inferred from 2D conductive modelling. Geophys. J. Int. 172, 464–476.

Luth, S.W., and Willingshofer, E. 2008. Mapping of the Post-Collisional Cooling History of the Eastern Alps. Swiss Journ. Geosci. 101, Sup1., 201-223.

Mancktelow, N. and Pavlis, T.L., 1994. Fold-fault relationships in low-angle detachment systems. Tectonics, 13, 668-685.

Mancktelow, N.S. and Grasemann, 1997. Time-dependent effects of heat advection and topography on cooling histories during erosion, Tectonophysics 270, 167–195.

Mancktelow, N.S., 1985. The Simplon line: a major displacement zone in the western Lepontine Alps. Eclogae Geol. Helv. 78, 73-96.

Mancktelow. N.S., 1992. Neogene lateral extension during convergence in the Central Alps: evidence from interrelated faulting and backfolding around the Simplonpass (Switzerland). Tectonophysics, 215:295-317.

Merle, O., Legal, P. and Mancel, P., 1986. Deformation and metamorphosis in the Simplon region of the central Alps, Eclogae Geol. Helv., 79, 705–718.

Müller, W, Prosser, G., Mancktelow, N., Villa, I.M., Kelley, S., Viola, G., and Oberli, F., 2001. Geochronological constraints on the evolution of the Periadriatic Fault System (Alps). Int. J. of Earth Sci., 90, 593-622.

Naeser, C. W., 1981. The fading of fission tracks in the geological environment: Data from deep drill holes, Nucl. Tracks, 5, 248 – 250.

Nagel, T.J., Herwartz, D., Rexroth, S., Münker, C., Froitzheim, N. and Kurz, W., 2013. Lu-Hf dating, petrography, and tectonic implications of the youngest Alpine eclogites (Tauern Window, Austria). Lithos, 170-171, 179-190.

Neubauer, F., Genser, J., Kurz, W. and Wang, X., 1999, Exhumation of the TW, Eastern Alps: Physics and chemistry of the Earth, ser. A, 24, 675-680.

Oberhänsli, R. Bousquet, R., Engi, M., Goffé, B., Gosso, G., Handy, M.R., Höck, V., Koller, F., Lardeaux, J.-M., Polino, R., Rossi, Ph., Schuster, R., Schwartz, St., Spalla, 2004. Metamorphic structure of the Alps. Scale 1:1.000.000, Commission for the Geological Map of the World, Paris.

Parrish, R. R., 1983. Cenozoic thermal evolution and tectonics of the Coast Mountains of British Columbia, 1, Fission track dating, apparent uplift rates, and patterns of uplift, Tectonics, 2, 601– 631.

Ramsay, J.G., 1967. Folding and fracturing of rocks : New York, McGrawHill, 568p.

Reiners, P.W., and Brandon, M. T., 2006. Using thermochronology to understand orogenic erosion. Annu. Rev. Earth Planet. Sci., 34, 419–66

Rosenberg, C.L., and Garcia, S., 2011. Estimating displacement along the Brenner fault and orogen parallel extension in the Eastern Alps. Int J Earth Sci 100:1129–1145.

Rosenberg, C.L., and Garcia, S., 2012. Reply to the comment of Fügenschuh et al. on the paper 'Estimating displacement along the Brenner Fault and orogen-parallel extension in the Eastern Alps' by Rosenberg and Garcia, Int J Earth Sci (Geol Rundsch) (2011) 100:1129–1145. Int J Earth Sci (Geol Rundsch) (2012) 101:1457–1464.

Scharf, A., Handy, M.R., Favaro, S., Schmid, S. M. and Bertrand, A., 2013. Modes of orogen-parallel stretching and extensional exhumation in response to microplate indentation and roll-back subduction (Tauern Window, Eastern Alps) Int J Earth Sci (Geol Rundsch), 102, 1627-1654.

Schmid, S.M., Fügenschuh, B., Kissling, E., and Schuster, R., 2004, Tectonic map and overall architecture of the Alpine orogen. Eclogae Geol. Helv., 97, 93-117.

Schmid S. M., Scharf, A., Handy, M.R., Rosenberg, C.L, 2013. The Tauern Window (Eastern Alps. Austria): a new tectonic map, with cross-sections and a tectonometamorphic synthesis. Swiss J. Geosci., 106, 1-32.

Selverstone, J., 1988. Evidence for East-West crustal extension in the Eastern Alps: implications for the unroofing history of the TW. Tectonics, 7, 87-105.

Sleep N. H., 1979. A thermal constraint on the duration of folding with reference to Acadian geology, New England (USA). J. Geol. 87, 583-9.

Steck, A., and Hunziker, J., 1994. The Tertiary structural and thermal evolution of the central Alps compressional and extensional structures in an orogenic belt, Tectonophysics, 238, 229–254.

Teyssier, C. and Whitney, D.L., 2002. Gneiss domes and orogeny. Geology v. 30, 1139-1142.

Vernon, 2008. Thermochronological approach to the late Neogene exhumation of the European Alps. The University of Edinburgh - PhD Thesis.

Wawrzyniec, T.F., Selverstone, J., and Axen, G.J., 2001. Styles of footwall uplift along the Simplon and Brenner normal fault systems, central and Eastern Alps. Tectonics, 20, 748-770.

Whitney, D.L., Teyssier, C. and Vanderhaeghe, O., 2004. Gneiss dome and crustal flow. In: *Gneiss domes in orogeny*, Whitney, D., Teyssier, C., Siddoway, S. (eds.). The Geological Society of America, Special Paper 380, 15-33.

Zimmermann, R., Hammerschmidt, K. and Franz, G., 1994. Eocene high pressure metamorphism in the Penninic units of the Tauern Window (Eastern Alps), evidence from 40Ar-39Ar dating and petrological investigations. Contrib. Mineral. Petrol. 117, 175-186.

Chapter V. Summary and Conclusion

Summary and conclusion

This thesis presents the results and interpretations of three different methods that have been combined to assess the mechanism of exhumation of the core of the Eastern Alpine chain, based on the studiy case of the Tauern Window. Combination of apatite and zircon fission track dating, paleostress field investigation and two-dimensional thermal models yields a good description of the cooling and exhumation histories underwent by the Tauern Window during Tertiary times.

The Tauern Window is described in the literature as the location of enhance exhumation from the Early Tertiary to Late Miocene. Indeed the exhumation of the Eastern Alps has been mostly localised in the Tauern Window from Oligocene onward. The geometry of the Tauern Window is marked by two major normal faults systems at its eastern and western borders and by large-scale upright folds forming two large sub-domes in its internal parts. Base on these observations, relative contribution of E-W extension and N-S shortening during exhumation of the Tauern Window is fairly debated and the main aim of this work was to bring a contribution to this debated. Exhumation along the low-angle Brenner and Katschberg fault systems may result in the juxtaposition of the high-grade deep crustal rocks of the European plate and lower-grade metamorphic upper crustal rocks of the Austroalpine units. However, part of the exhumation may also result from N-S oriented shortening during alpine convergence. N-S shortening may be accommodated by the formation large-scale upright folds with axial planes parallel to the Alpine orogeny.

Distributions of apatite and zircon fission track ages display heterogeneous distributions in the eastern sub-dome and ENE-WSW striking, elongate and concentric distributions with ages younging inward in the western sub-dome. Age distributions in the western sub-dome are sub-parallel to the axial plane of the upright fold suggesting that the cooling pattern of this sub-dome is related to the formation of the upright fold. As show by numerical thermal models, the younging of fission track ages towards the centre of the fold within the western sub-dome could be the result of higher exhumation rates within the central part of the sub-dome during amplification of the fold.

The same interpretation may be invoked to explain the difference in cooling ages between the eastern and western sub-domes of the Tauern Window. Indeed, both apatite and zircon fission track ages display younger ages in the eastern sub-dome when compared to the western one. Young ages of the eastern sub-dome may indicate either that the uplift of the rocks stopped earlier than in the western sub-dome or that the western sub-dome was exhumed with higher uplift rates but coevally to the eastern sub-dome. The second hypothesis is more relevant for the following reasons: (1) Along the Brenner and the Katschberg normal, very young apatite and zircon fission track ages indicating that both the Brenner and Katschberg fault were still active during Pliocene times, (2) Exhumation rates based on

age/elevation relationships are higher in the western sub-dome than in the eastern one, and (3) the high-amplitude (of more than 20 km) geometry of the fold of the western sub-dome and the plateau-type geometry of the eastern sub-dome may be related to the concentric distribution of the fission track ages in the western sub-dome and the more heterogeneous distributions of the ages over the eastern sub-dome, respectively.

We relate the higher uplift rates calculated in the western sub-dome, when compared to the one calculated in the western one to the geometry of the Pustertal Line, which marks the northern border of the Dolomite indenter involving a differential amount of shortening, north of the dolomite indenter. We propose that the present day geometry of the Pustertal Line results in a sinistral offset of the previously straight Periadriatic fault along the Guidicarie Line. This results in a same indentation process marked by a clockwise rotation of the Dolomite indenter, therefore by higher amount of shortening westward. Faster movement of the indenter in the west than in the east results in higher amount of shortening in front of the tip of the indenter, hence in higher exhumation rates and younger cooling ages in the western sub-dome of the Tauern Window than in the eastern one.

Since the Tauern Window is the only area of the Eastern Alps exposing rocks, which cooled below 300°C (Handy and Oberhänsli, 2004), the analysis of brittle structures and their associated paleo-stress fields allow one to investigate the Mid- to Late-Miocene tectonics of the Eastern Alps. The apatite and zircon fission track ages, which closure temperatures are below the assume temperature of the ductile-brittle transition provide information of the behaviours of the rocks of the 10 shallowermost km of the crust. Brittle structures observed in the Tauern Window can thus be linked to the cooling pattern provided by apatite and zircon fission track ages. The iso-age contours of zircon and apatite fission track ages follow the trend of the main axial planes of the major fold in the western part of the Tauern Window suggest that the cooling and exhumation histories of the Tauern Window is mainly related to folding and erosion. As a consequence, we expected to measure a large number of compressional structures associated to this folding event. Against our expectations, brittle deformations within the Tauern Window are characterised by the major occurrence of strike-slip faulting in its central part and extensional regimes, displaying E-W oriented σ_3, at the vicinity of the western and eastern margins. Only few compressive structures have been highlighted, mainly in the core of the Tauern Window.

In order to better understand the behaviour of the isotherm and to solve the apparent contradiction between structural results and fission track ages distributions over the Tauern Window, we performed a series of 2D-thermal models that provide the evolution of the temperatures by folding a lithosphere in function of (1) initial thermal states inheritate from earlier subduction history and (2) uplift rates and duration of deformation.

Results of 2D-thermal models indicate that (1) the perturbation of the geothermal gradient due to stacking of hot nappes induces a slower re-equilibration of the isotherms and

therefore results in younger ages than an initial undisturbed thermal state, and (2) the deformation and re-equilibration of the isotherms are highly dependant to the uplift rates of the rocks and duration of the deformation.

Models show that uplift rates higher than 1 $mm.yr^{-1}$ strongly enhances the deformation of the isotherms due the advection of hot deep material toward the surface. On the contrary, uplift rates lower than 0.5 $mm.yr^{-1}$ are not sufficient enough to counterbalance the re-equilibration of the isotherms tend to reach a horizontal steady state.

Models also show that a two-stage deformation history may result in a bell-shape distribution of cooling ages with younger ages in the centre of the dome. Indeed, the combination of higher uplift rates (> 1 $mm.yr^{-1}$) in the hinge of the folds during the first stage resulting in bending of the isotherms and lower amount of exhumation in the rims of the fold and the lower uplift rates (<0.5 $mm.yr^{-1}$) resulting in re-equilibration of the isotherm leads to younging of cooling ages toward the hinge of the fold.

A two-phase evolution would explain both the apatite and zircon fission track age distribution observed in the Tauern Window and the lack of compressive structures that should witness an age distribution resulting related to the formation of large-scale folds.

During the first stage of deformation, driven by N-S shortening and fast uplift rates, major large-scale folds of the Tauern Window where formed, bringing hot deep material to the surface, involving a bending of the isotherms. Due to its position in front of the tip of the indenter, the western sub-dome of the Tauern Window underwent higher uplift rates than the eastern sub-dome. The Dolomite indenter moves northward as a block but its movement is faster toward the west resulting in higher amount of shortening and higher amplitude of the fold in the western sub-dome than in the eastern sub- dome. Therefore during one and the same, coeval folding event, the eastern sub-dome underwent lower uplift rates, resulting in older ages than in the western sub-dome. This does not preclude that the tectonic process itself did not terminate earlier. During this stage, brittle compressional structures associated to N-S shortening may form in the brittle part of the upper crust. The occurrence of N-S compression and shortening during the first event due not preclude a coeval occurrence of E-W extension that would take place along the Katschberg and the Brenner normal faults.

The second stage is driven by E-W extension and strikes-slip faulting, as suggested by the occurrence of extensional brittle structures along the Brenner and the Katschberg faults and strike-slip regimes in the core of the Tauern Window. During the second stage, marked by lower uplift rates, when compared to the first stage, re-equilibration of the previously deformed isotherms occurred, resulting in the present-day apatite and zircon age distributions. During this second stage, N-S shortening and compression became of subordinate importance. Exhumation of the Tauern Window was taking place in an global E-W extensional context and strain partitioning of a regional paleostress field result in strike-slip faulting, yielding N-S shortening, in the central part of the Tauern Window and E-W extension along the Brenner and Katschberg normal fault systems. Compressive structures that were associated to the first

stage were thus eroded and the upper crust is mostly overprinted by the younger extensional/strike-slip faults.

Taken together the zircon and apatite fission tack data ages, the brittle deformations measured on the field and the 2D-thermal models we propose the following tectonic history of the Tauern Window.

Oligocene - Upper-Mid Miocene: The northward movement of the Dolomite indenter induces N-S shortening and exhumation of the Tauern Window characterised by folding and erosion and exhumation at high uplift rates. The upper brittle crust is affected by N-S compressive brittle structures associated to the formation of the upright folds. During this stage, advection of hot deep material at high uplift rates results in bending of the isotherms.

Mid-lower Miocene: The Periadriatic Line is sinistraly offset by the Giudicarie fault involving a clockwise rotation of the Dolomite indenter. The northward movement of the Dolomite indenter is therefore faster in the west than in the east resulting in higher amount of shortening and higher uplift rates in front of the tip of the indenter. In the Tauern window, this results in the formation of upright folds of high amplitudes in the western sub-dome and of folds of lower amplitudes in the eastern one. This stage is marked by folding and erosion and substantial extension along the Brenner and Katschberg Fault systems.

Pliocene: Pure N-S shortening is no longer active. In this context, extension of the upper crust is entirely accommodated, within the Tauern Window, by normal faulting along the two major normal fault systems, i.e. the Brenner and the Katschberg faults. E-W extension is accommodated in the central part of the Tauern Window by strike-slip faulting, yielding substantial N-S shortening. During this stage, the brittle upper crust affected by compressive structures, witnessing the older history, is eroded. Lower uplift rates allow for the re-equilibration of the previously bended isotherms, leading to the present-day age distributions provided the apatite and zircon fission track ages.

References

Allanic, C., 2013. Kinematics, Age and Dynamics of the brittle deformation within the Lepontine Dome (Central Alps), PhD, Orleans, 271p.

Anderson, E.M., 1942. The Dynamics of faulting (2nd edn). Olivier & Boyd, Edinburgh.

Angelier, J., 1984. Tectonic analysis of fault slip data sets. Journal of Geophysical Research, 89, , 5835-5848.

Angelier, J., 1989. From orientation to magnitudes in paleostress determinations using fault slip data. Journal of Structural Geology, 11, 37-50.

Angelier, J., 1990. Inversion of field data in fault tectonics to obtain the regional stress – III. A new rapid direct inversion method by analytical means. Geophysical Journal International, 103, 363-376.

Arthaud, F., Mattauer, M. and Proust, F., 1966. La structure et la microtectonique des nappes hercyniennes de la Montagne Noire. Colloq. Etages tectoniques

Axen, G. J., Bartley, J.M. and Selverstone, J., 1995, Structural expression of a rolling hinge in the footwall of the Brenner Line normal fault, Eastern Alps. Tectonics, 14, 1380-1392.

Batt, G. and Braun, J., 1997. On the thermomechanical evolution of compressional orogens. Geophys. J. Int., 128, 364-382.

Batt, G. E., Brandon, M. T., Farley, K. A. and Roden-Tice, M., 2001. Tectonic synthesis of the Olympic Mountains segment of the Cascadia wedge, using two-dimensional thermal and kinematic modeling of thermochronological ages, J. Geophys. Res., 106, 26,731–26,746.

Batt, G. and Brandon, M.T, 2002. Lateral thinking: 2D interpretation of thermochronology in convergent orogenic settings, Tectonophysics, 349, 185 –201.

Behrmann, J. H., 1988, Crustal-scale extension in a convergent orogen: The Sterzing-Steinach mylonite zone in the Eastern Alps. Geodynamica Acta, 2, 63-73.

Behrman, J.H. and Frisch, W., 1990. Sinistral ductile shearing associated with metamorphic decompression in the Tauern Window, Eastern Alps: Jahrbuch der Geologischen Bundesansalt, 133, 135-146.

Berner H., Hamberg, H. and Stephansson, O., 1972. Diapirism in theory and experiment: tectonophysics, 15, 197-218.

Bernet, M., M. Zattin, J. I. Garver, M. T. Brandon, and J. A. Vance, 2001. Steady-state exhumation of the European Alps, Geology, 29, 35-38.

Bigi, G., Castellarin, A., Coli M., Dalpiaz, G.V. and Vai, G.B., 1990. Structural model of Italy sheet 1 & 2, 1:500000. Consiglio Naz. Ricerche, Progetto Finalizzato Geodinamica, Selca Firenze.

Borsi, S., Del Moro, A., Sassi, F.P. and Zirpoli, G., 1973. Metamorphic evolution of the Austridic rocks to the South of the TW (Eastern Alps). Mem. Soc. Geol. It., v. XII, 549-571.

Borsi, S., Del Moza, A., Sassi, F., Zanferrari, A. and Zirpoli, G. 1978. New geopetrologic and radiometeric data on the alpine history of the Austridic continental margin South of the Tauern window (Eastern Alps). Memorie dell'Istituto della Regia Universitá di Padova 32, 1–20.

Bousquet, R., Oberhänsli, R., Goffé, B., Wiederkehr, M., Koller, F., Schmid, S.M., Schuster, R., Engi, M., Berger, A. and Martinotti, G., 2008. Metamorphism of metasediments in the scale of an orogen: A key to the Tertiary geodynamic evolution of the Alps. In: Tectonic Aspects of the Alpsine-Carpathian-Dinaride System, edited by Siegesmund, S., Fügenschuh, B. and Froitzheim, N., Geol. Soc. Spec. Publ., 298, 393-411.

Brandon M.T., Roden-Tice, M.K. and Garver, J.I., 1998. Late Cenozoic exhumation of the Cascadia accretionary wedge in the Olympic Mountains, northwest Washington State. GSA Bulletin 110, 985–1009.

Braun, J., van der Beek, P. and Batt, G., 2006. Quantitative thermochronology: Numerical methods for the interpretationof thermochronological data. Cambridge University Press, 258.

Brun, J.P. and Van Den Driessche, J., 1994. Extensional gneiss domes and detachment faults-structure and kinematics. Bulletin de la Société Géologique de France 165, 519–530.

Brun, J.P., 1983. L'origine des dômes gneissiques : modèles et tests. Bulletin de la société géologique de France 25, 219-228.

Burg, J.P., Klaus, B.J.P. and Podladchikov, Y.Y., 2004. Dome structures in collision orogens: Mechanical investigations of the gravity/compression interplay. In: Gneiss domes in orogeny. Whitney, D., Teyssier, C., Siddoway, S. (eds.), The Geological Society of America, Special Paper 380, 47-66.

Campani, M., 2009. Temporal and spatial evolution of a syn-orogenic extensional system: the Simplon Fault Zone (Central Alps). PhD thesis, ETH Zurich.

Caporali, A., Neubauer, F., Ostini, L., Stangl, G. and Zuliani, D., 2013. Modeling surface GPS velocities in the southern and Eastern Alps by finite dislocations at crustal depths. Tectonophysics, 590, 136-150.

Carey, E. and Brunier, B., 1974. Analyse théorique et numérique d'un modèle mécanique élémentaire appliqué à l'étude d'une population de failles. C.r. Acad. Sci., Paris D179, 891-894.

Carry, N., Gueydan, F., Brun, J.P. and Marquer, D., 2009. Mechanical decoupling of high-pressure crustal units during continental subduction. Earth and planetary Sciences Letters, 278, 13-25.

Castellarin A., 1992. Alpine compressional tectonics in the Southern Alps. Relationships with the N-Apennines. Annales Tectonicae 6, 62-95.

Carey, E. and Brunier, B., 1974. Analyse théorique et numérique d'un modèle mécanique élémentaire appliquée à l'étude d'une population de failles. C.r. Acad. Sci., Paris D179, 891-894.

Christensen, J. N., Selverstone, J., Rosenfeld, J. L. and DePaolo, D. J., 1994. Correlation by Rb- Sr geochronology of garnet growth histories from different structural levels within the Tauern Window, Eastern Alps. - Contrib. Mineral. Petrol., 118, 1-12.

Cliff, R., Droops, G. and Rex, D., 1985. Alpine metamorphism in South-East Tauern Window, Austria, 2. Rates of heating, cooling and uplift. Journal of Metamorphic geology 3, 403-415.

Coney, P.J., 1980. Cordilleran metamorphic core complexes: An overview, In: Cordilleran Metamorphic Core Complexes, Crittenden, M. D., Coney, P. J. and Davis, G. H. (Eds.), 1980. Geol. Soc. Am. Mem., 153, 7-34.

Coney, P.J. and Harms, T.A., 1984. Metamorphic core complexes: Cenozoic extensional relics of Maesozoic compression. Geology 12, 550-554.

Corrigan, J.D., 1991. Inversion of apatite fission track data for thermal history information. J Geophys Res 96: 10347-10360.

Cornelius, H.P., 1940. Zur Auffassung der Ostalpen im Sinne der Deckenlehre. Zeitsch. Deutsch. Geol. Ges., 92, 271-312.

Coyle, D.A, 1994. The application of apatite fission track analysis to problem in tectonics. PhD thesis, La Trobe University, Bundoora, Victoria.

Crittenden, M. D., 1980. Metamorphic core complexes of the North American Cordillera: Summary. In: Cordilleran Metamorphic Core Complexes, Crittenden, M. D., Coney, P. J. and Davis, G. H. (Eds.), 1980. Geol. Soc. Am. Mem., 153, 485-590.

Crowley, K.D., Cameron, M. and Schaefer, R.L., 1991. Experimental studies of annealing of etched fission tracks in fuorapatite, Geochim. Cosmochim. Acta 55, 11449-1465.

D'Agostino, N., Cheloni, D., Mantenuto, S., Selvaggi, G., Michelini, A. and Zuliani, D., 2005. Strain accumulation in the southern Alps (NE Italy) and deformation at the north-eastern boundary of Adria observed by CGPS measurements. Geophysical Research Letters, 32.

Decker, K., Meschede M. and Ring, U., 1993. Fault slip analysis along the northern margin of the Eastern Alps (Molasse, Helvetic nappes, North and South Penninic flysch, and the Northern Calcareous Alps). Tectonophysics, 223, 291-312.

Decker, K. and Peresson, H., 1996. Tertiary kinematics in the Alpine–Carpathian–Pannonian system: links between thrusting, transform faulting and crustal extensions. In: Wessely, G., Liebl, W. (Eds.), Oil and gas in Alpidic thrustbelts and basins of Central and Eastern Europe. EAGE Spec. Publ. 5, 69–77.

Decker, K. and Reiter, F., 2006. Depth-extrapolated models of fracture orientation and fracture density for the Brenner Base Tunnel. In: Pangeo Austria 2006, Tessadri-Wackerle, E. (ed.), 44-45, Innsbruck University Press.

Dewey, J.F., Pitman, W.C. III, Ryan, W.B.F. and Bonnin, J., 1973. Plate tectonics and the evolution of the Alpine system. Bulletin of the Geological Society of America 84, 3137-3180.

Dewey, J.F., Helman, M. L., Knott, S.D., Turco, E. and Hutton, D.H.W., 1989. Kinematics of the western Mediterranean, in Alpine tectonics, M.P. Coward, D. Dietrich and R.G. Park. (eds.). Geol. Soc. Spec.. Publ., London, 45, 265-283.

Di Fiore, G., 2013. Evoluzione morfotettonica delle aree alpine "Sempione" e "Brennero" attraverso studi termocronologici di bassa temperature. Universita di Bologna.

Dodson, M.H., 1979. Theory of cooling ages. In: Isotope Geology Jäger, E. and Hunziker, J.C (Eds), Lectures in Isotope Geology. Springer-Verlag, Berlin (1979), 194–202.

Donelick R.A, Roden, M.K, Mooers, J.D, Carpenter, B.S. and Miller, D.S., 1990. Etchable lenght reduction of induced fission tracks in apatite at room temperature (~23°C): crystallographic orientation effects and "initial" mean lenghts. Nucl. Tracks Radiat Meas. 17:261-265.

Donelick, R.A., 1993. Apatite etching characteristics versus chemical composition. Nuclear Tracks and Radiation Measurements 21: 604.

Donelick, R. A., Ketcham, R. A., and Carlson, W. D., 1999. Variability of apatite fission track annealing kinetics II: crystallographic orientation efects, American Mineralogist, 84, 1224–1234.

Donelik R.A, O'Sullivan, P.B., Ketchman. and Richard, 2005. Apatite fission track analysis. Reviewz in Mineralogy and Geochemistry, 58, 49-94.

Dumitru, T. A., 2000. Fission track geochronology, in Quaternary Geochronology: Methods and Applications, Noller, J.S., Sowers, J.M. and Lettis, W.R., American Geophysical Union Reference Shelf, v. 4, p. 131-156.

Dunkl, I., 2002. TRAKKEY: a Windows program for calculating and graphical presentation of fission track data. Comput. Geosci., 28, 3–12.

Dunkl, I., Frisch, W. and Grundmann, G., 2003. Zircon fission track thermochronology of the south-eastern part of the TW and the adjacent Austroalpine margin, Eastern Alps. Eclogae geol. Helv., 96, 209-217.

Ebbing, J., Braitenberg, C. and Goetze, H.J., 2001. Forward and inverse modelling of gravity revealing insight into crustal structures of the Eastern Alps. Tectonophysics 337/3-4, 191–208.

Echtler, H. and Malavieille, J., 1990. Extensional tectonics, basement uplift and Stephano-Permian collapse basin in a late Variscan metamorphic core complex (Montagne Noire, Southern Massif Central). In: Terranes in the Variscan Belt of Europe and Circum-Atlantic Paleozoic Orogens, Matte, Ph. (Editor), tectonophycs, 177, p.125-138.

Ellenberger, F., 1967. Replis de micaschistes et tectonique d'infrastructure au sein du massif gneissique de Caroux (zone axiale de la Montagne Noire). C. R. Sot. Gtol Fr., 227-228.

Eskola, P.E., 1949. The problem of mantle gneiss domes: Geological Society of London, Quaterly Journal, 104, 253-283.

Fitzgerald, P.G. and Gleadow, A.J.W, 1988. Fission track geochronology, tectonics and structure of the transantartic Mountains – Nucl. Tracks 17, 351-357.

Fleischer R.L. and Price, P.B., 1964-a. Techniques for geological dating of minerals by chemical etching of fission fragment tracks. Geochimica et Cosmochimica Acta, Vol. 28, Issues 10–11, 1705–1712.

Fleischer R.L. and Price, P.B., 1964-b. Decay Constant for Spontaneous Fission of U238. Phys. Rev. 133, B63–B64 (1964).

Foeken, J.P.T., Persano, C. Stuart, F. and ter Voorde, M., 2007. Role of topography in isotherm perturbation: Apatite (U-Th)/He and fission track results from the Malta tunnel, Tauern Window, Austria. Tectonics, 26, TC3006.

Foster, D., Kohn, B., and Gleadow, A., 1996. Sphene and zircon fission track closure temperatures revisited; empirical calibrations from 40Ar/39Ar diffusion studies of K-feldspar and biotite, in International Workshop on Fission track.

Foster, D.A. and John, B. 1999. Quantifying tectonic exhumation in an extensional orogen with thermochronology: examples from the southern Basin and Range Province. In: Exhumation processes: normal faulting, ductile flow.Ring, U., Brandon, M., Lister, G. & Willett, S. (Eds).

Foster, D. A., Schafer, C., Fanning, M.C. and Hyndmann D. W., 2001. Relationships between crustal partial melting, plutonism, orogeny, and exhumation: Idaho-Bitterroot batholith. Tectonophysics, 342, 313-350.

Foster, D. A. and Raza A., 2002. Low-temperature thermochronological record of exhumation of the Bitterroot metamorphic core complex, northern Cordilleran Orogen. Tectonophysics, 349, 23-36.

Franck, W., Kralik, M., Schabert, S. and Thöni, M., 1987. Geochronological data from the Eastern Alps, in Geodynamics of the Eastern Alps, Flügel, H. and Faupl, P. (eds.), pp. 272-281, Deuticke, Vienna, 1987.

Frisch, W., 1979. Tectonic progradation and plate tectonic evolution of the Alps. Tectonophysics 60, 121-139.

Frisch, W., Dunkl, I. and Kuhlemann, J., 2000. Post-collisional orogen-parallel large-scale extension in the Eastern Alps. Tectonophysics, 327, 239-265.

Frisch, W., Kuhlemann, A., Dunkl, I. and Brügel, A., 1998. Palinspastic reconstruction and topographic evolution of the Eastern Alps during late Tertiary tectonic extrusion. Tectonophysics, 297, 1-15.

Frisch, W., Szekely, B., Kuhlemann, A. and Dunkl, I., 1999. Geomorphological evolution of the Eastern Alps in response to Miocene tectonics. Zeitschrift für Geomorphologie N.F., 44, 103-138.

Froitzheim, N., Schmid, S.M. Frey, M., 1996. Mesozoic paleogeography and the timing of eclogite facies metamorphism in the Alps: a working hypothesis. Eclogae Geologicae Helvetiae, 89, 81–110.

Fügenschuh, B., Seward, D. and Mantckelow, N. S., 1997. Exhumation in a convergent orogen: the western TW. Terra Nova, 9, 213-217.

Fügenschuh B., Mantckelow N.S. and Schmid S.M., 2011. Comment on ‘‘Estimating displacement along the Brenner Fault and orogenparallel extension in the Eastern Alps’’ by Rosenberg and Garcia. Int J Earth Sci (Geol Rundsch), 100: 1129-1145. Int J Earth Sci (Geol Rundsch), 101: 1451-1455.

Galbraith, R.F., 1982. Statistical analysis of some fission track counts and neutron fluence measurements. Nucl. Tracks, 6: 99-107.

Gallagher, K., Brown, R. and Johnson, C., 1998. Fission track analysis and its applications to geological problems. Annu. Rev. Earth Planet. Sci., 26, 519-572.

Genser, J. and Neubauer, F., 1989. Low angle normal faults at the eastern margin of the TW (Eastern Alps). Mitteilungen der Österreichische Geologische Gesellschaft, 81, 233-243.

Gapais, D., Pêcher A., Gilbert, E. and Ballèvre M., 1992. Synconvergence spreading of the higher Himalaya crystalline in Ladakh. Tectonics, 11, 5, 1045-1056

Gilbert, E., and Merle, O., 1987, Extrusion and radial sprading beyond a closing channel: Journal of Structural Geology, 9, 481–490.

Giese, P., Reutter, K.-J., Jacobshagen, V., Nicolich, R., 1982. Explosion seismic crustal studies in the Alpine Mediterranean region and their implications for tectonic processes. In: Berckhemer, H., Hsü, K.J. (Eds.), Alpine-Mediterranean Geodynamics. : Geodynamics Series, 7. American Geophysical Union, pp. 39–73.

Gleadow, A.J.W. and Lovering, J.F., 1977. Geometry factor for external detectors in fission track dating. Nucl. Track. Detect., 1: 99-106.

Gleadow, A.J.W., 1981. Fission track dating methods: what are the real alternatives? Nucl. Tracks, 5: 3-14.

Gleadow, A.J.W. and Duddy, I.R., 1982. A natural long-term annealing experiment for apatite. Nuclear Tracks Radiation Experiments, 5, 169-174.

Glodny J., Ring, U. Kühn, Gleissner, P. and Franz, G., 2005. Crystallization and very rapid exhumation of the youngest Alpine eclogites (Tauern Window, Eastern Alps) from Rb/Sr mineral assemblage analysis, Contrib. Mineral. Petrol. 149, 699-712.

Glodny J., Ring, U. and Kühn A., 2008. Coeval high-pressure metamorphism, thrusting, strike-slip, and extensional shearing in the Tauern Window, Eastern Alps, Tectonics, 27, TC4004.

Green, P.F., Duddy, I.R., Gleadow, A.J.W., Tingate, P.R. and Laslett, G.M., 1985. Fission track annealing in apatite : track lenght measurements and the form of the Arrhenius plot. Nucl. Tracks 10: 323-328.

Green, P.F., Duddy, I.R., Gleadow, A.J.W., Tingate, P.R. and Laslett, G.M., 1986. Thermal annealing of fission tracks in apatite. 1. A qualitative description. Chemical Geology (Isotope Geoscience Section), 59, 237-253.

Green, P.F., Duddy, I.R., Laslett, G.M., Hegarty, A.J.W., Gleadow, A.J.W. and Lovering, J.F., 1989. Thermal annealing of fission tracks in apatite. 4. Quantitative modeling techniques and extension to geological timescales. Chemical Geology (Isotope Geoscience Section), 79, 155-182.

Grundmann, G. and Morteani, G., 1985. The young uplift and thermal history of the central Eastern Alps (Austria/Italy), evidence from apatite fission track ages. Jahrbuch der Geologischen Bundesanstalt, 128, 197-216.

Gueydan, F., Leroy, Y.M. and Jolivet, L., 2004. Mechanics of low-angle extensional shearzones at the brittle–ductile transition. J. Geophys. Res. 109, B12407.

Handy, M. and Oberhänsli, R., 2004. Age of the Metamorphic Structure of the Alps - Tectonic Interpretation and Outstanding Problems. In: Explanatory Notes to the Map: Metamorphic Structure of the Alps. Oberhänsli., R. (eds). Mitteilungen der Österreichischen Mineralogischen Gesellschaft, 149, 97-121.

Handy, M.R., Schmid, S.M, Bousquet, R., Kissling, E. and Bernoulli, D., 2010. Reconciling plate-tectonic reconstructions of Alpine Tethys with the geological–geophysical record of spreading and subduction in the Alps. Earth-Science Reviews, vol. 102; issues 3-4, 121–158.

Höck, V., 1980. Distribution of minerals of the Alpine metamorphism on the Penninic Tauern Window, Austria, Mitt. Österr. Geol. Ges., 71/72, 119-127.

Hoernes, S. and Friedrichsen, H., 1974. Oxygen isotope studies of metamorphic rocks of the Western Hohe Tauern Area (Austria). SMPM 54, 769-788.

Hoinkes, G. Koller, F., Rantitsch, G., Dachs, E., Hock, V., Neubauer, F. and Schuster, R., 1999. Alpine metamorphism of the Eastern Alps. Schweizerische Mineralogische und petrographishe Mitteilungen 79, 155-181.

Holland, T.J.B and Ray, N.J., 1985. Glaucophane and pyroxene breakdown reactions in the Pennine units of the Eastern Alps. J. metamorph. Geol., 3, 417-438.

Hurford, A.J., 1986, Cooling and uplift patterns in the Lepontine Alps, South Central Switzerland and an age of vertical movement on the Insubric fault line: Contributions to Mineralogy and Petrology, 92, 413-427.

Hurford, A.J. and Green, P.F. 1983. The zeta age calibration of fission track dating. Chem. Geol., 41, 285-317.

Hurford A.J. and Hammerschmidt, K., 1985. 40Ar/39Ar and K/Ar dating of the Bishop and Fish Canyon Tuffs: camibration ages for fission track dating standards. Chemical Geology: Isotope Geoscience section 58: 23-32.

Hoschek, G., 2001. Thermobarometry of metasediments and metabasites from the eclogite zone of the Hohe Tauern, Eastern Alps, Austria. Lithos 59, 127–150.

Hoschek, G., 2007. Metamorphic peak conditions of eclogites in the Tauern Window, Eastern Alps, Austria: Thermobarometry of the assemblage garnet + omphacite+ phengite + kyanite + quartz. Lithos, 93, 1-16.

Hurley, P.M., Hughes, H., Pinson Jr., W.H., Fairbairn, H.W. 1962. Radiogenic argon and strontium diffusion parameters in biotite at low temperatures obtained from Alpine Fault uplift in New Zealand. Geochimica et Cosmochimica Acta 26, 67– 80.

Inger, S. and Cliff, R.A., 1994. Timing of Metamorphism in the Tauaern Window, Eastern Alps: Rb-Sr ages and fabric formation: J. met. Geol.12, 695-707.

Jolivet, L., Famin, V., Mehl, C., Parra, T., Avigad, D. and Aubourg, C., 2004. Progressive strain localisation, crustal-scale boudinage and extensional metamorphic domes in the Aegean Sea. In: Gneiss domes in orogeny. Whitney, D., Teyssier, C., Siddoway, S. (eds.). The Geological Society of America, Special Paper 380, 185–210.

Kleinschrodt, R., 1987. Quarzkorngefügeanalyse im Altkristallin südlich des westlichen Tauernfensters (Südtirol/Italien). - Erlanger geol. Abh., 114, 1-82, Erlangen.

Kuhlemann, J., Frisch, W., Dunkl, I. and Székely, B., 2001. Quantifying tectonic versus erosive denudation: The Miocene core complexes of the Alps.- Tectonophysics, 330, 1-23.

Kurz, W., Neubauer, F., Genser, J. and Horner, H., 1993. Sequence of Tertiary Brittle Deformations in the Eastern TW (Eastern Alps). Mitt. Österr. Geol. Ges., 86, 153-164.

Kurz, W. and Neubauer, F, 1996. Deformation partitioning during updoming of the Sonnblick area in the TW (Eastern Alps, Austria). Journal of Structural Geology, 18, 11, 1327-1343.

Kurz, W., Neubauer, F., Genser, J. and Dachs, E., 1998. Alpine geodynamic evolution of passive and active continenetal margin sequences in the Tauern window. (eastern A lps, Austria, Italy), Rev. Geol. Rundschau, 87, 225-242.

Kurz, W., Handler, R., Bertoldi., C., 2008. Tracing the exhumation oft he eclogite zone (Tauern Window, Eastern Alps) by 40Ar/39Ar dating of the white mica in eclogites. Swiss journal of Geosciences 101, 1, 191-206.

Lammerer, B., 1986. Das Autochthon im westlichen Tauernfenster. Jahrb. Geol. Bundesanst. 129, 51– 67.

Lammerer, B., 1988. Thrust-regime and transpressionregime tectonics in the Tauern Window (Eastern Alps), Geol. Rundsch., 77, 143-156.

Lammerer, B. and Weger, M., 1998. Footwall uplift in an orogenic wedge: the TauernWindow in the Eastern Alps of Europe, Tectonophys., 285, 213–230.

Lammerer, B. Gebrande, H., Lüschen, E. and Vesela, P., 2008. A crustal-scale cross-section through the Tauern Window (Eastern Alps) from geophysical and geological data. In: Tectonic Aspects of the Alpsine-Carpathian-Dinaride System, edited by Siegesmund, S., Fügenschuh, B. and Froitzheim, N., Geol. Soc. Spec. Publ., 219-229.

Laslett, G. M., Green, P. F., Duddy, I. R., and Gleadow, A. J. W., 1987. Thermal annealing of fission tracks in apatite: 2. A quantitative analysis: Chemical Geology, v. 65, p. 1–13.

Laubscher, H.P.V., 1971. Das Alpen-Dinariden-Problem und die Palinspastik der südlichen Tethys. International Journal of Earth Sciences, 40, 813-833.

Laubscher, H.P., 1988. Material balance in Alpine orogeny. Geol. Soc. America, Bull., 100, 1313-1328.

Laubscher, H.P., 1990. The problem of the Moho in the Alps. Tectonophysics 182, 9-20.

Laubscher, H.P., 2010. Jura, Alps and the boundary of the Adria subplate. Tectonophysics, v. 483, pp.223-239.

Lee, J., Hacker, B.R., Dinklage, W.S., Wang, Y., Gans, P., Calvert, A., Wan, J.L., Chen, W.J., Blythe, A.E., and McClelland, W., 2000, Evolution of the Kangmar Dome, southern Tibet: Structural, petrologic, and thermochronologic constraints: Tectonics, v. 19, p. 872–895.

Leroy, M., Gueydan, F. and Dauteuil, O., 2008. Uplift and strength evolution of passive margins inferred from 2D conductive modelling. Geophys. J. Int. 172, 464–476.

Linzer, H.-G., Moser, F., Nemes, F., Ratschbacher, L., Sperner, B., 1997, Build-up and dismembering of a classical fold-thrust belt: from non-cylindircal stacking to lateral extrusion in the eastern Northern Calcareous Alps. Tectonophysics 272, 97– 124.

Linzer, H.-G., Decker, K., Peresson, H., Dell'Mour, R., and Frisch, W., 2002. Balancing orogenic float of the Eastern Alps: Tectonophysics, 354, 211-237.

Lister, G.S., Banga, G. and Feenstra, A., 1984. Metamorphic core complexes of cordilleran type in the Cyclades, Aegean Sea, Greece, Geology 12, 221–225.

Luth, S.W., and Willingshofer, E. 2008. Mapping of the Post-Collisional Cooling History of the Eastern Alps. Swiss Journ. Geosci. 101, Sup1., 201-223.

Malavieille, J., 2010. Impact of erosion, sedimentation, and structural heritage on the structure and kinematics of orogenic wedges: Analog models and case studies. GSA Today, 20, 4-10.

Mancktelow, N. and Pavlis, T.L., 1994. Fold-fault relationships in low-angle detachment systems. Tectonics, 13, 668-685.

Mancktelow, N.S., 1985. The Simplon line: a major displacement zone in the western Lepontine Alps. Eclogae Geol. Helv. 78, 73-96.

Mancktelow. N.S.. 1992. Neogene lateral extension during convergence in the Central Alps: evidence from interrelated faulting and backfolding around the Simplonpass (Switzerland). Tectonophysics, 215, 295-317.

Mancktelow, N.S. and Grasemann, 1997. Time-dependent effects of heat advection and topography on cooling histories during erosion, Tectonophysics 270, 167–195.

McDowell, F. and Kreizer, P., 1977. Timing of Mid-Tertiary volcanism in the Sierra Madre Occidental between Durango City and Matzalan, Mexico. Geological Society of America Bulletin, 88, 1479-1487.

Merle, O., Legal, P. and Mancel, P., 1986. Deformation and metamorphosis in the Simplon region of the central Alps, Eclogae Geol. Helv., 79, 705–718.

Miller, D. S., Jaeger, E. and Schmidt, K.,. 1967. Rb-Sr Altersbestimmungen an Biotiten der Raibler Schichten des Brenner Mesozoikums und am Muscovitgranitgneis von Vent (Oetztaler Alpen), Eclogae. Geol. Helv., 60, 537-541.

Milnes, A.G., 1974. Structure of the Pennine Zone (Central Alps): A new working hypothesis, Geol. Soc. Am. Bull., 85, 1727–1732.

Milnes, A.G., 1978. Structural zones and continental collision, Central Alps. Tectonophysics, 47, 369-392.

Most, P., 2003. Late Alpine cooling histories of tectonic blocks along the central part of the Transalp-Traverse (Inntal-Gadertal): constraints from geochronology. PhD Thesis.

Müller, W, Prosser, G., Mancktelow, N., Villa, I.M., Kelley, S., Viola, G., and Oberli, F., 2001. Geochronological constraints on the evolution of the Periadriatic Fault System (Alps). Int. J. of Earth Sci., 90, 593-622.

Naeser, C.W., 1967. The use of apatite and sphene for fission track age determinations. Bull. Geol. Soc. Am., 78: 1523-1526.

Naeser, C. W., 1979. Lectures in Isotope Geology. In: Isotope Geology Jäger, E. and Hunziker, J.C (Eds), Springer-Verlag, Berlin (1979), 154-169.

Naeser, C. W., 1981. The fading of fission tracks in the geological environment: Data from deep drill holes, Nucl. Tracks, 5, 248 – 250.

Nagel, T.J., Herwartz, D., Rexroth, S., Münker, C., Froitzheim, N. and Kurz, W., 2013. Lu-Hf dating, petrography, and tectonic implications of the youngest Alpine eclogites (Tauern Window, Austria). Lithos, 170-171, 179-190.

Neubauer, F., Genser, J., Kurz, W., and Wang, X., 1999. Exhumation of the Tauern Window, Eastern Alps. Physics and Chemistry of the Earth (A), 24, 675-680.

Nollau, G., 1969. Kleintektonische Struktur en am Südrand des Tauernfensters und ihre Einbeziehung in großtektonische Konzepte. - Geol. Rundsch., 58. 755-788, Stuttgart 1969.

Oberhänsli, R. Bousquet, R., Engi, M., Goffé, B., Gosso, G., Handy, M.R., Höck, V., Koller, F., Lardeaux, J.-M., Polino, R., Rossi, Ph., Schuster, R., Schwartz, St., Spalla, 2004. Metamorphic structure of the Alps. Scale 1:1.000.000, Commission for the Geological Map of the World, Paris.

Osmundsen P.T. and Andersen, T.B., 2001. The middle Devonian basins of western Norway: sedimentary response to large-scale transtensional tectonics? Tectonophysics, 332, p. 51-68.

O'Sullivan, P.B., and Parrish, R. R., 1995. The importance of apatite composition and single-grain ages when interpreting fission track data from plutonic rocks: a case study from the Coast Ranges, British Columbia. Earth and Planetary Science Letters 132, 213-224.

Oxburgh, E. R., and D. L. Turcotte, 1974. Thermal gradients and regional metamorphism in overthrust terrains with special reference to the Eastern Alps, Schweiz. Mineral. Petrogr. Mitt., 54, 641 – 642.

Parrish, R. R., 1983. Cenozoic thermal evolution and tectonics of the Coast Mountains of British Columbia, 1, Fission track dating, apparent uplift rates, and patterns of uplift, Tectonics, 2, 601– 631.

Paul, T. A., and Fitzgerald, P. G., 1992. Transmission electron microscopic investigation of fission tracks in fluorapatite: American Mineralogist, 77, 336-344.

Peresson, H., and Decker, K., 1997. Far-field effects of late Miocene subduction in the Eastern Carpathians: E-W compression and inversion of structures in the Alpine-Carpathian-Pannonian region. Tectonics, 16, 38-56.

Petit, J.P., 1987. Criteria for the sense of movement on fault surfaces in brittle rocks. Journal of structural Geology, 9, 597-608.

Platt, J.P., 1986. Dynamics of orogenic wedges and the uplift of high pressure metamorphic rocks. Geological Society of American Bulletin, 97, 1037-1053.

Pomella, H., 2010. The Cenozoic evolution of the Giudicarie fault system (Eastern/Southern Alps, northern Italy) A geochronological, structural and paleomagnetic study. PhD thesis, Innsbruck, April 2010.

Price, P. B. and Walker, R. M., 1963. Fossil tracks of charged particles in mica and the age of minerals: Journal of Geophysical Research, 68, 4847-4862.

Raith, M., Raase, D., Kreuzer, H. and Muller, D, 1978. The age of the alpidic metamorphism in the western Tauern Window, Austrian Alps, according to radiometric dating. In: "Alps, Appenines, Hellenides" Closs, H., Roeder, D.H., Schmidt, K. (Eds.). Intre-Union commission on Geodynamics, Scientific Report No38. 140-148 ,Stuttgart.

Ramsay, J.G., 1967. Folding and fracturing of rocks: New York, McGrawHill, 568p.

Ratschbacher, L., Frisch, W., Neubauer, F., Schmid, S. M. and Neuebauer, J., 1989. Extension in compressional orogenic belts: The Eastern Alps. Geology, 17, 404-407.

Ratschbacher, L., Merle, O., Davy, P. and Cobbold, P., 1991-a. Lateral extrusion in the Eastern Alps, Part. 1: Boundary conditions and experiments scaled for gravity. Tectonics, 10, 245-256.

Ratschbacher, L., Frisch, W. and Linzer, H.-G., 1991-b. Lateral extrusion in the Eastern Alps: Part II. Structural analysis. Tectonics, 10, 257-271.

Ravenhurst, C.E. and Donelick, R.A., 1992. Fission track thermochronology. In: Short Course. Handbook on Low Temperature Thermochronology, Zentilli M. and Reynolds, P.H. (eds). pp.21-42.

Reddy, S.M., Cliff, R.A. and East, R., 1993. Thermal history of the Sonnblick Dome, South-East Tauern window, Austria: Implications for heterogeneous uplift within the Pennine basement. Geol. Rdsch. 82, 667-675.

Reiners, P.W. and Brandon, M. T., 2006. Using thermochronology to understand orogenic erosion. Annu. Rev. Earth Planet. Sci., 34, 419–66

Reinecker, J. and Lehnhardt, A.W., 1999, Present-day stress field and deformation in eastern Austria, Int J. Earth Sciences, 88, 532–550.

Reiter, F., Lenhardt, W.A. and Brandner, R., 2005. Indications for activity of the Brenner Normal Fault zone (Tyrol, Austria) from seismological and GPS data. Austrian journal of Earth Sciences, 97, 16-23.

Rosenberg, C.L. and Berger, A., 2009. On the causes and modes of lateral growth of the Alps. Tectonics 28, issue 6, TC6001.

Rosenberg, C.L. and Garcia, S., 2011. Estimating displacement along the Brenner fault and orogen parallel extension in the Eastern Alps. Int J Earth Sci 100:1129–1145.

Rosenberg, C.L. and Garcia, S., 2012. Reply to the comment of Fügenschuh et al. on the paper 'Estimating displacement along the Brenner Fault and orogen-parallel extension in the Eastern Alps' by Rosenberg and Garcia, Int J Earth Sci (Geol Rundsch) (2011) 100:1129–1145. Int J Earth Sci (Geol Rundsch) (2012) 101:1457–1464.

Rosenberg, C.L. and Schneider, S. 2008. The western termination of the SEMP fault (Eastern Alps) and its bearing on the exhumation of the TW. In: Siegesmund, S., Fügenschuh, B., Froitzheim, N. (eds) Tectonic aspects of the alpine-dinaride-carpathian system. Geol. Soc. Lond 298: 197-218.

Rosenberg, C. L., Brun, J.-P. and Gapais, D., 2004. An indentation model of the Eastern Alps and the origin of the Tauern Window. Geology, 32, 997-1000.

Rosenberg, C. L., Brun, J.-P., Cagnard, F. and Gapais, D., 2007. Oblique indentation in the Eastern Alps: Insights from laboratory experiments. Tectonics, 26.

Royden, L.H., 1993. Evolution of retreating subduction boundaries formed during continental collision. Tectonophysics, 12, 629-638.

Sassi, F.P., Cavazzini, G, Visona, D. and Del Morro, A., 1985. Radiometric geochronology in the Eastern Alps : Results and problems, rend. soc. Ital. Mineral. Petrol., 40, 187-24.

Satir, M., 1976. Die Entwicklungsgeschichte der westlichen Hohen Tauern und der suedlichen Oetzalermasse aud grund radiometischer altersbestimmungen, Mem. Ist. Geol. Mineral. Univ. Padova, 30, 1-84.

Scharf, A., Handy, M.R., Favaro, S., Schmid, S. M. and Bertrand, A., 2013. Modes of orogen-parallel stretching and extensional exhumation in response to microplate indentation and roll-back subduction (Tauern Window, Eastern Alps) Int J Earth Sci (Geol Rundsch), 102, 1627-1654.

Schmid, S.M. and Kissling, E., 2000. The arc of the Western Alps in the light of geophysikal data on deep crustal structure. Tectonics, 19, 62-85.

Schmid, S.M., Fügenschuh, B., Kissling, E. and Schuster, R., 2004; Tectonic map and overall architecture of the Alpine orogen. Eclogae Geol. Helv., 97, 93-117.

Schmid S.M., Pfiffner O A, Froitzheim N, Schönborn G and Kissling E., 1996. Geophysical-geological transect and tectonic evolution of the Swiss-Italian Alps. Tectonics 15, 1036-1064.

Schmid S. M., Scharf, A., Handy, M.R. and Rosenberg, C.L, 2013. The Tauern Window (Eastern Alps. Austria): a new tectonic map, with cross-sections and a tectonometamorphic synthesis. Swiss J. Geosci., 106, 1-32.

Schulz, 1989. Jungalpidische Gefügeentwicklung entlang der Defereggen-Antholz-Vals-Linie (Osttirol, österreich). Jahrb. Geol. B-A Wien 132, 775-789.

Selverstone, J., Spear, F.S., Franz, G. and Morteani, G., 1984. Highpressure metamorphism in the SW Tauern Window, Austria: P-T paths from hornblende-kyanite-staurolite schists. J. Petrol. 25, 501-531.

Selverstone, J., 1985. Petrologic constraints on imbrications, metamorphism, and uplift in the SW Tauern Window, Eastern Alps. Tectonics, 4, 687-704.

Selverstone, J., 1988. Evidence for East-West crustal extension in the Eastern Alps: implications for the unroofing history of the TW. Tectonics, 7, 87-105.

Selverstone, J., Franz, G., Thomas, S. and Getty, S., 1992. Fluid variability in 2 GPa eclogites as an indicator of fluid behavior during subduction. Contributions to Mineralogy and Petrology 112, 341–357.

Selverstone, J., Axen, G. and Bartley, J., 1995. Fluid inclusion constraints on the kinematics of footwall uplift beneath the Brenner Line normal fault, Eastern Alps. Tectonics 14, 264-278.

Selverstone. J., 2005. Are the Alps collapsing? Annual Review of Earth and Planetary Science, 33, 2.1-2.20.

Senftl, E. and Exner, C., 1973. Rezente Hebung der Hohen Tauern und geologische Interpretation. Verhandlungen der Geologischen Bundesansalt, 1973, 209-234.

Sleep N. H., 1979. A thermal constraint on the duration of folding with reference to Acadian geology, New England (USA). J. Geol. 87, 583-9.

Soom, M.A., 1990. Abkühlungs- und Hebungsgeschichte der Externmassive und der penninischen Decken beidseits der Simplon-Rhone-Linie seit dem Oligozän: Spaltspurdatierungen an Apatit/Zirkon und K-Ar-Datierungen an Biotit/Muskowit (westliche Zentralalpen). PhD thesis, Universität Bern.

Spencer, J.E., 1984. The role of tectonic denudation in the wrapping and uplift of low-angle normal faults, Geology 12, 95-98.

Staufenberg, H., 1987. Apatite fission track evidence for postmetamorphic uplift and cooling history of the eastern Tauern Window and the surrounding Austroalpine (Central Eastern Alps, Austria). Jahrbuch der Geologischen Bundesanstalt, 130, 571-586.

Steck, A., and Hunziker, J., 1994. The Tertiary structural and thermal evolution of the central Alps compressional and extensional structures in an orogenic belt, Tectonophysics, 238, 229–254.

Steininger, F., Roegl, F., Hoehuli, P. and Muller, C., 1989. Lignite deposition and marine cycles. The Austrian Tertiary lignite deposits. A case history, Sitzungsber. Akad. Wiss.Wien, mnath-naturwiss Kl., 197(5-10), 309-332, 1989.

Steenken, A., Siegesmund, S., Heinrichs, T., and Fügenschuh, B., 2002. Cooling and exhumation of the Rieserferner Pluton (Eastern Alps, Italy/Austria). International Journal of Earth Sciences, 91, 799–817.

Stampfli, G.M., 1993. Le Brianconnais, terrain exotique dans les Alpes? - Eclogae geol. Helv, 86, 1-45

Steenken, A., Siegesmund, S., Heinrichs, T., and Fügenschuh, B., 2002. Cooling and exhumation of the Rieserferner Pluton (Eastern Alps, Italy/Austria). International Journal of Earth Sciences, 91, 799–817.

Stipp, M., Stünitz, H., Heilbronner, R. and Schmid S.M., 2002. The eastern Tonale fault zone: a "natural laboratory" for crystal plastic deformation of quartz over a temperature range from 250 to 700 °C. Journal of Structural Geology, 24, 1861-1884.

Stöckhert, B., Brix, M.R., Kleinschrodt, R., Hurford, A.J., and Wirth, R., 1999. Thermochronometry and the microstructures of quartz - A comparison with experimental flow laws and predictions on the temperature of the brittle-plastic transition. Journal of Structural Geology, 21, 351–369.

Sue, C., Delacou, B., Champagnac, J-D., Allanic, C, Tricart, P. and Burkhard, M., 2007. Extensional neotectonics around the Western /Central Alps: an overview. Int. J. Earth Sci., 96, 1101-1129.

Tagami, T., and Shimada, C., 1996. Natural long-term annealing of the zircon fission track system around a granitic pluton. J. Geophys. Res. 101, 8245-8255.

Termier, P. 1903. Les nappes des Alpes orientales et la synthèse des Alpes. Bull. Soc. Géol. France IVe Ser., 3, 711-766.

Teyssier, C. and Whitney, D.L., 2002. Gneiss domes and orogeny. Geology 30, 1139-1142.

Thöni, M., 1981. Degree and Evolution of the Alpine Metamorphism in the Austroalpine Unit W of the Hohe Tauern in the light of K/Ar and Rb/Sr Age Determinations in Micas. Jahrb. Geol. B.-A., 124 (1): 111-174.

Thöni, M., 1999. A review from geochronological data from the Eastern Alps, Schweizerische Mineralogische und petrographische Mitteilungen 79, 209-230.

Tollmann, A., 1963. Ostalpensynthese. 256p., Deuticke, Wien.

Tollmann, A., 1975. Ozeanische Kruste im Pennin des Tauemfensters und die Neugliederung des Deckenbaus der Hohen Tauem. Neues Jahrb. Geol. Pal/iontol. Abh. 148, 286-319.

Vernon, 2008. Thermochronological approach to the late Neogene exhumation of the European Alps. The University of Edinburgh - PhD Thesis.

Villa, I. and Von blanckenburg, F.,1992. A hornblende Ar- Ar age traverse of the Bregaglia tonalite (SE Central Alps). Schweizerische Mineralogische und Petrographische Mitteilungen, 71, 73-87.

Viola, G., Mancktelow, N. S. and Seward, D., 2001. Late Oligocene-Neogene evolution of Europe-Adria collision: New structural and geochronological evidence from the Giudicarie fault system (Italian Eastern Alps). Tectonics, 20, 999-1020.

Von Blanckenburg, F., Villa, I.M., Baur, H., Morteani, G. and steiger R.H., 1989. Time calibration of a PT-path from the Western Tauern Window, Eastern Alps: the problem of closure temperatures. Contributions to mineralogy and Petrology, 101, 1-11.

Wagner GA. 1979. Correction and interpretation of fission track ages. In: Isotope Geology Jäger, E. and Hunziker, J.C (Eds), Lectures in Isotope Geology. Springer-Verlag, Berlin (1979), 170-177.

Wagner, G. A., and Van den Haute, P., 1992. Fission track dating: Dordrecht; Boston, Kluwer, 285 p.

Wagner, G.A., 1968. Fission track dating of apatite. Earth Planet. Sci. Lett., 4, 411-415.

Wallace, R.E., 1951. Geometry of shearing stress and relation to faulting, J. Geol., 59, 118-130.

Wang, X., and Neubauer, F., 1998. Orogen-parallel strike-slip faults bordering metamorphic core complexes: the Salzach-Enns fault zone in the Eastern Alps. Journal of Structural Geology, 20, 799-818.

Wawrzyniec, T.F., Selverstone, J., and Axen, G.J., 2001. Styles of footwall uplift along the Simplon and Brenner normal fault systems, central and Eastern Alps. Tectonics, 20, 748-770.

Wernicke, B., 1985. Uniform-sense normal simple shear of the continental lithosphere. Can. J. Earth Sci. 88, 108-125.

Whitney, D.L., Teyssier, C. and Vanderhaeghe, O., 2004. Gneiss dome and crustal flow. In: Whitney, D., Teyssier, C., Siddoway, S. (eds.), Gneiss domes in orogeny: The Geological Society of America, Special Paper 380, 15-33.

Withjack, M.O. and Sheiner, C., 1982. Fault Patterns Associated with Domes – An Experimental and Analytical Study. The American Association of Petroleum Geologists Bulletin, 66, 302-316.

Wölfler, A., Dekant, C., Danisìk, M., Kurz, W., Dunkl, I., Putis, M. and Frisch, W., 2008. Late stage differential exhumation of crustal blocks in the central Eastern Alps: evidence from fission track and (U–Th)/He thermochronology. Terra Nova, 20, 378–384,

Yamada, R., Tagami, T. Nishimura, S. and Ito H., 1995. Annealing kinematics of fission tracks in zircon: an experimental study. Chem. Geol. 122, 249-258.

Yin, A.,1989. Origin of regional, rooted low-angle normal faults: a mechanical model and its tectonic implications. Tectonics, 8, p. 469-482.

Yin, A., 2004. Gneiss domes and gneiss dome systems. In: Gneiss dome and orogeny Whitney, D.L., Teyssier, C. and Siddoway, C.S. (eds), Boulder, Colorado. Geological Society of America Special Paper 380, p.1-14.

Zaun P.E., and Wagner G.A., 1985. Fission track stability in zircons under geological conditions. Nuclear Tracks, 10, 303–307.

Zimmermann, R., Hammerschmidt, K. and Franz, G., 1994. Eocene high pressure metamorphism in the Penninic units of the Tauern Window (Eastern Alps), evidence from 40Ar-39Ar dating and petrological investigations. Contrib. Mineral. Petrol. 117, 175-186.

Zwingmann, H., and Mancktelow, N., 2004. Timing of alpine fault gouges. Earth and Planetary Science letters, 223, 415-425.

Caption list

Figures

Tables

Appendixes

Appendix 1. Apatite fission track data set

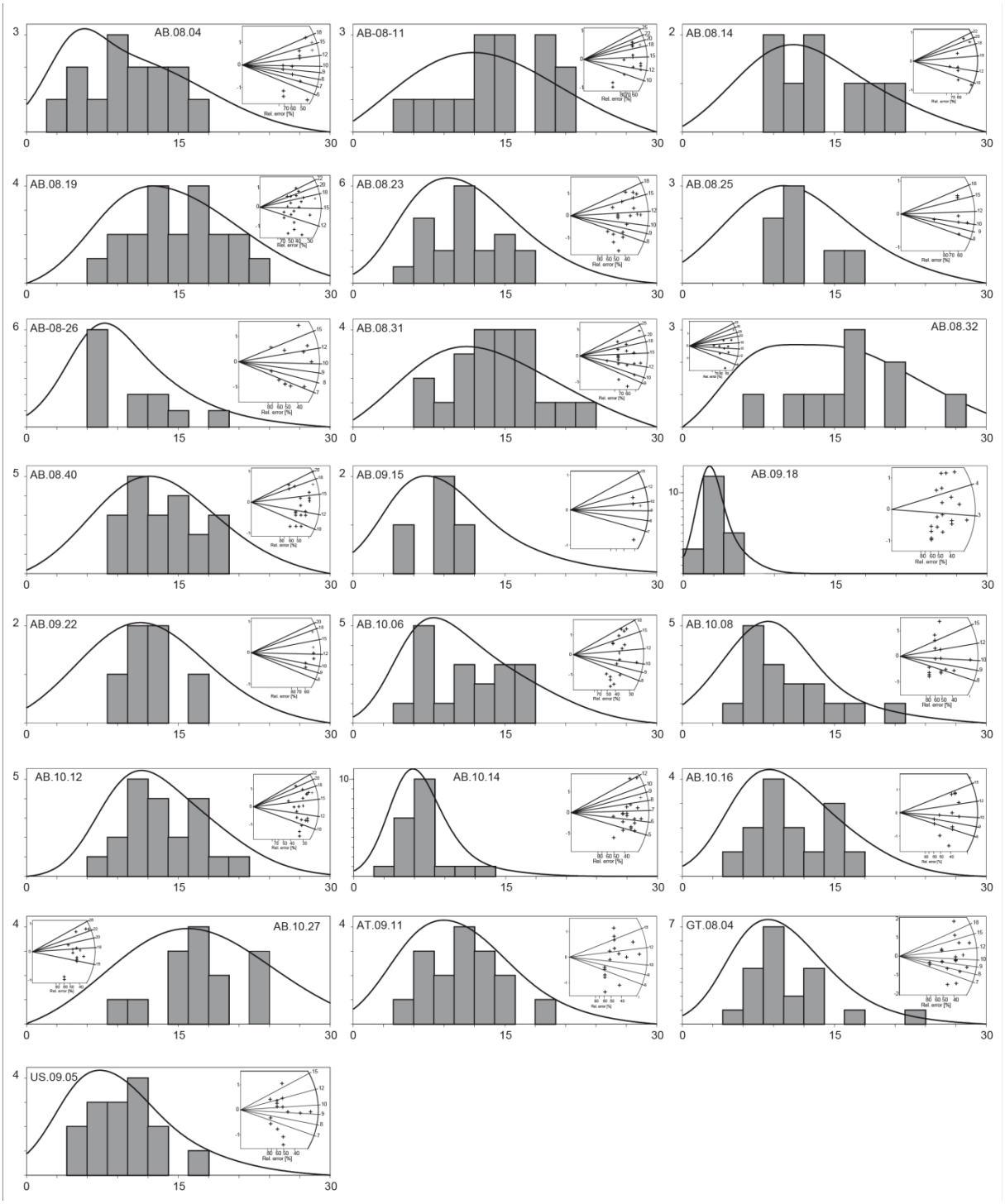

Appendix 2. Zircon fission track data set

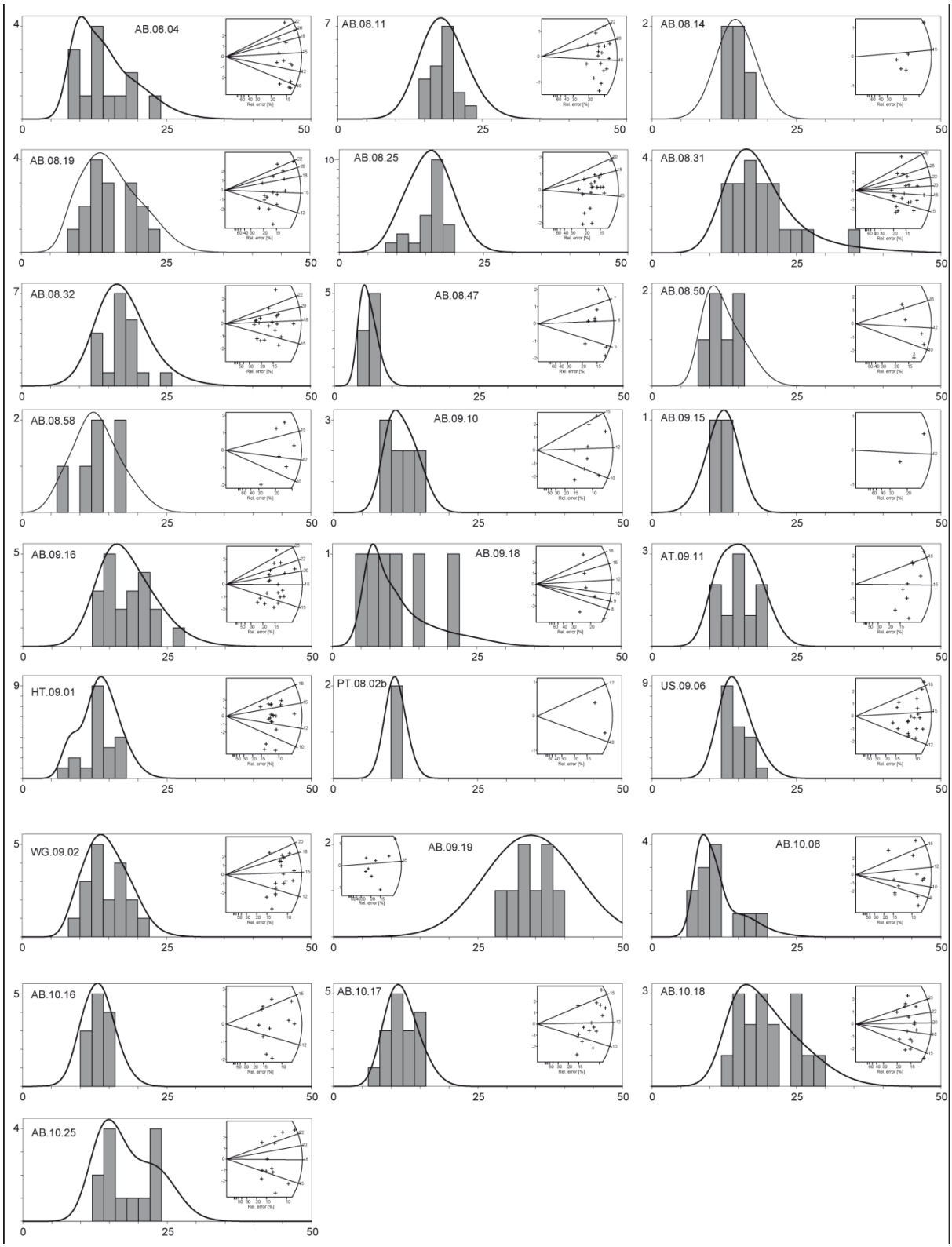

Appendix 3: Compilation of apatite fission track ages normalized at 1000 m elevation

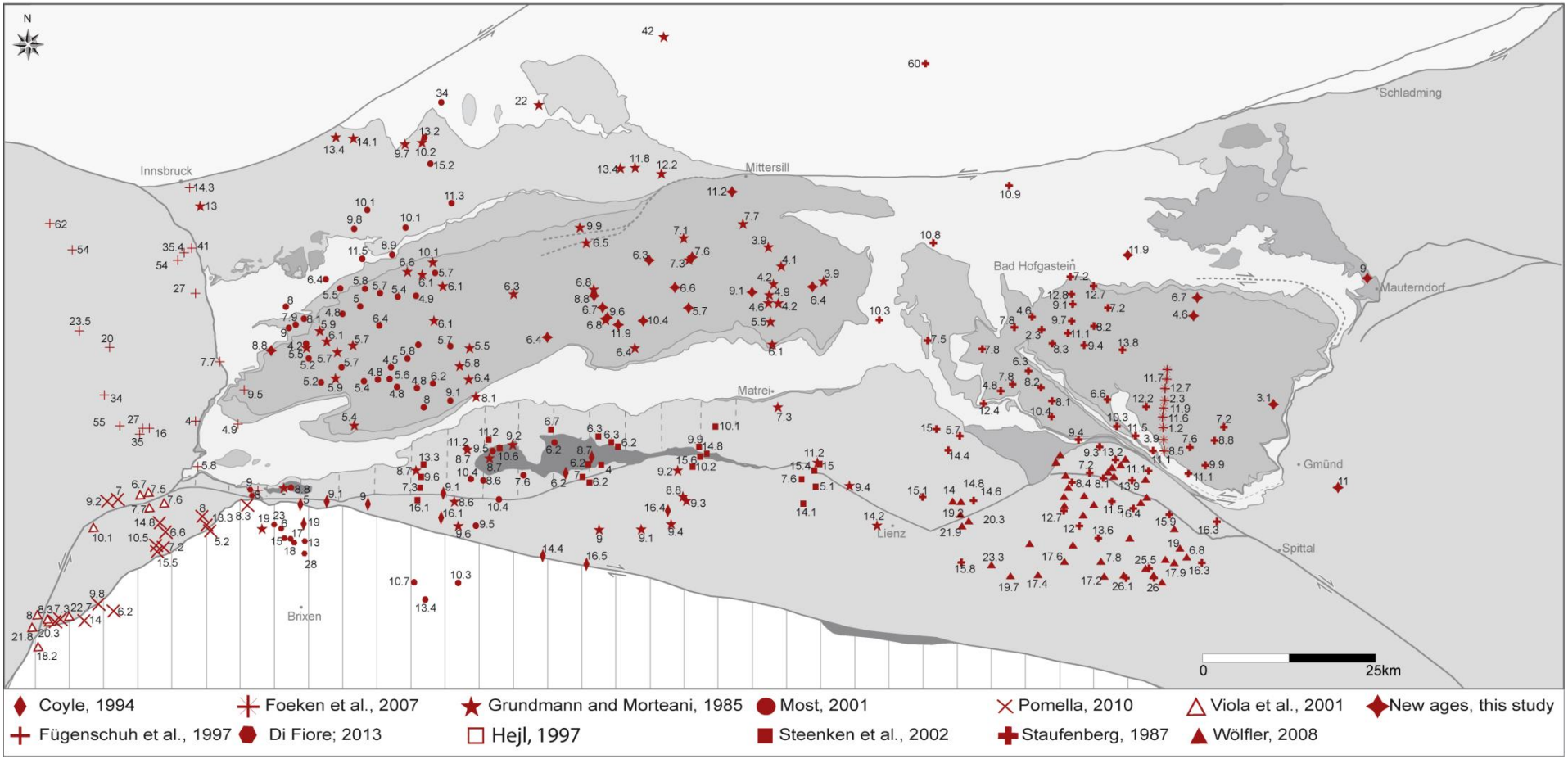

Appendix 4: Compilation of zircon fission track ages normalized at 1000 m elevation

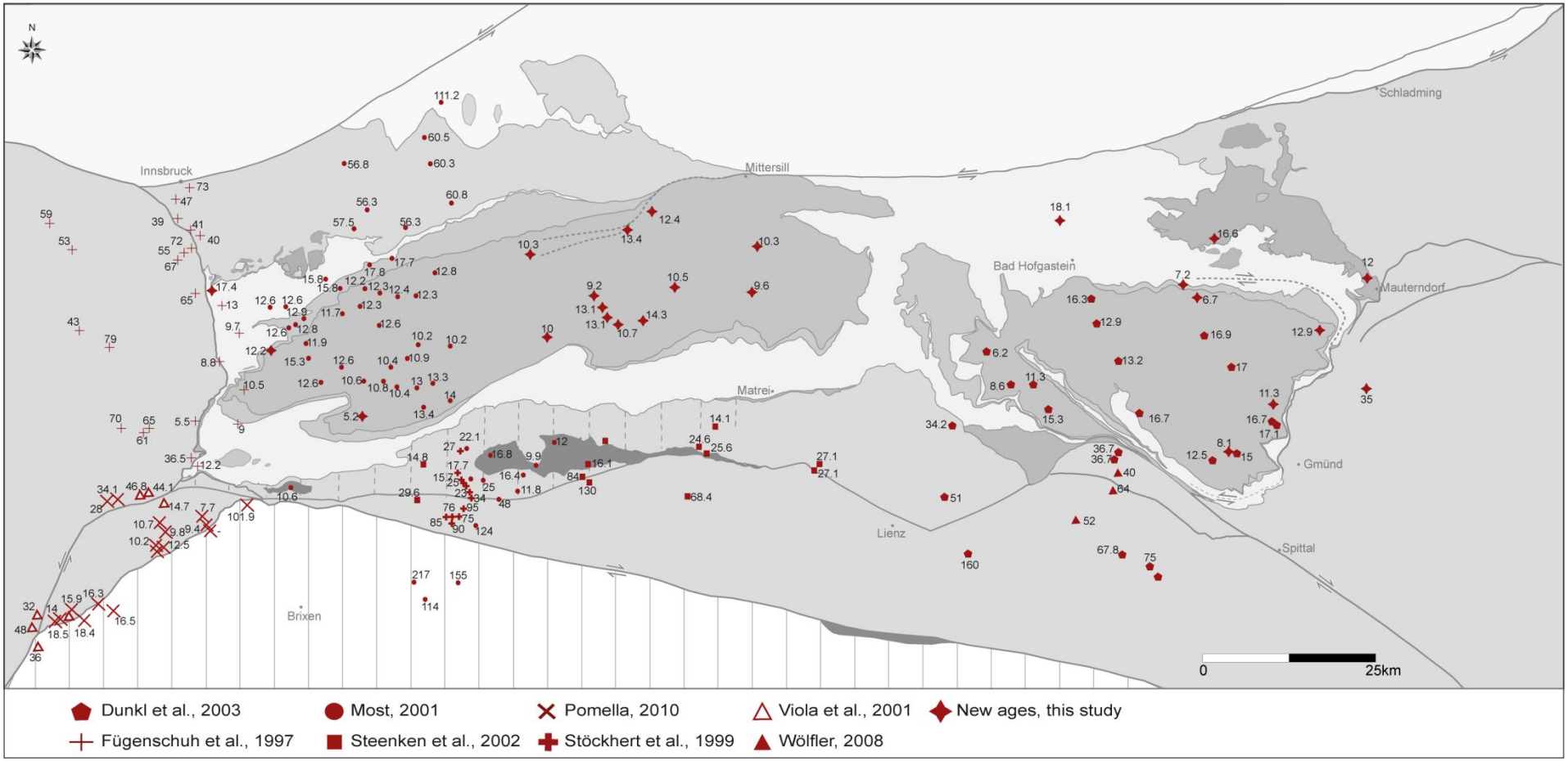

Appendix 5. Extrapolation of apatite fission track ages normalized at 1000 elevation

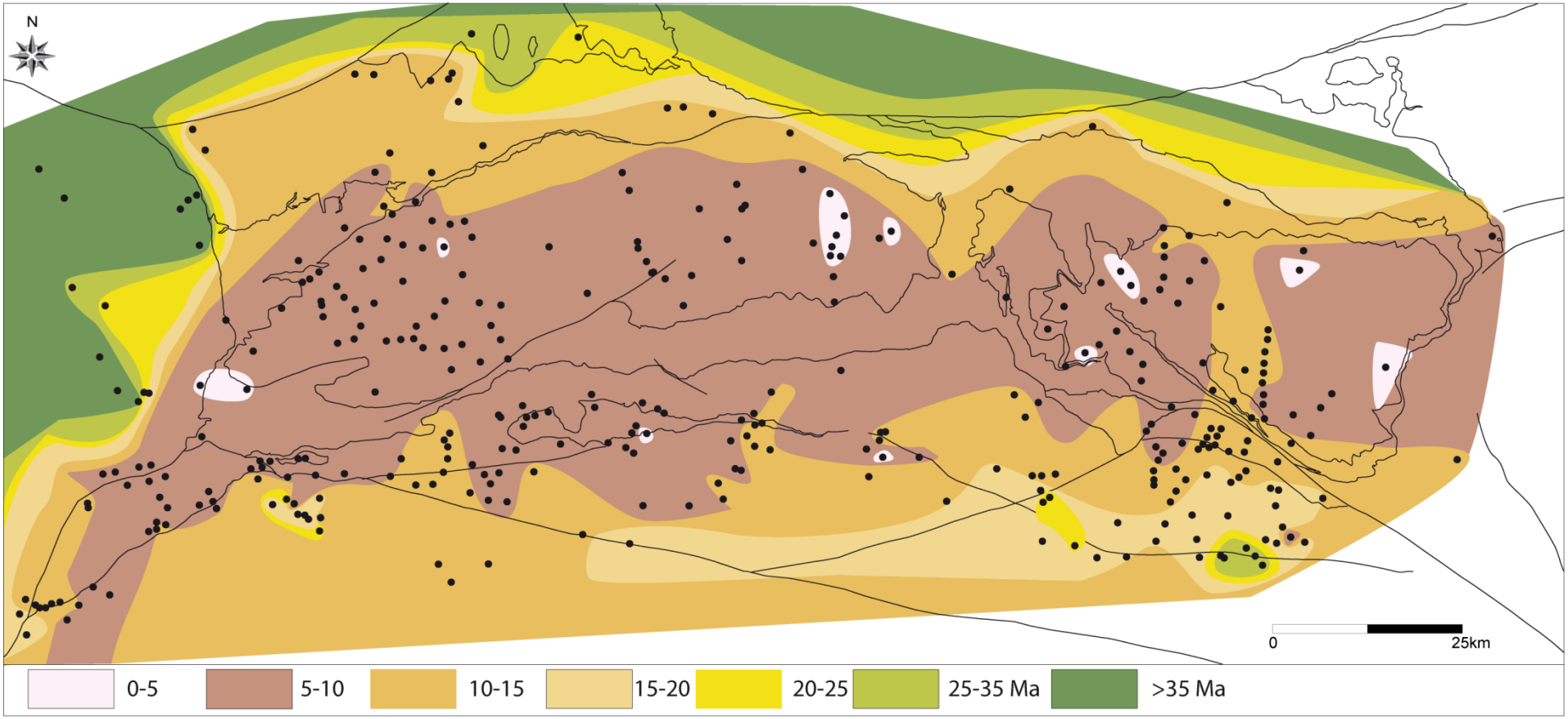

Appendix 6. Extrapolation of zircon fission track ages over the Tauern Window normalized at 1000 elevation